



University of Kentucky  
UKnowledge

---

Theses and Dissertations--Chemical and  
Materials Engineering

Chemical and Materials Engineering

---

2017

## FORMULATION AND CHARACTERIZATION OF POLY( $\beta$ -AMINO ESTER) NETWORKS FOR CONTROLLED DELIVERY OF ANTIOXIDANTS IN PHARMACEUTICAL APPLICATIONS

Vinod Shivaji Patil

University of Kentucky, [vinod.patil@uky.edu](mailto:vinod.patil@uky.edu)

Author ORCID Identifier:

<http://orcid.org/0000-0003-4093-8979>

Digital Object Identifier: <https://doi.org/10.13023/ETD.2017.023>

[Right click to open a feedback form in a new tab to let us know how this document benefits you.](#)

---

### Recommended Citation

Patil, Vinod Shivaji, "FORMULATION AND CHARACTERIZATION OF POLY( $\beta$ -AMINO ESTER) NETWORKS FOR CONTROLLED DELIVERY OF ANTIOXIDANTS IN PHARMACEUTICAL APPLICATIONS" (2017). *Theses and Dissertations--Chemical and Materials Engineering*. 70.

[https://uknowledge.uky.edu/cme\\_etds/70](https://uknowledge.uky.edu/cme_etds/70)

This Doctoral Dissertation is brought to you for free and open access by the Chemical and Materials Engineering at UKnowledge. It has been accepted for inclusion in Theses and Dissertations--Chemical and Materials Engineering by an authorized administrator of UKnowledge. For more information, please contact [UKnowledge@lsv.uky.edu](mailto:UKnowledge@lsv.uky.edu).

## **STUDENT AGREEMENT:**

I represent that my thesis or dissertation and abstract are my original work. Proper attribution has been given to all outside sources. I understand that I am solely responsible for obtaining any needed copyright permissions. I have obtained needed written permission statement(s) from the owner(s) of each third-party copyrighted matter to be included in my work, allowing electronic distribution (if such use is not permitted by the fair use doctrine) which will be submitted to UKnowledge as Additional File.

I hereby grant to The University of Kentucky and its agents the irrevocable, non-exclusive, and royalty-free license to archive and make accessible my work in whole or in part in all forms of media, now or hereafter known. I agree that the document mentioned above may be made available immediately for worldwide access unless an embargo applies.

I retain all other ownership rights to the copyright of my work. I also retain the right to use in future works (such as articles or books) all or part of my work. I understand that I am free to register the copyright to my work.

## **REVIEW, APPROVAL AND ACCEPTANCE**

The document mentioned above has been reviewed and accepted by the student's advisor, on behalf of the advisory committee, and by the Director of Graduate Studies (DGS), on behalf of the program; we verify that this is the final, approved version of the student's thesis including all changes required by the advisory committee. The undersigned agree to abide by the statements above.

Vinod Shivaji Patil, Student

Dr. Thomas D. Dziubla, Major Professor

Dr. Thomas D. Dziubla, Director of Graduate Studies

FORMULATION AND CHARACTERIZATION OF POLY( $\beta$ -AMINO ESTER)  
NETWORKS FOR CONTROLLED DELIVERY OF ANTIOXIDANTS IN  
PHARMACEUTICAL APPLICATIONS

---

DISSERTATION

---

A dissertation submitted in partial fulfillment of the  
requirements for the degree of Doctor of Philosophy in the  
College of Engineering  
at the University of Kentucky

By

Vinod Shivaji Patil

Lexington, Kentucky

Co-Directors: Dr. Thomas D. Dziubla, Professor of Chemical Engineering  
and Dr. Douglass S. Kalika, Professor of Chemical Engineering

Lexington, Kentucky

Copyright © Vinod Shivaji Patil 2016  
<http://orcid.org/0000-0003-4093-8979>

## ABSTRACT OF DISSERTATION

### FORMULATION AND CHARACTERIZATION OF POLY( $\beta$ -AMINO ESTER) NETWORKS FOR CONTROLLED DELIVERY OF ANTIOXIDANTS IN PHARMACEUTICAL APPLICATIONS

Oxidative stress, which reflects an imbalance between oxidants and endogenous antioxidants, is known to be a cause as well as an effect of health conditions such as cancer, diabetes, Alzheimer's disease, Parkinson's disease and ischemia-reperfusion injury. Antioxidants have shown promising results *in vitro* in controlling oxidative stress. However, years of *in vitro* studies have failed to translate into effective clinical interventions for controlling oxidative stress in the disease conditions. This has been due to low bioavailability and lower stability of antioxidants. Poly(antioxidant  $\beta$ -amino esters) (PABAE) are a recently-developed class of biodegradable polymeric hydrogels that have shown promise in their ability to control cellular response and reduce oxidative stress while simultaneously enhancing material biocompatibility. In this dissertation, poly(curcumin  $\beta$ -amino ester) (PCBAE) hydrogels were synthesized and tuned using process parameters for the controlled release of curcumin, an antioxidant.

Curcumin was functionalized with acrylate groups to form curcumin multiacrylate (CMA) so that it could be covalently incorporated into a polymer network. Liquid chromatography-mass spectrometry (LCMS) and nuclear magnetic resonance (NMR) were used to identify individual acrylate species present in the resulting multiacrylate mixture. A series of hydrogel networks were formed by polymerization of a commercial diacrylate, polyethylene glycol diacrylate (PEG400DA), and a primary diamine, 4,7,10-trioxa-1,13-tridecanediamine (TTD), in combination with CMA. Aqueous degradation and curcumin release were evaluated, along with the thermomechanical properties of the networks using dynamic mechanical analysis and broadband dielectric spectroscopy. The network properties and curcumin release characteristics were tuned through systematic variations in curcumin composition, amine crosslinker, PEG diacrylate, and ratio of total acrylate to amine. The degradation and resulting antioxidant properties of these biomaterials are closely related to the composition and architecture of the networks established during polymerization. The PCBAEs developed in this study had degradation times ranging from 5 hours to up to 58 hours. Based on these results, one PCBAE variant was selected for the development of tablet formulations for colon specific delivery, and these tablets exhibited a sustained release for 20 hours. Overall, the PCBAE series shows a wide range of

degradation and thermomechanical characteristics with potential use in drug delivery, tissue engineering and biomedical applications.

**KEYWORDS:** Oxidative stress, antioxidants, crosslinked networks, controlled release, curcumin

Vinod Shivaji Patil

December 9<sup>th</sup>, 2016

FORMULATION AND CHARACTERIZATION OF POLY( $\beta$ -AMINO ESTER)  
NETWORKS FOR CONTROLLED DELIVERY OF ANTIOXIDANTS IN  
PHARMACEUTICAL APPLICATIONS

By  
Vinod Shivaji Patil

Dr. Thomas D. Dziubla  

---

Co-Director of Dissertation

Dr. Douglass S. Kalika  

---

Co-Director of Dissertation

Dr. Thomas D. Dziubla  

---

Director of Graduate Studies

December 9<sup>th</sup>, 2016  

---

Date

## DEDICATION

I dedicate this dissertation to my Mom and Dad, Phulwanti Patil and Shivaji Patil.

Thank you for going through so many hardships so that we (Jeetendra, myself and Sachin) could have a better tomorrow.

## ACKNOWLEDGMENTS

I would like to acknowledge my advisors Dr. Kalika and Dr. Dziubla for guiding me during my PhD research. I feel privileged to have had an opportunity to benefit from their enormous experience and work ethics which will help me throughout my life. They always motivated me to come up with new ideas and gave freedom to explore them. I will cherish the weekly research meetings, where Dr. Dziubla shared lot of exciting novel ideas. Dr. Kalika's expertise in polymer engineering helped throughout my research. Dr. Kalika's discipline in research and in life has had an immense influence on me. I would also like to acknowledge my committee members Dr. Berron and Dr. DeRouchey for providing insight and guidance during the research, and Dr. Munson for being an external examiner for the defense of this dissertation.

I would like to thank my past and present lab members Dr. Sundar Authimoolam, Dr. Prachi Gupta, Dr. Andrew Lakes, Angela Maria Gutierrez, Mark Bailey, Irfan Ahmed and Carolyn Jordan for in depth discussions and providing thoughtful inputs. I am also grateful to have had great friends in Lexington who made me feel at home. I would like to thank my friends Dr. Suraj Nagpure, Dr. Raghava Bhamidipati, Sebastian Hernandez, Abhishek Kognole, Ashish Aher and Priyesh Wagh.

No words are enough, but I would like to thank my Mom and Dad for instilling good habits and discipline, which has helped me enormously till now. I am grateful to my brothers, Jeetendra and Sachin, have always been there for me and for helping me learn new things all my life. I would also like to thank my *Vaini*, Shwetali. I thank all my family members for taking time to Skype with me weekly and sometimes even daily so that I never felt I was away from them. I would also like to thank my fiancé Bhavana for listening to

my ideas, giving me a different point of view to look at things and life. She kept me sane during ups and downs in my research and life.

## TABLE OF CONTENTS

ACKNOWLEDGMENTS .....	iii
LIST OF TABLES.....	xi
LIST OF FIGURES .....	xii
Chapter 1: Introduction and background .....	1
1.0 Introduction.....	1
1.1 Background.....	3
1.1.1 Oxidative stress.....	3
1.1.1.1 ROS/RNS generation pathways.....	4
1.1.2 Role of OS in pathology .....	5
1.1.2.1 Lipid peroxidation.....	6
1.1.2.2 Protein oxidation.....	7
1.1.2.3 Oxidative DNA damage.....	7
1.1.3 Role of OS in biomaterial compatibility .....	8
1.1.4 Strategies to counter OS.....	10
1.1.5 Measurement of antioxidant activity .....	11
1.1.6 Polymers for drug delivery .....	12
1.1.6.1 Non-degradable polymers.....	14
1.1.6.2 Degradable polymers .....	15
1.1.7 Hydrogels.....	18
1.1.8 Polymers for antioxidant delivery.....	21
1.1.8.1 Antioxidant loaded polymer systems.....	21
1.1.8.2 Antioxidant embedded in the polymer chain .....	22
Chapter 2: Research goals.....	30

2.1 Specific aim 1: Synthesize and characterize curcumin multiacrylate (CMA) monomers for use in PCBAE synthesis .....	31
2.1.1 Hypothesis # 1.....	31
2.1.2 Significance and outcome .....	31
2.2 Specific aim 2: Synthesize biodegradable poly(antioxidant $\beta$ -amino ester) (PABAE) networks based on incorporation of curcumin multiacrylate and characterize their static and dynamic properties.....	31
2.2.1 Hypothesis #2.....	32
2.2.2 Significance and outcome .....	32
2.2 Specific aim 3: Determine the influence of total acrylate to amine ratio, amine crosslinker and diacrylate monomer on mechanical and degradation properties of PCBAE.....	32
2.2.1 Hypothesis # 3.....	33
2.2.2 Significance and outcome .....	33
2.4 Specific aim 4: Develop poly( $\beta$ -amino ester) (PBAE) based tablet formulation for improved bioavailability of a hydrophobic drug .....	34
2.4.1 Hypothesis # 4.....	34
2.4.2 Significance and outcome .....	34
Chapter 3: Curcumin acrylation for biological and environmental applications.....	35
3.1 Introduction.....	35
3.2 Experimental.....	36
3.2.1 Materials .....	36
3.2.2 Curcumin multiacrylate (CMA) synthesis.....	36
3.2.3 High performance liquid chromatography (HPLC).....	37
3.2.3 Liquid chromatography-mass spectrometry (LCMS).....	38
3.2.4 $^1\text{H}$ Nuclear magnetic resonance ( $^1\text{H-NMR}$ ).....	38

3.2.5 Thermogravimetric analysis (TGA).....	38
3.3 Results and discussion .....	38
3.3.1 High performance liquid chromatography (HPLC).....	39
3.3.2 Liquid chromatography-mass spectrometry (LCMS).....	40
3.3.3 <sup>1</sup> H Nuclear magnetic resonance ( <sup>1</sup> H-NMR).....	43
3.3.4 Thermogravimetric analysis (TGA).....	44
3.4 Conclusions.....	45
Chapter 4: Static and dynamic properties of biodegradable poly(antioxidant β-amino ester) networks based on incorporation of curcumin multiacrylate.....	62
4.1 Introduction.....	62
4.2 Experimental .....	65
4.2.1 Materials .....	65
4.2.2 Curcumin multiacrylate synthesis.....	65
4.2.3 Synthesis of PCβAE gel films .....	66
4.2.4 Swelling studies .....	67
4.2.5 Degradation studies.....	67
4.2.6 Dynamic Mechanical Analysis .....	68
4.2.7 Broadband Dielectric Spectroscopy.....	68
4.3 Results & discussions .....	69
4.3.1 Synthesis and characterization of CMA .....	69
4.3.2 Swelling characteristics .....	70
4.3.3 Aqueous degradation .....	71
4.3.4 Dynamic mechanical analysis.....	71
4.3.5 Broadband dielectric spectroscopy .....	74
4.3.5.1 Analysis of the glass-rubber relaxation.....	75

4.3.5.2 Analysis of sub-glass relaxations.....	76
4.4 Conclusions.....	77
Chapter 5: Influence of ratio of total acrylate to amine (RTAA) and monomer selection on network and degradation properties of poly(curcumin $\beta$ -amino ester) (PCBAE).....	95
5.1 Introduction.....	95
5.2 Experimental.....	97
5.2.1 Materials.....	97
5.2.2 Gel synthesis.....	97
5.2.3 Dynamic mechanical analysis (DMA).....	98
5.2.4 Degradation.....	99
5.2.5 Trolox equivalent antioxidant capacity (TEAC).....	100
5.3 Results and discussion .....	100
5.3.1 Amine crosslinker .....	100
5.3.1.1 Effect of amine crosslinker on mechanical properties of 0:100 CMA:PEG400DA hydrogels .....	101
5.3.1.2 Effect of amine crosslinker on degradation properties of 0:100 CMA:PEG400DA hydrogels .....	101
5.3.2 Commercial diacrylate .....	102
5.3.2.1 Effect of diacrylate on mechanical properties of 0:100 CMA:PEGDA hydrogels.....	103
5.3.2.2 Effect of diacrylate on degradation properties of 0:100 CMA:PEGDA hydrogels.....	104
5.3.3 Influence of RTAA on functional properties of PCBAE hydrogels .....	104
5.3.3.1 Effect of RTAA on monomer extraction during washing of gels.....	105
5.3.3.2 Effect of RTAA on mechanical properties of 50:50 CMA:PEG400DA hydrogels.....	105

5.3.3.3 Effect of RTAA on degradation properties of 50:50 CMA:PEG400DA hydrogels.....	106
5.3.3.4 Effect of RTAA on mechanical properties of 90:10 CMA:PEG400DA hydrogels.....	107
5.3.3.5 Effect of RTAA on degradation properties of 90:10 CMA:PEG400DA hydrogels.....	108
5.3.4 CMA composition dependence for PCBAE-EDBE and PCBAE-HMD hydrogels.....	108
5.3.4.1 Effect of CMA composition on mechanical properties of PCBAE-EDBE hydrogels.....	109
5.3.4.2 Effect of CMA composition on degradation of PCBAE-EDBE hydrogels .....	110
5.3.4.3 Effect of CMA composition on mechanical properties of PCBAE-HMD hydrogels.....	110
5.3.4.4 Effect of CMA composition on degradation of PCBAE-HMD hydrogels .....	111
5.4 Conclusions.....	112
Chapter 6: Poly( $\beta$ -amino ester) based tablet formulation for improved oral bioavailability of a hydrophobic drug.....	140
6.1 Introduction.....	140
6.2 Experimental.....	142
6.2.1 Materials .....	142
6.2.2 Synthesis of poly(curcumin $\beta$ amino ester) gel films .....	143
6.2.3 Particle size analysis .....	143
6.2.4 PCBAE prodrug tablet synthesis .....	144
6.2.5 Tablet dissolution and curcumin release.....	144
6.2.6 Anti-oxidant activity using TEAC assay .....	145

6.2.7 Standard and accelerated storage stability .....	146
6.3 Results.....	146
6.3.1 Film degradation and tablet dissolution.....	146
6.3.2 Tablet storage stability.....	148
6.3.3 Antioxidant activity .....	152
6.4 Discussion.....	152
6.5 Conclusions.....	156
Chapter 7: Conclusions.....	171
References:.....	174
VITA.....	188

## LIST OF TABLES

<b>Table 1.1:</b> Endogenous sources of ROS/RNS.....	23
<b>Table 3.1:</b> Composition of curcumin, acryloyl chloride and TEA in the initial reaction mixture. ....	46
<b>Table 3.2:</b> UV-Vis absorbance peaks for different forms of curcumin multiacrylate. ....	47
<b>Table 3.3:</b> Proportion of different acrylates in CMA prepared with different curcumin: acryloyl chloride ratios. The values are based on the peak areas from LCMS.....	48
<b>Table 4.1:</b> Compositions of synthesized poly(curcumin $\beta$ amino esters). ....	79

## LIST OF FIGURES

<b>Figure 1.1:</b> Formation of strong ROS/RNS from superoxide anion .....	24
<b>Figure 1.2:</b> Mechanism of lipid peroxidation. L – lipid, A – antioxidant.....	25
<b>Figure 1.3:</b> Mechanism for the formation of malonaldehyde (MDA), where PUFA is poly(unsaturated fatty acid). .....	26
<b>Figure 1.4:</b> Reaction scheme in CUPRAC and FRAP assays.....	27
<b>Figure 1.5:</b> Schematic for drug release from a polymer matrix due to swelling response caused by stimuli such as temperature, or pH in aqueous media.....	28
<b>Figure 1.6:</b> Steps involved in the bulk degradation of polymers. ....	29
<b>Figure 3.1:</b> Chemical structure of curcumin (A), curcumin monoacrylate (B), curcumin diacrylate (C), and curcumin triacrylate (D). R <sub>1</sub> and R <sub>2</sub> are both OCH <sub>3</sub> for curcumin, H and OCH <sub>3</sub> for demethoxycurcumin, and both H for bisdemethoxycurcumin.....	49
<b>Figure 3.2:</b> HPLC chromatograms for curcumin and curcumin multiacrylate with different curcumin:acryloyl chloride ratios (viz. 1:1, 1:2 and 1:3). The curcumin peak intensity decreases with an increase in acryloyl chloride in the reaction mixture.....	50
<b>Figure 3.3:</b> Absorbance spectra for individual peaks from HPLC analysis for CMA 1:3. The time noted in the legend is the peak elution time obtained from HPLC. Possible peak assignments for the different acrylates are indicated in the legend. CMoA – curcumin monoacrylate, CTA – curcumin triacrylate, CDA – curcumin diacrylate, DCDA – demethoxycurcumin diacrylate, BDCDA – bisdemethoxycurcumin diacrylate.....	51
<b>Figure 3.4:</b> LCMS data for curcumin. Mass spectroscopy results are shown in the top three plots, while the result from the UV-vis detector connected before the mass spectrometer is shown in the bottom plot.....	52
<b>Figure 3.5:</b> LCMS data for CMA synthesized using 1:1 curcumin:acryloyl chloride ratio. Mass spectroscopy results are shown in the top three plots, while the result from the UV-vis detector connected before the mass spectrometer is shown in the bottom plot. ....	53
<b>Figure 3.6:</b> LCMS data for CMA synthesized using 1:2 curcumin:acryloyl chloride ratio. Mass spectroscopy results are shown in the top three plots, while the result from the UV-vis detector connected before the mass spectrometer is shown in the bottom plot. ....	54

<b>Figure 3.7:</b> LCMS data for CMA synthesized using 1:3 curcumin:acryloyl chloride ratio. Mass spectroscopy results are shown in the top three plots, while the result from the UV-vis detector connected before the mass spectrometer is shown in the bottom plot. ....	55
<b>Figure 3.8:</b> Curcumin triacrylate (CTA) elution collection samples rerun in HPLC using 12 minute gradient method file from 60/40 (ACN/aqueous) to 100/0 (ACN/aqueous). Inset plot shows same data, but expanding triacrylate range. For curcumin triacrylate, peaks 1, 2 and 3 correspond to the 14.8, 15.8 & 17.3 minute peaks in Figure 3.2. ....	56
<b>Figure 3.9:</b> Isolated curcumin triacrylate “peak 2” elution collection samples (0.5 and 5 hours after collection) rerun in HPLC using 12 minute gradient method file from 60/40 (ACN/water) to 100/0 (ACN/water). Inset plot shows same data, but expanding triacrylate range.....	57
<b>Figure 3.10:</b> Isolated curcumin triacrylate “peak 3” elution collection samples (0.5 and 5 hours after collection) rerun in HPLC using 12 minute gradient method file from 60/40 (ACN/water) to 0/100 (ACN/water). Inset plot shows same data, but expanding triacrylate range.....	58
<b>Figure 3.11:</b> <sup>1</sup> H NMR (400 MHz, DMSO- <i>d</i> <sub>6</sub> ) spectrum of curcumin and CMA prepared with different curcumin:acryloyl chloride ratios. Acrylation is evident from the decrease in hydroxyl proton peaks (9.5 to 10.5 ppm) and the emergence of acrylate proton peaks (between 6.1 and 6.7 ppm).....	59
<b>Figure 3.12:</b> Comparison of extent of acrylation values obtained from LCMS and NMR analysis of CMA with different curcumin to acryloyl chloride ratios. All the data reported in the current figure is for n = 1. ....	60
<b>Figure 3.13:</b> Thermogravimetric analysis (TGA) for curcumin and CMA synthesized with different curcumin:acryloyl chloride ratios. ....	61
<b>Figure 4.1:</b> Chemical structure of curcumin [A] and acrylate-functionalized curcumin (diacrylate form) [B]. R <sub>1</sub> and R <sub>2</sub> can be either H or OCH <sub>3</sub> . ....	80
<b>Figure 4.2:</b> Simplified schematic for synthesis of PAβAE hydrogels. ....	81
<b>Figure 4.3:</b> HPLC comparison plot for curcumin and curcumin multiacrylate at 420 nm. ....	82
<b>Figure 4.4:</b> Swelling ratio in ACN for CMA:PEG400DA PCβAE hydrogels.....	83

<b>Figure 4.5:</b> PC $\beta$ AE degradation in PBS at 37°C. (a) Swelling ratio vs. time for PC $\beta$ AE degradation. Inset table shows the total degradation time for each film. (b) Initial swelling ratio for CMA:PEG400DA PC $\beta$ AE hydrogels. ....	84
<b>Figure 4.6:</b> Dynamic mechanical properties of PCBAE films synthesized using different CMA:PEG400DA molar ratios. (a) Storage modulus (Pa) vs. temperature (°C) at 1 Hz. (b) Tan $\delta$ vs. temperature (°C) at 1 Hz. ....	86
<b>Figure 4.7:</b> Time-temperature superposition results for 0:100 and 50:50 CMA:PEG 400DA. Solid curves are KWW best-fits. 50:50 result is shifted downward by one decade for clarity (re: right axis).....	88
<b>Figure 4.8:</b> Dielectric response for 50:50 CMA:PEG400DA network. (a) Dielectric constant ( $\epsilon'$ ) vs. temperature (°C); frequencies from 1 Hz to 1.3 MHz. (b) Dielectric loss ( $\epsilon''$ ) vs. temperature (°C); frequencies from 1 Hz to 1.3 MHz. Inset plot shows sub-glass transitions for 1, 11, and 110 Hz.....	89
<b>Figure 4.9:</b> Dielectric loss ( $\epsilon''$ ) vs. frequency (Hz) in the vicinity of the glass transition for 50:50 CMA:PEG400DA; temperatures from 15°C to 65°C at 5°C intervals. Data are corrected for conduction according to equation 3. Solid curves are HN fits.....	91
<b>Figure 4.10:</b> Dielectric loss ( $\epsilon''$ ) vs. frequency (Hz) for 50:50 CMA:PEG400DA sub-glass transitions; temperatures from -95°C to -45°C at 5°C intervals. Solid curves are HN fits. ....	92
<b>Figure 4.11:</b> Arrhenius plot of $f_{MAX}$ (Hz) vs. 1000/T (K) for PC $\beta$ AE hydrogels with different CMA:PEG400DA molar ratios.....	93
<b>Figure 4.12:</b> Dielectric loss ( $\epsilon''$ ) vs. frequency (Hz) at -60°C for PC $\beta$ AE hydrogels with different CMA:PEG400DA molar ratios. Solid curves are HN fits. ....	94
<b>Figure 5.1:</b> Chemical structures of (a) curcumin, (b) curcumin multiacrylate (CMA), (c) 4,7,10-Trioxatridecane-1,13-diamine (TTD), (d) 2,2'(ethylenedioxy) bis ethylamine (EDBE), (e) Hexamethylene diamine (HMD), (f) Diacrylate monomer. n = 13 for poly(ethylene glycol)576 diacrylate (PEG576DA), n = 9 for poly(ethylene glycol) 400 diacrylate (PEG400DA), and n = 2 for diethylene glycol diacrylate (DEGDA). R <sub>1</sub> and R <sub>2</sub> can be H or -OCH <sub>3</sub> and R <sub>3</sub> , R <sub>4</sub> and R <sub>5</sub> can be -OH or an acrylate group. ....	113

<b>Figure 5.2:</b> Dynamic mechanical properties of PCBAE films synthesized using different amines for 0:100 CMA:PEG400DA gel. (a) Storage modulus vs. Temperature (°C) at 1 Hz; (b) Tan $\delta$ vs. Temperature (°C) at 1 Hz. ....	114
<b>Figure 5.3:</b> Swelling ratio for 0:100 CMA:PEG400DA films with different amine crosslinkers during degradation in PBS (0.1 % SDS).....	116
<b>Figure 5.4:</b> Dynamic mechanical properties for PCBAE films of different diacrylates for 0:100 gel. (a) Storage modulus vs. Temperature (°C) at 1 Hz; (b) Tan $\delta$ vs. Temperature (°C) at 1 Hz. ....	117
<b>Figure 5.5:</b> Swelling ratio for 0:100 CMA:PEGDA films made with TTD using different commercial diacrylates during degradation in PBS (0.1 % SDS). ....	119
<b>Figure 5.6:</b> Weight loss during the washing of hydrogels as a function of RTAA for 50:50, 70:30 and 90:10 CMA:PEG400DA films.....	120
<b>Figure 5.7:</b> Dynamic mechanical properties for 50:50 CMA:PEG400DA films made with TTD for different RTAA. (a) Storage modulus vs. Temperature (°C) at 1 Hz; (b) Tan $\delta$ vs. Temperature (°C) at 1 Hz.....	121
<b>Figure 5.8:</b> Degradation in PBS (0.1 % SDS) for 50:50 CMA:PEG400DA films made with TTD for different RTAA. (a) Swelling ratio as a function of degradation time; (b) Curcumin release profile measured using absorbance @ 420 nm; (c) Antioxidant capacity of supernatants measured using TEAC in-vitro antioxidant capacity measurement assay. ....	123
<b>Figure 5.9:</b> Dynamic mechanical properties for 90:10 CMA:PEG400DA films made with TTD for different RTAA. (a) Storage modulus vs. Temperature (°C) at 1 Hz; (b) Tan $\delta$ vs. Temperature (°C) at 1 Hz.....	126
<b>Figure 5.10:</b> Degradation in PBS (0.1 % SDS) for 90:10 CMA:PEG400DA films made with TTD for different RTAA. (a) Swelling ratio as a function of degradation time; (b) Curcumin release profile measured using absorbance @ 420 nm. ....	128
<b>Figure 5.11:</b> Dynamic mechanical properties of different CMA:PEG400DA composition made with EDDBE crosslinker. (a) Storage modulus vs. Temperature (°C) at 1 Hz; (b) Tan $\delta$ vs. Temperature (°C) at 1 Hz. ....	130
<b>Figure 5.12:</b> Degradation in PBS (0.1 % SDS) for different CMA:PEG400DA films made with EDDBE crosslinker. (a) Swelling ratio as a function of degradation time; (b) Curcumin	

release profile measured using absorbance @ 420 nm; (c) Antioxidant capacity of supernatants measured using TEAC in-vitro antioxidant capacity measurement assay.	132
<b>Figure 5.13:</b> Dynamic mechanical properties for PCBAE films of different CMA:PEG 400DA composition made with HMD crosslinker. (a) Storage modulus vs. Temperature (°C) at 1 Hz; (b) Tan $\delta$ vs. Temperature (°C) at 1 Hz.....	135
<b>Figure 5.14:</b> Degradation in PBS (0.1 % SDS) for different CMA:PEG400DA films made with HMD crosslinker. (a) Swelling ratio as a function of degradation time; (b) Curcumin release profile measured using absorbance @ 420 nm; (c) Antioxidant capacity of supernatants measured using TEAC in-vitro antioxidant capacity measurement assay.	137
<b>Figure 6.1:</b> Particle size distribution for 90:10 CMA:PEG400DA PCBAE microparticles analyzed using Shimadzu SALD-7101 nano particle size analyzer. ....	158
<b>Figure 6.2:</b> Curcumin release profiles for 90:10 CMA:PEG400DA PCBAE hydrogel film and tablets containing PCBAE microparticles (i.e. prodrug tablet) and free curcumin powder, respectively, in PBS (0.1 % SDS) at 37°C using USP apparatus II. Inset plot shows curcumin release for prodrug tablet vs 90:10 CMA:PEG400DA microparticles. ....	159
<b>Figure 6.3:</b> HPLC peak elution profile (420 nm) for supernatant samples collected during aqueous dissolution of the PCBAE prodrug tablet. ....	160
<b>Figure 6.4:</b> PCBAE tablets after 1week storage. (i) unexposed tablet; (ii) tablet from standard storage conditions i.e., 25°C and 57% RH; (iii) tablet from accelerated storage conditions i.e., 40°C and 75% RH. ....	161
<b>Figure 6.5:</b> Prodrug (PCBAE) tablet moisture absorption as a function of storage time for standard and accelerated storage conditions. ....	162
<b>Figure 6.6:</b> Curcumin release profiles from dissolution of PCBAE prodrug tablets stored at (a) standard conditions of 25°C & RH = 57%; (b) accelerated conditions of 40°C & RH = 75%. ....	163
<b>Figure 6.7:</b> HPLC analysis of the final degradation supernatants collected from the dissolution of PCBAE prodrug tablets stored at standard and accelerated conditions. ..	165
<b>Figure 6.8:</b> Curcumin release profiles for PCBAE prodrug tablets stored at accelerated conditions for 4 weeks. Crushed tablet compared with non-crushed tablet. ....	166
<b>Figure 6.9:</b> Curcumin release profiles for PCBAE prodrug tablets stored at 25°C and 40°C for 2 weeks in the absence of surrounding moisture.....	167

**Figure 6.10:** Curcumin release profiles in PBS for 90:10 CMA:PEG400DA PCBAE hydrogel films as-prepared at ambient conditions, and stored at 40°C for 2 weeks in the absence of moisture (i.e. RH = 0%)..... 168

**Figure 6.11:** Antioxidant capacity of tablet dissolution supernatants measured for all storage times at standard conditions using TEAC in-vitro antioxidant measurement assay. (a) Standard conditions of 25°C & RH = 57%; (b) Accelerated conditions of 40°C & RH = 75%..... 169

## Chapter 1: Introduction and background

### 1.0 Introduction

Oxidative stress (OS), which is characterized by an imbalance between reactive oxygen species and antioxidant defenses, occurs in a wide variety of cardiovascular, neurological and inflammatory diseases. As such, controlling OS through addition of antioxidants should be able to control these diseases. A range of antioxidant enzymes (AOEs) and small molecule antioxidants have been explored to achieve this goal. Each system has its benefits and limitations, with AOEs being able to scavenge millions of copies of a specific oxidant, while small molecule antioxidants are capable of scavenging a wide variety of oxidants, although limited to stoichiometric proportions. While these antioxidants have been able to control OS *in vitro*, years of studies have failed in demonstrating benefit in controlling OS in clinical trials for the treatment of disease conditions mentioned above. This has been due to lower bioavailability and rapid excretion of antioxidants from the body and also their lower stability rendering them inactive before reaching the OS site. In this work, we propose to overcome these challenges through development of polymeric prodrug of polyphenolic antioxidant i.e., poly(antioxidant  $\beta$ -amino esters) (PABAE). PABAE can provide antioxidant release over a wide range of time, while improving the bioavailability and stability of an antioxidant. An additional advantage with PABAE is it opens up new possibilities of controlling biomaterial biocompatibility, which is also OS dependent. One of the way to achieve this is through casting a PABAE layer on the bioimplants, which can reduce the OS caused by bioimplant and thereby improve the biocompatibility.

Among small molecule antioxidants, polyphenols have been studied extensively due to their promising antioxidant activities. Curcumin is a poly-phenol which has high antioxidant activity as well as anti-inflammatory and anti-angiogenic properties, and has received a GRAS (Generally Recognized As Safe) status from the United States Food and Drug Administration. However, curcumin has limited aqueous solubility and undergoes degradation when exposed to UV light. Approaches used for curcumin delivery have focused on developing a dispersion of polyphenols in aqueous phase through entrapment of curcumin in polymer nanoparticles, polymeric micelles, liposomes or molecules such as cyclodextrin. Unfortunately, these approaches accommodate only low levels of drug loading and don't actively improve the solubility of curcumin when released in the body.

In this work, we have developed a polymeric pro-drug containing curcumin, i.e., poly(curcumin  $\beta$ -amino ester) (PCBAE) for drug-delivery and biomedical applications. The PCBAE undergoes hydrolytic degradation to release the original form of curcumin. PCBAE hydrogels were synthesized through a Michael-addition type reaction, which allows the synthesis of PCBAE without the use of free radical polymerization. Being a pro-drug system, it protects the labile groups on the curcumin molecule. The solubility of curcumin is improved due to the amorphous nature of PCBAE, and the release of degradation products that help to solubilize the curcumin.

Curcumin was functionalized with acrylate groups as a monomeric precursor to PCBAE. Curcumin multiacrylate (CMA) was characterized using nuclear magnetic resonance (NMR) and liquid chromatography mass spectrometry (LCMS) to identify different acrylate species in CMA and to determine the extent of acrylation. Following this work, a systematic study of the effect of independent parameters such as ratio of total

acrylate to amine (RTAA), amine crosslinker, diacrylate monomer and CMA composition on the mechanical and functional properties of PCBAE is required. The rubbery modulus, glass transition temperature and degradation kinetics of the PCBAEs networks were investigated to guide the strategic design of these polymers for drug delivery and biomedical applications.

A background for developing controlled release formulations for curcumin is presented in this chapter. This includes discussion on oxidative stress generation pathways along with its role in pathology and biomaterial compatibility. Strategies to counter oxidative stress are presented with a focus on delivery of exogenous antioxidants. With this approach in mind, literature on different polymers (degradable as well as non-degradable) used for drug delivery and biomedical applications is presented followed by an emphasis on the antioxidant polymers, which have been explored to improve bioavailability of antioxidants.

## **1.1 Background**

### **1.1.1 Oxidative stress**

Cardiovascular diseases, cancer, chronic lower respiratory disease, neurodegenerative diseases and diabetes are among the leading causes of death in United States [1, 2]. In 2013 and 2014, about 1 in 4 deaths was caused by heart diseases, which include conditions such as atherosclerosis, heart attack, and rheumatic heart disease [1]. Cancer has a similar death rate (i.e., 1 in 4 deaths). One of the key pathophysiological features that is common among all of these conditions, as a cause or an effect, is oxidative stress (OS) [3-5]. OS is defined as the condition when reactive oxygen species are produced in excess compared to the antioxidant defense system in the body. As with most processes

in the body, an equilibrium is present between the generation of reactive oxygen species and consumption (e.g., through antioxidants) in healthy cells. A low concentration of oxygen species such as superoxide radical anion ( $O_2^{\cdot-}$ ), hydrogen peroxide ( $H_2O_2$ ), and hydroxyl radical ( $OH^{\cdot}$ ) is in fact needed for various biological processes in the body. However, when this equilibrium is disturbed due to endogenous or exogenous factors, causing an increase in reactive oxygen species, it leads to an oxidative stress state.

#### 1.1.1.1 ROS/RNS generation pathways

Classically, the oxidizing compounds produced in the living systems are classified either as reactive oxygen species (ROS) or reactive nitrogen species (RNS). ROS include radicals such as superoxide radical anion ( $O_2^{\cdot-}$ ), hydroxyl radical ( $OH^{\cdot}$ ), hydroperoxyl radical ( $HO_2^{\cdot}$ ), in addition to non-radical species such as hypochlorous acid (HOCl), hydrogen peroxide ( $H_2O_2$ ) and singlet oxygen; while RNS include nitrogen containing species such as nitric oxide ( $NO^{\cdot}$ ), and peroxynitrite ( $ONOO^-$ ). A low concentration of ROS/RNS is required for cell signaling, controlling cell proliferation and apoptosis, and activation of transcription factors such as necrosis factor  $\kappa$ B (NF- $\kappa$ B) [6-8]. **Table 1.1** shows the endogenous sources of ROS/RNS. A major endogenous source of superoxide anion are mitochondria [9, 10]. Although the superoxide anion is not a strong oxidant by itself, it leads to the formation of strong oxidant species, which can cause oxidative damage, through a series of reactions which is presented in **Figure 1.1** [9].

External environmental factors such as atmospheric pollution, tobacco smoke, as well as ionizing radiation including ultraviolet (UV) radiation, X-ray radiation and gamma ray radiation can also induce the generation of excess ROS/RNS [11-13]. ROS/RNS are generated as a response to pollutants such as polychlorinated biphenyls, automotive

exhaust, and airborne particulates including metal nanoparticles (e.g., silver, ferric oxide or copper oxide nanoparticles) [14-17]. Metal oxide nanoparticles are used as catalysts in many industries, which leads to an increase in their concentration in the ambient air and has been shown to be correlated with the occurrence of pulmonary diseases [14, 18, 19].

Oxidative species are also generated when the body recognizes a bioimplant as a foreign entity, which leads to an immune system response directing macrophages to the bioimplant site; these macrophages generate oxidative species to neutralize the foreign entity [15]. This mechanism is also present in the response of infectious agents through phagocytosis [20]. Additionally, cyclic stretching of cells has been shown to cause the generation of superoxide anion and nitric oxide in mechanical ventilator induced lung injury [21-23].

### **1.1.2 Role of OS in pathology**

OS plays a vital role in the pathology of various diseases as it can cause indiscriminate damage to cellular components including lipids, proteins and DNA, ultimately leading to cellular apoptosis and tissue damage [20]. OS also leads to neuronal cell death, an important step in neurodegenerative diseases such as Parkinson's disease, Alzheimer's disease, and also in traumatic brain injury [24]. Changes in the cell signaling caused by OS is seen in many cancer cells [11]. OS caused by cigarette smoking has been implicated in the pathogenesis of chronic obstructive pulmonary disease [12]. OS is also a result of conditions such as ischemia-reperfusion injury, where reperfusion of oxygen in the oxygen deprived tissues leads to OS [25, 26]. The role of OS in ulcerative colitis (UC) has been shown, where increased levels of lipid peroxidation, SOD, catalase and decreased levels of glutathione were observed for patients with UC [27].

### 1.1.2.1 Lipid peroxidation

Lipid peroxidation occurs as a result of oxidative stress damage. Peroxidation of lipids such as polyunsaturated fats (PUFAs) involves attack of ROS on carbon-carbon double bond leading to the formation of lipid peroxides [28, 29]. The lipid peroxidation usually proceeds through three steps seen with a typical radical mediated reaction: initiation, propagation and termination [28]. The reaction steps are shown in **Figure 1.2** [29]. ROS attack on lipid leads to the formation of lipid radical (L<sup>•</sup>), which can react with oxygen to form lipid peroxide radical. Lipid peroxide radical can react with another lipid to form lipid radical and propagate the reaction. The termination reaction involves quenching of radicals through antioxidants to form non radical products [28]. Lipid peroxidation leads to the formation of products such as malonaldehyde (MDA), 4-hydroxynonenal (HNE), alkanes, isoprostanes, and cholesteroloxides [30]. Formation of MDA follows a multiple step mechanism starting with the peroxidation of poly(unsaturated fatty acids) (PUFAs) as shown in **Figure 1.3** [28, 31]. MDA and HNE are known to be toxic, while MDA is also known to be carcinogenic in rats [11, 32]. MDA is mainly formed through oxidative degradation of poly(unsaturated fatty acids) (PUFAs) such as arachidonic acid and docosahexaenoic acid [31]. MDA and HNE can also form adducts with DNA and proteins, which can affect their activity and lead to more systemic damage [30]. Isoprostanes are stable compounds which make them good markers of oxidative stress [33]. The brain has a high concentration of fatty acids making it more susceptible to lipid peroxidation, which plays role in neurodegenerative diseases [20, 34, 35].

### **1.1.2.2 Protein oxidation**

Protein oxidation leads to the formation of functional groups such as hydroxyls and carbonyls on the proteins [30]. Bityrosine, L-DOPA, and ortho-tyrosine are other products that are formed as a result of protein oxidation, and are used commonly, along with protein carbonyls, as biomarkers for the protein damage due to oxidative stress [30]. Protein carbonyls have been found to be present at much higher levels in various neurodegenerative and cardiovascular diseases as well as during aging and in premature aging diseases such as Werner's syndrome [36-39]. Proteins with oxidative damage become functionally inactive and are degraded to a greater extent compared to non-oxidized proteins [39, 40]. The oxidized proteins, at low concentrations, can be generally eliminated from the cell environment through a proteolytic process. However, excess production of oxidized proteins can eventually lead to accumulation of oxidized proteins in the cell [40]. Since most of the enzymes are proteins, protein oxidative damage has a much higher impact than stoichiometric proportion on the health of a cell [36, 39]. The oxidized proteins play a vital role in aging and pathologies such as diabetes, atherosclerosis and neurological disorders [40].

### **1.1.2.3 Oxidative DNA damage**

The attack of ROS on DNA can cause pyrimidine and purine base changes or single or double strand breaks [30, 41]; both nuclear and mitochondrial DNA are damaged by ROS. Mitochondrial DNA can suffer higher oxidative damage than nuclear DNA as it does not contain the histones needed for DNA repair [9, 42]. This lower ability of mitochondrial DNA to self-repair following an oxidative attack has been linked to the aging [9]. In addition to this, accumulation of oxidized DNA, proteins, and lipids is known to be

correlated to the aging [43]. Hydroxyl radicals can react with DNA to form DNA adducts such as 8-hydroxyguanine (8-OH-G) also known as 8-oxoguanine. 8-OH-G is a commonly used biomarker for DNA oxidation measurement [41]. DNA damage is a major factor in carcinogenesis as well as neurodegenerative disorders such as Parkinson's disease and Alzheimer's disease [44-46]. Oxidative stress also plays a role in causing and proliferating cancer as tumorous cells favor ROS rich regions [11, 47]. Additionally, 8-OH-G produced as a result of DNA damage has been shown to correlate directly to the size of tumors [48]. An increase in damaged DNA has been observed in the brain for neurological diseases [41], DNA damage is also encountered in diabetic conditions. Exposure of high glucose levels (i.e. hyperglycemia) to microvascular endothelial cells (MVEC) and human umbilical vein endothelial cells (HUVEC) has been reported to lead to an increase in 8-oxoguanine levels caused by increased ROS [41, 49].

### **1.1.3 Role of OS in biomaterial compatibility**

Apart from OS damage, another application where role of OS is key is biomaterial compatibility. The utility of biomaterials has grown extensively over time to include classical orthopedic implants as well as ventilators, biosensors, drug delivery implants, and cosmetic implants [50-52]. Apart from the functionality of the biomaterial to perform its intended purpose, another factor that is equally important is the body's response to the biomaterial i.e., biomaterial compatibility. Biomaterial compatibility is affected by inflammation caused by the immune system response to the biomaterial [53]. When the body recognizes a biomaterial as a foreign object, the biomaterial can experience a chronic phagocytic attack from the immune system leading to macrophages releasing ROS/RNS with the intended goal of eliminating the biomaterial from the body [54, 55]. This OS

signaling can lead to a chronic inflammatory state at the biomaterial site. As such, OS and the inflammatory response to the biomaterial are intricately related [53].

Inflammation is also orchestrated as a part of the body's healing response to an injury caused by a bioimplant [56, 57]. The role of inflammation in the healing response to injury is to remove the germs from the affected site to prevent further damage [58]. However, the surgical wounds, which occur in a sterile environment, differ from traumatic injury, consequently the reduction of the inflammation stage through the control of OS can expedite the wound healing response to bioimplants [59]. Additionally, the functioning of bioimplants such as drug depot can be severely affected due to inflammatory response related fibrous formation around the implant [56, 60]. The fibrous formation can reduce the drug release, and create an additional physical barrier for drug delivery that in the worst case renders the device completely ineffective.

Not surprisingly, biomaterial compatibility is also vital for the success of orthopedic implants. For instance, titanium alloys, which are widely used in orthopedic implants, can fail due to corrosion processes [61]. Metal ions produced during corrosion or through any other process have been known to affect the redox status of cells [32, 62]. In a study on titanium alloy (Ti6Al4V), a simulated corrosive environment showed reduction in the glutathione levels and produced an OS state leading to a chronic inflammation [61, 63]. ROS generation has also been shown to occur in alveolar cells due to mechanical stretch and ventilation, leading to an increase in epithelial permeability, which is one of the characteristics of ventilator-induced lung injury [21]. In another study on bioimplants, Sanchez et al. studied the role of soft-tissue dermal fillers such as calcium hydroxylapatite, acrylamides and silicone present in dermal bioimplants in orchestrating OS, where they

found evidence of oxidative damage and an increase in myeloperoxidase concentration [15].

Biomaterials in the form of nanoparticles have been widely researched for drug delivery and tissue culture applications due their ability to cross physiological barriers such as blood-brain barriers or intestinal epithelium, and for their tendency to be internalized to a greater extent by cells [64]. However, there have also been studies showing that nanoparticles can induce OS through an immune response [65]. Apart from the chemical properties of the biomaterial, surface characteristics such as surface charge, surface morphology, and hydrophobicity can also induce an immune response [66-68]. For instance, a study on gold nanoparticles demonstrated an increase cytokine gene expression with an increase in hydrophobicity of nanoparticles [66].

#### **1.1.4 Strategies to counter OS**

Oxidative stress can be relieved by reducing the concentration of oxidants, which can be achieved through decrease in the exposure to environmental factors or reduction in the *in vivo* ROS production [6]. ROS can be actively intercepted from damaging the biomolecules in the body through targeted delivery of antioxidants. Environmental factors can be eliminated by avoiding exposure to UV light, tobacco smoke and ambient pollution. To decrease the excess ROS/RNS generated due to disease state or from the immune response to a biomaterial, targeted delivery of antioxidants at the desired site is required. Two types of antioxidants are present in the body, viz., small molecule antioxidants and large molecule enzyme antioxidants. Small molecule antioxidants include compounds such as curcumin, quercetin, trolox, glutathione (GSH), thioredoxin, lipoic acid, N-acetyl cysteine, ascorbic acid (vitamin C), alpha-tocopherol (vitamin E) gallic acid, and apigenin,

while antioxidant enzymes include catalase, superoxide dismutase (SOD), glutathione peroxidase, glutathione reductase and peroxiredoxins [6, 64, 69]. Each of these have a specific advantage in radical scavenging. Small molecule antioxidants can alleviate the oxidative stress through ROS scavenging as well as by chelation with ROS forming transition metals [32]. Small molecule antioxidants can scavenge various types of oxidative species, but they are consumed in the process, which necessitates a drug delivery system that provides a sustained release of antioxidants. Alternatively, antioxidant enzymes can scavenge millions of copies of radicals before becoming deactivated. However, they are very specific, which means that each enzyme can scavenge only a certain type of radical. In addition, antioxidant enzymes face stability challenges, which require additional storage and handling considerations, and which preclude oral administration

#### **1.1.5 Measurement of antioxidant activity**

The antioxidant activity is usually measured for: 1) the selection of antioxidant to be used in the treatment of oxidative stress, and 2) to monitor the endogenous antioxidant levels. Antioxidant activity assays are classified as hydrogen atom transfer (HAT) assays and electron transfer assays [70]. HAT assays include assays such as oxygen radical absorbance capacity (ORAC) and total radical-trapping potential (TRAP). Electron transfer assays include assays such as cupric ion reducing antioxidant assay (CUPRAC), ferric reducing/antioxidant power (FRAP), and trolox equivalent antioxidant capacity (TEAC). ORAC and TRAP can be used for hydrophilic as well as lipophilic antioxidants [71]. ORAC and TRAP involve use of a substrate, which brings a variable factor (i.e. the substrate's reactivity with peroxy radicals) into the picture [70].

Electron transfer assays are colorimetric assays, which correlate change in absorbance with antioxidant activity. The advantages with these assays over HAT assays is that they don't use any competing substrates. For instance, the CUPRAC assay involves reduction of Cu(II) to Cu(I) in the presence of an antioxidant; (re: **Figure 1.4**). Bathocuprione, a chromogenic agent, forms a chelating complex with Cu(II). The absorbance of the solution containing this complex increases when Cu(II) is reduced to Cu(I) by an antioxidant [70, 72]. The FRAP assay involves a similar response where reduction of Fe(III) to Fe(II) takes place in the presence of antioxidant. FRAP uses ferric salt, Fe(III)(2,4,6-tripyridyl-s-triazine)<sub>2</sub>Cl<sub>3</sub> as an electron donating species [70]. FRAP has a limitation in that it cannot be used for antioxidants such as glutathione and ascorbic acid [73]. Another electron transfer assay which is based on colorimetric response is the TEAC assay. It uses 2,2'-azinobis-(3-ethylbenzothiazoline-6-sulfonate) (ABTS) to create a cation radical solution, which is prepared by reacting ABTS and potassium persulfate. TEAC assay is used for measuring the antioxidant capacity of water soluble systems. It is a simple colorimetric assay, which is widely used due to its robustness, operational simplicity and linear response to antioxidant concentration [70].

### **1.1.6 Polymers for drug delivery**

Polymers have been used as excipients in pharmaceutical formulations for many years. Furthermore, their application as drug delivery vehicles has also gained importance over last several decades and as such they play a vital role in the development of novel drug delivery systems. Polymers are used for controlled release, sometimes called modified release, as well as for targeted delivery of drugs. For instance, enteric coating polymers such as Eudragit® (a poly(methacrylate) based polymer) are used in tablet formulations

for protecting drugs which display loss of activity under the low pH environment of the stomach or for delivery of drugs to the lower gastrointestinal tract (GI). Additionally, crosslinked polymer hydrogel networks, as well as linear polymers, have been widely used for developing novel drug delivery systems to overcome the challenges associated with bioavailability and drug distribution in the body.

Apart from drug delivery in humans, controlled release also has applications in veterinary drug delivery, in agriculture for the controlled release of fertilizers and pesticides, and in the packaging industry. For instance, controlled antioxidant release packaging films have been prepared with low density polyethylene (LDPE), polypropylene and poly(vinyl alcohol) (PVA) for lipid oxidation inhibition [74].

The selection of polymer for the development of drug delivery vehicles is dependent on the specific requirements of the drug delivery approach to be used. Apart from functional properties, one factor that is vital in pharmaceutical and biomedical applications is that the polymer and its degradation products should be non-toxic, non-carcinogenic and non-thrombogenic. Hydrophilicity of the drug is another factor that dictates specific polymers to be used for drug-delivery. Controlled release of drugs is necessary for both hydrophilic and hydrophobic drugs. For instance, a controlled release is required for hydrophilic drugs to avoid rapid dissolution and excretion from the body. Also, a high level of drug can move the drug concentration out of therapeutic window and into the toxic range, which can have an adverse effect on the subject. For a hydrophobic drug, a controlled release is desired to slow introduction of the drug, thereby avoiding potential precipitation due to low solubility, followed by rapid excretion of the drug. A targeted delivery ensures that the desired site receives a therapeutic quantity of drug, while avoiding

systemic side effects on other regions. A targeted delivery is also desired for lowering the overall dose administered to patients [64].

Polymers used for drug delivery can be generally classified as non-degradable and degradable polymers. Even though degradable polymers are typically preferred due to its inherent advantages, non-degradable polymers have also been used in numerous applications. These are discussed in the following sections. Polymers can undergo degradation through hydrolysis, oxidation or through exposure to radiation. The classification of polymers as non-degradable sometimes depends on the timescale of degradation as compared to the time the polymer is used in the application [75].

#### **1.1.6.1 Non-degradable polymers**

Non-degrading polymers have been used as orthopedic implants or implant supports, and also as drug delivery vehicles. These polymers when used as drug delivery vehicles usually follow a diffusion-based drug release mechanism. Once drug release is complete, the drug delivery vehicle can be excreted (e.g. drug delivery particles) or removed via surgery (i.e. implants) [76]. A schematic for drug release from non-degrading polymer is shown in **Figure 1.5**, where drug diffuses out of the polymer matrix as the matrix undergoes swelling. Apart from this, non-degradable polymers are also important as catheters, syringes, dialysis tubing or vascular grafts in the field of medicine [77].

The degradation characteristics of polymers are dependent on the nature of the chemical bonds present in the polymer chain. Non-degrading polymers usually undergo minimal or no degradation. In general, polymers can offer a high mechanical strength, as well as an ease of processing, without an increase in weight that is typically associated with the use of metal implants. A good overview of non-degrading polymers in medicine is

presented by Shastri, who highlights numerous non-degradable polymers based technologies that have been commercialized [77]. These applications incorporate synthetic polymers such as high density poly(ethylene) (HDPE), poly(propylene) (PP), poly(tetra fluoroethylene) (PTFE or Teflon), poly(ethylene terephthalate) (PET), poly(methyl methacrylate) (PMMA), poly(dimethyl siloxane) (PDMS), poly(ethylene vinyl acetate) (PEVA), and poly(ethylene glycol) (PEG) [77]. HDPE exhibits excellent mechanical and structural properties, due to which it has been used for hip and knee replacement [77, 78]. PP, owing to its fiber forming properties, has been used to make meshes for prosthetics as well as for periodontal drug delivery systems [79, 80]. The extruded form of PTFE (e-PTFE) has good oxygen permeability to oxygen due to the pores developed in the extrusion process [77]. In addition to its good permeability, its inert character is advantageous for making meshes used as surgical barriers and for vascular grafts [77, 81, 82]. Similarly, PET has also been used to make vascular grafts [83]. PMMA is used as bone cement in surgeries involving artificial joints, and also as a bone substitute in cranioplasty [77, 84-86]. PDMS and PEVA have been used for drug delivery [77, 87, 88] and PDMS in the form of silicone gels is also widely used in plastic surgeries. PEG coatings have been used to improve the circulation of drug delivery vehicles. PEG based hydrogels have been explored for contact lenses, drug delivery and tissue engineering scaffolds. This material platform will be discussed in detail in the section on hydrogels.

#### **1.1.6.2 Degradable polymers**

All polymers undergo thermal degradation when exposed to high temperatures. However, when polymers are specifically classified as degradable polymers, the classification is based on degradation through biological means or through exposure to

light. Polymers degrading in a biological setting are classified as biodegradable polymers and polymers degrading through light exposure are classified as photodegradable polymers. These polymers have been used in applications such as drug delivery vehicles or depots, wound dressings, surgical sutures and surgical implants [76]. Apart from this, biodegradable polymers are very important in packaging applications to mitigate the environmental impact of the non-degradable polymers used in packaging.

Biodegradable polymers are especially advantageous for drug delivery and biomedical applications as no removal surgery is required. A strictly diffusion based release obtained with non-degradable polymers is not viable for large molecules such as proteins and polypeptides that exhibit inherently low diffusion rates and thus necessitate the use of degradable polymers [76, 89]. Biodegradable polymers usually contain labile groups such as esters, or anhydrides that can undergo hydrolysis [90]. Biodegradable polymers can be broadly classified based on the mode of degradation as either enzymatically degradable or hydrolytically degradable polymers. Enzymatically degradable polymers include poly(amino acids), fibrin, and polysaccharides [91]. Hyaluronic acid is one such polysaccharide which has been gaining significant interest for drug delivery and tissue culture applications [92]. Hydrolytically degradable polymers that have been used for drug delivery include polyesters, polyanhydrides, poly(orthoesters), poly(phosphoesters), poly(ester amides) and poly(phosphazenes) [91, 93, 94]. Natural degradable polymers such as polysaccharides have been explored as an enteric coating for oral formulations [95]. Polyesters such as poly(glycolic acid) (PGA), poly(lactic acid) (PLA), poly(lactic-co-glycolic acid) (PLGA), and polycaprolactone (PCL) have been

widely investigated for biomedical applications such as sutures, clips, bone pins and plates [76, 91, 96, 97].

The terms erosion and degradation are sometimes used interchangeably in the literature when discussing degradable polymers. For the current work, the term erosion will be used to describe the physical loss of material from the polymer, while the term degradation will be used for chemical degradation of the polymer through chemical cleavage of bonds. Polymers can undergo either surface erosion or bulk erosion. These two modes are discussed in detail in the following sections.

#### **1.6.1.2.1 Surface eroding polymers**

Surface eroding polymers involve erosion of material from the surface of the polymer either through a dissolution of polymer or through removal of degradation products formed from the chemical degradation of a polymer. The rate of water intake for these polymers is much slower than the rate of degradation of the polymer leading to a higher degradation at the surface [98]. These polymers typically maintain their geometric shape while the overall size decreases as the polymer degrades [75]. For drug delivery applications, the drug molecule is physically entrapped or encapsulated in the polymer matrix and is released as the polymer erodes. The advantage with these polymers is that zero order release can be obtained since the release is proportional to the rate of polymer erosion [75]. Poly(anhydrides) and poly(ortho esters) are widely studied degradable polymers that undergo surface erosion [99]. Poly(sebacic acid) (PSA), poly(1,3-bis(p-carboxyphenoxy) propane-co-isophthalic acid) (PCPP-IPA), and poly(1,3-bis(p-carboxyphenoxy) propane-co-sebacic acid) (PCPP-SA) are few examples of polyanhydrides used for drug delivery [100]. Other surface eroding polymer systems such

as cellulose acetate phthalate complexed with pluronic F-127, have been used for sequential release of multiple drugs [101, 102].

#### **1.6.1.2.2 Bulk eroding polymers**

Bulk eroding polymers undergo weight loss homogeneously throughout the polymer sample instead of just on the surface. The rate of water intake for these polymers is much higher than the rate of degradation of polymer leading to hydrolysis or degradation throughout the polymer matrix [98]. As the polymer matrix breaks down, the diffusivity of the drug changes with both position and time, requiring complex mathematical models to predict the drug release [99, 103]. The bulk degradation of polymers follows four overlapping steps shown in **Figure 1.6** [103]. Polyesters such as PLA, PGA, PLGA, and poly( $\beta$ -amino esters) (PBAE), which have been widely used in the pharmaceutical and biomedical fields are known to undergo bulk degradation [99].

#### **1.1.7 Hydrogels**

Hydrogels are crosslinked polymer networks which have been widely explored as drug delivery vehicles and as a scaffold for tissue engineering applications. The popularity of hydrogels has been partly due to their ability to have a high water intake uptake properties that enhance their compatibility in the body. In addition to this, hydrogels can be tuned across a wide range of functional characteristics such as degradation/drug release time, mechanical properties, thermal properties, and surface properties. Furthermore, hydrogels can be tuned to be pH responsive, thermoresponsive as well as responsive to various biomarkers in the body. The literature on the synthesis and application of novel hydrogels has been growing continuously over the years. Numerous excellent review

articles highlight their use in bionanotechnology, biomedical applications, diagnostic devices, regenerative medicine, and drug delivery [104-107].

Hydrogels can be synthesized in various sizes and shapes from the bulk scale to the nanoscale. Bulk gels or films are used in wound healing or biomedical applications, while microscale or nanoscale hydrogels are commonly used in pharmaceutical formulations. Nanoparticles have garnered a lot of interest in drug delivery applications due to their ability to cross intestinal epithelium and the blood-brain barrier, in addition to being internalized by cells much more easily as compared to microparticles [64]. Apart from conventional spherical shape, hydrogels can be synthesized in different geometries such as circular or elliptical discs, rods, conical shape, toroidal shape, plug shape as well as vase shape [96, 108-113]. The particle shape has been known to affect the phagocytosis, which is undesirable in the context of drug delivery [109]. Particle shape has also been shown to affect degradation properties and transport of particles in the body and across organs such as the spleen [96, 114].

Hydrogels can be formed through physical as well as chemical crosslinks. Physical crosslinks can be formed through ionic bonding, hydrogen bonding and even through molecular entanglements [106, 115-117]. For instance, hydrogels based on affinity of avidin and streptavidin with biotin polymers were developed for controlled release of curcumin [118]. Hydrogels based on chemical crosslinks have been synthesized through a multitude of reaction mechanisms. Free radical polymerization of monomers containing groups such as acrylate functional groups is one of the most commonly used methods for making chemically-crosslinked hydrogels that are non-degradable [119]. Free radical polymerization can be carried out through exposure of a radical generator (i.e. initiator)

and monomer solution to radiation. Free radical generating solutions such as mixtures of ammonium persulfate and tetramethylethylenediamine (TEMED) are used for hydrogel synthesis when radiation cannot be used.

Reaction methods which do not involve free radicals have also been developed for *in-situ* crosslinking at milder reaction conditions [107]. These involve reaction between monomers such as aldehyde and amine, aldehyde and hydrazine, acrylate and amine, and acrylate and thiols [107, 120]. Reaction between acrylate and amine, and acrylate and thiol follows Michael addition mechanism. The reaction between acrylate and amine leads to the formation of PBAE hydrogels. PBAE are a class of hydrogels which are efficient drug delivery vehicles and can be synthesized with relative ease [121, 122]. These are hydrolytically degradable polymers that can be tuned to achieve a wide range of degradation times.

Hydrogels based on PEG and PVA have been studied extensively for drug delivery and tissue engineering applications due to the low protein adsorption tendency of PEG and PVA which aides in the biocompatibility of these systems. Hydrogels used for controlled release of drugs can be degradable or non-degradable depending on the nature of the crosslinks present in the matrix. The drug release mechanism for non-degradable hydrogels is the same as shown in Figure 3. Bulk degrading hydrogels follow the steps shown in Figure 4, along with the release of entrapped drug molecules. In addition to the physical drug encapsulation, binding of the drug molecules to chains in the network is a technique which has been explored to provide a better control of the drug release [123]. Prodrug approaches, where the drug is a part of the hydrogel network and is released as the network undergoes degradation, have also been investigated [124].

### **1.1.8 Polymers for antioxidant delivery**

Antioxidant delivery is one of the approaches used for reducing oxidative stress. For the efficient introduction of antioxidants, controlled and targeted delivery is vital. Controlled release of antioxidants is important since antioxidants can also act as pro-oxidants depending on the dose [125]. Another key consideration in antioxidant therapy is stability, as antioxidants can easily react with oxygen and lose their activity. To overcome this challenge, different techniques have been developed which include entrapment or encapsulation of antioxidant in a polymer, encapsulation in another molecule such as cyclodextrin, and prodrug polymers containing antioxidant as a part of polymer matrix that release antioxidants upon degradation [69, 126]. These approaches are discussed in the sub-sections that follow.

#### **1.1.8.1 Antioxidant loaded polymer systems**

Antioxidant delivery via physical loading in a polymer matrix (i.e. encapsulation approach) has been explored for antioxidant enzymes (AOEs) as well as small molecule antioxidants to improve the targeting and stability of the antioxidants. The encapsulation approach is helpful for protection of AOEs during delivery, as AOEs can be inactivated through proteolytic processes [127]. For instance, encapsulation of catalase was demonstrated through the use of filamentous PEG-b-PLA diblock copolymers [128]. Biodegradable microspheres of PLGA and PLA were used for encapsulation of SOD and catalase, and controlled release of these AOEs was obtained [129]. PLGA based encapsulation has been used for small molecule antioxidants such as curcumin, quercetin and catechin [130, 131]. Hydrogels formed by self-assembling peptides were also used for the encapsulation and controlled release of curcumin [132]. Encapsulation of drugs in

hydrogels synthesized through free radical polymerization is widely explored, however this approach is not feasible for antioxidants due to the inherent radical scavenging property of antioxidants. Polymer syntheses based on the Michael addition reaction which can form polymers such as PBAE under mild conditions have been explored for antioxidant delivery [69, 133].

#### **1.1.8.2 Antioxidant embedded in the polymer chain**

The prodrug approach, in which antioxidants are covalently embedded directly in the polymer backbone, has been explored for small molecule antioxidants. Small molecule antioxidants which require large overall doses that can lead to an increase in local toxicity as well as lower bioavailability in the absence of a controlled release system. Controlled antioxidant release is desired for hydrophilic antioxidants such as vitamin C, trolox as well as for hydrophobic antioxidants such as curcumin, quercetin as each type can have low bioavailability due to rapid excretion and poor dissolution, respectively. Additionally, the prodrug approach can enhance drug loading and improve the stability of small molecule antioxidants through protection of labile groups. Hydrolytically degradable prodrug antioxidant systems have been studied for trolox, apigenin, curcumin and quercetin, and show a reduction in OS generated by copper oxide nanoparticles and iron oxide nanoparticles [124, 133, 134]. Polymeric prodrugs of vanillin and glutathione have also been studied for the controlled release and reduction of oxidative stress [135, 136].

**Table 1.1:** Endogenous sources of ROS/RNS.

<b>Source</b>	<b>ROS/RNS</b>	<b>References</b>
Mitochondrial respiration	Superoxide anion	[9, 10]
Nicotinamide Adenine Dinucleotide Phosphate oxidase (NADPH-oxidase), xanthine oxidase, cytochrome P450 metabolism	Superoxide anion	[6, 11, 137]
Neutrophils and macrophages during inflammation	Superoxide anion	[138]
Reaction of superoxide anion with superoxidase dismutase (Ref. Figure 1.1)	H <sub>2</sub> O <sub>2</sub>	[11]
Reaction of H <sub>2</sub> O <sub>2</sub> with transition metals (Ref. Figure 1.1)	Hydroxyl radical	[138]
Reaction of superoxide anion with nitric oxide (Ref. Figure 1.1)	Peroxynitrite	[125]

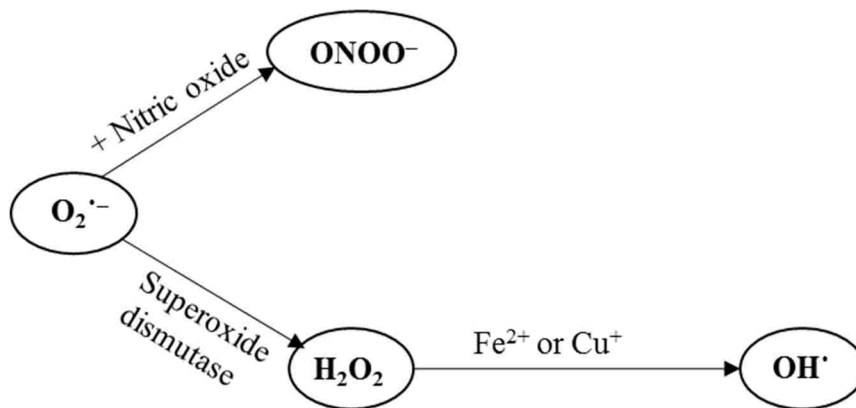


**Figure 1.1:** Formation of strong ROS/RNS from superoxide anion

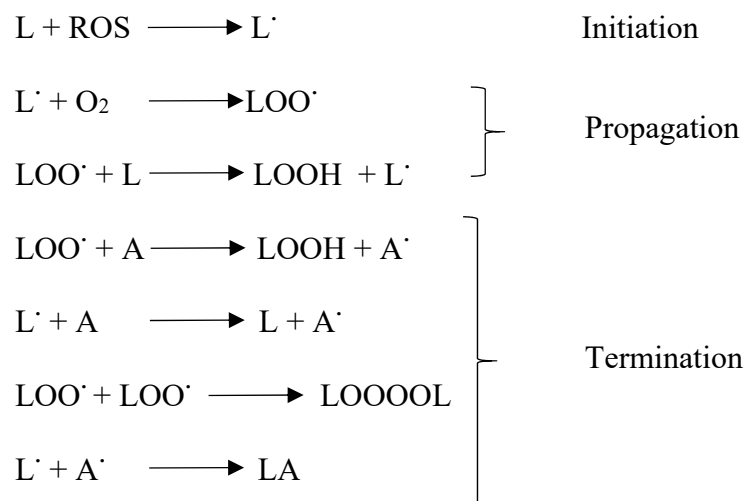


**Figure 1.2:** Mechanism of lipid peroxidation. L – lipid, A – antioxidant.

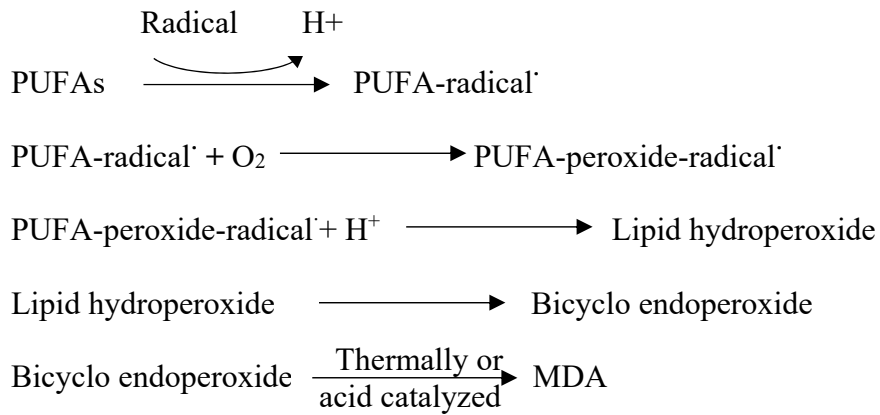


**Figure 1.3:** Mechanism for the formation of malonaldehyde (MDA), where PUFA is poly(unsaturated fatty acid).

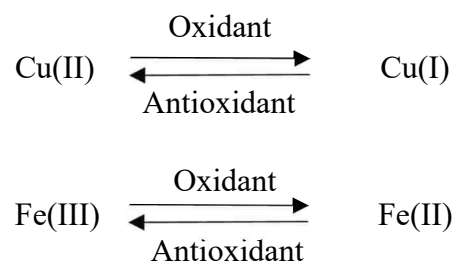


**Figure 1.4:** Reaction scheme in CUPRAC and FRAP assays.

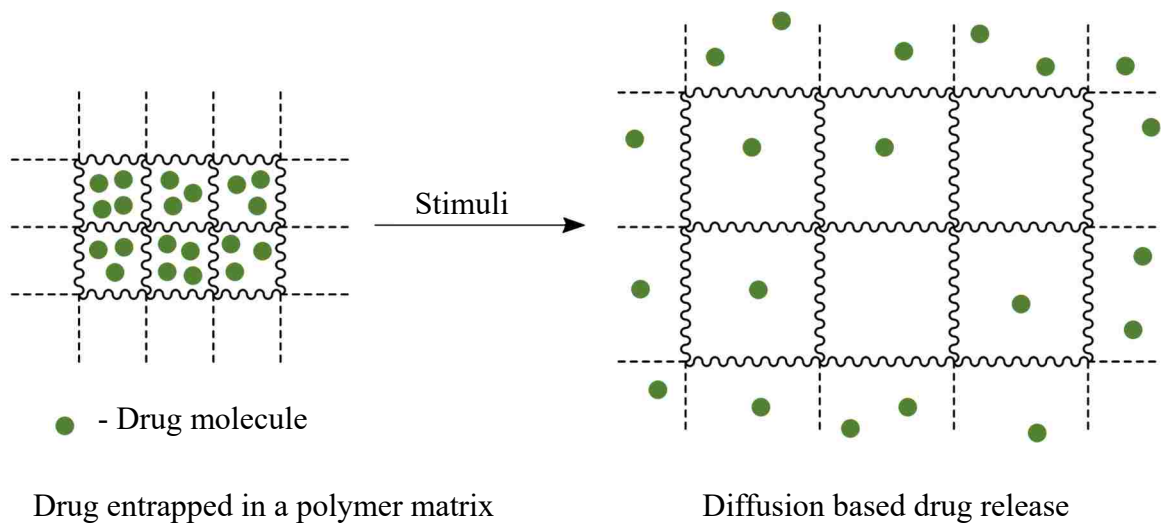


**Figure 1.5:** Schematic for drug release from a polymer matrix due to swelling response caused by stimuli such as temperature, or pH in aqueous media.

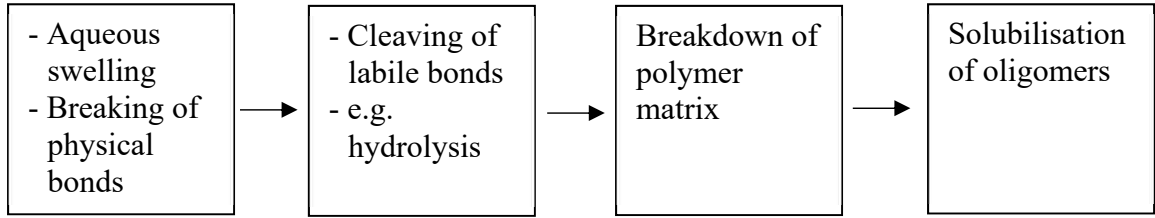


**Figure 1.6:** Steps involved in the bulk degradation of polymers.

## Chapter 2: Research goals

In this work, poly(curcumin  $\beta$ -amino esters) (PCBAEs), which are crosslinked amorphous polymer networks, have been developed for drug-delivery and biomedical applications. As a model antioxidant compound, this work focuses on curcumin, a natural polyphenol found in the Indian spice, turmeric, which has been shown to possess antioxidant and anti-inflammatory properties. However, due to its low aqueous solubility and biological instability, curcumin possesses poor pharmaceutical properties that have greatly limited its clinical use. It is theorized that a sustained delivery of solubilized, intact curcumin can achieve therapeutic concentrations of curcumin, and thereby reduce oxidative stress. Here, PCBAEs were synthesized and characterized for their ability to achieve this sustained release and improved stability. The overall goal of this work was to explore the role of various synthesis parameters in tuning the degradation and thermomechanical properties of the PCBAE networks, which could enable the development of novel pharmaceutical and biomedical applications. The PCBAE networks were characterized through swelling response, curcumin release profiles, and antioxidant activity measurements. In addition, the molecular relaxation properties of PCBAE were characterized using broadband dielectric spectroscopy, and thermomechanical properties were characterized using dynamic mechanical analysis. Finally, a PCBAE based tablet formulation was developed for colon specific drug delivery, as a proof of principle case demonstrating the potential application of PCBAE in pharmaceutical settings. The overall goal has been split into four specific aims, which are explained below.

## **2.1 Specific aim 1: Synthesize and characterize curcumin multiacrylate (CMA) monomers for use in PCBAE synthesis**

Synthesize different grades of CMA through variation of curcumin to acryloyl chloride ratio and identify the curcumin acrylate products present in the curcumin acrylate.

### **2.1.1 Hypothesis # 1**

The extent of curcumin acrylation can be tuned in a reproducible fashion by controlling reaction stoichiometry.

### **2.1.2 Significance and outcome**

This hypothesis was tested using the experiments presented in **Chapter 3**. Different grades of CMA were prepared through variation of curcumin to acryloyl chloride ratios. Different curcumin acrylates (mono, di and tri) present in CMA was characterized through liquid chromatography mass spectrometry (LCMS) and nuclear magnetic resonance (NMR). The thermal properties of different grades of CMA were characterized through thermogravimetric analysis (TGA). Through this detailed analysis of the acrylation products, it was confirmed that curcumin multiacrylate systems of known extents of acrylation can be synthesized in a batch to batch reproducible fashion.

## **2.2 Specific aim 2: Synthesize biodegradable poly(antioxidant $\beta$ -amino ester) (PABAE) networks based on incorporation of curcumin multiacrylate and characterize their static and dynamic properties**

Synthesize series of PCBAE hydrogels through a reaction between CMA, along with PEG400DA, and 4,7,10-trioxa-1,13-tridecanediamine (TTD) as a crosslinker, and characterize the molecular relaxation properties, thermomechanical properties and degradation properties of PCBAE.

### **2.2.1 Hypothesis #2**

By increasing network hydrophobicity, CMA can slow down PCBAE network degradation and increase thermomechanical stability.

### **2.2.2 Significance and outcome**

This hypothesis was tested through the experiments presented in **Chapter 4**. A series of PCBAE hydrogels was synthesized through varying the molar ratio of CMA to PEG400DA. PCBAEs with high CMA content (i.e. PCBAE with 90:10 CMA:PEG400DA) were synthesized successfully, which allowed for high drug loading (50.94 % w/w) in the gels. The swelling response of the series was measured in acetonitrile to characterize network properties, such as relative crosslinking density. The degradation properties of PCBAEs were characterized through measurement of aqueous swelling response. The molecular relaxation properties of PCBAEs were characterized using broadband dielectric spectroscopy (BDS). Time-temperature plots were developed for glass to rubber and sub-glass relaxations. The thermomechanical properties of PCBAEs were characterized using dynamic mechanical analysis (DMA). An overall increase in degradation time and glass transition temperature was observed with an increase in CMA content.

### **2.3 Specific aim 3: Determine the influence of total acrylate to amine ratio, amine crosslinker and diacrylate monomer on mechanical and degradation properties of PCBAE**

Synthesize PCBAEs with a broad range of functional properties through a systematic variation of independent synthesis parameters such as total acrylate to amine ratio, amine crosslinker and diacrylate monomer.

### **2.3.1 Hypothesis # 3**

A) The degradation time and crosslink density of PCBAE can be reduced by reducing the molecular length and hydrophilicity of amine crosslinker and commercial diacrylate monomer.

B) An increase in total acrylate to amine ratio can increase the degradation time and thermomechanical stability of PCBAE networks.

C) An increase in CMA composition can increase the degradation time of PCBAE for PCBAEs synthesized with 2,2'(ethylenedioxy) bis ethylamine (EDBE) and hexamethylene diamine (HMD).

### **2.3.2 Significance and outcome**

This set of hypotheses was tested through experiments presented in **Chapter 5**. The independent process parameters, such as amine crosslinker, commercial diacrylate monomer, and ratio of total acrylate to amine (RTAA), were used to synthesize series of PCBAE hydrogels with wide range of functional properties thereby enabling novel applications of PCBAEs. The glass to rubber transition and rubbery modulus was characterized using dynamic mechanical analysis, and the degradation properties were characterized through measurement of swelling response and drug release. Amine crosslinker had a significant effect on degradation characteristics, but no significant effect on thermomechanical characteristics. An increase in CMA composition for PCBAEs made with EDBE and HMD increased the degradation times. An increase in total acrylate to amine ratio led to an increase in thermomechanical stability.

## **2.4 Specific aim 4: Develop poly( $\beta$ -amino ester) (PBAE) based tablet formulation for improved bioavailability of a hydrophobic drug**

Develop a PBAE based oral tablet formulation for improved bioavailability of curcumin and study the stability of formulation under different storage conditions.

### **2.4.1 Hypothesis # 4**

PBAE based tablet formulations can be developed for improving bioavailability of curcumin.

### **2.4.2 Significance and outcome**

To test this hypothesis, oral tablet formulations based on PCBAE microparticles were synthesized and stability of this formulation was tested under standard and accelerated storage conditions. These experiments are discussed in **Chapter 6**. Tablet formulation consisted of PCBAE microparticles and microcrystalline cellulose along with magnesium stearate. A sustained release of curcumin was obtained for over 20 hours. PCBAE being hydrolytically degradable, tablet stability was found to be sensitive to moisture.

## Chapter 3: Curcumin acrylation for biological and environmental applications

### 3.1 Introduction

Curcumin is the main constituent of the Indian spice turmeric and has been shown to possess anti-oxidant, anti-inflammatory and anti-angiogenic properties [139-141]. The major challenge with the use of curcumin as an experimental or therapeutic agent is its limited aqueous solubility and photoinstability [142]. Multiple strategies have been proposed to overcome these limitations including conjugation, polymerization, amorphous dispersion and encapsulation [143-146]. Many of these approaches can be facilitated through the acrylation of curcumin. Curcumin acrylation was first explored by Wattamwar et al. for the preparation of hydrolytically degradable poly(curcumin  $\beta$  amino ester) hydrogels for use in drug delivery applications [124]. These materials improve the stability of curcumin for controlled release and also increase its bioavailability through enhanced solubility. Curcumin acrylation has since been used to make antibacterial nanofibers, chemical sensing materials and as a drug carrier in the form of curcumin microspheres [147-149]. Curcumin has also been explored recently for its radical scavenging potential and its capacity to inhibit toxicity of dioxin and dioxin-like molecules such as polychlorinated biphenyl (PCB) and for its potential use in environmental remediation [13, 150, 151]. The acrylation approach has similarly been used for other phenolic molecules such as apigenin and quercetin [152, 153]; the identification methods discussed in this work can be extended to these molecules and other phenols, such as myricetin and catechin [154, 155].

Curcumin contains three hydroxyl groups available for modification, and curcumin acrylation can lead to the formation curcumin mono-, curcumin di- and curcumin triacrylates. The relative proportion of these species in the resulting curcumin multiacrylate (CMA) mixture can influence the subsequent synthesis of curcumin-containing materials, with the potential for endcapping and branching in the context of polymerization reactions [156]. However, a full characterization and identification of the individual acrylate species produced by the acrylation procedure described by Wattamwar et al. has not yet been reported. In this chapter, we present the identification of curcumin acrylate species that result from the synthesis protocol of Wattamwar, and consider the influence of reaction stoichiometry on the relative populations of the various acrylate species and the overall extent of acrylation that is achieved.

## **3.2 Experimental**

### **3.2.1 Materials**

Curcumin was purchased from Chem-Impex International, Inc. Triethyl amine (TEA) and acryloyl chloride were purchased from Sigma-Aldrich. All solvents (tetrahydrofuran (THF), dichloromethane (DCM), and acetonitrile (ACN)) were obtained from Pharmco-Aaper. Molecular sieves (3Å) were added to the solvents to remove any moisture present and to maintain the anhydrous state of the solvents.

### **3.2.2 Curcumin multiacrylate (CMA) synthesis**

Curcumin was functionalized with acrylate to form curcumin multiacrylate by reaction with acryloyl chloride according to the method reported previously [69]. Briefly, curcumin was dissolved in THF to a final concentration of 50 mg/mL. TEA was added to this solution at the desired curcumin:TEA ratio as presented in **Table 3.1**. After the TEA

addition, acryloyl chloride was added drop wise to the THF solution while the mixture was stirred on an ice bath. The reaction mixture was allowed to react for 16 hours under dark conditions. The mixture was then subjected to vacuum filtration to remove the precipitated triethylammonium chloride salts formed by the reaction between TEA and acryloyl chloride, which release HCl. THF from filtrate was evaporated under vacuum using a liquid N<sub>2</sub> trap. The recovered CMA mass was re-dissolved in DCM. This solution was then purified by multiple washes with 0.1 M K<sub>2</sub>CO<sub>3</sub> and then 0.1 M HCl to remove unreacted acryloyl chloride and TEA, respectively. Magnesium sulfate was added to remove residual moisture from the solution; the amount of magnesium sulfate needed was usually small (around 1% of curcumin weight). The resulting solution was filtered to remove magnesium sulfate, and DCM was then evaporated under vacuum using a liquid N<sub>2</sub> trap to obtain the final product in powdered form. Three different batches were synthesized by varying the curcumin to acryloyl chloride ratio (viz. 1:1, 1:2 and 1:3) to demonstrate control over the acrylation. The curcumin:TEA ratio selected was the same as the curcumin:acryloyl chloride ratio (e.g., for 1:1 curcumin:acryloyl chloride, 1:1 curcumin:TEA was used). The molar ratios of curcumin, acryloyl chloride and TEA used for preparing these batches is presented in Table 3.1. Chemical structures of curcumin and the different acrylates possible through acrylation are presented in **Figure 3.1**.

### **3.2.3 High performance liquid chromatography (HPLC)**

The synthesized CMA was characterized using reverse-phase HPLC (Waters Phenomenex C18 column, 5 μm, 250 mm (length) X 4.6 mm (I.D.) on a Shimadzu Prominence LC-20 AB HPLC system). Samples were prepared with a final concentration of 50 μg/mL in ACN. A gradient from 50/50 ACN/water to 100/0 ACN/water over 30

minutes at 1 mL/min was used with the column chamber set at 40°C. The absorbance was measured from 220 nm to 500 nm.

### **3.2.4 Liquid chromatography-mass spectrometry (LCMS)**

LCMS was performed using a Shimadzu high-performance liquid chromatograph (HPLC) equipped with a ZORBAX Eclipse XDB-C18 column, coupled with an ABSciex 5600 “Triple TOF” hybrid quadrupole time of flight mass spectrometer. For LCMS, the same elution method was used as for HPLC, but the flow rate was 0.5 mL/min and the column chamber temperature was 35°C. A UV-Vis detector was present before the mass spectrometer which measured absorbance at 420 nm.

### **3.2.5 <sup>1</sup>H Nuclear magnetic resonance (<sup>1</sup>H-NMR)**

<sup>1</sup>H NMR spectroscopy was performed using a Varian UNITY INOVA 400 MHz instrument equipped with a 5 mm quadrupole-nucleus probe. 7.5 mg of sample was dissolved in 750 μL of deuterated dimethyl sulfoxide (DMSO). Deuterated DMSO was used for analysis of all compounds. The chemical shifts are reported in ppm relative to TMS (trimethyl silane).

### **3.2.6 Thermogravimetric analysis (TGA)**

A TA Instruments Q50 TGA instrument was used to measure the thermal stability of the different CMA samples. The heating rate was 10°C/min from 35°C to 550°C. Sample amount was approximately 3 mg. All samples were analyzed under nitrogen purge in a closed aluminum pan with perforated lid.

## **3.3 Results and discussion**

Curcumin is known to display keto-enol tautomerism across the central moiety connecting the benzene rings [157]. In commonly used organic solvents such as DMSO,

acetone, chloroform, and acetonitrile, the enol is present as the majority form compared to the keto form [158, 159]. During the acrylation of curcumin, hydroxyl groups are functionalized with acrylate groups: based on the number of hydroxyl groups replaced, different mono-, di- and triacrylates are possible (Figure 1). To study curcumin acrylation in detail, different grades of curcumin multiacrylate (CMA) were prepared through a systematic variation of the curcumin:acryloyl chloride ratio. The synthesized grades of CMA were characterized with HPLC, LCMS and NMR. LCMS and NMR data was used to determine the extent of acrylation, and LCMS was used to identify monoacrylate, diacrylate and triacrylate species of curcumin.

### 3.3.1 High performance liquid chromatography (HPLC)

In **Figure 3.2**, the HPLC chromatograms for curcumin, CMA 1:1, CMA 1:2 and CMA 1:3 are presented. A group of peaks was present from 8 minutes to 9.5 minutes, which correspond to different forms of curcumin. The intensity of this set of peaks decreased as the amount of acryloyl chloride in the initial reaction mixture was increased, demonstrating an increase in the extent of curcumin conversion to curcumin acrylates. Also, additional peaks around 14 minutes and 19 minutes emerge for CMA 1:1, 1:2 and 1:3, along with peaks at 14.8, 15.8 & 17.3 minutes for CMA 1:3, which could potentially be different acrylates of curcumin. Based on an increase in the inherent hydrophobicity of the acrylated curcumin, the peaks evident at 14 and 19 minutes in Figure 3.2 were anticipated to be monoacrylate and diacrylate forms of curcumin, respectively. As the curcumin:acryloyl chloride ratio was increased to 1:2, the relative proportion of monoacrylate decreased while the diacrylate proportion increased. This trend continued for CMA 1:3, where the proportion of monoacrylate relative to diacrylate was even lower. The

emergence of peaks between 14 minutes and 19 minutes (i.e. peaks at 14.8, 15.8 & 17.3 minutes) for CMA 1:3, which could potentially be triacrylate peaks, was unexpected. Since the triacrylate form is presumably more hydrophobic than the diacrylate, the triacrylate species would be expected to elute after the diacrylate form. To explore the elution sequence in detail and to establish the molecular weight corresponding to each peak, LCMS analysis was completed for all CMA formulations as discussed below.

The absorbance spectrum for each HPLC elution peak was recorded using a photodiode array (PDA) detector connected with the HPLC instrument. The absorbance spectrum for each peak present in the CMA 1:3 HPLC chromatogram is presented in **Figure 3.3**; the absorbance spectra for CMA 1:1 and CMA 1:2 are provided in the supplemental section. A blue shift in peak wavelengths is seen for the different acrylated forms of curcumin as compared to unmodified curcumin, which has an absorbance peak maximum at 420 nm. The peak wavelengths for the different curcumin acrylate species are listed in the **Table 3.2**. The UV-vis absorbance peaks shift to lower wavelengths due to acrylation, with the curcumin peak maximum at approximately 420 nm, monoacrylates at 410 nm, diacrylates around 400 nm and triacrylates at 370 nm.

### **3.3.2 Liquid chromatography-mass spectrometry (LCMS)**

The LCMS data for curcumin and CMA with curcumin:acryloyl chloride formulation ratios of 1:1 and 1:2 is presented in the **Figure 3.4** and **Figure 3.5**. The elution times for all elution peaks in LCMS are approximately 2 minutes higher than those obtained from HPLC; this is due to a lower column temperature (35°C) used for LCMS as compared to HPLC (40°C), which does not affect the nature or sequence of the elution peaks. The LCMS data for curcumin (Figure 3.4) identify three forms of curcumin:

bisdemethoxycurcumin, demethoxycurcumin and curcumin. These forms are present in the molar amounts 3.5%, 25.4% and 71.1%, respectively, which are similar to the proportions obtained from the HPLC absorbance peak areas (3.9%, 23.0% and 73.1%, respectively). The comparable values obtained from LCMS and HPLC absorbance show that the molar extinction coefficients are similar for the three forms of curcumin.

The LCMS data for CMA 1:1 are presented in Figure 3.5. A cluster of four peaks around 16.5 minutes was found to be a group of monoacrylate peaks, corresponding to bisdemethoxycurcumin monoacrylate, demethoxycurcumin monoacrylate, curcumin monoacrylate, followed by an additional demethoxycurcumin monoacrylate peak. As seen in **Figure 3.6**, these monoacrylate peaks are present in CMA 1:2 as well, but in a lower proportion. A group of three diacrylate peaks are present at 22.5 minutes for both CMA 1:1 and CMA 1:2, representing curcumin diacrylate, demethoxycurcumin diacrylate and bisdemethoxycurcumin diacrylate, respectively. For CMA 1:2, the proportion of diacrylate peaks is relatively higher than in CMA 1:1. The LCMS data for CMA 1:3 are shown in **Figure 3.7**. For CMA 1:3, a curcumin monoacrylate peak and a set of diacrylate peaks are present. Along with these peaks, three additional peaks were present at 17.8, 18.9 and 20.5 minutes. These peaks had a molecular weight of 531, which corresponds to curcumin triacrylate. Based on the peak area analysis, the extent of acrylation (number of acrylate groups per molecule) was calculated to be 1.34, 1.84 and 2.56 for CMA 1:1, 1:2 and 1:3, respectively. The various elution peaks observed in the HPLC data in Figure 2 were identified using LCMS (re: Figure 3.5, 3.6 & 3.7). The CMA 1:1 sample had unreacted curcumin, along with monoacrylates and diacrylates of the three forms of curcumin. The CMA 1:2 sample had the same constituent species as CMA 1:1, but with a higher amount

of diacrylate species and a lower amount of unreacted curcumin. The monoacrylate and diacrylate peak elution sequence was found to be based on the hydrophobicity of the respective molecules. Additionally, it was observed that demethoxycurcumin monoacrylate had two peaks in the elution profile. This was due to two possible forms of monoacrylation of demethoxycurcumin, viz., acrylation on the benzene ring with  $R_1 = \text{OCH}_3$ , or acrylation on the benzene ring with  $R_2 = \text{H}$ . CMA 1:3 showed complete conversion of curcumin, forming a mixture of curcumin triacrylate and diacrylate species along with a trace amount of curcumin monoacrylate species. The relative proportions of the various acrylates for different curcumin:acryloyl chloride ratios are shown in **Table 3.3**.

It was seen from both the HPLC and LCMS analysis of CMA 1:3 that the curcumin triacrylates elute before the diacrylate species. This result was not anticipated, given the higher hydrophobicity of curcumin triacrylate. The observed elution order most likely reflects additional factors that govern the elution of the triacrylates such as electrical charge on the molecule due to ion pairing, or molecular shape. Acrylation at the central linkage can potentially give the triacrylate molecule a more kinked geometry as compared to the overall linear character of the diacrylate molecule, and this kinked configuration can contribute to a lower adsorption tendency on the column leading to earlier elution of the triacrylates [160, 161].

An additional phenomenon observed with curcumin triacrylate elution is the appearance of three distinct elution peaks as seen from LCMS (re: Figure 3.7). This could reflect different conformational isomers of curcumin triacrylate, which have varying adsorption tendencies and hence elute at different times. To explore this further, each of

the triacrylate peak elutions for the CMA 1:3 sample were collected separately and reinjected into the HPLC. HPLC runs for isolated curcumin triacrylate (CTA) peak 1, isolated CTA peak 2 and isolated CTA peak 3 are reported in **Figure 3.8**. It can be seen that each of these isolated samples redistribute across the original CTA peak positions observed for CMA 1:3. For the peak collection from HPLC, an extended method file was used, which provided approximately 3 minutes of peak time separation. A sample collection window of 25 seconds was used to collect samples. Based on these data, there is ample evidence to indicate that these species are redistributing across triacrylate peak positions, which would imply that they correspond to three different conformers of CTA formed by the rotation of acrylate groups. This is a commonly observed phenomenon in non-planar molecules that experience hindrance in the free rotation around the sigma bond due to the presence of neighboring chemical groups [162, 163]. To explore if the three CTA peaks represent species that are in equilibrium with each other, or if they interconvert over time to reach equilibrium, the influence of holding time on peak positions was studied. As seen from **Figures 3.9 and 3.10**, the peak positions and relative areas didn't change even after 5 hours, suggesting that conformations are stable and don't convert over time. This implies that the conformational kinetics are fast enough to obtain equilibrium within 30 minutes.

### **3.3.3 <sup>1</sup>H Nuclear magnetic resonance (<sup>1</sup>H-NMR)**

The degree of acrylation of curcumin was further characterized by NMR. The <sup>1</sup>H-NMR data for all samples are presented in **Figure 3.11**. The phenolic proton peaks (9.5 to 10.5 ppm) decrease with increasing acryloyl chloride ratio, reflecting an increase in the extent of curcumin to curcumin acrylate conversion. The smaller peak at 10.1 ppm

corresponds to the hydroxyl proton present at the enol while the 9.7 ppm peak corresponds to the phenolic protons. Also, acrylate proton peaks (6 to 6.6 ppm) emerge, confirming the presence of acrylate groups on the curcumin molecule. Based on NMR data, the extent of acrylation (number of acrylate groups per molecule) was calculated to be 1.03, 1.73, and 2.82 for 1:1, 1:2 and 1:3 CMA, respectively. A comparison of the extent of acrylation for the different formulation ratios using LCMS and NMR is reported in **Figure 3.12**.

### **3.3.4 Thermogravimetric analysis (TGA)**

Thermal stability of monomers is an important parameter when developing polymers for different applications, where the monomer might be exposed to elevated temperatures during polymer synthesis or other processing steps. TGA was performed on curcumin and CMA to explore the thermal stability of these samples; see **Figure 3.13**. Volatiles are evaporated initially from all samples as indicated by the ~ 4% weight loss prior to samples reaching 250°C. The curcumin decomposition begins at the lowest temperature, suggesting the greatest degree of thermal instability amongst the samples. Interestingly, decomposition begins around 350°C for CMA 1:2 and CMA 1:3, while for CMA 1:1, decomposition starts around 250°C. For CMA 1:1, the decomposition curve was broader as compared to CMA 1:2 and CMA 1:3. The earlier onset and broader decomposition was due to the higher amount of residual (i.e., unmodified) curcumin present in the CMA 1:1 sample. The amount of carbon residue (~ 40%) left at the end of TGA analysis was consistent with estimates obtained by considering the full pyrolysis of curcumin and CMA.

### 3.4 Conclusions

In this work, a synthesis method for curcumin acrylation was presented and the resulting curcumin multiacrylate product was characterized using HPLC, LCMS and NMR. Control over the extent of acrylation was demonstrated, and it was confirmed that the degree of acrylation correlates with the curcumin:acryloyl chloride ratio in the formulation mixture. All acrylate species present in the CMA samples were identified using LCMS, and the extent of acrylation was determined using both LCMS and NMR. The extent of acrylation was found to be 1.34 and 1.03 for CMA 1:1, 1.84 and 1.73 for CMA 1:2, and 2.56 and 2.82 for CMA 1:3 using LCMS and NMR, respectively. Overall, it was seen that an increase in acrylation led to an increase in thermal stability of the parent compound. The full characterization of these multiacrylate products is essential for their use in the design and synthesis of future curcumin-based materials for biological and environmental applications.

**Table 3.1:** Composition of curcumin, acryloyl chloride and TEA in the initial reaction mixture.

	<b>Curcumin (moles)</b>	<b>Acryloyl chloride (moles)</b>	<b>TEA (moles)</b>
CMA 1:1	1	1	1
CMA 1:2	1	2	2
CMA 1:3	1	3	3

**Table 3.2:** UV-Vis absorbance peaks for different forms of curcumin multiacrylate.

	<b>Absorbance peak wavelength</b>
<b>Curcumin</b>	<b>420 nm</b>
Curcumin monoacrylate	412 nm
Curcumin diacrylate	400 nm
Curcumin triacrylate	370 nm
<b>Demethoxycurcumin</b>	<b>420 nm</b>
Demethoxycurcumin monoacrylate	408 nm
Demethoxycurcumin diacrylate	397 nm
Demethoxycurcumin triacrylate	370 nm
<b>Bisdemethoxycurcumin</b>	<b>420 nm</b>
Bisdemethoxycurcumin monoacrylate	412 nm
Bisdemethoxycurcumin diacrylate	395 nm

**Table 3.3:** Proportion of different acrylates in CMA prepared with different curcumin:acryloyl chloride ratios. The values are based on the peak areas from LCMS.

	CMA 1:1	CMA 1:2	CMA 1:3
Curcumin	16.0 %	2.3 %	0 %
Monoacrylates	38.5 %	23.3 %	1.0 %
Diacrylates	40.6 %	62.0 %	42.4 %
Triacrylates	4.9 %	12.4 %	56.6 %

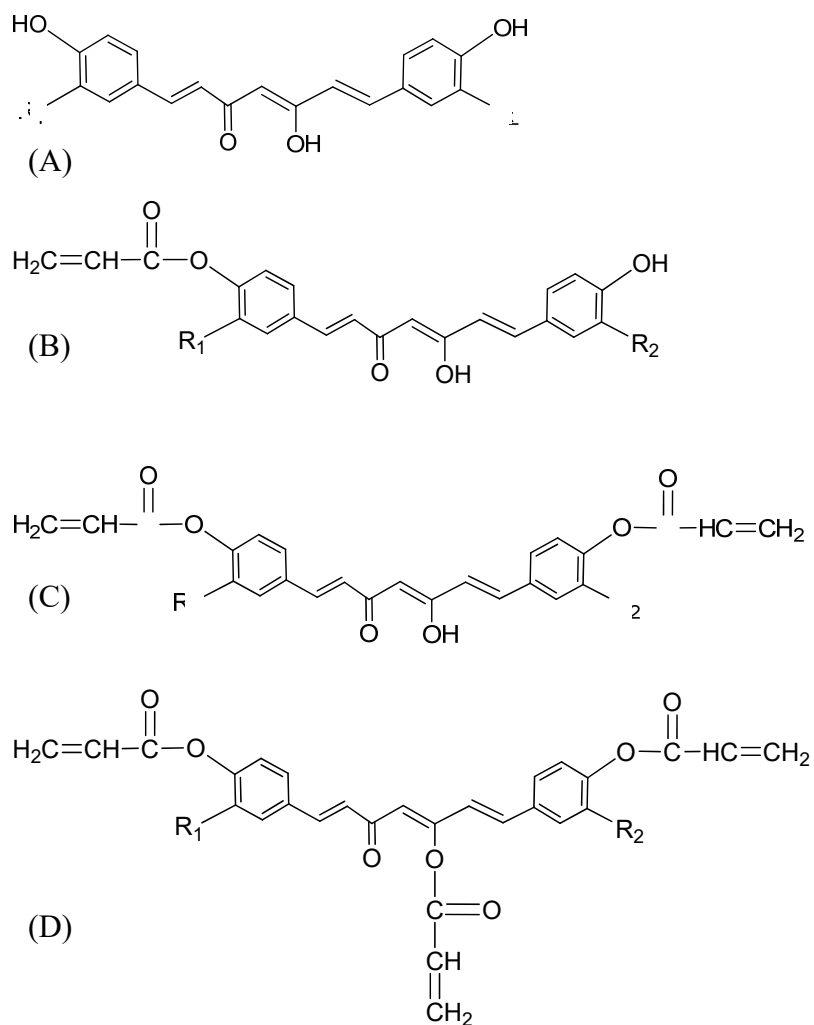


**Figure 3.1:** Chemical structure of curcumin (A), curcumin monoacrylate (B), curcumin diacrylate (C), and curcumin triacrylate (D). R<sub>1</sub> and R<sub>2</sub> are both OCH<sub>3</sub> for curcumin, H and OCH<sub>3</sub> for demethoxycurcumin, and both H for bisdemethoxycurcumin.

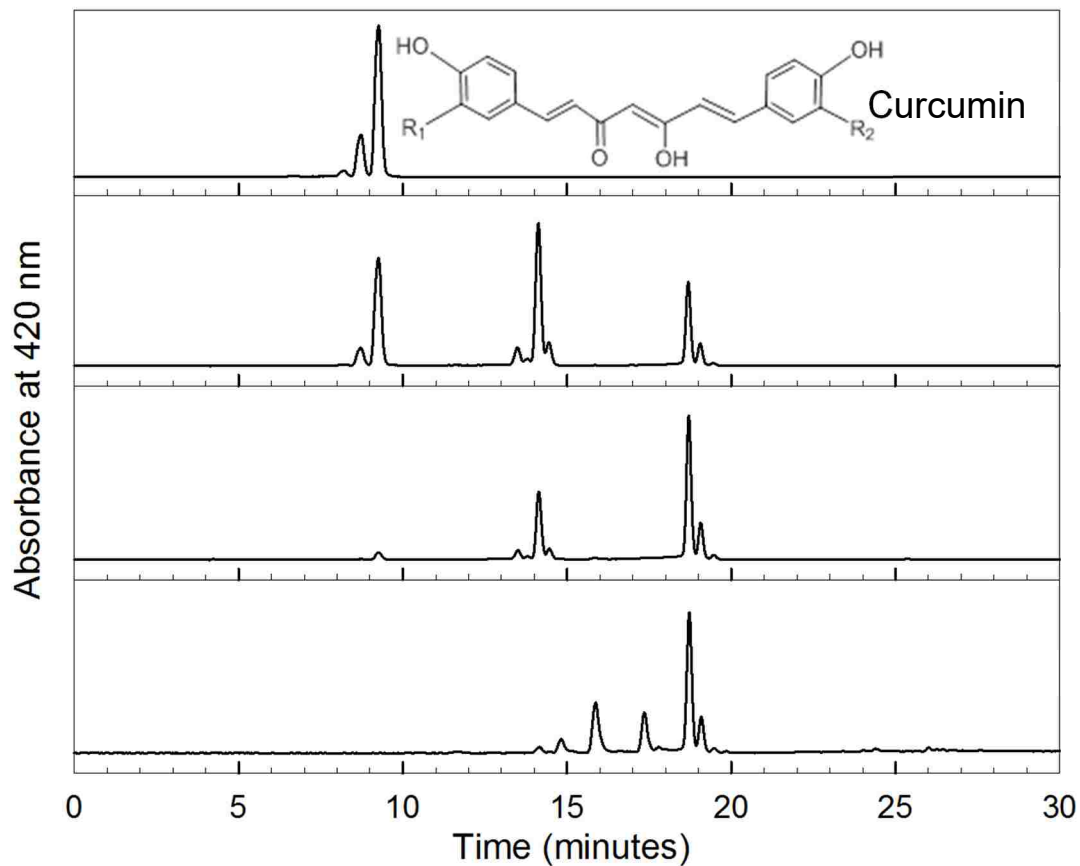


**Figure 3.2:** HPLC chromatograms for curcumin and curcumin multiacrylate with different curcumin:acryloyl chloride ratios (viz. 1:1, 1:2 and 1:3). The curcumin peak intensity decreases with an increase in acryloyl chloride in the reaction mixture.

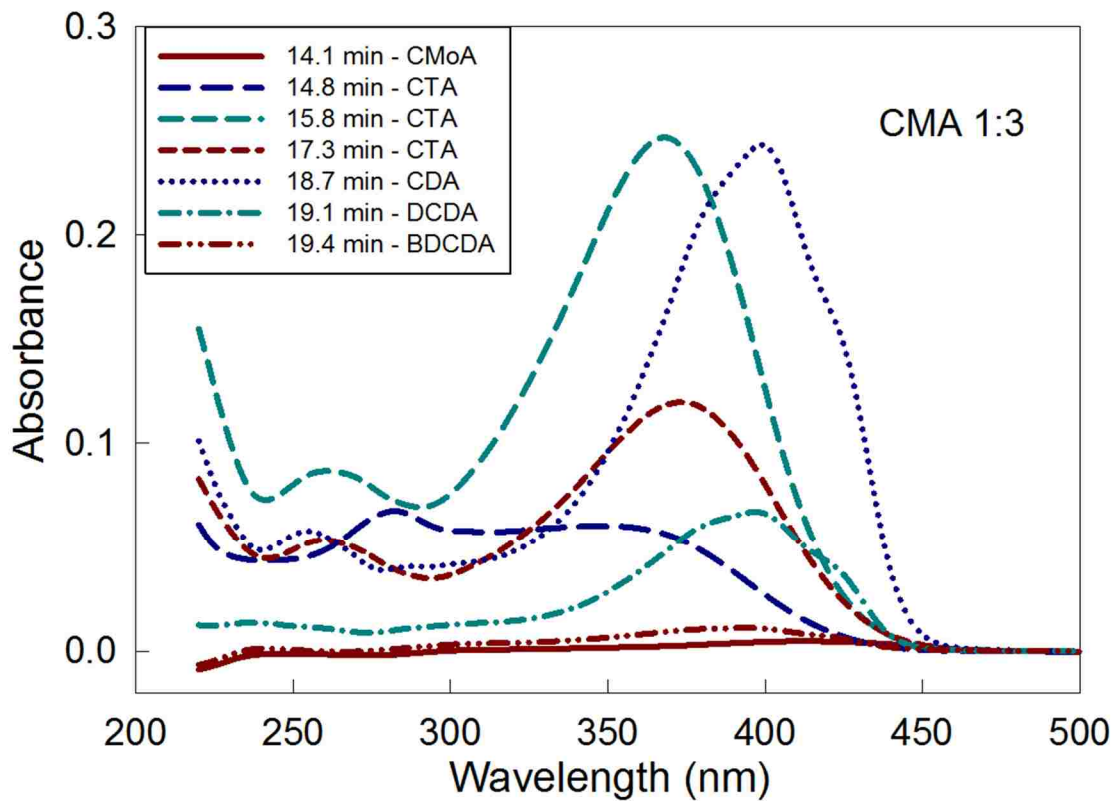


**Figure 3.3:** Absorbance spectra for individual peaks from HPLC analysis for CMA 1:3. The time noted in the legend is the peak elution time obtained from HPLC. Possible peak assignments for the different acrylates are indicated in the legend. CMoA – curcumin monoacrylate, CTA – curcumin triacrylate, CDA – curcumin diacrylate, DCDA – demethoxycurcumin diacrylate, BDCDA – bisdemethoxycurcumin diacrylate.

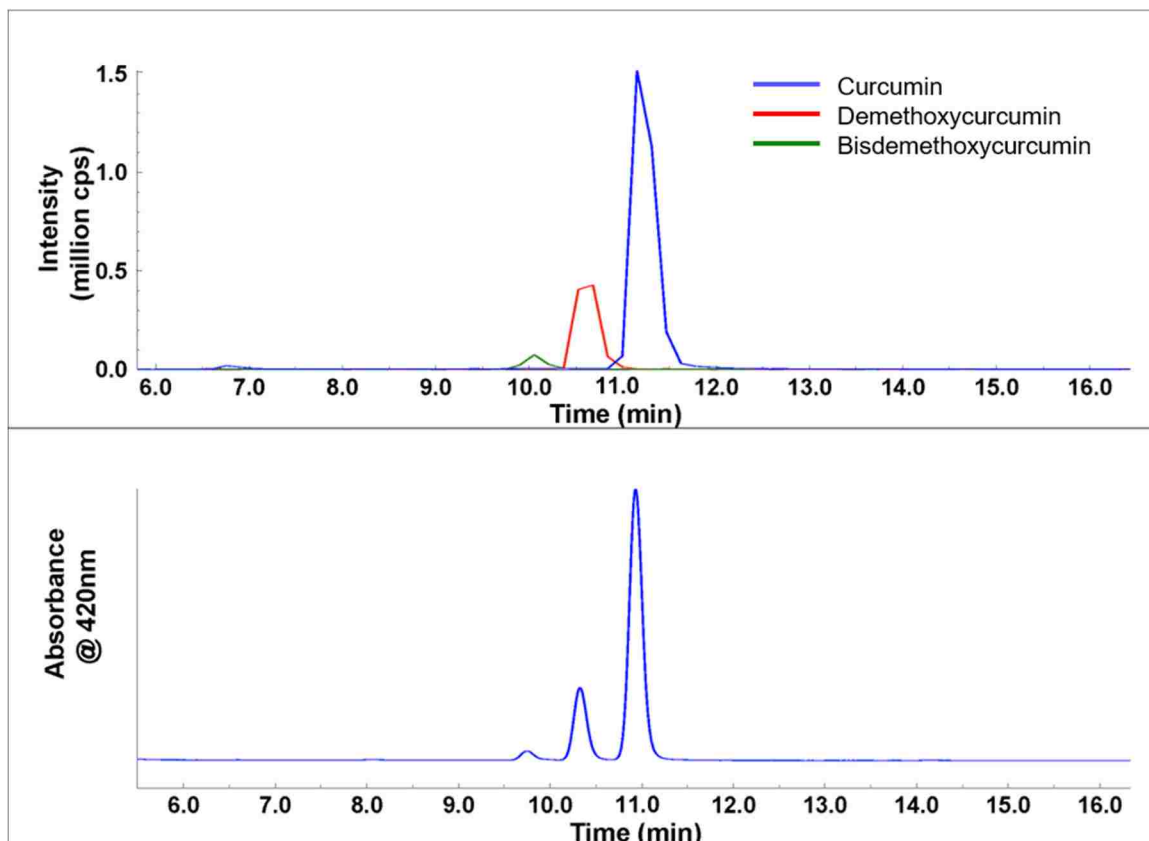


**Figure 3.4:** LCMS data for curcumin. Mass spectroscopy results are shown in the top three plots, while the result from the UV-vis detector connected before the mass spectrometer is shown in the bottom plot.

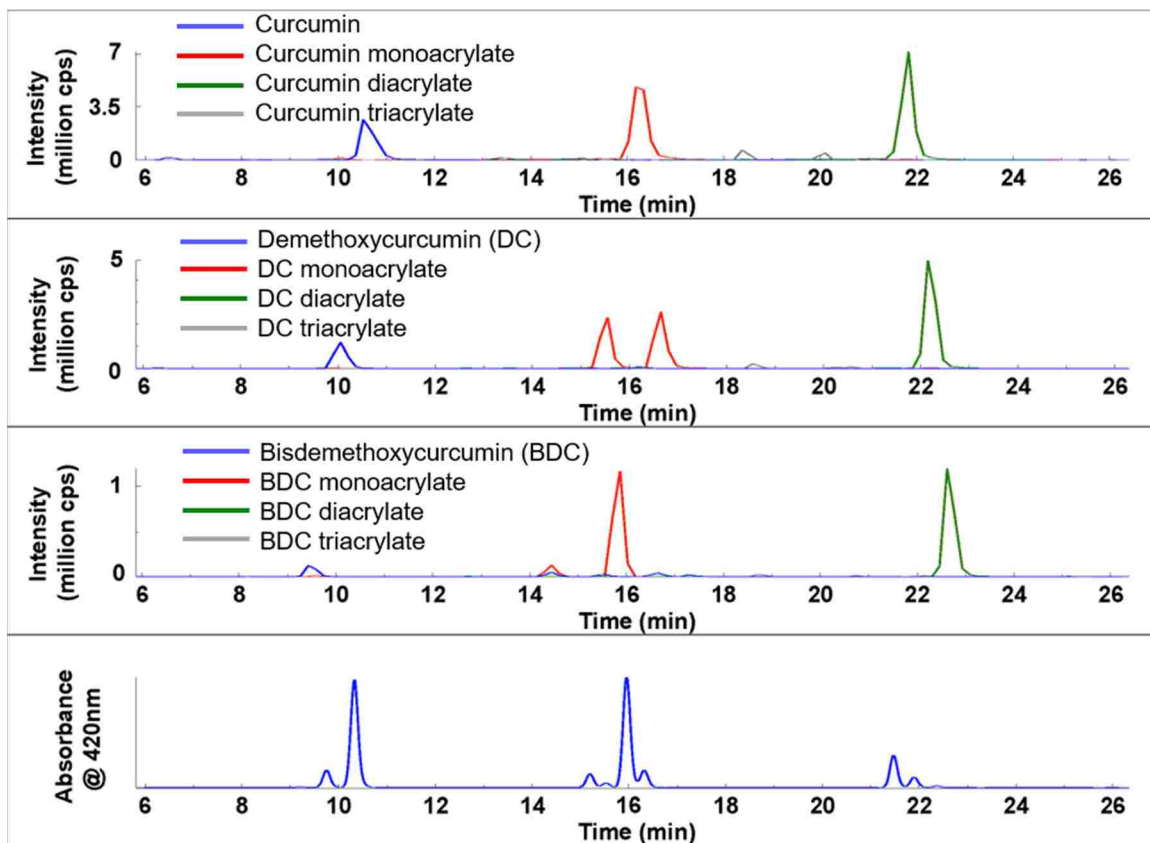


**Figure 3.5:** LCMS data for CMA synthesized using 1:1 curcumin:acryloyl chloride ratio. Mass spectroscopy results are shown in the top three plots, while the result from the UV-vis detector connected before the mass spectrometer is shown in the bottom plot.

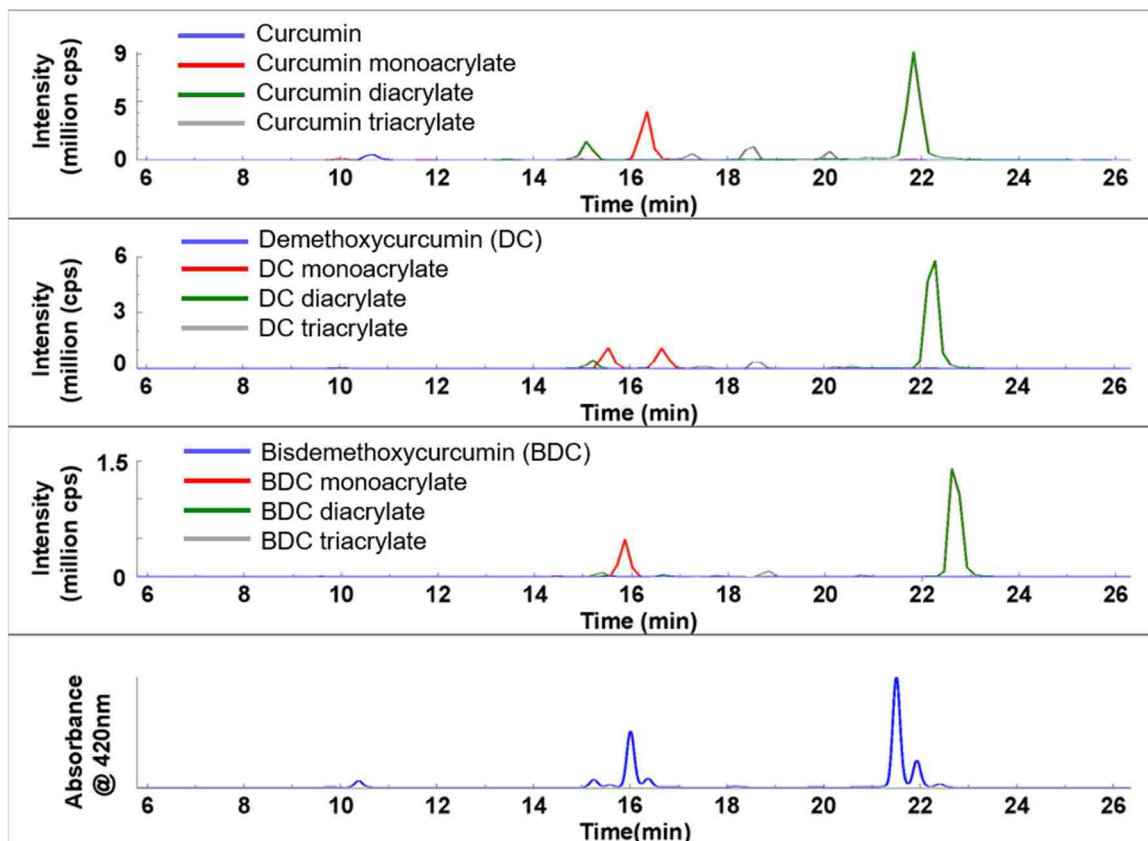


**Figure 3.6:** LCMS data for CMA synthesized using 1:2 curcumin:acryloyl chloride ratio. Mass spectroscopy results are shown in the top three plots, while the result from the UV-vis detector connected before the mass spectrometer is shown in the bottom plot.

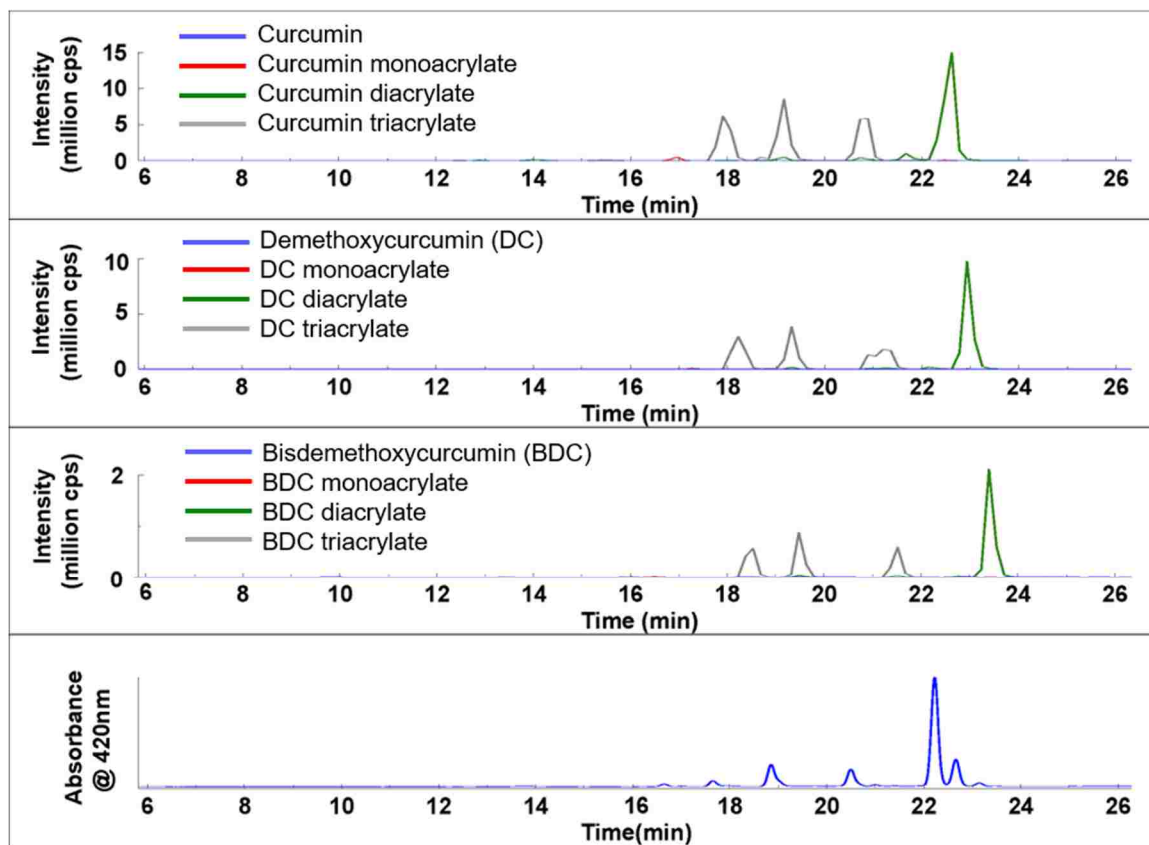


**Figure 3.7:** LCMS data for CMA synthesized using 1:3 curcumin:acryloyl chloride ratio. Mass spectroscopy results are shown in the top three plots, while the result from the UV-vis detector connected before the mass spectrometer is shown in the bottom plot.

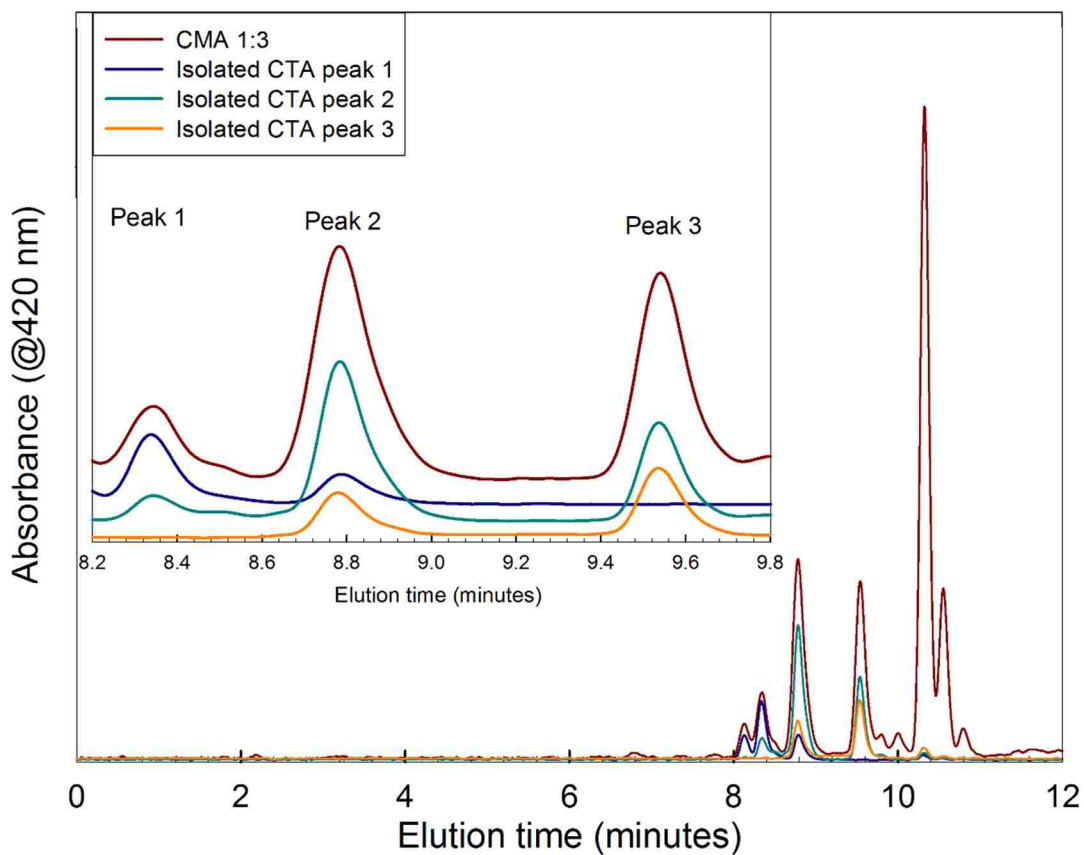


**Figure 3.8:** Curcumin triacrylate (CTA) elution collection samples rerun in HPLC using 12 minute gradient method file from 60/40 (ACN/aqueous) to 100/0 (ACN/aqueous). Inset plot shows same data, but expanding triacrylate range. For curcumin triacrylate, peaks 1, 2 and 3 correspond to the 14.8, 15.8 & 17.3 minute peaks in Figure 3.2.

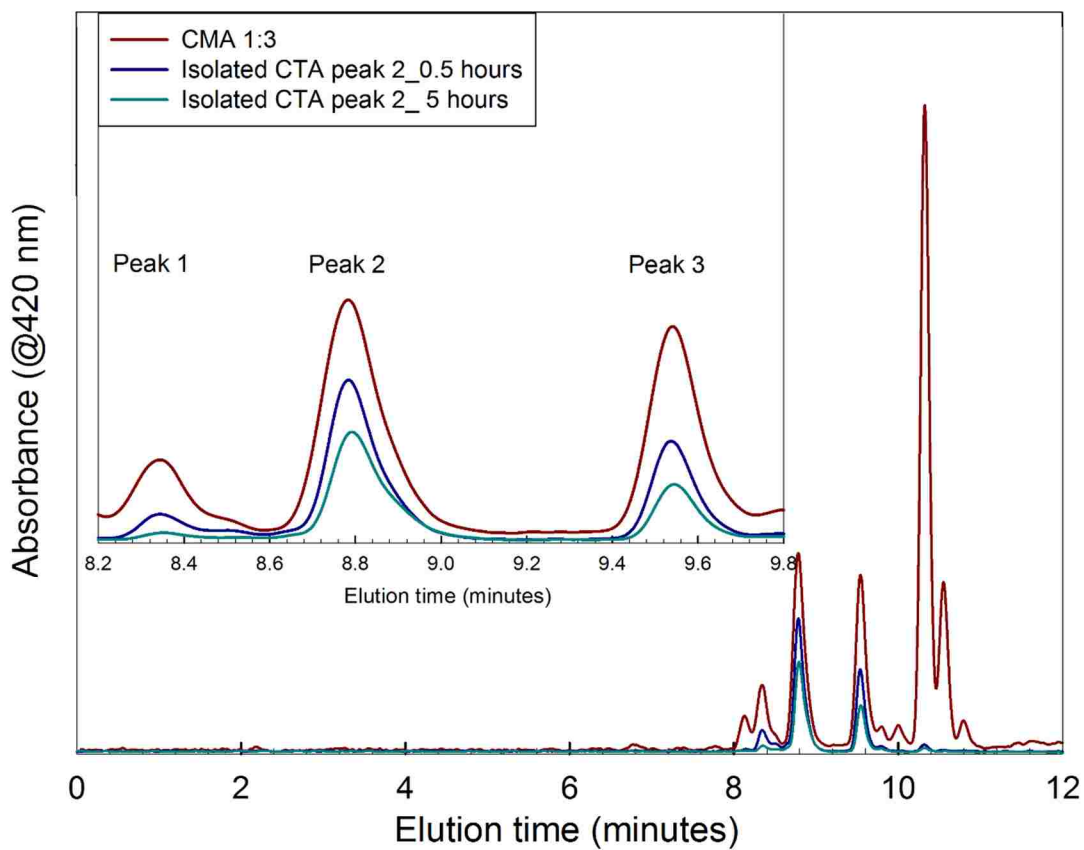


**Figure 3.9:** Isolated curcumin triacrylate “peak 2” elution collection samples (0.5 and 5 hours after collection) rerun in HPLC using 12 minute gradient method file from 60/40 (ACN/water) to 100/0 (ACN/water). Inset plot shows same data, but expanding triacrylate range.

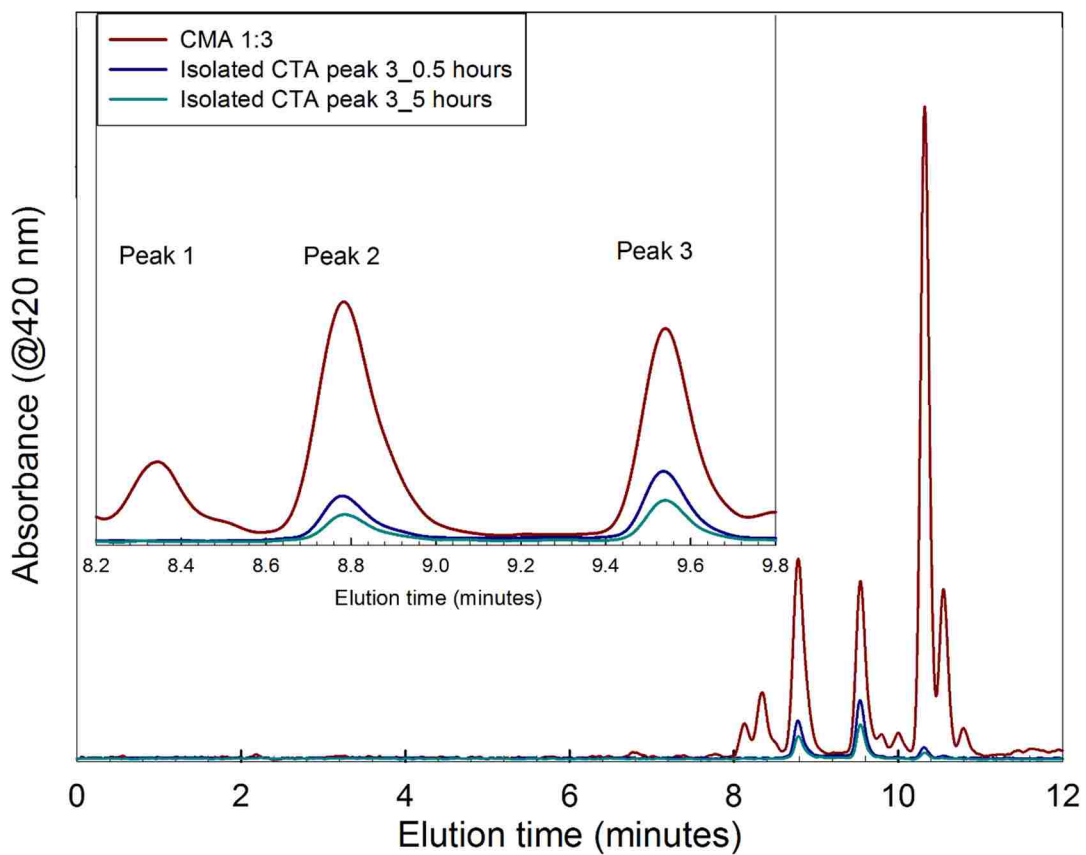


**Figure 3.10:** Isolated curcumin triacrylate “peak 3” elution collection samples (0.5 and 5 hours after collection) rerun in HPLC using 12 minute gradient method file from 60/40 (ACN/water) to 0/100 (ACN/water). Inset plot shows same data, but expanding triacrylate range.

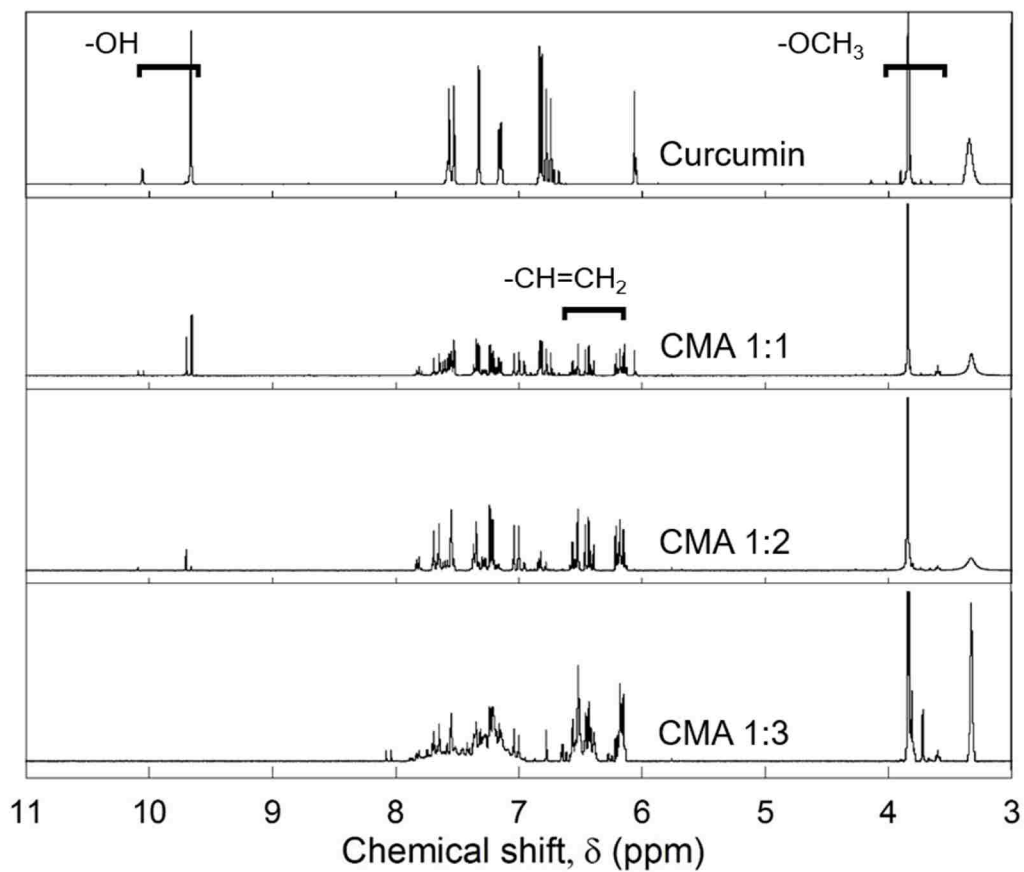


**Figure 3.11:** <sup>1</sup>H NMR (400 MHz, DMSO-*d*<sub>6</sub>) spectrum of curcumin and CMA prepared with different curcumin:acryloyl chloride ratios. Acrylation is evident from the decrease in hydroxyl proton peaks (9.5 to 10.5 ppm) and the emergence of acrylate proton peaks (between 6.1 and 6.7 ppm).

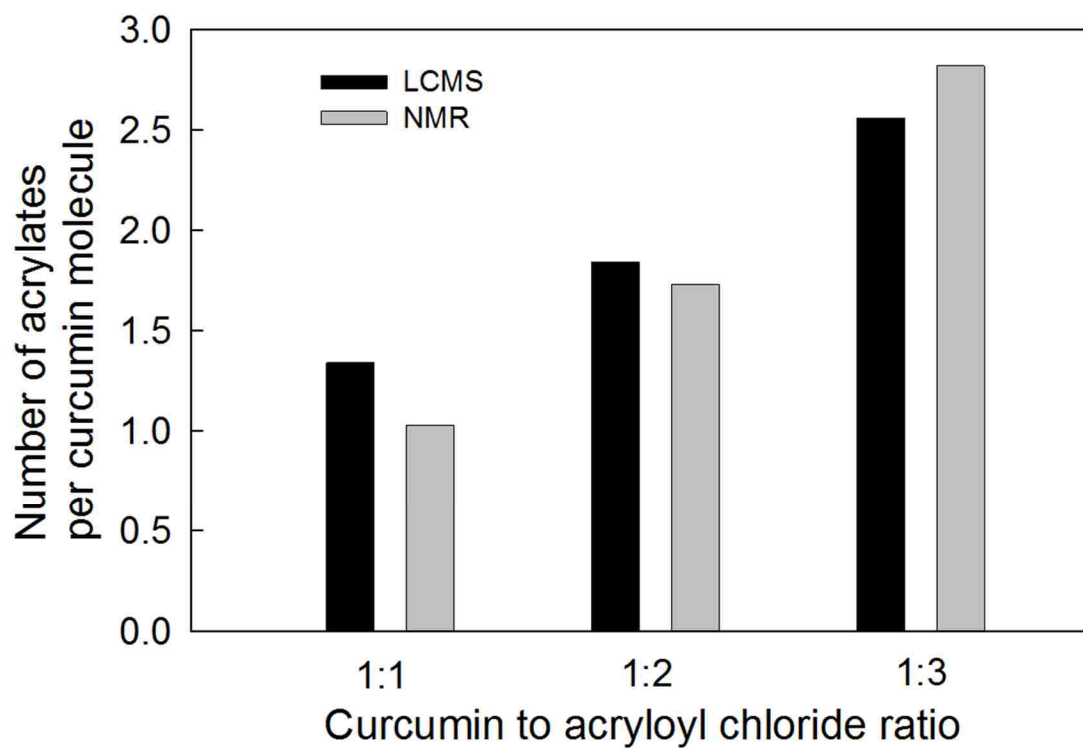


**Figure 3.12:** Comparison of extent of acrylation values obtained from LCMS and NMR analysis of CMA with different curcumin to acryloyl chloride ratios. All the data reported in the current figure is for  $n = 1$ .

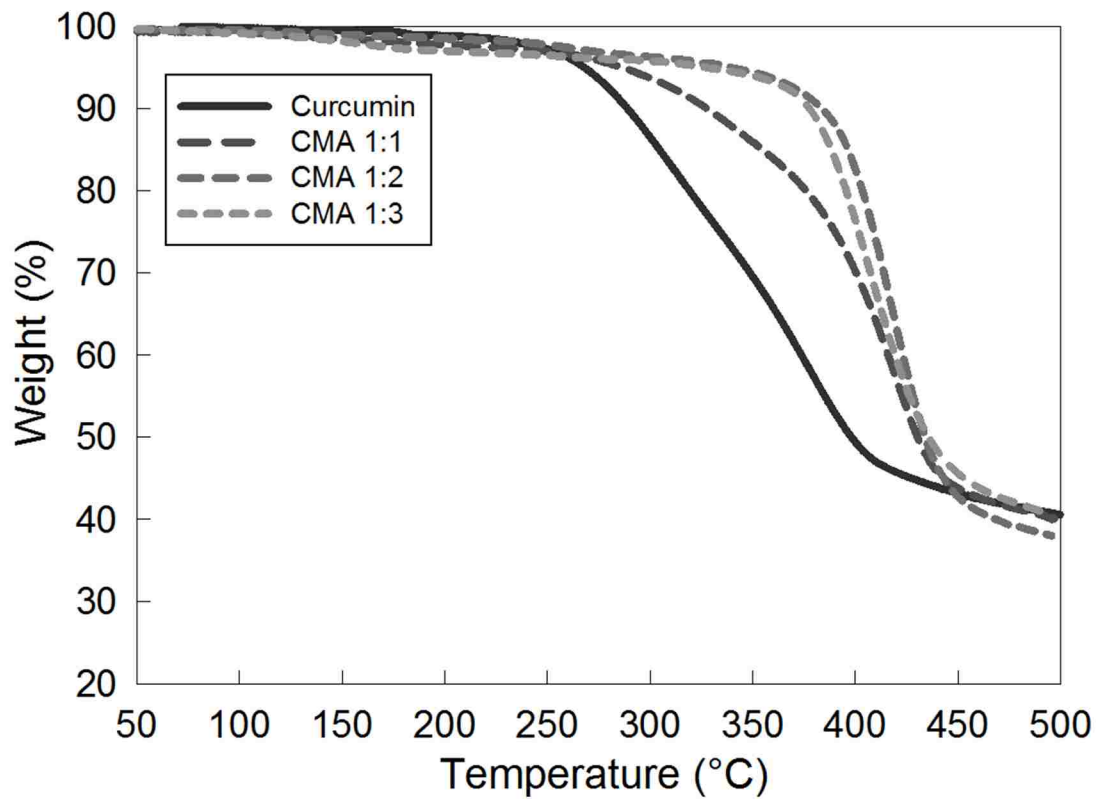


**Figure 3.13:** Thermogravimetric analysis (TGA) for curcumin and CMA synthesized with different curcumin:acryloyl chloride ratios.

## **Chapter 4: Static and dynamic properties of biodegradable poly(antioxidant $\beta$ -amino ester) networks based on incorporation of curcumin multiacrylate**

This chapter is based on the following published work:

Patil, V.S.; Dziubla, T.D.; Kalika, D.S. “ Static and dynamic properties of biodegradable poly(antioxidant  $\beta$ -amino ester) networks based on incorporation of curcumin multiacrylate”, *Polymer* 2015, 75, 88.

### **4.1 Introduction**

Biodegradable polymers have found use in a variety of biomedical applications including sutures, drug delivery, tissue engineering and orthopedic implants [54, 98]. As with all biomaterials, their use is dictated by the observed situational biocompatibility. In acute settings, this is largely determined by the inflammatory response. For instance, when surrounding macrophages become activated, either through bulk mechanical cues, surface response, or the degradation products of the implanted polymers, they will release a burst of superoxide anions and digestive enzymes which can lead to the loss of function of the biomedical device [164-166]. This results in the initiation of oxidative stress in the neighboring tissues, a condition where excess reactive oxygen species are produced, leading to the propagation of inflammation, apoptosis and cell death.

Acute oxidative stress can be eliminated by re-establishing the balance of oxidants and antioxidants, which can be achieved by increasing levels of antioxidants [6]. Antioxidants can scavenge free radicals or oxidative species and reduce them to stable molecules and thus suppress oxidative stress. Polymer conjugation of small molecule antioxidants has been used as a means of suppressing biomaterial induced oxidative stress

through long-term sustained release [167]. In this work, we have used curcumin, a potent naturally-derived dietary antioxidant, for the suppression of oxidative stress. Curcumin is a polyphenolic compound derived from the Indian spice turmeric and along with its antioxidant attributes, it is also known to have anti-tumor and anti-inflammatory properties [139, 168, 169] and has shown promising free radical scavenging capabilities [168]. Despite this potential, the use of curcumin is restricted by its poor solubility [126] and limited chemical stability: oxygen is known to cause curcumin degradation, and curcumin has also been shown to break down with mechanisms independent of oxygen in the presence of light, resulting in severe color fading of curcumin-coated tablets and solutions [142].

Recently, our laboratory has developed poly(antioxidant  $\beta$ -amino ester) (PA $\beta$ AE) hydrogels that incorporate polyphenolic antioxidants (e.g., quercetin, curcumin) as a way to suppress biomaterial associated inflammatory response and to increase antioxidant bioavailability [124]. These polymers are based upon the poly( $\beta$ -amino ester) (P $\beta$ AE) synthesis approach, which relies on the Michael addition reaction of amines to acrylates. The benefit of this chemistry over more traditional free radical acrylate polymerization is that the resulting ester bonds of the P $\beta$ AE polymers are sensitive to hydrolysis, allowing for controlled degradation and antioxidant release [170-172]. Advantages of PA $\beta$ AE chemistry within this context are: (i) it does not involve a free radical initiator which can be problematic when working with antioxidants; (ii) degradation products improve the overall solubility of the poorly soluble antioxidant compounds; (iii) the network can undergo controlled, pH-dependent degradation through hydrolysis of ester bonds; and (iv)

antioxidant stability is increased due to its incorporation in the PA $\beta$ AE three-dimensional network backbone structure.

In this Chapter, we report the influence of changes in curcumin content on the structure and thermomechanical properties of poly(curcumin  $\beta$ -amino ester) hydrogel networks, i.e. PC $\beta$ AE. PC $\beta$ AE networks of varying composition were studied with a goal of achieving tunable drug release properties with controlled release rates. Hydrophobic curcumin was covalently linked into the hydrogel networks using PA $\beta$ AE chemistry: each PC $\beta$ AE network was synthesized by reacting poly(ethylene glycol) diacrylate (PEGDA) with a primary diamine, 4,7,10-trioxa-1,13-tridecanediamine (TTD), in combination with acrylate-functionalized curcumin. The introduction of functionalized curcumin into the polymerization mixture has the potential to substantively change the intrinsic chemical composition of the resulting hydrogels and the topology and inherent flexibility of the networks, which are core material aspects that strongly influence the swelling and degradation response of the polymers and their bulk mechanical properties. In an effort to fully elucidate the relationships between antioxidant content, mechanical response and tunable release, the relaxation properties of the networks were studied by dynamic mechanical analysis and broadband dielectric spectroscopy. These spectroscopic techniques were employed to establish the glass-rubber and sub-glass relaxation characteristics of the gels as a function of antioxidant content, and to provide insight regarding the structure and overall crosslink density achieved in the networks as a function of reaction conditions.

## 4.2 Experimental

### 4.2.1 Materials

Curcumin used for the curcumin multiacrylate (CMA) synthesis was purchased from Chem-Impex International, Inc. Acryloyl chloride, 4,7,10-trioxa-1,13-tridecanediamine (TTD) and triethyl amine were all purchased from Sigma-Aldrich. Poly(ethylene glycol) 400 diacrylate (PEG400DA) was purchased from Polysciences. All organic solvents were purchased from Pharmco-AAPER and used as received.

### 4.2.2 Curcumin multiacrylate synthesis

Curcumin was functionalized with acrylate by reaction with acryloyl chloride to form curcumin multiacrylate using a method similar to that reported previously [124]; see **Figure 4.1**. Curcumin was dissolved in tetrahydrofuran (THF) at a concentration of 50 mg/mL. Triethylamine (TEA) was added at a 1:3 molar ratio of curcumin:TEA. Acryloyl chloride, at a 1:3 molar ratio of curcumin:acryloyl chloride, was slowly added to the solution using an addition funnel while the reaction mixture was stirred on an ice bath. The reaction was allowed to proceed for 16 hours at room temperature under dark conditions. The precipitated triethylammonium chloride salt was removed by vacuum filtration. THF from filtrate was evaporated under vacuum using a liquid N<sub>2</sub> trap. The recovered CMA mass was re-dissolved in dichloromethane (DCM) and subjected to multiple 0.1 M HCl and 0.1 M K<sub>2</sub>CO<sub>3</sub> washes to remove excess TEA and acryloyl chloride, respectively. The residual water was removed by adding magnesium sulfate salt. After filtration, DCM was removed by evaporation under vacuum using the liquid N<sub>2</sub> trap and the final product was obtained in powdered form. The curcumin multiacrylate synthesized via this method was characterized via Fourier transform infrared (FTIR) and <sup>1</sup>H-nuclear magnetic resonance

(NMR) spectroscopy, with detailed spectra reported by Wattamwar et al [124]. The CMA was further characterized using reverse-phase high-performance liquid chromatography (HPLC; Waters Phenomenex C18 Column, 5  $\mu\text{m}$ , 250 mm (length) x 4.6 mm (I.D.) on a Shimadzu Prominence LC-20 AB HPLC system). The column was maintained at 40°C. A gradient from 50/50 acetonitrile/water to 100/0 acetonitrile/water over 15 minutes at 1 mL/min flow rate was used for analysis of CMA. The wavelength used for detection was 420 nm, with all samples injected as 50  $\mu\text{l}$  injection volumes. In addition, independent liquid chromatography-mass spectrometry (LC/MS) studies were conducted to establish the molecular weight of the individual elution fractions. The LC/MS unit was comprised of a Shimadzu high-performance liquid chromatograph (HPLC) equipped with a ZORBAX Eclipse XDB-C18 column, coupled with an ABSciex 5600 “Triple TOF” hybrid quadrupole time of flight mass spectrometer [173].

#### 4.2.3 Synthesis of PC $\beta$ AE gel films

Crosslinked copolymer networks were synthesized via Michael addition with primary diamine (TTD) in anhydrous dichloromethane (DCM) as shown in **Figure 4.2**. DCM was added at a ratio of 1.5 ml of solvent per gram of total monomer weight, which facilitates heat dissipation when synthesizing PC $\beta$ AE with higher amounts of CMA. The molar ratio of CMA to PEG400DA was systematically varied, as shown in **Table 4.1**. The ratio of total acrylates to total amine hydrogens (RTAA) was fixed at 1.0 for all formulations, based on an assumed CMA functionality of two (i.e. diacrylate). The film synthesis process was as follows: half of the total solvent was mixed with CMA powder, while the remaining half was mixed with PEG400DA. TTD was added to the PEG400DA solution and the resulting mixture was kept at room temperature for 5 minutes. The CMA

solution was then added to the PEG400DA solution while mixing on a vortex mixer. The final reaction solution was poured into a casting ring assembly which was covered with a watch glass to control the solvent evaporation rate. The casting ring assembly was kept at room temperature for 1 hour and then transferred to a convection oven for 24 hours at 50°C. The resulting gels were washed in anhydrous acetonitrile for 5 hours with solvent change every hour to remove unreacted monomer and then dried under vacuum at 50°C. Films with thickness in the range of 100 microns to 300 microns were prepared.

#### **4.2.4 Swelling studies**

The swelling characteristics of the networks were measured in anhydrous acetonitrile. Each sample was kept in acetonitrile for 30 minutes to reach equilibrium swelling. Upon removal, excess solvent was removed from the surface and the sample was weighed immediately. The swelling ratio was calculated as the ratio of the equilibrium (swollen) weight,  $W_s$ , to the dry weight,  $W_d$ .

$$\text{Swelling ratio} = \frac{W_s}{W_d} \quad (1)$$

Three replicates were completed for each sample and values are reported with standard deviation.

#### **4.2.5 Degradation studies**

Degradation studies were performed in phosphate buffered solution (PBS) with 0.1% sodium dodecyl sulfate (SDS) at 37°C (7.4 pH). After each time point, supernatant was removed and the mass of swollen gel was measured; the gel was then transferred to a fresh reservoir of PBS. During the degradation of the gels, a point is reached where the

sample begins to lose mechanical integrity, making further handling impractical such that swelling ratio could not be measured. Degradation time was defined as the point where the gel had completely degraded and no solid gel could be detected even after centrifuging the sample at 10,000 rpm for 5 minutes. Three replicates were completed for each sample and values are reported with standard deviation.

#### **4.2.6 Dynamic Mechanical Analysis**

Dynamic mechanical analysis (DMA) experiments were performed using the TA Instruments Q800 dynamic mechanical analyzer operating in tensile geometry. Storage modulus ( $E'$ ) and loss tangent ( $\tan \delta$ ) were recorded at a heating rate of  $1^\circ\text{C}/\text{min}$  at 1 Hz. The temperature range was from  $-100^\circ\text{C}$  to  $150^\circ\text{C}$ . Test samples were in the form of strips with thickness of  $\sim 0.3$  mm, width 3 mm and length 20 mm. Samples were dried under vacuum at  $50^\circ\text{C}$  prior to measurement. All measurements were carried out under an inert ( $\text{N}_2$ ) atmosphere.

#### **4.2.7 Broadband Dielectric Spectroscopy**

Broadband dielectric spectroscopy (BDS) measurements were performed using a Novocontrol "Concept 40" broadband dielectric spectrometer (Hundsangen, Germany). Each sample was placed between aluminum foils and mounted between gold platens in the Novocontrol Quatro Cryosystem. Dielectric constant ( $\epsilon'$ ) and dielectric loss ( $\epsilon''$ ) were measured across a range of frequencies at fixed temperature (isothermal measurement mode). The frequency range was 1 Hz to 1.3 MHz, while the temperature range was  $-150^\circ\text{C}$  to  $100^\circ\text{C}$  (or  $150^\circ\text{C}$ ), with a  $5^\circ\text{C}$  interval. For BDS analysis, samples were prepared in the form of films with 22 mm diameter and thickness in the range of 150 to 200 microns. The

thickness of each sample was measured using a micrometer gauge with precision to  $\pm 1 \mu\text{m}$ . Samples were dried under vacuum at  $50^\circ\text{C}$  prior to measurement.

## 4.3 Results & discussions

### 4.3.1 Synthesis and characterization of CMA

Curcumin multiacrylate (CMA) was prepared according to the method detailed above and was characterized using HPLC. The HPLC plot for curcumin and the resulting CMA is shown in **Figure 4.3**. Commercially available curcumin contains two curcuminoids, desmethoxycurcumin and bis-desmethoxycurcumin, along with curcumin. This is reflected in a set of three peaks for curcumin at a retention time of  $7.5 \pm 0.5$  minutes. The curcumin peak is not seen in the HPLC plot of CMA, which implies that all curcumin has been functionalized. Since the acrylation of curcumin increases its hydrophobicity (and the HPLC column contains a hydrophobic stationary phase), it is expected that the curcumin acrylates will be eluted sequentially after the unmodified curcumin elution time point. The group of peaks located from 11 minutes to 14 minutes retention time corresponds to a mixture of curcumin multiacrylates, specifically curcumin monoacrylate, curcumin diacrylate and curcumin triacrylate. LC/MS measurements confirmed the molecular weight of these individual populations, with a minimal amount of monoacrylate indicated (less than 1%) and diacrylate and triacrylate species present in comparable proportion. This result is consistent with prior  $^1\text{H-NMR}$  studies indicating an average functionality of 2.66 acrylate groups per curcumin molecule for CMA synthesized under similar conditions [124]. Details of the full analysis are presented in reference [173].

### 4.3.2 Swelling characteristics

The measurement of network swelling ratio provides a convenient (indirect) characterization of crosslink density. Also, the mechanical strength of the crosslinked polymer is a sensitive function of crosslink density [174, 175]. The use of an organic solvent, such as acetonitrile, allows for determination of the network swelling response without simultaneously degrading the network, which is the case with aqueous media. PC $\beta$ AE swelling was characterized in anhydrous acetonitrile (aACN) for hydrogels incorporating varying ratios of CMA to PEG400DA in the pre-polymerization reaction mixture. Since the solubility of curcumin in ACN is lower than that of PEG400DA, from a compositional standpoint the swelling ratio would be expected to decrease as we increase curcumin content in the network. Simultaneously, from a structural point of view, curcumin is shorter and stiffer than the relatively long and flexible PEGDA segment. This should render the network stiffer and also lead to a decrease in the average distance between crosslinks (i.e., an increase in crosslink density). With an increase in crosslink density, we also expect the swelling ratio to decrease. However, as seen in the equilibrium swelling results shown in **Figure 4.4**, a maximum value of the equilibrium swelling ratio was obtained for the 30:70 gel, beyond which the swelling ratio progressively decreased with increasing curcumin content. The increase in swelling ratio with increasing curcumin (up to 30:70) suggests that a looser network is forming with the introduction of curcumin multiacrylate in the reaction mixture, resulting in a lower overall network crosslink density. This aspect of network formation was further explored via measurement of the rubbery modulus using dynamic mechanical analysis, as discussed below.

### 4.3.3 Aqueous degradation

The aqueous degradation profiles for different hydrogels are shown in **Figure 4.5a**. As the CMA:PEG400DA ratio was increased, network hydrophobicity increased. The effect of hydrophobicity can be seen from the swelling response in the aqueous phase, with the initial swelling increment in PBS decreasing with increasing CMA content (see **Figure 4.5b**). Inspection of Figure 4.5a shows that, in general, network degradation slows with increasing CMA content. The total degradation time for the hydrogel with CMA:PEG400DA molar ratio 0:100 was 3 hours, and increased to as much as 25 hours for the 90:10 gel (see inset table in Figure 4.5a). These degradation times are consistent with previous studies on PA $\beta$ AE networks comprised of PEG400DA and curcumin multiacrylates [124, 171]. For the 10:90 and 30:70 compositions, the degradation profiles are nearly identical, despite the nominally more hydrophobic character of the 30:70 network. This specific result likely reflects the somewhat looser character of the 30:70 network, as suggested by the ACN swelling measurements.

### 4.3.4 Dynamic mechanical analysis

While PC $\beta$ AE has been characterized from a functional point of view [124], little is known about its network properties. The network properties of hydrogels are important in determining potential biomedical applications, as these biomaterials need to have optimum mechanical characteristics for appropriate use. When used in tissue engineering applications, for example, it is necessary for the implant and surrounding native tissue to have a similar modulus while ensuring that the material has enough mechanical strength to survive *in vivo* and not deteriorate before desired function is achieved [176]. Also,

knowledge of the glass transition and mobility of the network is helpful in predicting the stability of these polymer systems at storage temperature or in application environments.

Dynamic mechanical results for all compositions from 0:100 to 90:10 CMA:PEG400DA are presented in **Figure 4.6**, with storage modulus ( $E'$ ) and  $\tan \delta$  plotted vs. temperature at 1 Hz. A strong, step-wise decrease in storage modulus is seen as the material goes from the glassy to the rubbery state, with an accompanying peak in  $\tan \delta$ . The glass transition temperature for the networks is offset to higher temperatures with increasing CMA content;  $T_{\alpha}$ , defined as the peak temperature in  $\tan \delta$  at 1 Hz, varies from  $-39^{\circ}\text{C}$  for the 0:100 film to  $67^{\circ}\text{C}$  for the 90:10 composition. The 0:100 network film displays a very narrow relaxation peak in  $\tan \delta$ , with a progressive broadening in the glass-rubber relaxation with increasing CMA content. For the 90:10 composition, a low-temperature shoulder is evident just below  $40^{\circ}\text{C}$ , suggesting the coexistence of PEGDA- and curcumin-rich phases within the network.

According to rubber elasticity theory, the rubbery modulus is proportional to the crosslink density of the polymer network [177]. With increasing CMA content, relatively long and flexible PEG chains are replaced with shorter and stiffer curcumin segments, such that a systematic increase in both network crosslink density and rubbery modulus could be reasonably anticipated. However, the storage modulus curves plotted in Figure 4.6a show an initial decrease in rubbery plateau modulus with CMA content, with a relative minimum in rubbery modulus observed for the 30:70 composition. Only at CMA:PEG400DA ratios beyond 50:50 does the trend in rubbery modulus reverse, with stiffer networks obtained at the highest curcumin contents. This outcome may be a reflection of steric impediments to network formation that are introduced by the presence of the stiffer curcumin moieties in

the emerging gels. For the fixed reaction conditions, this has the potential to result in lower overall extents of crosslinking. It is notable that the maximum in (ACN) swelling ratio that is observed for the 30:70 composition aligns directly with the measured minimum in rubbery modulus.

To further compare the characteristics of the homopolymer and copolymer networks, time-temperature superposition (TTS) was applied to the dynamic mechanical results for the 0:100 and 50:50 network compositions; modulus master curves were obtained and are plotted as  $E'$  vs.  $\omega a_T$  in **Figure 4.7**, where  $\omega$  is the applied test frequency and  $a_T$  is the dimensionless shift factor. In each case, the reference temperature was selected based on the peak maximum in  $\tan \delta$  at 1 Hz.

TTS curves for both compositions were fit using the Kohlrausch-Williams-Watts (KWW) “stretched exponential” relaxation time distribution function:

$$\phi(t) = \exp[-(t / \tau_o)^{\beta_{KWW}}] \quad (2)$$

where  $\tau_o$  is the network relaxation time and  $\beta_{KWW}$  is the distribution parameter [178].  $\beta_{KWW}$  ranges from 0 to 1, with values below unity reflecting relaxation broadening as compared to the single-relaxation time Debye response. The 0:100 homopolymer network could be described by a single KWW fit with a value of  $\beta_{KWW} = 0.31$ , which is comparable to the result obtained for similar PEG-based homopolymer networks [179]. Copolymerization with CMA results in a marked increase in glass-rubber relaxation breadth, with the 50:50 network relaxation corresponding to a distribution parameter,  $\beta_{KWW} = 0.12$ .

### 4.3.5 Broadband dielectric spectroscopy

Broadband dielectric spectroscopy is a powerful tool for the detection of relaxation mechanisms in polymers owing to its wide range of temperature and frequency combined with the ability to probe local dipolar motions which are not easily detected via dynamic mechanical analysis. In dielectric studies, the measured polarization response is comprised of instantaneous polarization, orientation polarization and interfacial polarization. The focus in this study is orientation polarization, as it is the basis for the detection of motional transitions. Interfacial (or electrode) polarization and conduction are generally observed at high temperatures and low frequencies (i.e., beyond the glass transition), with a strong increase in the dielectric constant and loss intensity [180].

Dielectric results for a representative 50:50 CMA:PEG400DA poly(curcumin  $\beta$ -amino ester) sample are plotted isochronally as dielectric constant and dielectric loss vs. temperature in **Figure 4.8**. In the dielectric constant plot, an incremental step change in  $\epsilon'$  is evident above  $-25^\circ\text{C}$  corresponding to polarization associated with the glass-rubber relaxation. Similarly, in the dielectric loss plot, a loss peak is present at the glass-rubber relaxation. Dielectric loss peaks associated with sub-glass relaxations in the sample are shown in the inset plot of dielectric loss for selected lower frequencies. PC $\beta$ AE hydrogels show three molecular relaxations with increasing temperature which have been designated as the  $\beta_1$ ,  $\beta_2$  and  $\alpha$  relaxations. The  $\beta_1$  and  $\beta_2$  relaxation processes correspond to local sub-glass transitions while the higher temperature  $\alpha$  relaxation corresponds to large-scale dipolar reorientations associated with the glass transition [181]. Each transition shifts to higher temperature with increasing measurement frequency.

#### 4.3.5.1 Analysis of the glass-rubber relaxation

The glass-rubber transition involves large-scale translational motions of polymer segments and associated dipoles leading to a distinct, step-change increase in dielectric constant,  $\Delta\varepsilon = \varepsilon_R - \varepsilon_U$ . The dielectric data for all samples were analyzed using the Havriliak–Negami (HN) modification of the single-relaxation time Debye expression to obtain the relaxation characteristics at each temperature; an expanded form of the Havriliak-Negami equation was used in order to remove the influence of conduction above the glass-rubber relaxation [182]:

$$\varepsilon^*(\omega) = \varepsilon_U + \frac{(\varepsilon_R - \varepsilon_U)}{\{1 + (i\omega\tau_{HN})^{\alpha_{HN}}\}^{\beta_{HN}}} - i \left( \frac{\sigma}{\varepsilon_o \omega} \right)^N \quad (3)$$

where  $\varepsilon_R$  is the relaxed dielectric constant (i.e., dielectric constant value as  $\omega \rightarrow 0$ ),  $\varepsilon_U$  is the unrelaxed dielectric constant (i.e., dielectric constant value as  $\omega \rightarrow \infty$ ),  $\tau_{HN}$  is the relaxation time,  $\alpha_{HN}$  and  $\beta_{HN}$  are the broadening and skewing parameters respectively,  $\sigma$  is the conductivity and  $\varepsilon_o$  is vacuum permittivity. For an ideal conduction process, N assumes a value of 1 [182, 183].

The WINFIT software package provided with the Novocontrol spectrometer was used to obtain HN best-fits for the dielectric loss vs. frequency data at each temperature. Representative HN fits of dielectric loss are shown for the glass-rubber (**Figure 4.9**) and sub-glass (**Figure 4.10**) transitions; the relaxation times ( $\tau_{MAX}$ ) associated with the peak maxima were extracted from the HN fits and related to the position of the frequency maximum for each temperature, with  $\tau_{MAX} = 1/\omega_{MAX} = (2\pi f_{MAX})^{-1}$ .

The frequency-temperature relation for the glass-rubber relaxation is shown via an Arrhenius plot in **Figure 4.11**, where  $\log(f_{\text{MAX}})$  is plotted vs.  $1000/T$  (K). For the range of accessible test frequencies, the data could be fit using the Williams-Landel-Ferry (WLF) relation across the glass transition [184]. The glass transition curves shift to higher temperatures as the level of curcumin incorporation is increased, consistent with the trend observed using dynamic mechanical analysis. PEG400DA is a relatively flexible component compared to CMA, and the presence of PEG imparts network flexibility. As the PEG400DA content is reduced, flexible PEG chains are replaced by the stiffer curcumin component, which leads to a reduction in network flexibility. This reduction in network flexibility means that higher temperatures are required for the chains to overcome the energy barriers inherent to long-range segmental motion, leading to an increase in the glass transition temperature.

#### 4.3.5.2 Analysis of sub-glass relaxations

PC $\beta$ AE shows two sub-glass transitions ( $\beta_1$  and  $\beta_2$ ) with increasing temperature. Isothermal dielectric data for each sub-glass transition were analyzed using the HN equation (Eq. 3). For the sub-glass transitions, satisfactory HN fits were obtained by setting the skewing parameter ( $\beta_{\text{HN}}$ ) equal to 1 (Figure 4.10). In **Figure 4.12**, dielectric loss data for the sub-glass transitions are presented for PC $\beta$ AE with different CMA:PEG400DA ratios. The data shown correspond to the mid-range of the sub-glass transition region ( $\sim 60^\circ\text{C}$ ) where both sub-glass transitions could be compared. For all network compositions, two overlapping sub-glass transitions were evident:  $\beta_1$  is on the high-frequency side (lower temperature sub-glass transition) while  $\beta_2$  is on the low-frequency side (higher temperature sub-glass transition). It can be observed from Figure 4.10 that peak positions for the sub-

glass transitions shift minimally relative to the 0:100 film, which contains only ethylene oxide units. This suggests that the sub-glass transitions originate solely due to the local motion of ethylene oxide moieties: as the proportion of PEG400DA in the network decreases, the intensities of the sub-glass transitions also decrease due to the reduced ethylene oxide content. The presence of curcumin does not appear to affect the position of the sub-glass relaxations, suggesting that the curcumin moiety is not participating in the measured sub-glass processes. This likely is a reflection of the relatively bulky character of curcumin and the substantial energy barrier associated with localized motions of the curcumin moiety along the chain backbone. In prior publications, both crystalline poly(ethylene oxide) (PEO) and UV-crosslinked PEGDA were reported to have two sub-glass transitions which originate from similar dipolar motions [181, 185, 186]. In these previous studies, it was hypothesized that the  $\beta_1$  relaxation originates from local motions of the ethylene oxide moieties occurring far from the crystal surface or crosslink junctions, whereas the  $\beta_2$  process reflects more constrained motions originating in the vicinity of the crystals/crosslinks.

The Arrhenius data for the sub-glass transitions are shown in Figure 9. There is minimal variation in the position of the sub-glass transitions with network composition, with each relaxation defined by a common activation energy. For  $\beta_1$ , the activation energy is 40 kJ/mol and for  $\beta_2$ , it is higher with a value of 52 kJ/mol, consistent with prior studies [181].

#### **4.4 Conclusions**

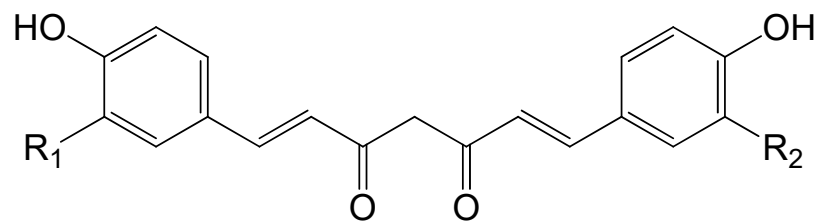
The incorporation of curcumin in PA $\beta$ AE hydrogels was achieved using a one-step method based on a Michael addition reaction. A series of PC $\beta$ AE films was synthesized by

varying the relative proportion of curcumin multiacrylate in the reaction mixture using an improved film synthesis protocol based on ring casting with in-situ polymerization. This protocol allowed preparation of PC $\beta$ AE hydrogels with reproducible degradation and thermomechanical properties. Curcumin, by its rigid character, alters the flexibility and architecture of the network, which then affects the degradation and release profile. Overall degradation times ranging from 3 hours to 25 hours were obtained by varying the CMA composition. An increase in curcumin content in the networks resulted in an increase in the glass transition temperature, as measured by dynamic mechanical analysis and broadband dielectric spectroscopy, owing to the replacement of long and flexible PEG chains with the shorter and more rigid curcumin moiety. Dielectric spectroscopy measurements indicated three relaxation processes in the PC $\beta$ AE networks: two sub-glass relaxations ( $\beta_1$  &  $\beta_2$ ) and the glass-rubber ( $\alpha$ ) relaxation with increasing temperature. The sub-glass relaxations originated from the localized motion of ethylene oxide units, consistent with previous studies on PEG-based networks. It was demonstrated that network hydrophilicity, crosslink density, and overall flexibility could all be modified directly by variations in curcumin content as a basis by which to control the degradation properties of the resulting materials.

**Table 4.1:** Compositions of synthesized poly(curcumin  $\beta$  amino esters).

CMA:PEG400DA (molar ratio)	mole %		
	CMA	PEG400DA	TTD
0:100	0.00	66.67	33.33
10:90	6.67	60.00	33.33
30:70	20.00	46.67	33.33
50:50	33.33	33.33	33.33
70:30	46.67	20.00	33.33
90:10	60.00	6.67	33.33

[A]



[B]

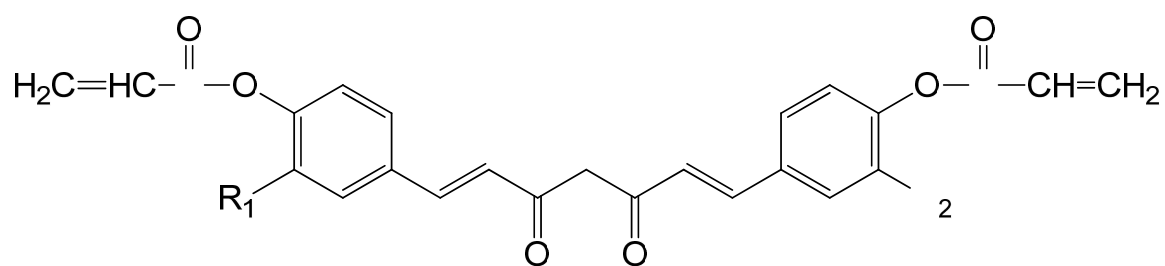


**Figure 4.1:** Chemical structure of curcumin [A] and acrylate-functionalized curcumin (diacrylate form) [B]. R<sub>1</sub> and R<sub>2</sub> can be either H or OCH<sub>3</sub>.

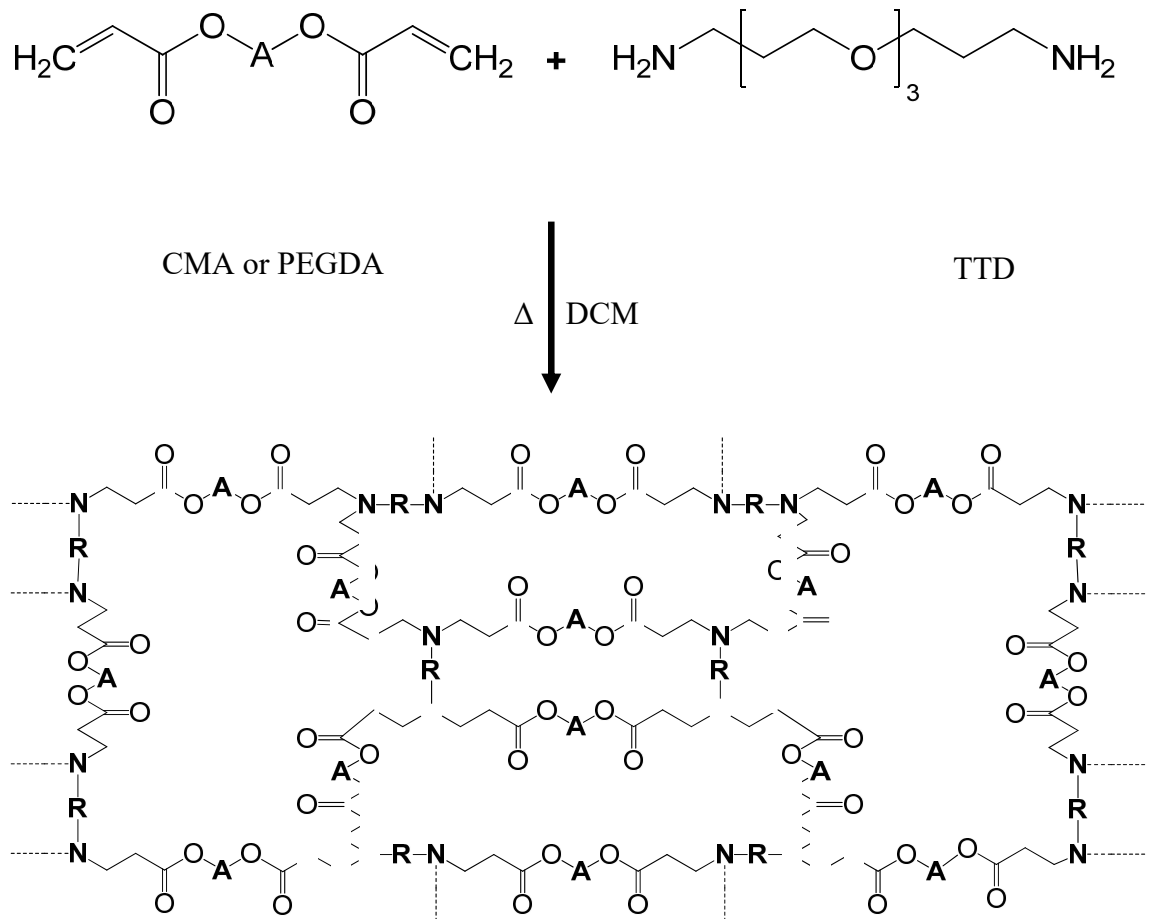


**Figure 4.2:** Simplified schematic for synthesis of PAβAE hydrogel.

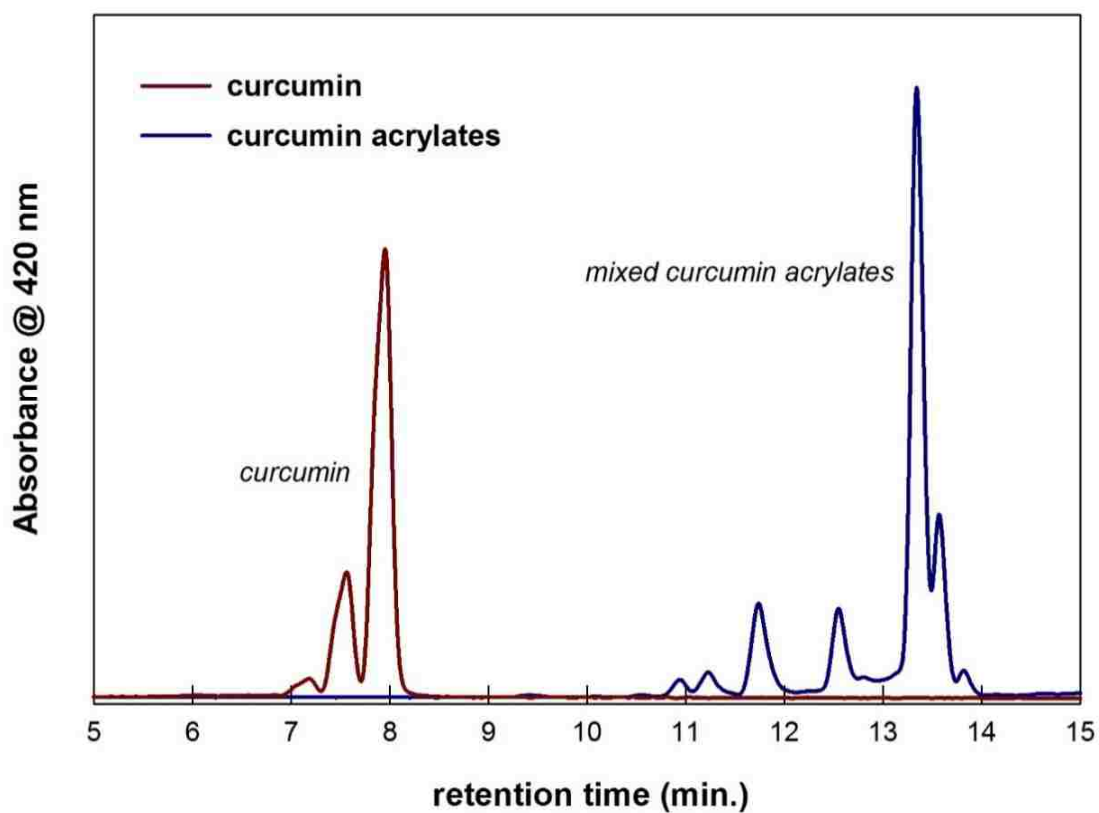


**Figure 4.3:** HPLC comparison plot for curcumin and curcumin multiacrylate at 420 nm.

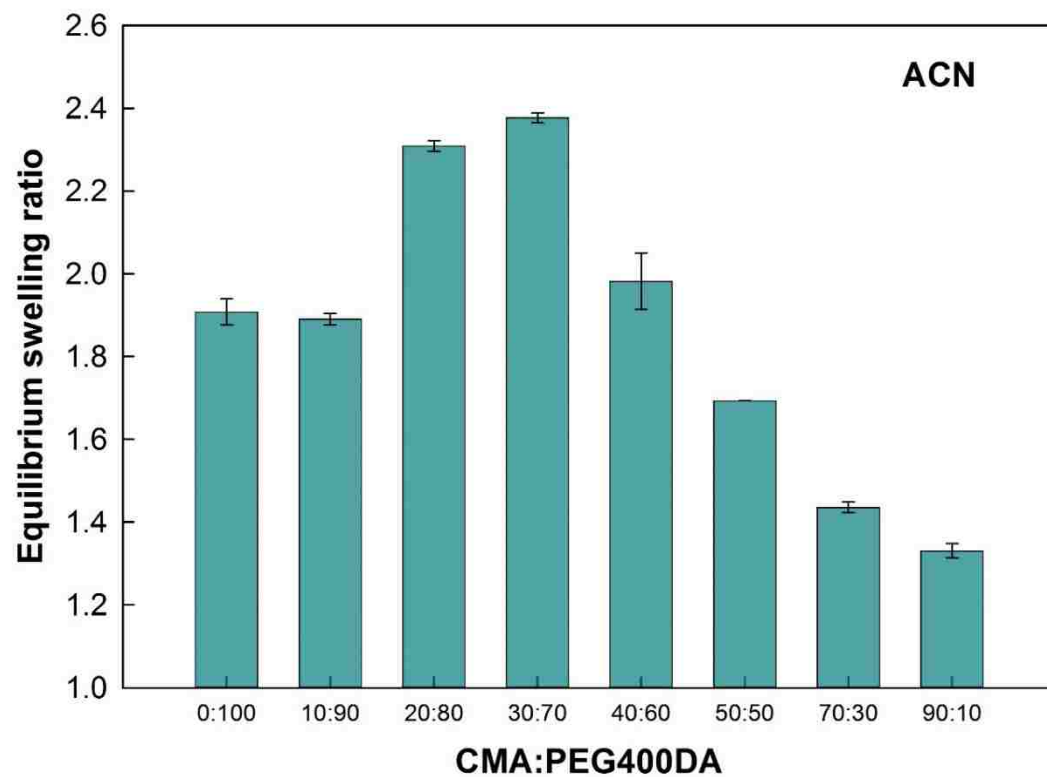


**Figure 4.4:** Swelling ratio in ACN for CMA:PEG400DA PC $\beta$ AE hydrogels.

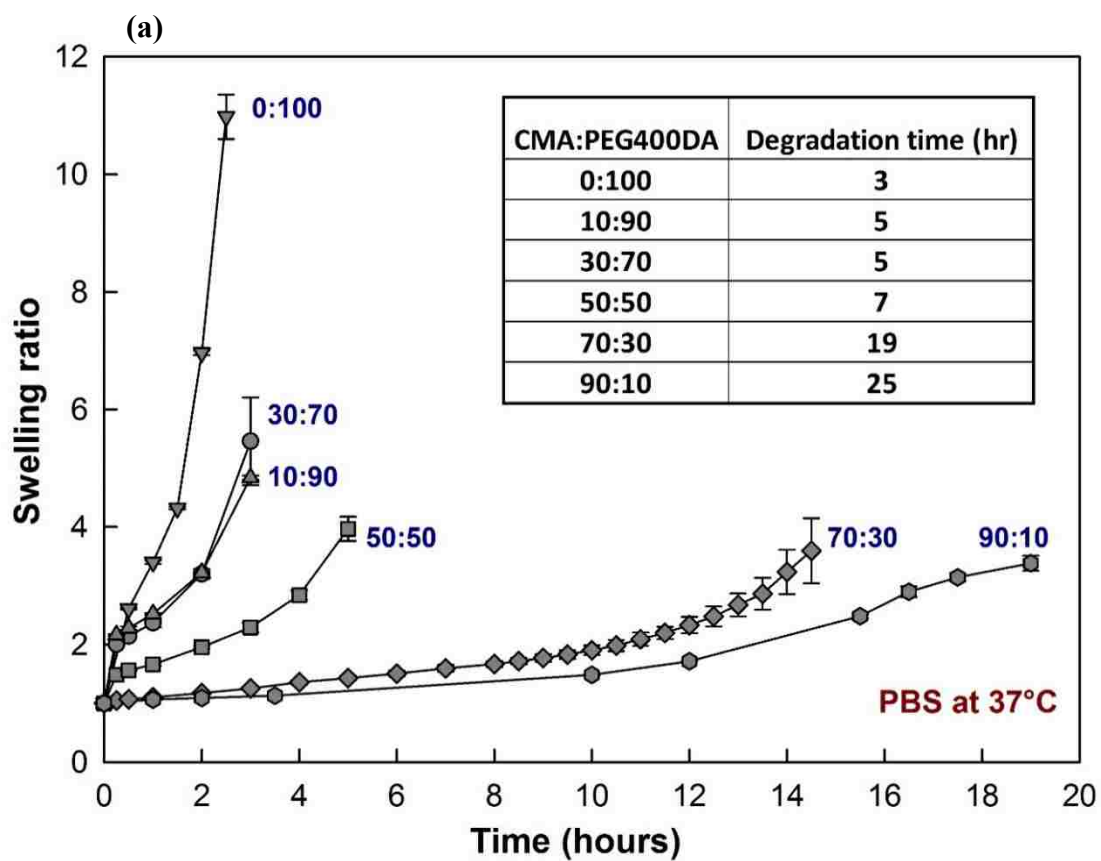


**Figure 4.5:** PC $\beta$ AE degradation in PBS at 37°C. (a) Swelling ratio vs. time for PC $\beta$ AE degradation. Inset table shows the total degradation time for each film. (b) Initial swelling ratio for CMA:PEG400DA PC $\beta$ AE hydrogels.

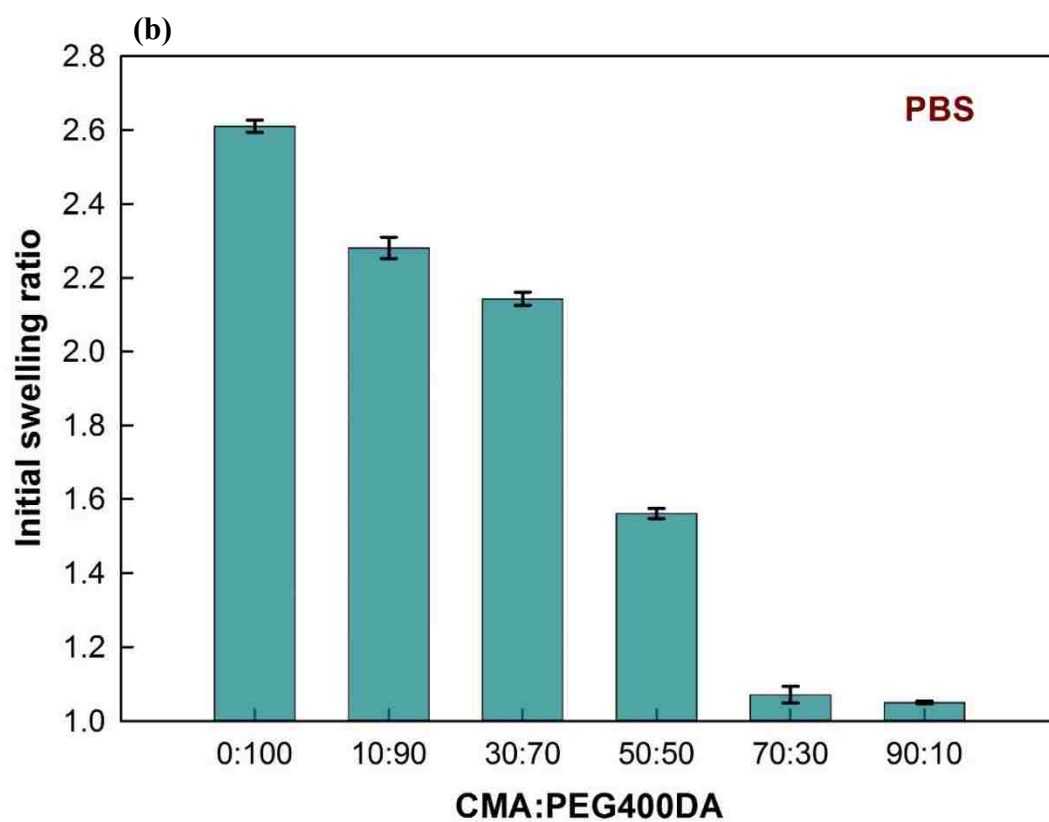


**Figure 4.5:** PC $\beta$ AE degradation in PBS at 37°C. (a) Swelling ratio vs. time for PC $\beta$ AE degradation. Inset table shows the total degradation time for each film. (b) Initial swelling ratio for CMA:PEG400DA PC $\beta$ AE hydrogels.

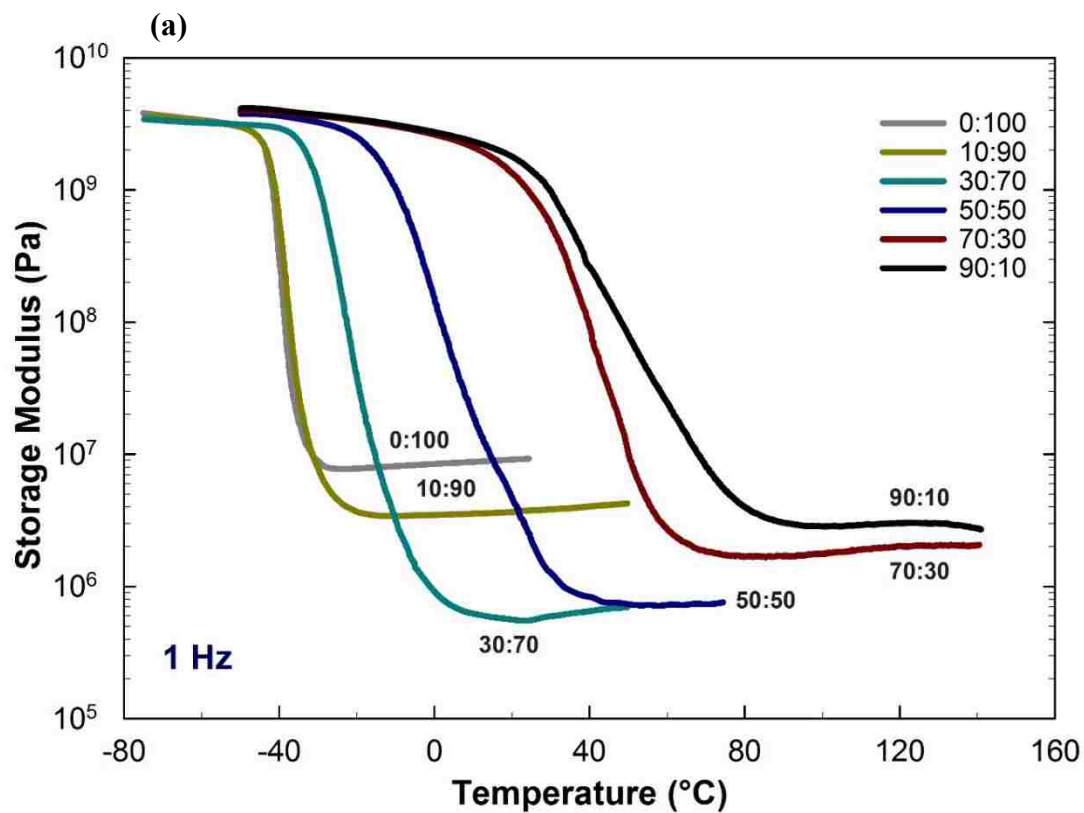


**Figure 4.6:** Dynamic mechanical properties of PCBAE films synthesized using different CMA:PEG400DA molar ratios. (a) Storage modulus (Pa) vs. temperature (°C) at 1 Hz. (b) Tan  $\delta$  vs. temperature (°C) at 1 Hz.

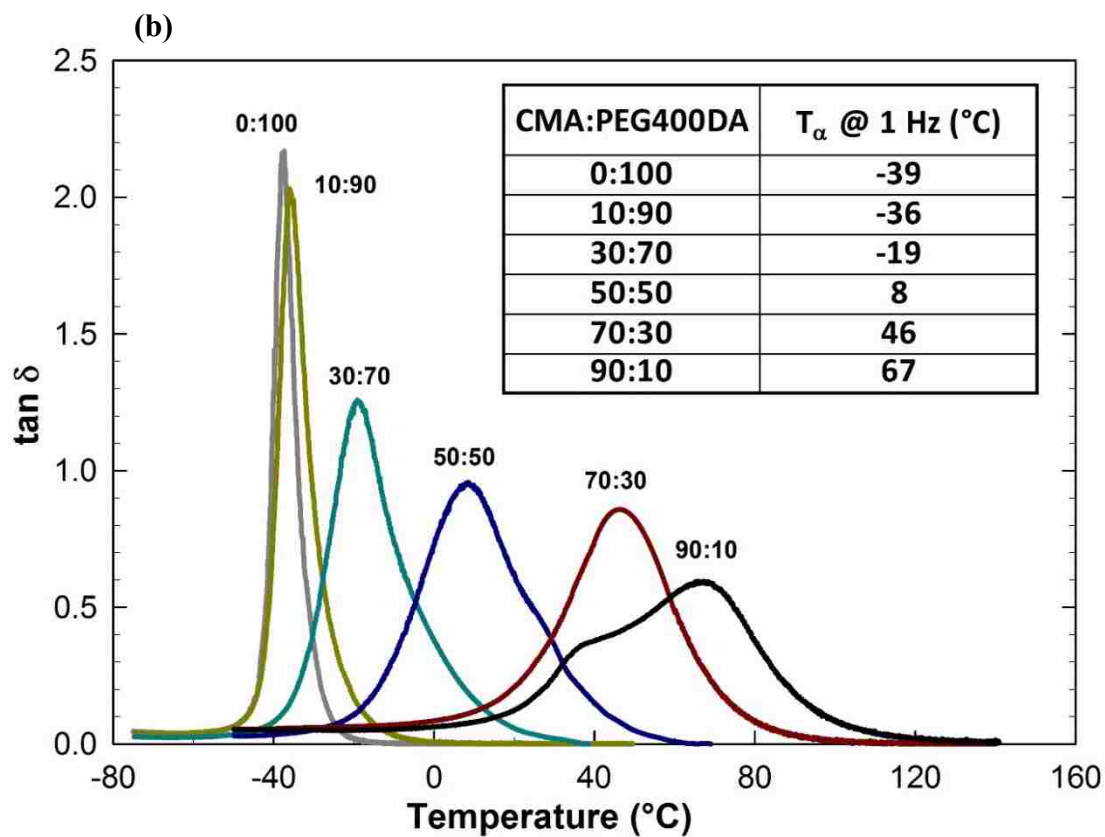


**Figure 4.6:** Dynamic mechanical properties of PCBAE films synthesized using different CMA:PEG400DA molar ratios. (a) Storage modulus (Pa) vs. temperature ( $^{\circ}\text{C}$ ) at 1 Hz. (b) Tan  $\delta$  vs. temperature ( $^{\circ}\text{C}$ ) at 1 Hz.

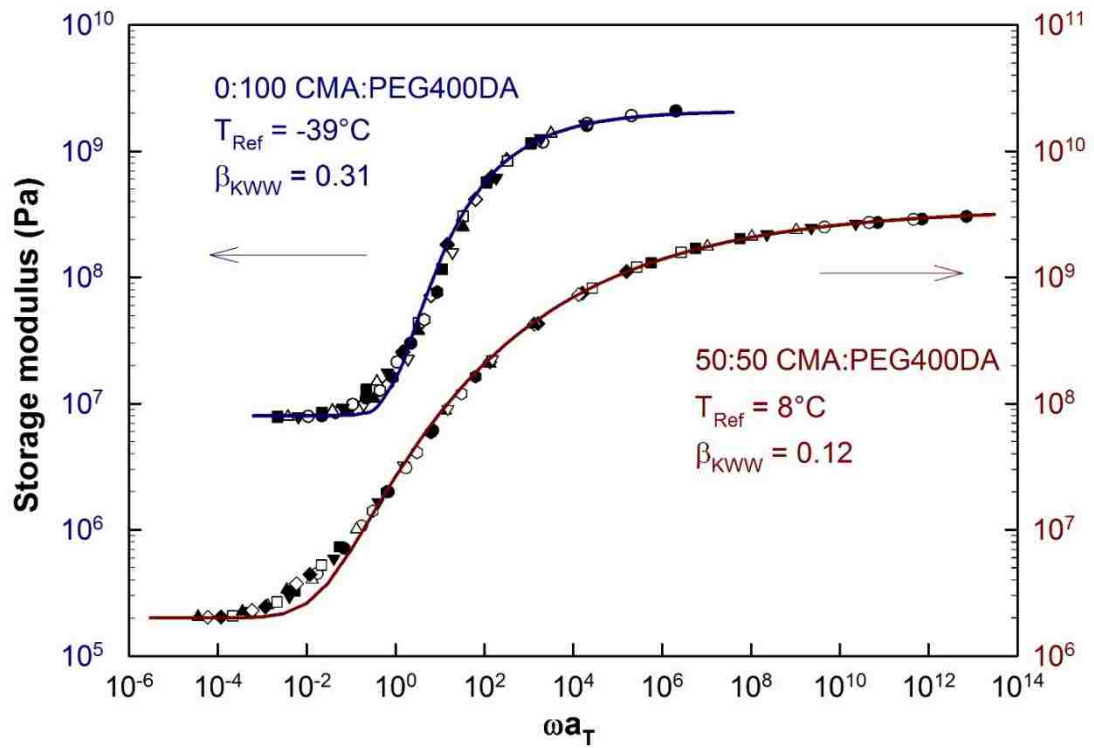


**Figure 4.7:** Time-temperature superposition results for 0:100 and 50:50 CMA:PEG400DA. Solid curves are KWW best-fits. 50:50 result is shifted downward by one decade for clarity (re: right axis).

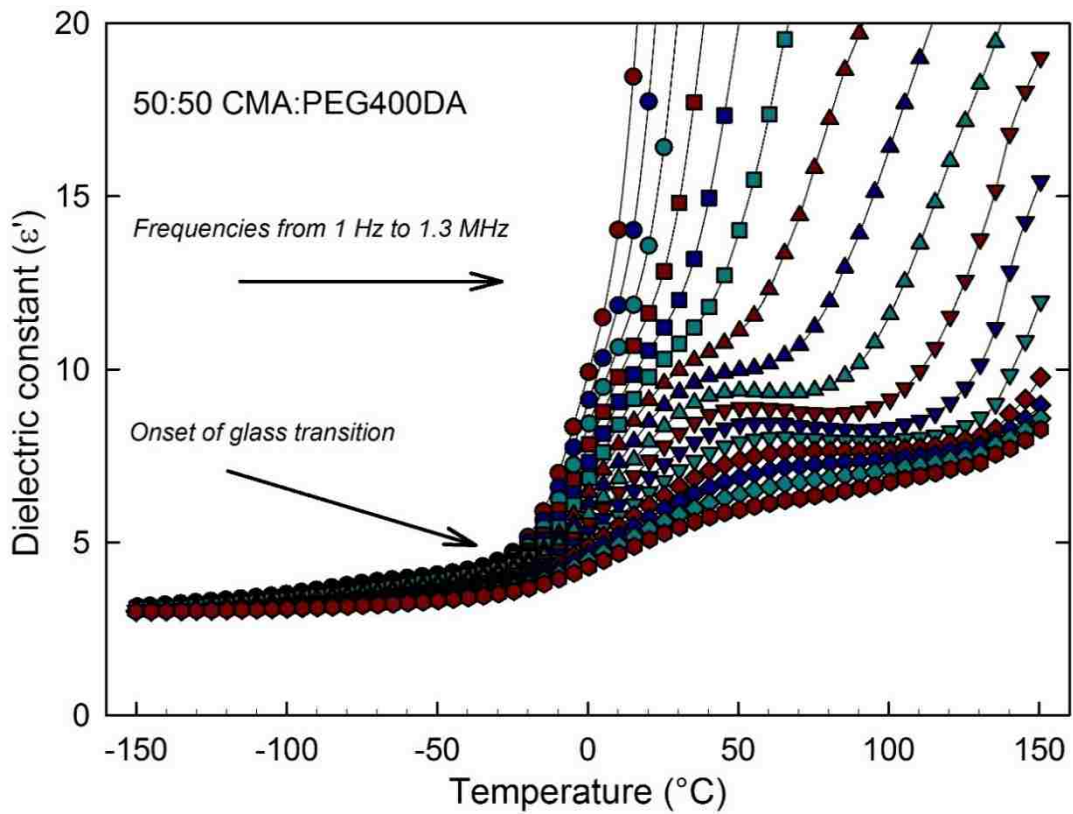


**Figure 4.8:** Dielectric response for 50:50 CMA:PEG400DA network. (a) Dielectric constant ( $\epsilon'$ ) vs. temperature ( $^{\circ}\text{C}$ ); frequencies from 1 Hz to 1.3 MHz. (b) Dielectric loss ( $\epsilon''$ ) vs. temperature ( $^{\circ}\text{C}$ ); frequencies from 1 Hz to 1.3 MHz. Inset plot shows sub-glass transitions for 1, 11, and 110 Hz.

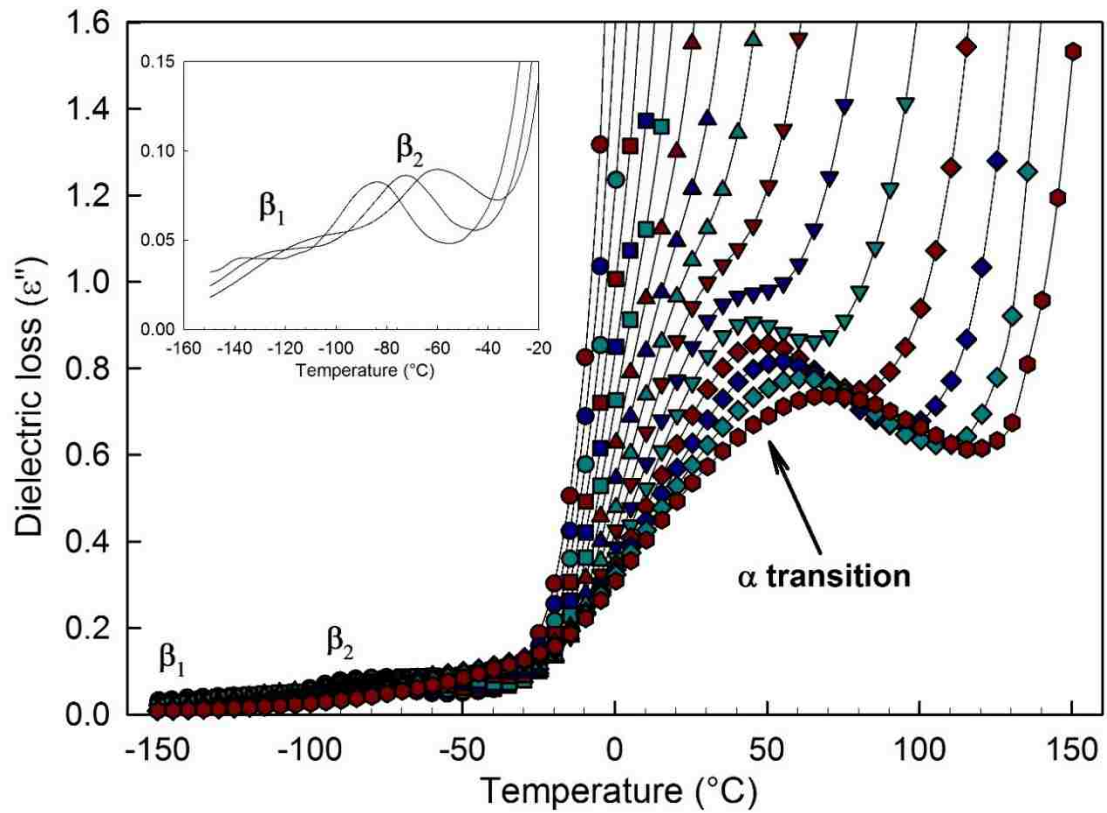


**Figure 4.8:** Dielectric response for 50:50 CMA:PEG400DA network. (a) Dielectric constant ( $\epsilon'$ ) vs. temperature ( $^{\circ}\text{C}$ ); frequencies from 1 Hz to 1.3 MHz. (b) Dielectric loss ( $\epsilon''$ ) vs. temperature ( $^{\circ}\text{C}$ ); frequencies from 1 Hz to 1.3 MHz. Inset plot shows sub-glass transitions for 1, 11, and 110 Hz.

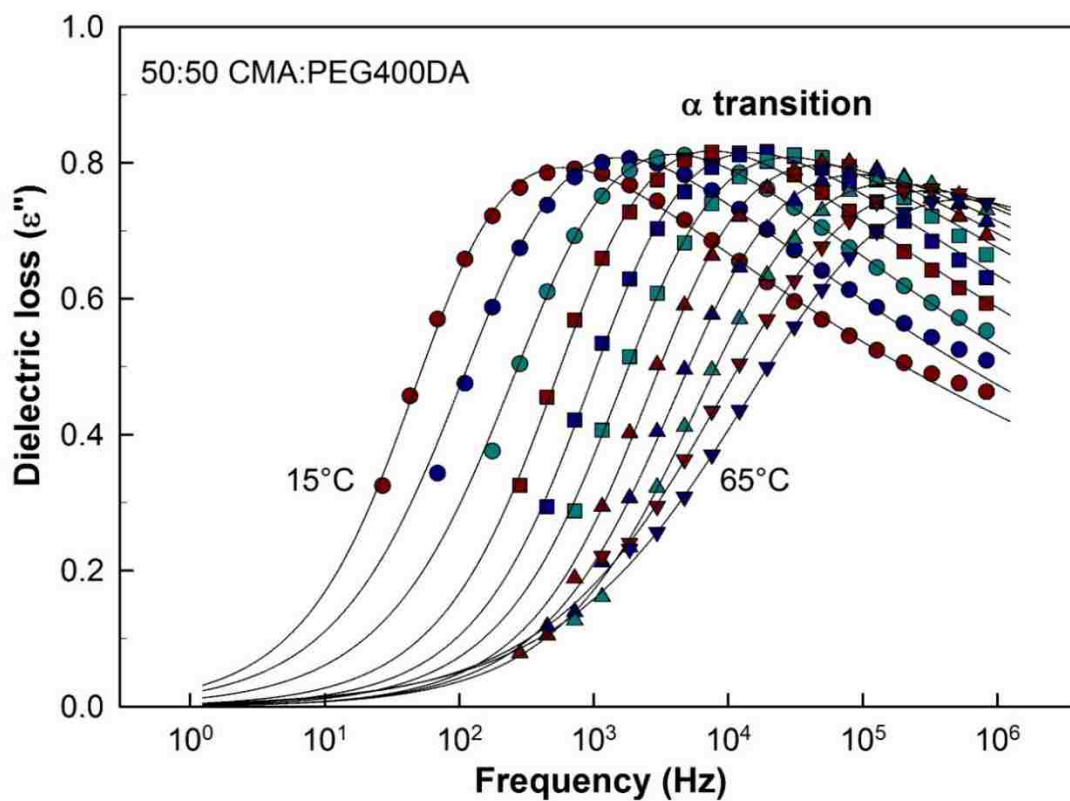


**Figure 4.9:** Dielectric loss ( $\epsilon''$ ) vs. frequency (Hz) in the vicinity of the glass transition for 50:50 CMA:PEG400DA; temperatures from 15°C to 65°C at 5°C intervals. Data are corrected for conduction according to equation 3. Solid curves are HN fits.

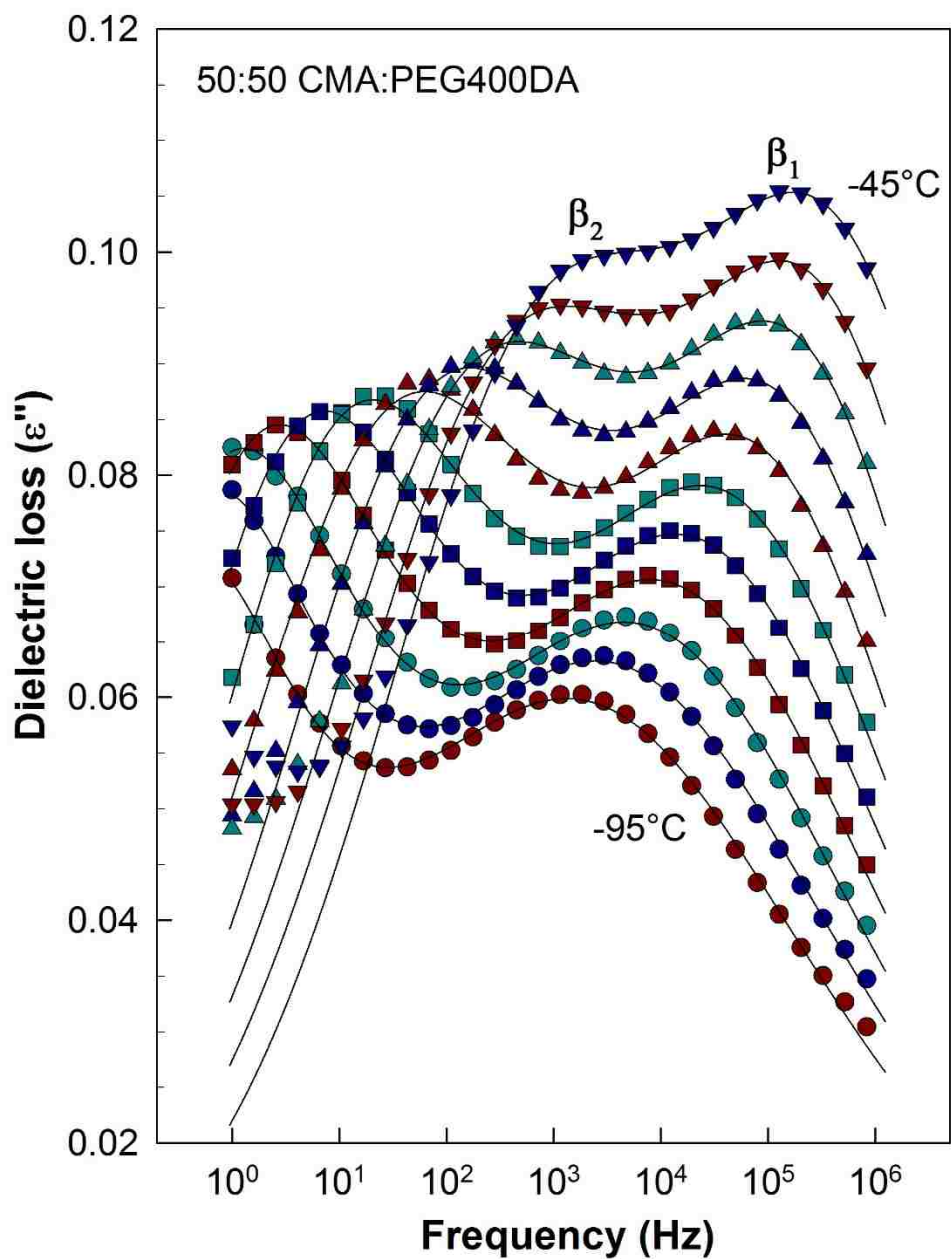


**Figure 4.10:** Dielectric loss ( $\epsilon''$ ) vs. frequency (Hz) for 50:50 CMA:PEG400DA sub-glass transitions; temperatures from  $-95^\circ\text{C}$  to  $-45^\circ\text{C}$  at  $5^\circ\text{C}$  intervals. Solid curves are HN fits.

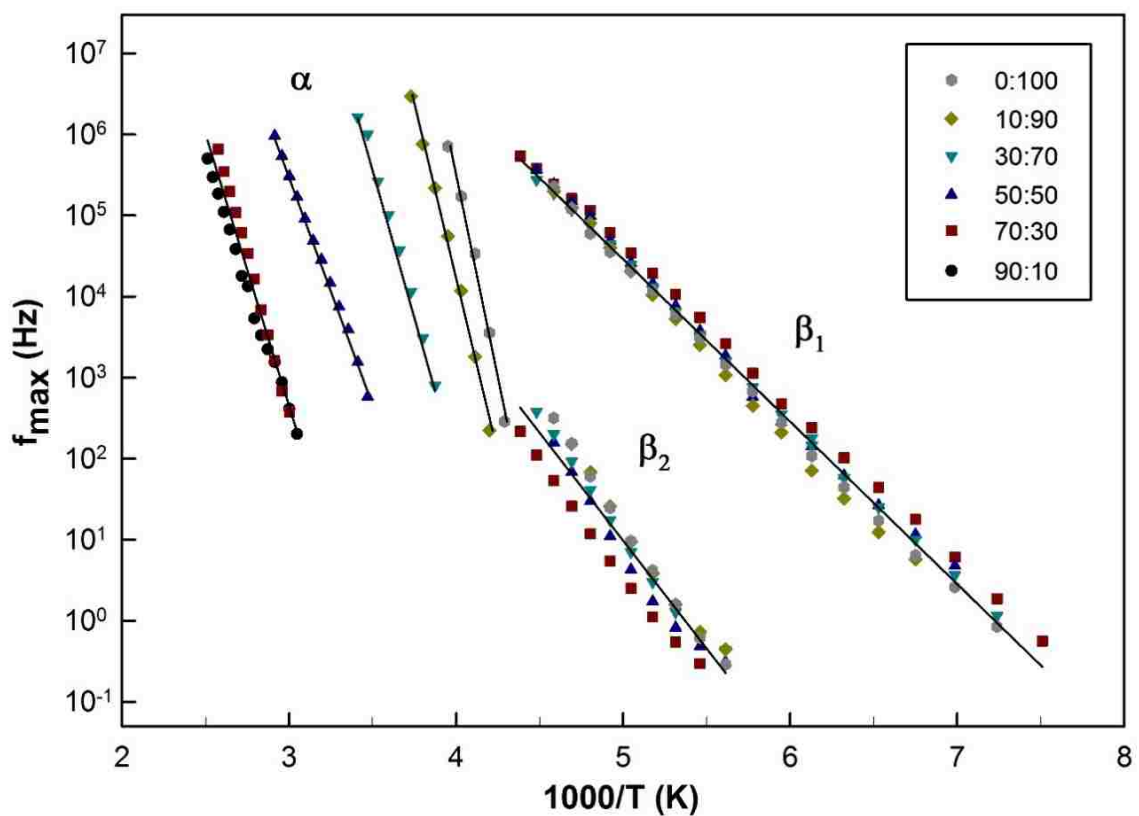


**Figure 4.11:** Arrhenius plot of  $f_{\max}$  (Hz) vs.  $1000/T$  (K) for PC $\beta$ AE hydrogels with different CMA:PEG400DA molar ratios.

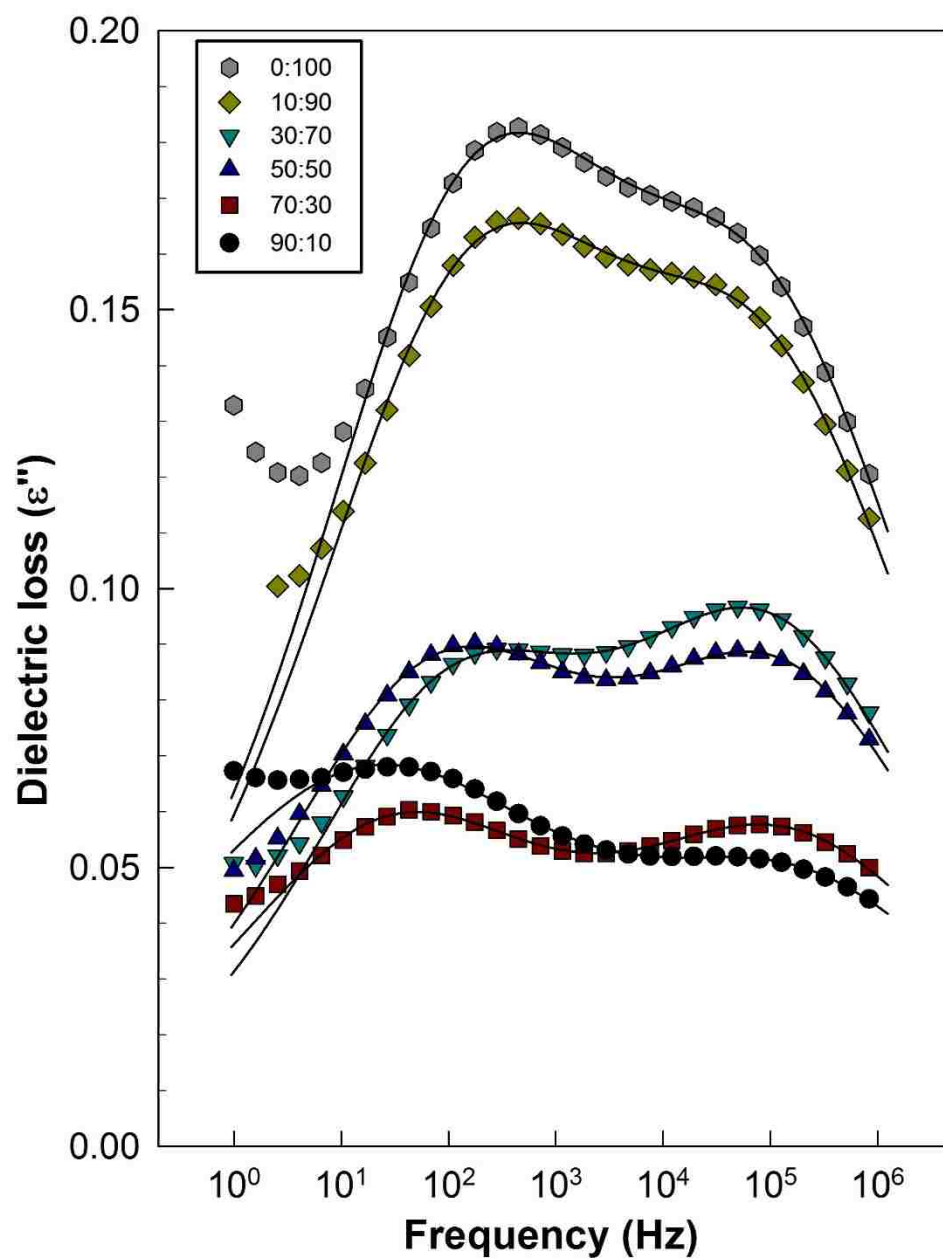


**Figure 4.12:** Dielectric loss ( $\epsilon''$ ) vs. frequency (Hz) at  $-60^\circ\text{C}$  for PC $\beta$ AE hydrogels with different CMA:PEG400DA molar ratios. Solid curves are HN fits.

**Chapter 5: Influence of ratio of total acrylate to amine (RTAA) and monomer selection on network and degradation properties of poly(curcumin  $\beta$ -amino ester) (PCBAE)**

## **5.1 Introduction**

Hydrogels have been used for drug delivery, tissue regeneration, orthopedic implants, contact lenses, and biosensors due to their high water intake capability, biocompatibility and mechanical properties that can be tuned to match those of biological tissue [106, 187-189]. Among biodegradable hydrogels, poly( $\beta$ -amino esters) (PBAE) have gained interest for drug delivery and biomedical applications [121, 190-192]. PBAEs have been used for delivery of small molecules as well as macromolecules such as proteins and peptides using standard encapsulation techniques with wide drug release times ranging from hours to months [122, 156, 193-200]. The mechanical properties of PBAEs can also be adjusted to match the mechanical properties of tissue, which is crucial in tissue engineering applications [115, 201]. PBAE, which is subject to hydrolytic degradation, is advantageous when used as a bioimplant or depot for drug delivery or orthopedic applications, since no removal surgery is required. PBAE has been shown to be biocompatible, as evidenced from its low cytotoxicity, as well as the low cytotoxicity of its degradation products [202-204].

While encapsulation of drugs in PBAE networks has been widely studied, covalent incorporation of a drug in the PBAE network as a part of the polymer backbone has only recently been explored. PBAE networks containing antioxidants such as curcumin, quercetin and apigenin have been developed with promising results for suppressing the

oxidative stress caused by copper oxide and iron oxide nanoparticles, as well as for the protection of mitochondria against oxidative stress [124, 133, 152, 204, 205]. Incorporation of antioxidants in the PBAE network offers advantages towards improving stability, bio-availability of the drugs and targeted drug delivery. In our prior work, we explored the tuning of network and functional properties of poly(curcumin  $\beta$ -amino esters) with varying curcumin composition [69]. Curcumin is a major component of the Indian spice turmeric, which has antioxidant and anti-inflammatory properties. Antioxidant delivery is one of the approaches used for reduction of oxidative stress, which is a cause or an effect of various conditions such as Parkinson's disease, Alzheimer's disease, ischemia reperfusion injury, cancer, and also cardiovascular diseases [3, 4, 45, 46]. However, low solubility and instability of antioxidants limit their applications. This necessitates the development of efficient antioxidant delivery systems to overcome the pathological conditions related to oxidative stress. Even though curcumin has displayed various advantageous properties, its application has been limited by its photo-instability and low aqueous solubility caused by its hydrophobic and crystalline character [206, 207]. Incorporation of curcumin into an amorphous PBAE polymer network improves its stability by reducing the mobility of labile groups and also limits the access of reactive agents to these labile groups. This approach has been shown to improve the dissolution of curcumin, which is believed to be a result of its incorporation into a fully degradable amorphous solid and by the solubility enhancements that result from the presence of co-degradation products. In this work, acrylate functionalized curcumin along with a commercial poly(ethylene glycol) diacrylate was reacted with a primary diamine to form poly(curcumin  $\beta$ -amino ester) (PCBAE) through a Michael-type conjugate addition reaction. The impact of independent parameters

such as the specific amines and diacrylates used in the reaction, curcumin composition, and the ratio of total acrylate to amine on the functional properties of PCBAE was investigated. The understanding of these process parameters is vital in being able to tune the PCBAE properties to a desired application. A systematic study of thermomechanical properties, degradation and curcumin release of PCBAE as a function of these independent parameters is presented. Thermomechanical properties were investigated using dynamic mechanical analysis, while degradation and curcumin release were measured via swelling response and UV-Vis spectrophotometry, respectively.

## **5.2 Experimental**

### **5.2.1 Materials**

Curcumin was purchased from Chem-Impex and used as received. Acryloyl chloride, triethyl amine (TEA), poly(ethylene glycol) 576 diacrylate (PEG576DA), poly(ethylene glycol) 400 diacrylate (PEG400DA), diethylene glycol diacrylate (DEGDA), 4,7,10-trioxa-1,13-tridecanediamine (TTD), 2,2'(ethylenedioxy) bis ethylamine (EDBE) and hexamethylene diamine (HMD) were all purchased from Sigma-Aldrich. Tetrahydrofuran (THF), dichloromethane (DCM) and acetonitrile (ACN) were all purchased from Pharmco-AAPER. Molecular sieves were added to all solvents to remove any trace moisture.

### **5.2.2 Gel synthesis**

The hydrogels were synthesized through a Michael-addition based step polymerization reaction between a primary diamine and curcumin multiacrylate (CMA) in combination with a commercial diacrylate in anhydrous DCM as solvent. The amount of DCM used was in the ratio of 1.5 mL of solvent per gram of total monomer weight. A ratio

of total acrylate to total amine (RTAA) was selected according to the gel to be synthesized. (Note: A diacrylate molecule has two total acrylates, while a primary diamine has four total amines, so two moles of diacrylate with one mole of primary amine would have a RTAA value of 1.0). CMA used for the gel synthesis had approximately 2.8 acrylate groups per molecule of curcumin [173]. The gel synthesis protocol involved dissolving CMA in half of the total solvent required and dissolving commercial diacrylate, i.e. PEG576DA, PEG400DA or DEGDA in the remaining half of the solvent. Amine was added to the commercial diacrylate solution and allowed to react for 5 minutes at room temperature. The CMA solution was added to this mixture while mixing on a vortex mixer. The reaction solution was then transferred to a casting ring kept on a glass plate covered with a teflon sheet. The ring was covered with a watch glass to provide controlled evaporation of the solvent. The reaction mixture was allowed to react at room temperature for an hour and then kept in a convection oven at 50°C for 24 hours. To create films with uniform thickness, the assembly was kept on a level platform during the entire synthesis. The resulting gels were washed in ACN for 5 hours by changing the solvent every hour. The gels were dried overnight in a vacuum oven at 50°C followed by drying at 100°C for an hour. The synthesized gels had an average thickness of 350 microns. Unless specified, monomers used for synthesis of PCBAE hydrogels were PEG400DA and TTD along with CMA at a RTAA value of 1.0.

### **5.2.3 Dynamic mechanical analysis (DMA)**

The thermomechanical properties of the hydrogel samples were measured using a TA Instruments Q800 dynamic mechanical analyzer operating in tensile geometry. The samples were cut into a rectangular geometry and had approximate dimensions of 30 mm

x 3 mm x 0.35 mm (length x width x thickness). The samples were dried under vacuum at 50°C prior to measurement. Storage modulus ( $E'$ ) and loss tangent ( $\tan \delta$ ) values were measured as a function of temperature at a heating rate of 1°C/min at 1 Hz under an inert nitrogen flow. The temperature range was from -75°C to 140°C.

#### **5.2.4 Degradation**

The hydrogels were cut to an appropriate size for the degradation studies. The degradation of hydrogels was performed in a phosphate buffered saline (PBS) solution with 0.1% sodium dodecyl sulfate (SDS) at 37°C (7.4 pH) in a United States Pharmacopeia (USP) dissolution apparatus II (VanKel VK 700). The degradation of the gels was monitored through the swelling ratio and curcumin release profile. At each time point, gel was taken out of the dissolution apparatus; the excess water was removed from the gel by blotting with Kimwipe®, and the weight of gel was measured. The swelling ratio was expressed as the ratio of weight of gel at time  $t$ ,  $W_t$ , and weight of gel before degradation i.e., dry weight,  $W_d$ .

As each gel degraded, it reached a point where it began losing mechanical integrity, making further handling unfeasible such that swelling ratio could not be measured. Degradation time was defined as the point where the gel had degraded completely and no solid gel could be seen even after centrifuging at 10,000 rpm for 5 min. A 1 mL supernatant was collected at each time point during the degradation of the curcumin containing gels, and stored at -20°C until further analysis. All the degradation studies were done with  $n=3$  and values are reported with standard deviation. All the supernatants collected during the degradation of hydrogel films were analyzed by UV-Visible spectrophotometry (Cary® 50 UV spectrophotometer).

### 5.2.5 Trolox equivalent antioxidant capacity (TEAC)

The antioxidant activity of curcumin released during the degradation was evaluated by running a standard colorimetric assay, viz., trolox equivalent antioxidant capacity (TEAC) assay. 2,2'-azinobis-(3-ethylbenzothiazoline-6-sulfonate) (ABTS) cation radical solution was prepared by reacting ABTS and potassium persulfate overnight under dark conditions. The absorbance intensity of the cation radical solution was decreased to 0.4 by dilution with PBS. Using a 96-well microplate, 10  $\mu$ L of sample to be analyzed was introduced to each well followed by 200  $\mu$ L of cation radical solution. The absorbance was measured after 5 minutes at 734 nm and compared against the standard trolox curve.

## 5.3 Results and discussion

### 5.3.1 Amine crosslinker

One of the main factors that can affect the properties of crosslinked polymer networks is the crosslinker, which in the current study is amine. Amine crosslinker characteristics that can change the network properties are amine chain length and its hydrophilicity. For instance, an amine with shorter chain length can increase the crosslink density and the glass transition temperature of the network, which can lead to an increase in its degradation time. Additionally, a decrease in hydrophilicity of the amine can render the network more hydrophobic, which will likely increase its degradation time. To explore these factors systematically, three primary amines with a decreasing degree of hydrophilicity and average molecular contour length were selected in this study. Primary amines used were 4,7,10-trioxatridecane-1,13-diamine (TTD), 2,2'(ethylenedioxy) bis ethylamine (EDBE), and hexamethylene diamine (HMD) (Ref: **Figure 5.1**). The hydrophilicity comparison of amines is based on the number of ethylene oxide units present

in the molecule: TTD has three ethylene oxide units, EDDBE has two ethylene oxide units while HMD has none. Amine crosslinker was used to manipulate the thermomechanical and functional properties of 0:100 CMA:PEG400DA microfilms i.e., PCBAE microfilms made without curcumin before exploring PCBAE prepared with curcumin.

#### **5.3.1.1 Effect of amine crosslinker on mechanical properties of 0:100 CMA:PEG400DA hydrogels**

Dynamic mechanical analysis (DMA) was performed on 0:100 CMA:PEG400DA films synthesized with TTD, EDDBE and HMD. Storage modulus and  $\tan \delta$  as a function of temperature for these films is presented in **Figure 5.2**. All samples had similar rubbery modulus as well as glass transition temperature ( $T_g$ ). Based on the chain length of amines, it would be expected that rubbery modulus would increase when EDDBE or HMD was used instead of TTD. However, contrary to the expectation, it was seen that the amine structure did not have a significant effect on the rubbery modulus and glass transition temperature of the 0:100 CMA:PEG400DA films. The reason for this could be understood when the overall topology of the network is considered. For every molecule of amine, two molecules of PEG400DA are present; since PEG400DA is a relatively long and flexible component compared to the amines that were used, the network mechanical properties are not affected appreciably by the change in the amine details.

#### **5.3.1.2 Effect of amine crosslinker on degradation properties of 0:100 CMA:PEG400DA hydrogels**

The degradation of hydrogels can be assessed through various methods, including swelling ratio, hydrogel mass loss and drug release [124, 197]. For the current study, the effect of amine crosslinker type on degradation was tracked by measuring the swelling

ratio of the hydrogels as a function of time, as presented in **Figure 5.3**. As seen from the degradation profile, the 0:100 CMA:PEG400DA-TTD hydrogel had the shortest degradation time, followed by the 0:100 CMA:PEG400DA-HMD and 0:100 CMA:PEG400DA-EDBE hydrogels. Since all films display a similar rubbery modulus and glass transition temperature, degradation of the gels would be expected to primarily depend on the hydrophilicity of the network, which was true for the gels made with TTD and EDBE, where the 0:100 CMA:PEG400DA-EDBE hydrogels had a longer degradation time compared to the 0:100 CMA:PEG400DA-TTD hydrogels. However, the HMD hydrogel had a degradation time that was in between the gels made with TTD and EDBE. Such deviation from the expected trend was also seen for gels made with these amines at RTAA of 0.6, where gels made with HMD had the same degradation time as gels made with EDBE [171]. This is possibly due to the relatively slower rate of gel formation observed during the synthesis of the 0:100 CMA:PEG400DA-HMD gels. The slower reaction rate for HMD is due to the absence of ethylene oxide units in the HMD structure, and hence, the absence of favorable interactions present between reactants such as PEG400DA and TTD (or EDBE). This affects the reaction rate and potentially the network architecture, since HMD is not able to react with PEG400DA as efficiently as TTD or EDBE.

### **5.3.2 Commercial diacrylate**

Apart from amine crosslinker, another independent parameter in terms of monomer selection is the commercial diacrylate used for PCBAE synthesis. Similar to the amine crosslinker selection, commercial diacrylate can be used to tune the network properties through variation in the hydrophilicity and chain length of the diacrylate. A decrease in the overall network hydrophilicity can increase the degradation time and a reduction in chain

length (and a corresponding increase in crosslink density) can potentially increase the degradation time as well. Three diacrylates with decreasing average molecular length and relative hydrophilicity (PEG576DA, PEG400DA and DEGDA) were selected to explore the role of commercial diacrylates on the mechanical and functional properties of PCBAE.

### **5.3.2.1 Effect of diacrylate on mechanical properties of 0:100 CMA:PEGDA hydrogels**

The effect of diacrylate molecular weight on hydrogel mechanical properties was studied for the 0:100 CMA:PEGDA hydrogels by dynamic mechanical analysis; see **Figure 5.4**. An increase in rubbery modulus and glass transition temperature was observed with a decrease in the average length of the diacrylate monomer. DEGDA, being the shortest of the diacrylates, led to gels with the highest crosslink density and correspondingly the highest rubbery modulus and glass transition temperature in this series. Other than rubbery modulus and glass transition temperature, the nature of the storage modulus curve for the 0:100 CMA:PEG576DA hydrogel was found to be different compared to the PEG400DA and DEGDA hydrogels. This change in the storage modulus curve indicates that the PEG576DA undergoes a cold-crystallization process during the slow heating (1°C/min) in the DMA. During heating, as the gel transitions to the rubbery phase, polymer segments have enough mobility to rearrange to form the crystals, which undergo melting upon further heating. Such cold-crystallization has also been reported for UV-crosslinked PEG576DA hydrogels [179]. The cold-crystallization phenomenon was not seen for the 0:100 CMA:PEG400DA or 0:100 CMA:DEGDA hydrogels since the length of the PEG400DA and DEGDA segments does not provide enough mobility between crosslinks for the chains to form ordered crystals.

### **5.3.2.2 Effect of diacrylate on degradation properties of 0:100 CMA:PEGDA hydrogels**

The degradation properties for hydrogels synthesized with different diacrylates were studied by measuring the swelling ratios during the degradation of these gels; the corresponding data are presented in **Figure 5.5**. The three diacrylates, i.e., PEG576DA, PEG400DA and DEGDA, contain 13, 9 and 2 ethylene oxide units, respectively, and hence are listed in order of decreasing hydrophilicity. The 0:100 CMA:PEG576DA and 0:100 CMA:PEG400DA hydrogels had similar degradation profiles even though the PEG576DA network had a lower overall crosslink density, as reflected in its rubbery modulus, and a somewhat higher overall hydrophilic character. The 0:100 CMA:DEGDA hydrogels had the longest degradation time in this series, which was due to their considerably higher crosslink density and ethylene oxide content.

### **5.3.3 Influence of RTAA on functional properties of PCBAE hydrogels**

While variations in the amine crosslinker and diacrylate were found to affect the functional properties of the 0:100 CMA:PEGDA hydrogels differently, changes in the relative acrylate to amine ratios can potentially alter the properties of PCBAE without changing the CMA:PEGDA composition. This was studied through variations in RTAA (ratio of total acrylate to amine) in the current work. RTAA is a crucial process parameter as changes in the corresponding stoichiometric ratio can alter the reaction rate as well as the structure of the resulting crosslinked network. The effect of RTAA on weight loss during washing was explored for 50:50 CMA:PEG400DA, 70:30 CMA:PEG400DA and 90:10 CMA:PEG400DA hydrogel films made with TTD. The mechanical characteristics

and degradation properties were explored for the 50:50 CMA:PEG400DA, and 90:10 CMA:PEG400DA hydrogel films.

#### **5.3.3.1 Effect of RTAA on monomer extraction during washing of gels**

During the washing of gels with ACN, unreacted monomers were removed from the films. The weight loss was calculated by measuring the weight of the gel before washing, and then after washing and drying steps. The weight loss data as a function of RTAA for the 50:50 CMA:PEG400DA hydrogel is presented in **Figure 5.6**. An increase in weight loss was seen as RTAA was increased. At lower RTAA values, a higher concentration of amine crosslinker is present which tends to increase the extent of polymerization, and hence leads to a lower weight loss of unreacted monomers in the washing step. A similar effect of RTAA on the weight loss was observed for the 70:30 CMA:PEG400DA and 90:10 CMA:PEG400DA hydrogel films (re: Figure 5.6).

#### **5.3.3.2 Effect of RTAA on mechanical properties of 50:50 CMA:PEG400DA hydrogels**

The influence of RTAA on the mechanical properties of 50:50 CMA:PEG400DA hydrogels synthesized with TTD as a crosslinker was explored for films with RTAA values of 0.6, 0.8, 1.1, 1.2 and 1.4. The storage modulus and  $\tan \delta$  as a function of temperature for these films are presented in **Figure 5.7**. The rubbery modulus for the films varied from approximately 1 MPa to 4 MPa, and displayed an overall trend of increasing crosslink density (i.e., increasing rubbery modulus) with increasing acrylate to amine ratio in the reaction mixture. In addition, an increase in the measured glass transition temperature was observed with an increase in RTAA. This increase in glass transition temperature is the result of an overall increase in curcumin content in the network with increasing RTAA.

The curcumin moiety is relatively short and rigid as compared to the longer and more flexible PEG and TTD components. The increased presence of curcumin reduces the mobility of the network chains thereby requiring more energy for the chain motion, and thus increasing the glass transition temperature of the hydrogels. An increase in glass transition temperature with increasing curcumin composition was also seen with PCBAE networks synthesized from PEG400DA and TTD, and with a fixed RTAA of 1.0 [69].

### **5.3.3.3 Effect of RTAA on degradation properties of 50:50 CMA:PEG400DA hydrogels**

The impact of RTAA on the degradation properties of 50:50 CMA:PEG400DA hydrogels made with TTD was studied for selected RTAA values (0.6, 1.1 and 1.4). The swelling ratio of the hydrogels, their curcumin release profiles during degradation, and the antioxidant activity profiles of the release supernatants are presented in **Figure 5.8**. At the one hour time point, the 50:50 CMA:PEG400DA-0.6 hydrogel had the highest swelling ratio for the current series, followed by the 50:50 CMA:PEG400DA-1.1 and 50:50 CMA:PEG400DA-1.4 hydrogels. This was consistent with the inherent hydrophilicity of these hydrogels, where films with lower RTAA had higher hydrophilic content due to lower relative incorporation of curcumin as well as higher amounts of the hydrophilic amine. The total degradation time for these films was measured through the curcumin release profile. The curcumin release profile of the hydrogels followed the swelling response, where the 50:50 CMA:PEG400DA-1.4 hydrogel had the slowest swelling response and longest total degradation time in the series. Interestingly, an increase in degradation time was seen with both increase and decrease in RTAA from 1.1. At higher RTAA (1.4), curcumin composition is increased which increases the degradation time due

to increased hydrophobicity of networks. At lower RTAA (0.6), two competing effects are present where an increase in amine composition leads to an increase in hydrophilicity of the network but also leads to a much tighter network. This tighter network leads to an increase in degradation time. The antioxidant activity of the curcumin released was measured using the colorimetric TEAC assay. The TEAC profiles were found to be similar to the curcumin release profiles for each corresponding PCBAE, thereby confirming that the curcumin released was in its native form. However, the proportionality was different for each PCBAE, which could be due to different constituent species present in the degradation sample for PCBAEs made with different RTAA.

#### **5.3.3.4 Effect of RTAA on mechanical properties of 90:10 CMA:PEG400DA hydrogels**

The effect of RTAA on the network and functional properties of PCBAE was explored for 90:10 CMA:PEG400DA hydrogels to understand how variations in RTAA affect the PCBAE at higher curcumin loading. The 90:10 CMA:PEG400DA network has a much higher hydrophobicity compared to 50:50 CMA:PEG400DA, owing to its much higher curcumin content. The effect of RTAA on the mechanical properties of the 90:10 CMA:PEG400DA hydrogels made with TTD was studied for RTAA values of 0.6, 1.0 and 1.4. The storage modulus and  $\tan \delta$  results for 90:10 CMA:PEG400DA films with different RTAA are reported in **Figure 5.9**. The rubbery modulus did not change appreciably with RTAA for this series, while the glass transition temperature increased with an increase in RTAA. These results are similar to the results observed for the study involving 50:50 CMA:PEG400DA films, and suggest that the effect of RTAA on the PCBAE network properties is independent of the hydrophobicity of the network under study.

### **5.3.3.5 Effect of RTAA on degradation properties of 90:10 CMA:PEG400DA hydrogels**

The role of RTAA on the degradation properties of the 90:10 CMA:PEG400DA hydrogels was also studied; the 90:10 film is the most hydrophobic sample in this series. The swelling data and curcumin release profiles from these films is presented in **Figure 5.10**. The RTAA values were selected such that a wide range of RTAA was covered. Swelling response for these films was different from the swelling response observed for the 50:50 CMA:PEG400DA films. The 90:10 CMA:PEG400DA-0.6 film had higher swelling than the 90:10 CMA:PEG400DA-1.0 film at the start, which was later overtaken by the 90:10 CMA:PEG400DA-1.0 film. The final degradation time as a function of RTAA for the 90:10 CMA:PEG400DA films was similar to the 50:50 CMA:PEG400DA films, where the 90:10 CMA:PEG400DA-1.0 film had the fastest degradation time, while the 90:10 CMA:PEG400DA-0.6 and 90:10 CMA:PEG400DA-1.4 films had similar final degradation times. At RTAA=1.4, curcumin is present in higher proportion which increases the network hydrophobicity. In addition to this, curcumin being short and stiff reduces the mobility of the polymer chains as reflected in the glass transition temperature increase (re: Figure 5.9). This also contributes to a lower swelling response and the correspondingly slower degradation observed for these films. Similar to the study involving the 50:50 CMA:PEG400DA films, at lower RTAA (0.6), an increase in degradation time was seen due to tighter network formation.

### **5.3.4 CMA composition dependence for PCBAE-EDBE and PCBAE-HMD hydrogels**

As discussed in chapter four, a wide range of hydrogel functional properties and degradation characteristics could be obtained for the PCBAE-TTD networks by varying

the relative amount of curcumin covalently incorporated into the hydrogel network (i.e. variation of CMA composition in the pre-polymerization reaction mixture). To extend this investigation further, it is appropriate to consider the influence of other diamine crosslinkers (i.e. EDBE, HMD) for similar series of PCBAE networks. As is evident from their chemical structure (re: Figure 5.1), the EDBE and HMD crosslinkers afford additional tuning capability for the networks owing to their shorter length and correspondingly higher hydrophobicity.

#### **5.3.4.1 Effect of CMA composition on mechanical properties of PCBAE-EDBE hydrogels**

The mechanical properties of PCBAE hydrogels made with EDBE as a crosslinker were studied for selected CMA:PEG400DA compositions. The storage modulus and  $\tan \delta$  are presented in **Figure 5.11** as a function of temperature at 1Hz. The glass-rubber transition for these materials shifted to higher temperatures with an increase in CMA as seen from the shift in the storage modulus curves and  $\tan \delta$  peaks. This behavior is similar to the composition dependence observed for the PCBAE hydrogels made with TTD. However, the rubbery modulus did not change with CMA content for the CMA:PEG400DA composition range studied here. The rate of reaction between CMA and EDBE is much faster than CMA and TTD due to the shorter chain length of EDBE. This leads to a network where the average crosslink distance doesn't vary with composition and is controlled primarily by the EDBE crosslinker, leading to a similar rubbery modulus in each case.

#### **5.3.4.2 Effect of CMA composition on degradation of PCBAE-EDBE hydrogels**

The effect of CMA composition on the degradation properties of hydrogels made with EDBE crosslinker was explored for 50:50 CMA:PEG400DA, 70:30 CMA:PEG400DA and 90:10 CMA:PEG400DA gels. These CMA compositions were selected for hydrogel synthesis since it has been observed previously that CMA composition has a major impact on the degradation properties of PCBAE gels at CMA:PEG400DA compositions higher than 50:50 [69]. The swelling ratio, curcumin release and antioxidant activity profiles for these hydrogels are presented in **Figure 5.12**. 50:50 CMA:PEG400DA-EDBE, 70:30 CMA:PEG400DA-EDBE and 90:10 CMA:PEG400DA-EDBE hydrogels had total degradation times of 10 hours, 18 hours and 23 hours, respectively. A relatively lower extent of swelling and an increase in degradation time was observed with increase in CMA composition compared with gels made with TTD. An increase in CMA composition increases the hydrophobicity and glass transition temperature of the network, which delays the swelling response and increases the total degradation time.

#### **5.3.4.3 Effect of CMA composition on mechanical properties of PCBAE-HMD hydrogels**

The mechanical properties of PCBAE hydrogels made with HMD were explored for selected CMA compositions. The storage modulus and  $\tan \delta$  results for this series are presented in **Figure 5.13**. As seen from the  $\tan \delta$  curves, an increase in glass transition temperature was again observed with an increase in CMA composition. This was similar to the composition dependence seen with gels made using TTD and EDBE as the crosslinker. Also, it is expected that the rubbery modulus wouldn't be affected by the

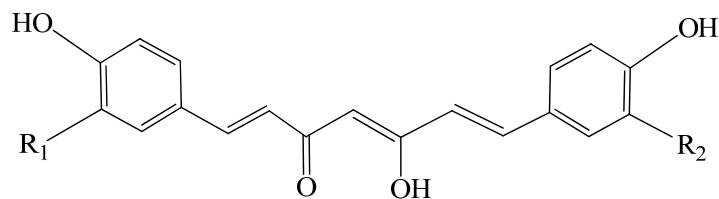
change in CMA composition, as the shorter length of the HMD spacer controls the distance between crosslinks. This was, in fact, observed and the rubbery modulus for the current series did not change appreciably with composition. One interesting point with this series was that the breadth of  $\tan \delta$  peak decreased with an increase in CMA composition. Contrary to this observation, for hydrogels made with TTD, an increase in the breadth of the  $\tan \delta$  peak was seen [69]. This shows that hydrogel homogeneity increased with CMA composition for gels made with HMD as the crosslinker. This behavior is, in part, due to the hydrophobicity of HMD, which allows it to blend more uniformly with hydrophobic CMA during the reaction step.

#### **5.3.4.4 Effect of CMA composition on degradation of PCBAE-HMD hydrogels**

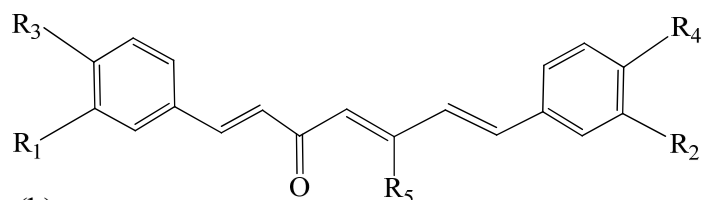
The degradation properties of PCBAE gels made with HMD were studied for CMA:PEG400DA compositions of 50:50, 70:30 and 90:10. The swelling ratio, curcumin release and antioxidant activity during the degradation of PCBAE gels made with HMD crosslinker are shown in **Figure 5.14**. The swelling response and curcumin release profiles were found to be dependent on the CMA composition, where slower swelling response and longer degradation times were seen for PCBAEs with higher CMA content. 90:10 CMA:PEG400DA-HMD gels had the longest curcumin release time (~58 hours) yet reported for PCBAE hydrogels. This sample had some non-degraded residue evident at the end, which was thought to be the result of very hydrophobic regions created by the combination of CMA and HMD rendering a portion of the gel non-degradable under the observation time of the study.

## 5.4 Conclusions

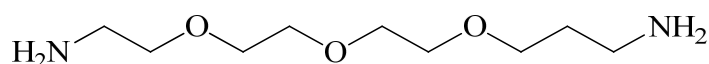
A systematic study of the independent process parameters involved in the synthesis of PCBAE was completed. These parameters included amine crosslinker, diacrylate monomer, and acrylate to amine ratio (RTAA). For 0:100 CMA:PEG400DA hydrogels, the amine crosslinkers did not have an impact on the glass transition temperature or rubbery modulus, as measured by dynamic mechanical analysis. However, an increase in degradation time was observed with reduced hydrophilicity and chain length of amine crosslinker. On the other hand, for 0:100 CMA:PEGDA hydrogels, the diacrylate molecular weight had a major impact on the rubbery modulus, glass transition temperature and degradation time, where values for these parameters increased with decreasing chain length and hydrophilicity of the diacrylate. It was found that length of the monomer (i.e. amine or diacrylate) is a better control parameter for tuning 0:100 CMA:PEGDA hydrogel properties. An overall increase in glass transition temperature and degradation time was observed with an increase in RTAA for the multiple CMA:PEG400DA compositions that were explored. Increase in CMA content for PCBAE gels with EDDBE and HMD as crosslinkers was able to increase the glass transition temperature and degradation time to some extent. Additionally, caution must be exercised with hydrophobic monomers as too high a proportion of hydrophobic monomer can render the polymer non-degradable. With their wide degradation times and tunable mechanical properties, PCBAEs have great potential to address challenges in drug delivery, tissue engineering and orthopedic applications.



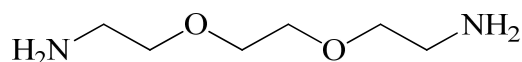
(a)



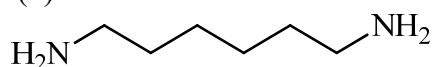
(b)



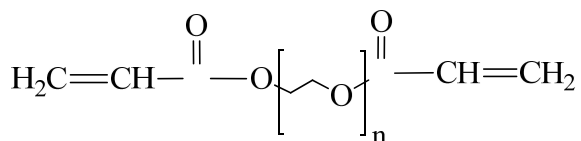
(c)



(d)



(e)



(f)

**Figure 5.1:** Chemical structures of (a) curcumin, (b) curcumin multiacrylate (CMA), (c) 4,7,10-Trioxatridecane-1,13-diamine (TTD), (d) 2,2'-(ethylenedioxy) bis ethylamine (EDBE), (e) Hexamethylene diamine (HMD), (f) Diacrylate monomer.  $n = 13$  for poly(ethylene glycol)576 diacrylate (PEG576DA),  $n = 9$  for poly(ethylene glycol) 400 diacrylate (PEG400DA), and  $n = 2$  for diethylene glycol diacrylate (DEGDA).  $R_1$  and  $R_2$  can be H or  $-OCH_3$  and  $R_3$ ,  $R_4$  and  $R_5$  can be  $-OH$  or an acrylate group.

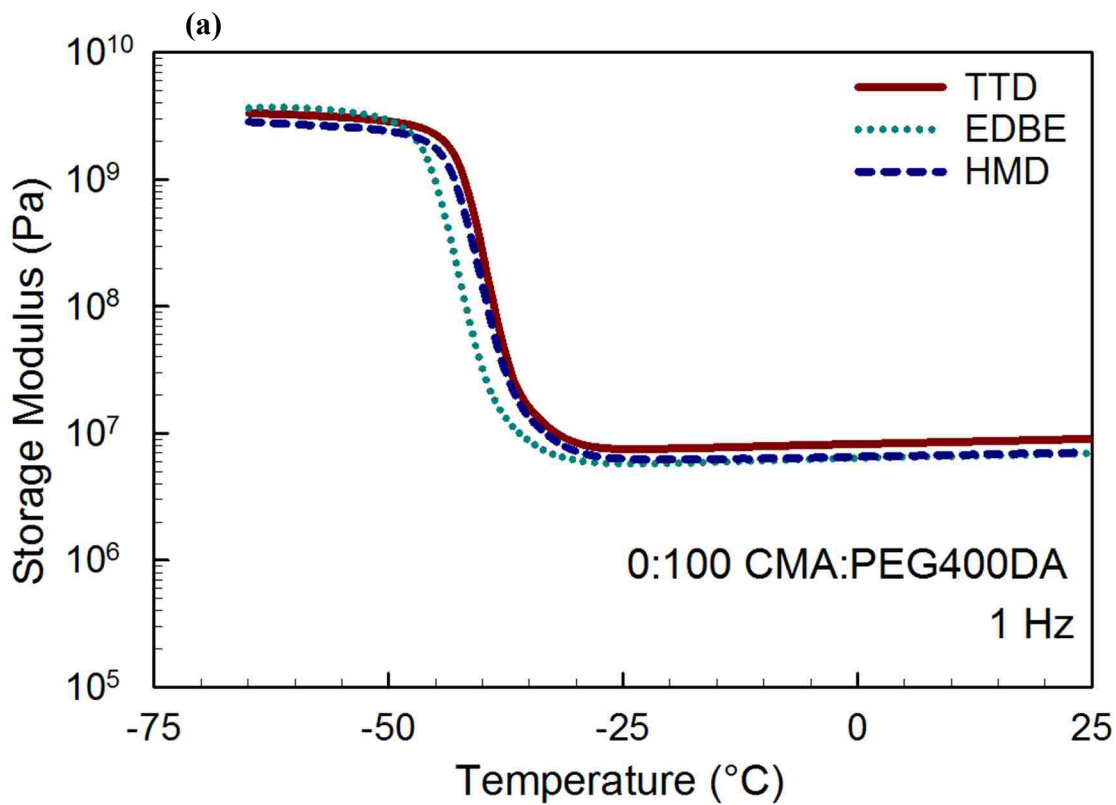


**Figure 5.2:** Dynamic mechanical properties of PCBAE films synthesized using different amines for 0:100 CMA:PEG400DA gel. (a) Storage modulus vs. Temperature ( $^{\circ}\text{C}$ ) at 1 Hz; (b) Tan  $\delta$  vs. Temperature ( $^{\circ}\text{C}$ ) at 1 Hz.

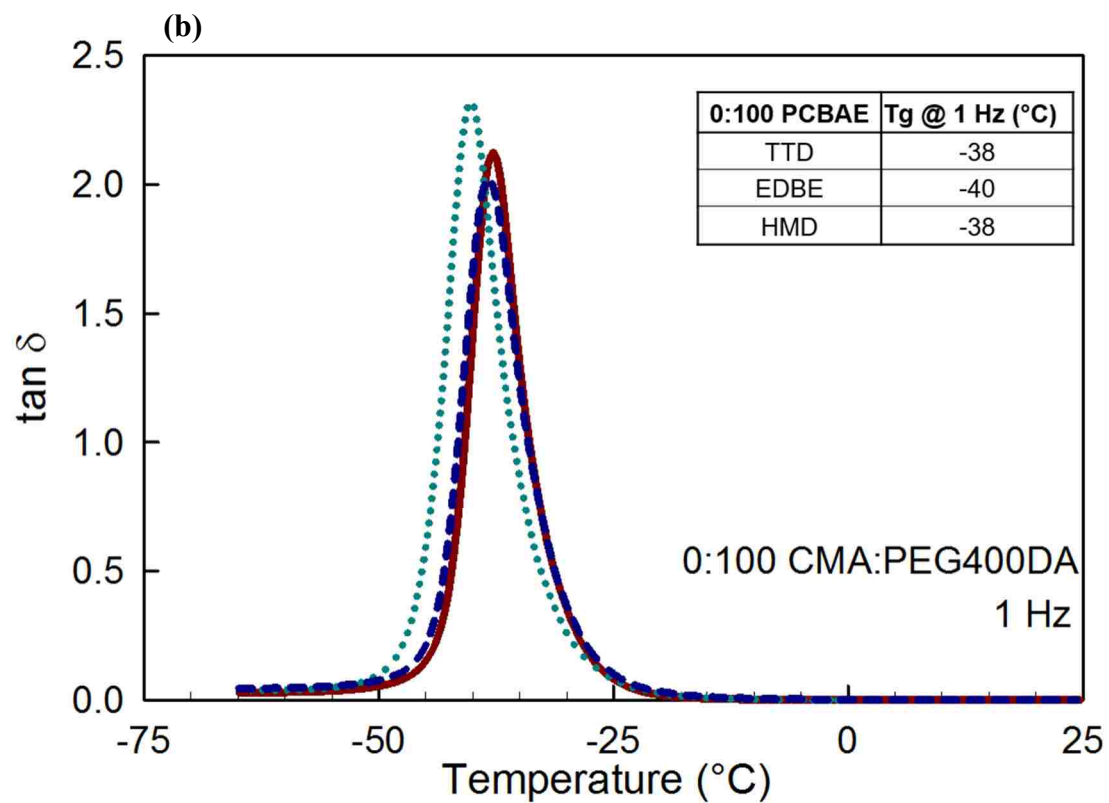


**Figure 5.2:** Dynamic mechanical properties of PCBAE films synthesized using different amines for 0:100 CMA:PEG400DA gel. (a) Storage modulus vs. Temperature (°C) at 1 Hz; (b) Tan  $\delta$  vs. Temperature (°C) at 1 Hz.

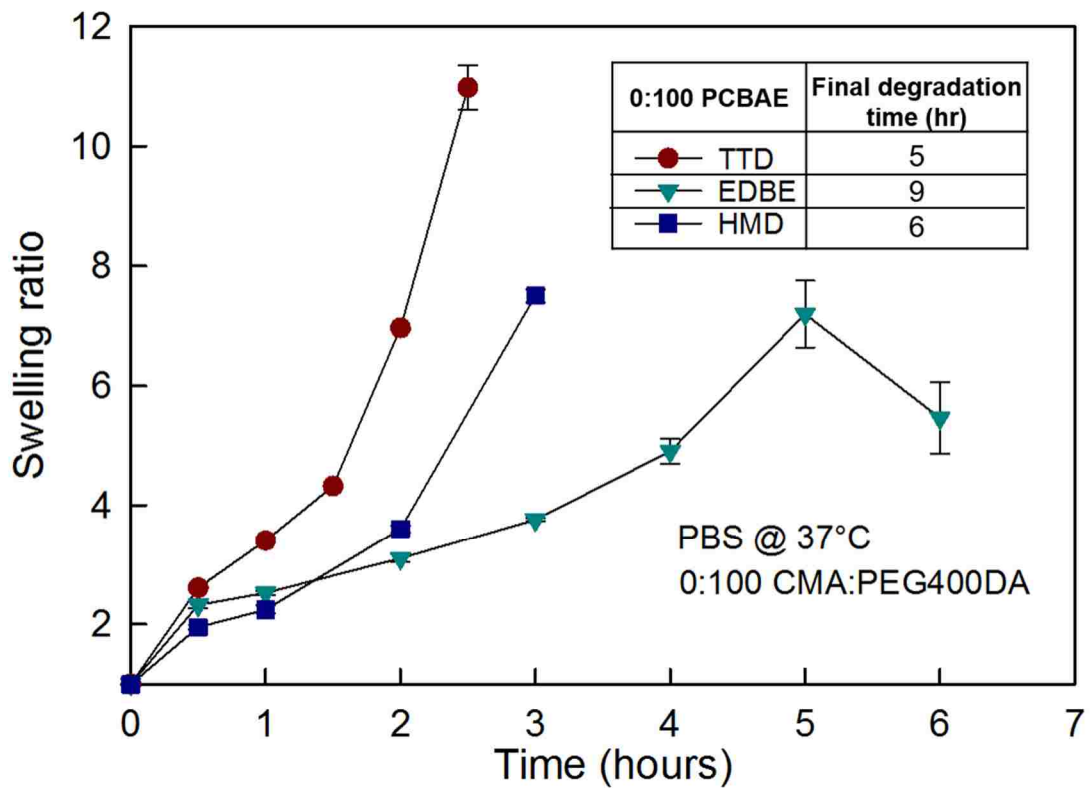


**Figure 5.3:** Swelling ratio for 0:100 CMA:PEG400DA films with different amine crosslinkers during degradation in PBS (0.1 % SDS).

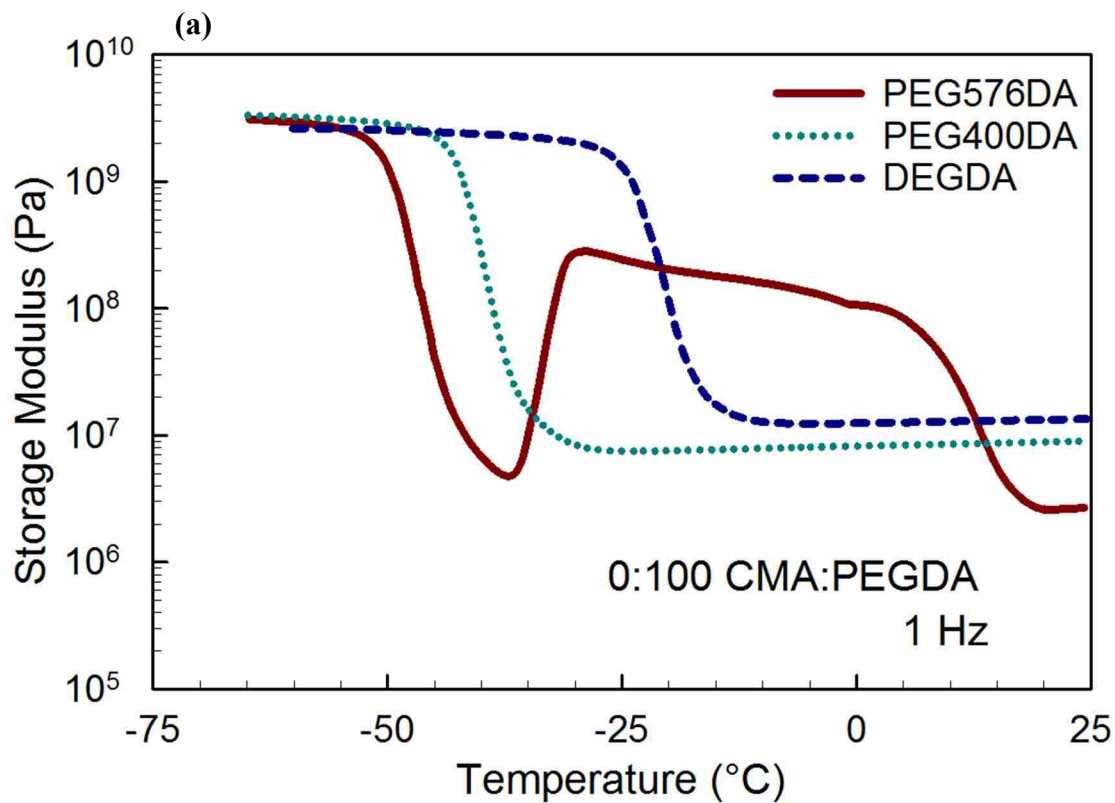


**Figure 5.4:** Dynamic mechanical properties for PCBAE films of different diacrylates for 0:100 gel. (a) Storage modulus vs. Temperature ( $^{\circ}\text{C}$ ) at 1 Hz; (b)  $\text{Tan } \delta$  vs. Temperature ( $^{\circ}\text{C}$ ) at 1 Hz.

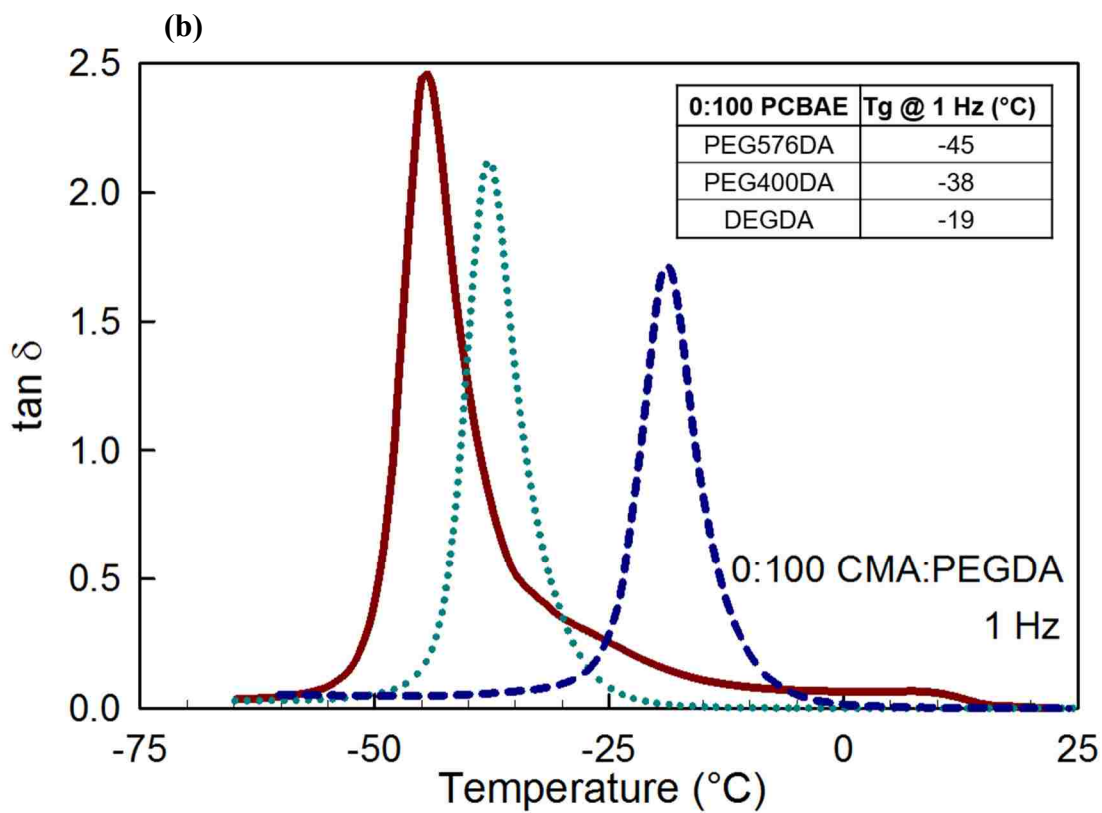


**Figure 5.4:** Dynamic mechanical properties for PCBAE films of different diacrylates for 0:100 gel. (a) Storage modulus vs. Temperature (°C) at 1 Hz; (b) Tan  $\delta$  vs. Temperature (°C) at 1 Hz.

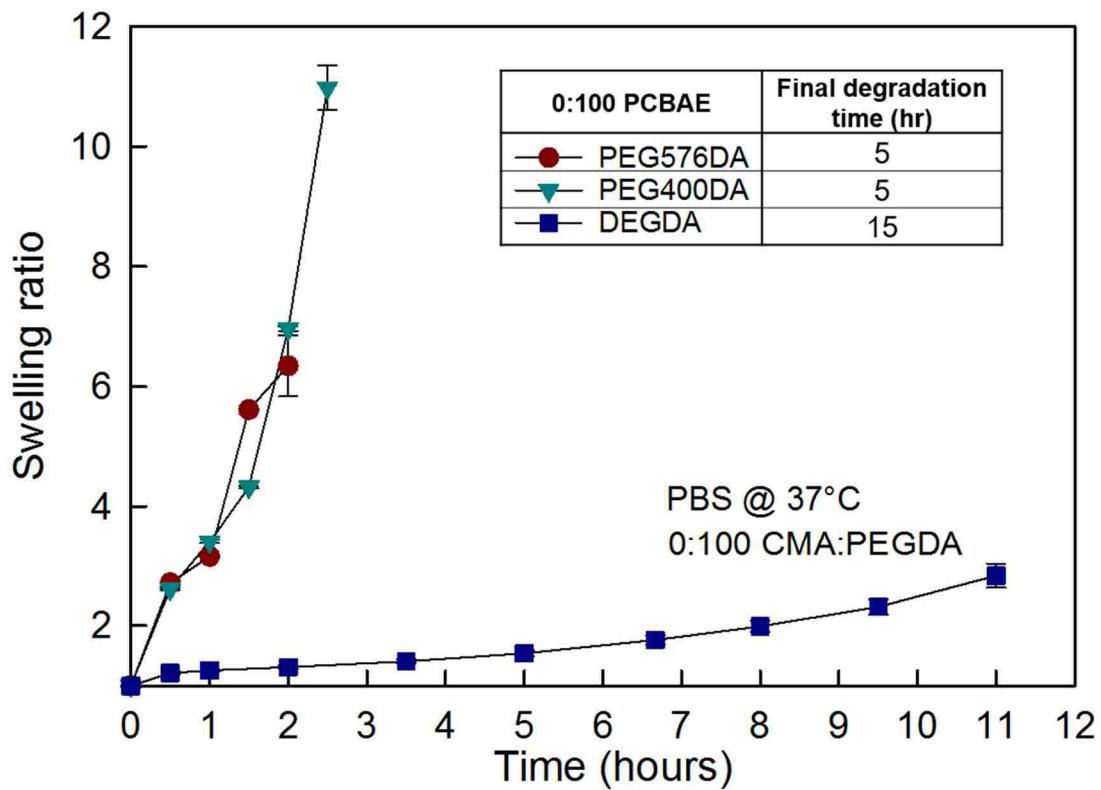


**Figure 5.5:** Swelling ratio for 0:100 CMA:PEGDA films made with TTD using different commercial diacrylates during degradation in PBS (0.1 % SDS).

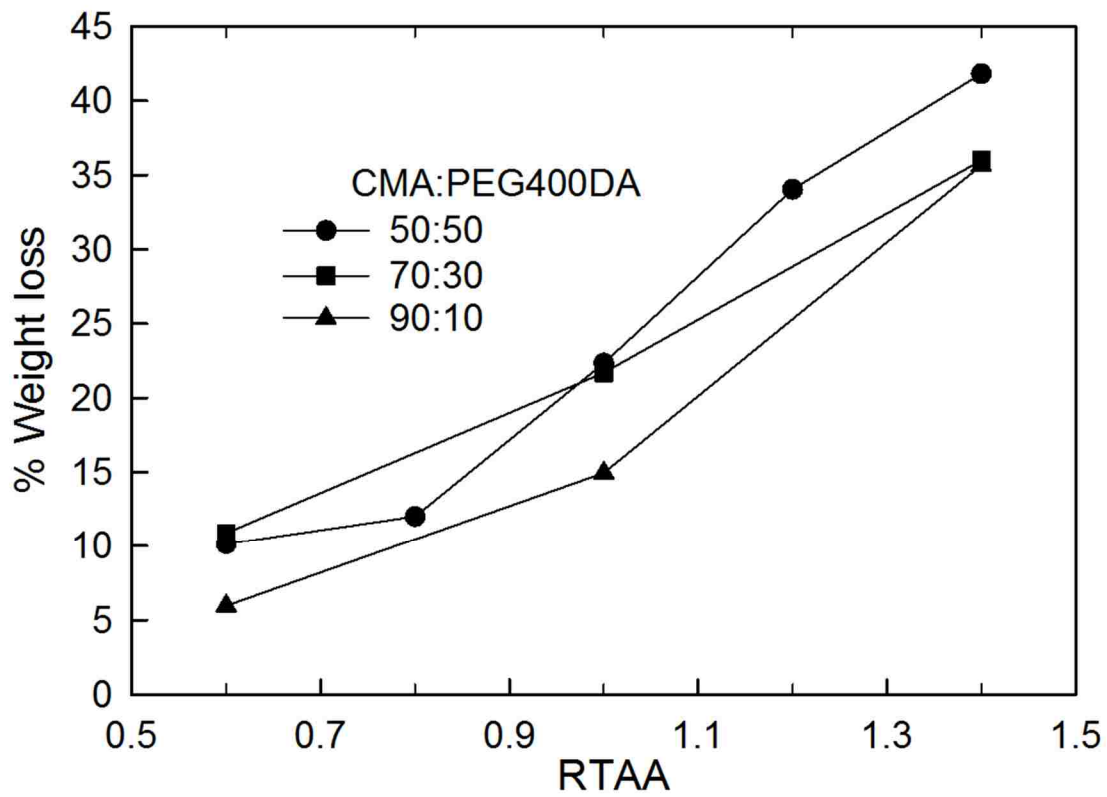


**Figure 5.6:** Weight loss during the washing of hydrogels as a function of RTAA for 50:50, 70:30 and 90:10 CMA:PEG400DA films.

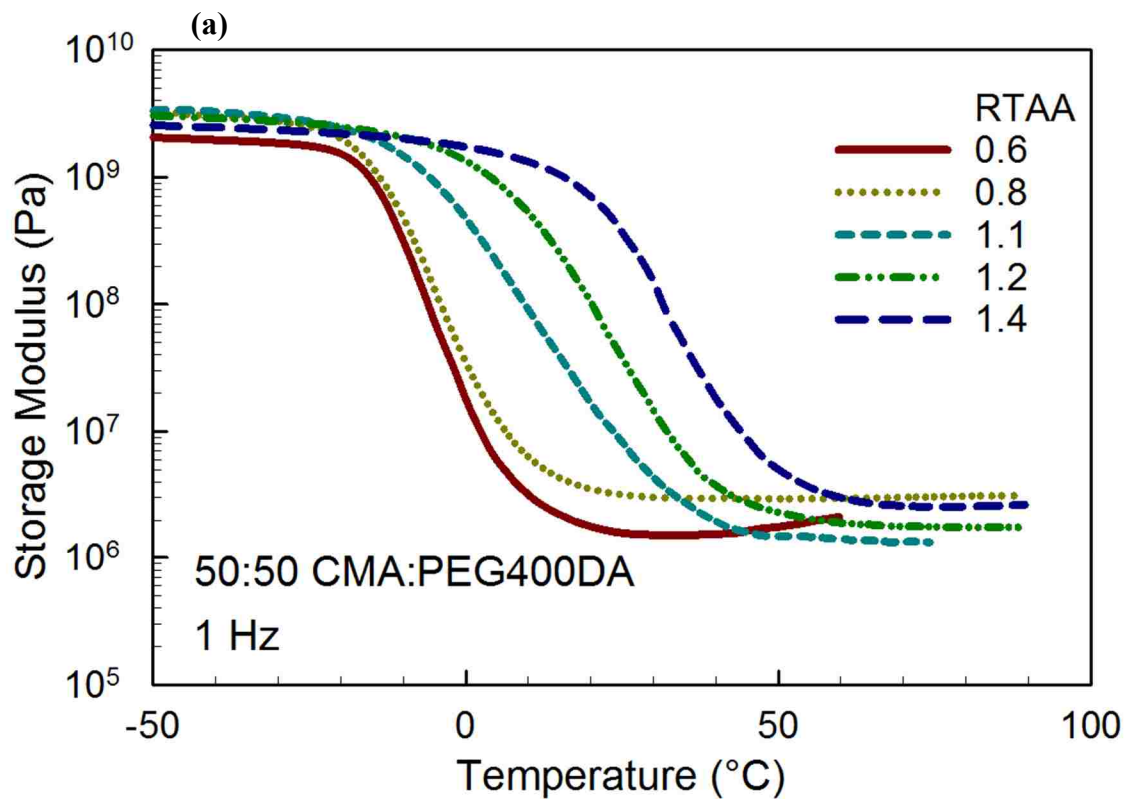


**Figure 5.7:** Dynamic mechanical properties for 50:50 CMA:PEG400DA films made with TTD for different RTAA. (a) Storage modulus vs. Temperature (°C) at 1 Hz; (b) Tan  $\delta$  vs. Temperature (°C) at 1 Hz.

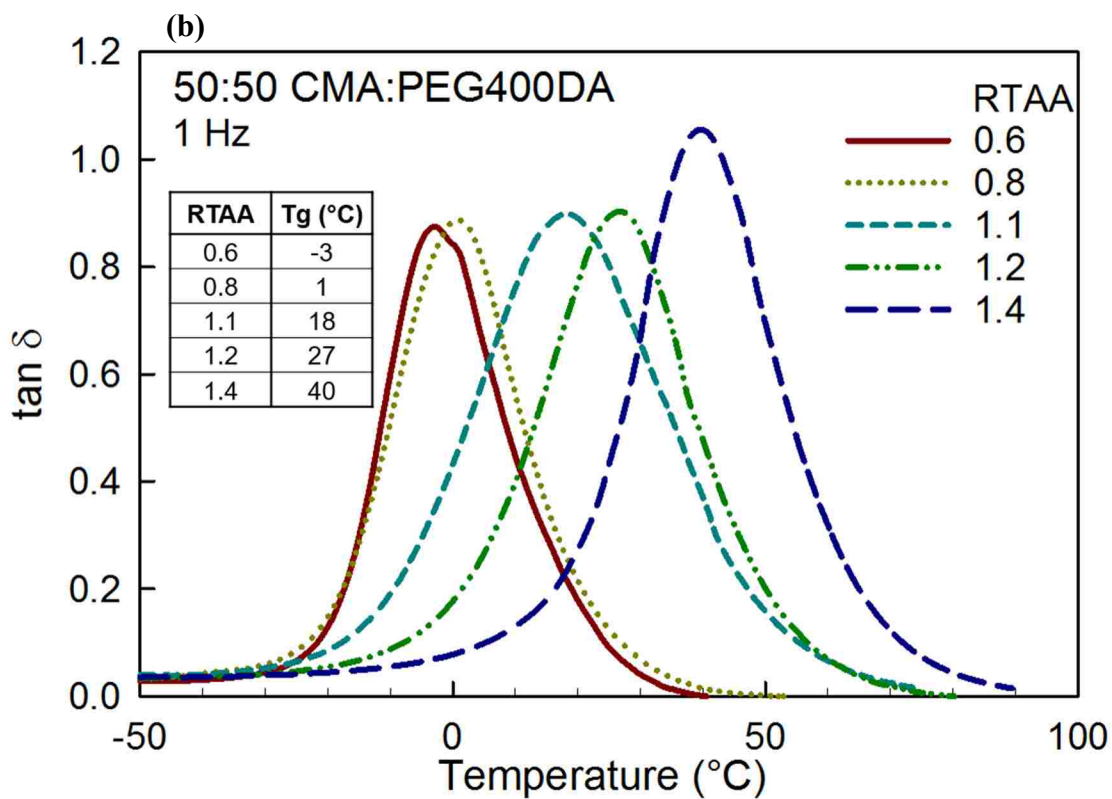


**Figure 5.7:** Dynamic mechanical properties for 50:50 CMA:PEG400DA films made with TTD for different RTAA. (a) Storage modulus vs. Temperature (°C) at 1 Hz; (b) Tan  $\delta$  vs. Temperature (°C) at 1 Hz.

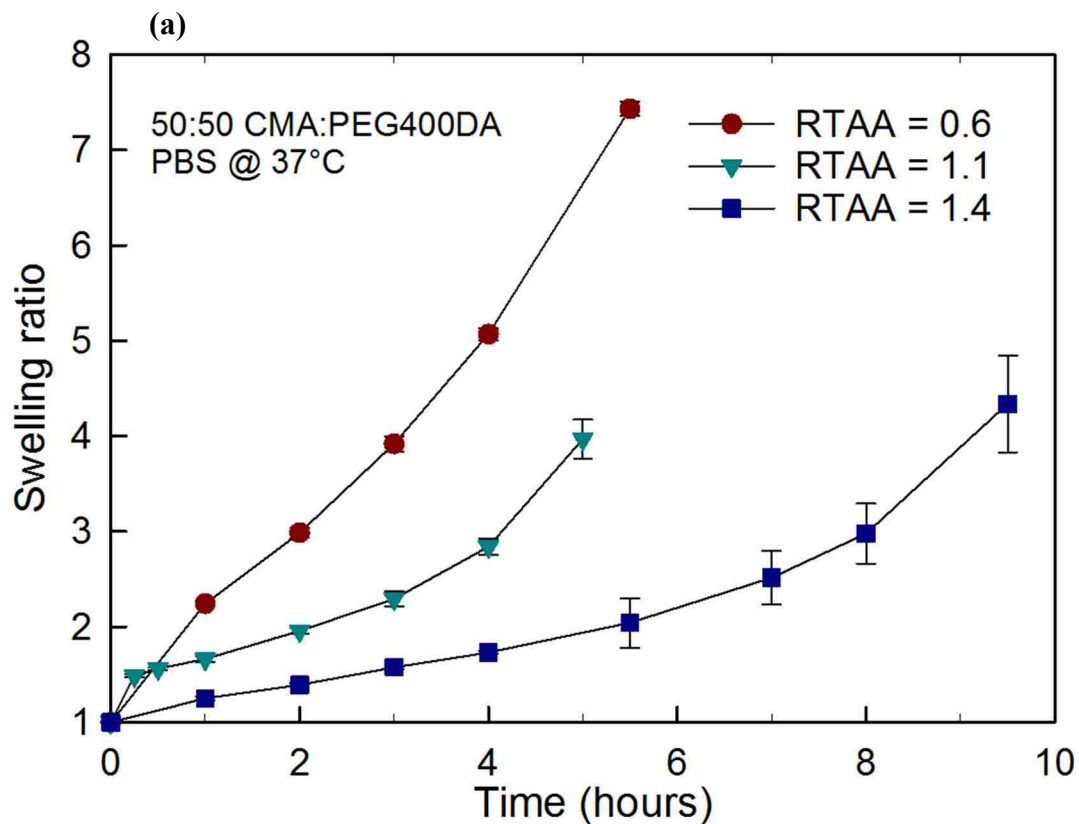


**Figure 5.8:** Degradation in PBS (0.1 % SDS) for 50:50 CMA:PEG400DA films made with TTD for different RTAA. (a) Swelling ratio as a function of degradation time; (b) Curcumin release profile measured using absorbance @ 420 nm; (c) Antioxidant capacity of supernatants measured using TEAC in-vitro antioxidant capacity measurement assay.

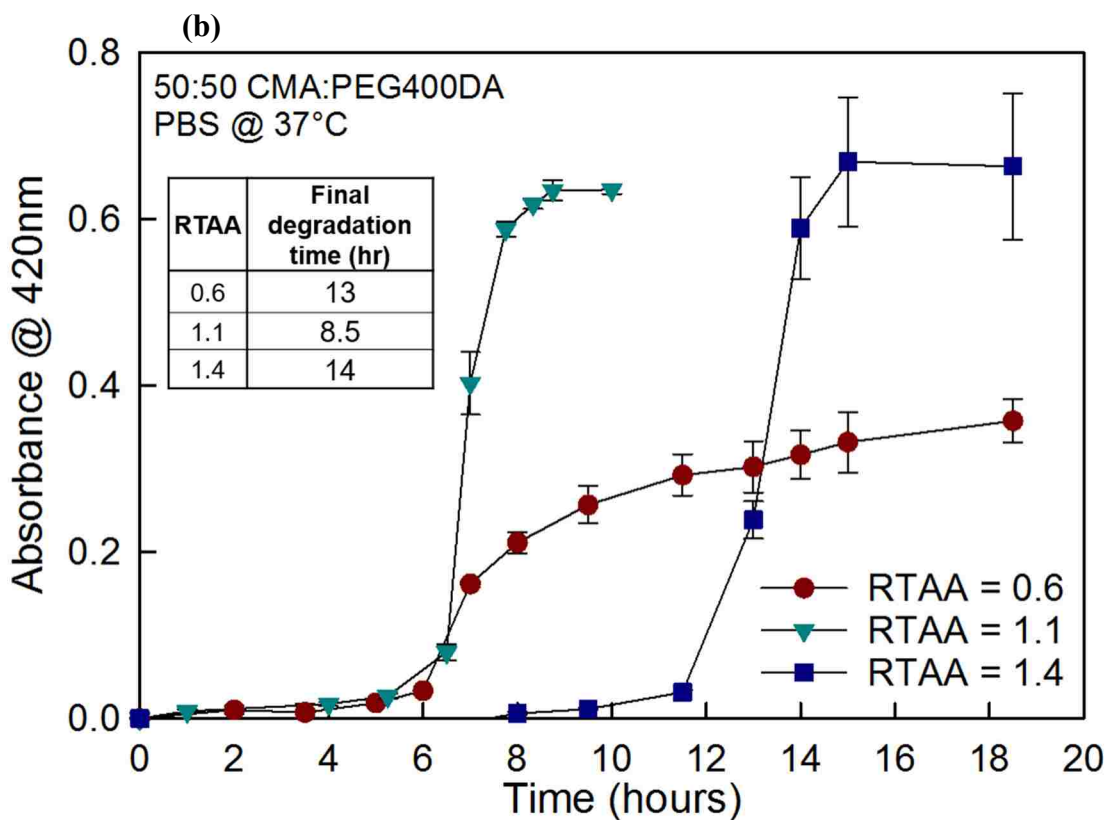


**Figure 5.8:** Degradation in PBS (0.1 % SDS) for 50:50 CMA:PEG400DA films made with TTD for different RTAA. (a) Swelling ratio as a function of degradation time; (b) Curcumin release profile measured using absorbance @ 420 nm; (c) Antioxidant capacity of supernatants measured using TEAC in-vitro antioxidant capacity measurement assay.

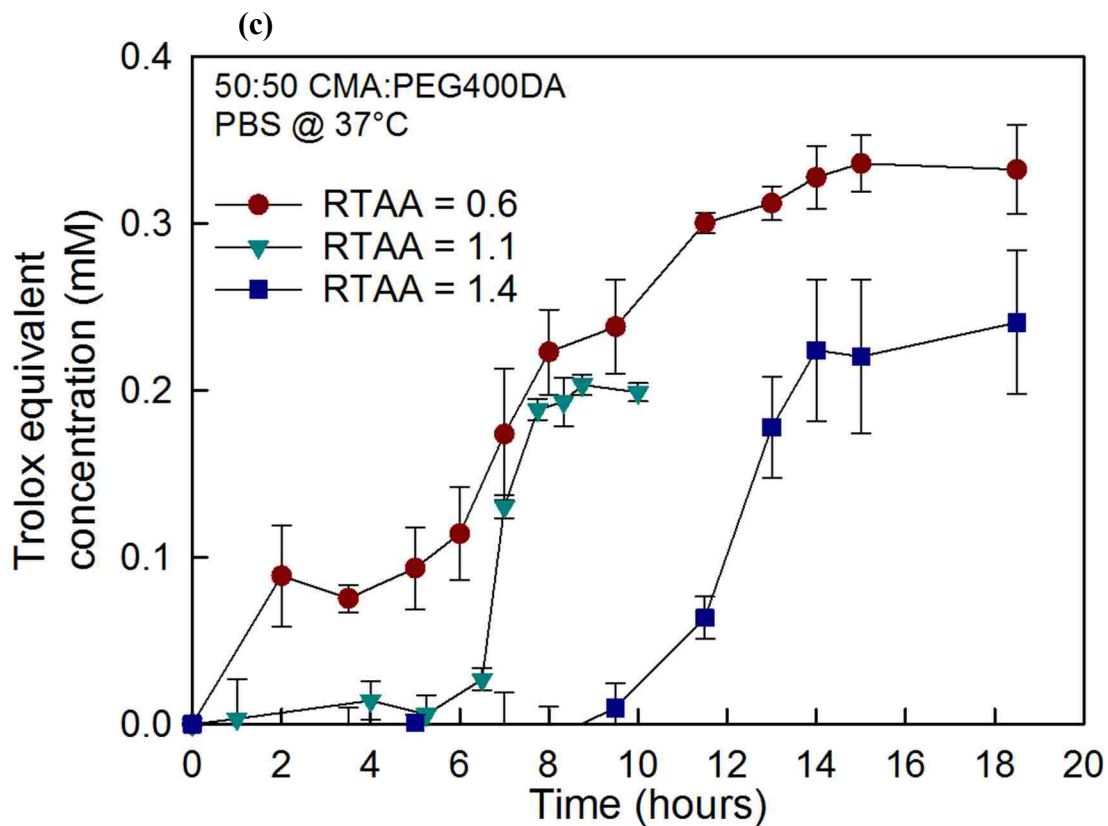


**Figure 5.8:** Degradation in PBS (0.1 % SDS) for 50:50 CMA:PEG400DA films made with TTD for different RTAA. (a) Swelling ratio as a function of degradation time; (b) Curcumin release profile measured using absorbance @ 420 nm; (c) Antioxidant capacity of supernatants measured using TEAC in-vitro antioxidant capacity measurement assay.

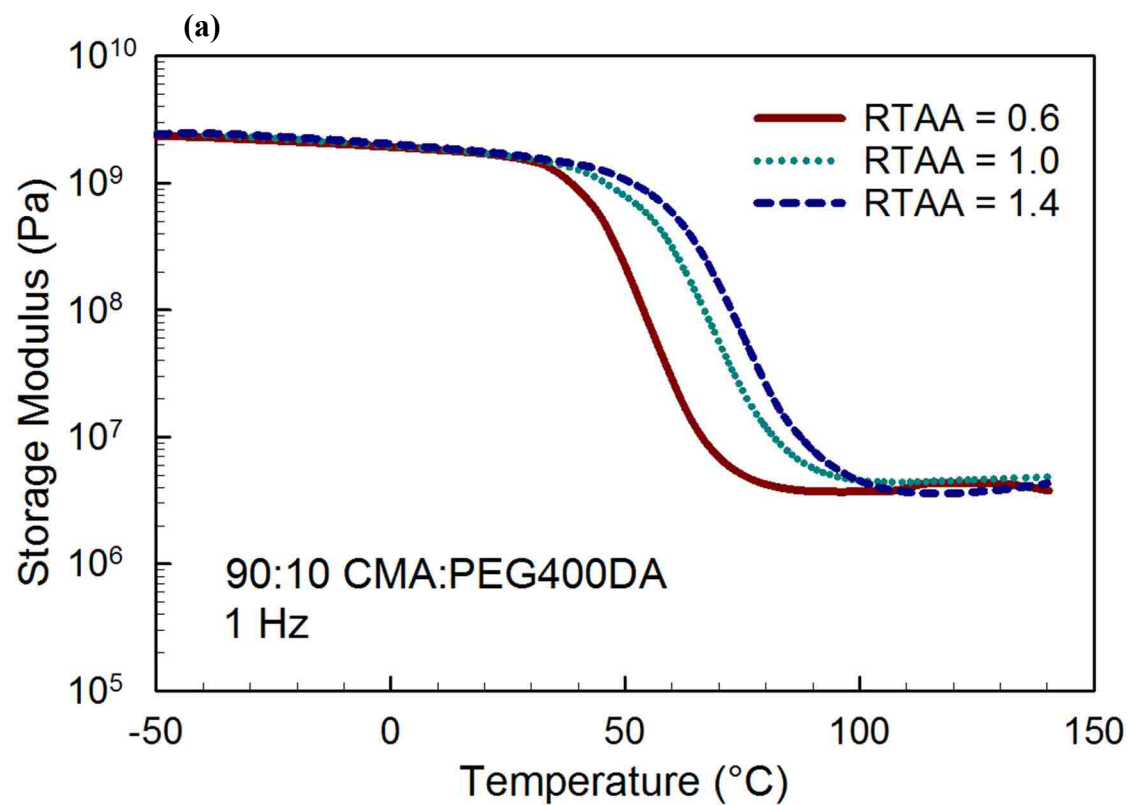


**Figure 5.9:** Dynamic mechanical properties for 90:10 CMA:PEG400DA films made with TTD for different RTAA. (a) Storage modulus vs. Temperature (°C) at 1 Hz; (b) Tan  $\delta$  vs. Temperature (°C) at 1 Hz.

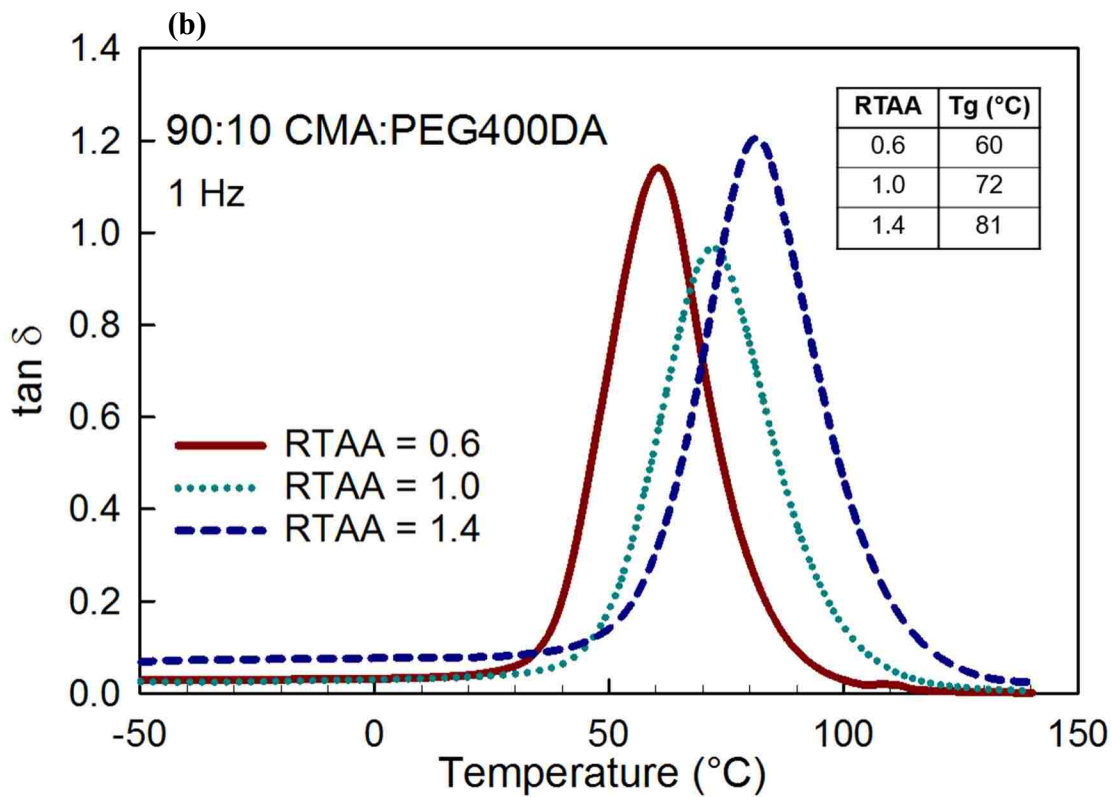


**Figure 5.9:** Dynamic mechanical properties for 90:10 CMA:PEG400DA films made with TTD for different RTAA. (a) Storage modulus vs. Temperature (°C) at 1 Hz; (b) Tan  $\delta$  vs. Temperature (°C) at 1 Hz.

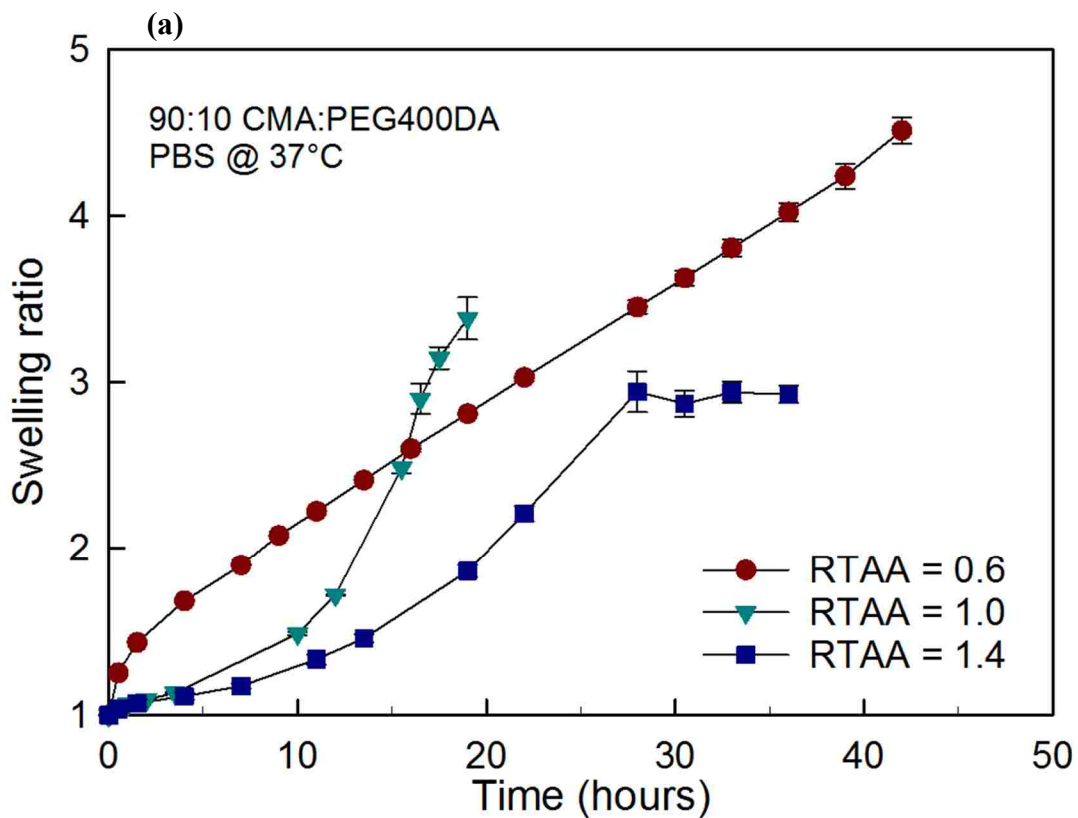


**Figure 5.10:** Degradation in PBS (0.1 % SDS) for 90:10 CMA:PEG400DA films made with TTD for different RTAA. (a) Swelling ratio as a function of degradation time; (b) Curcumin release profile measured using absorbance @ 420 nm.

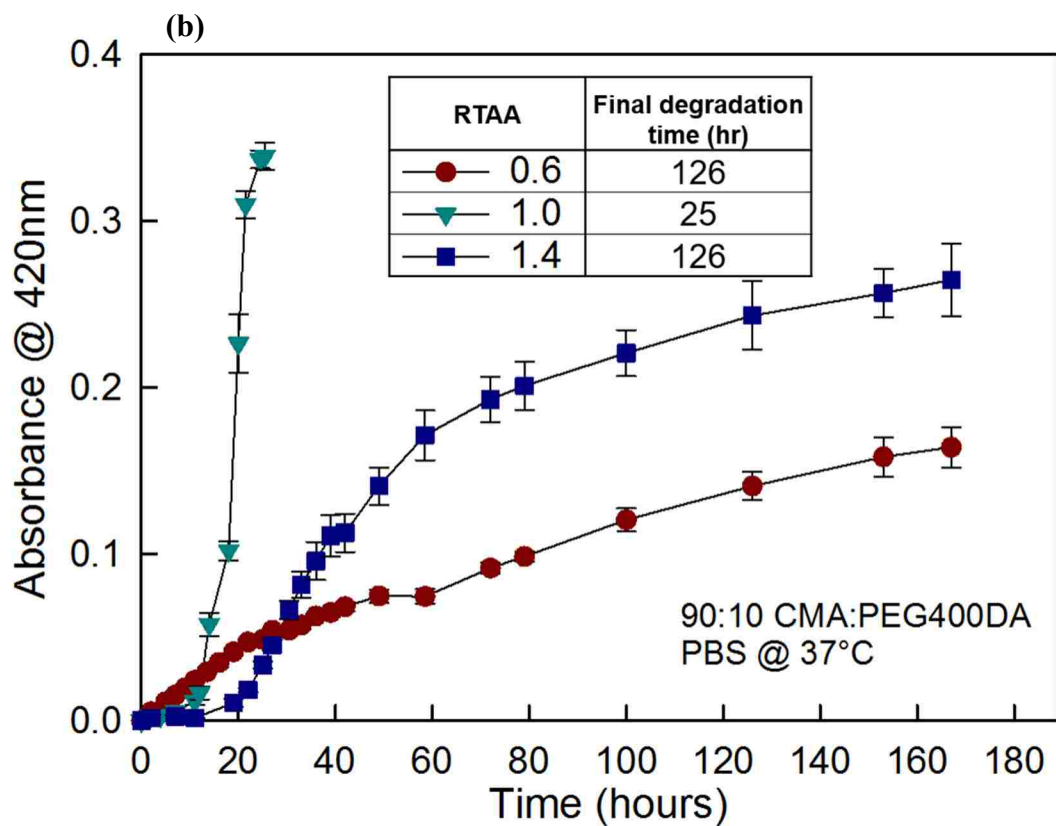


**Figure 5.10:** Degradation in PBS (0.1 % SDS) for 90:10 CMA:PEG400DA films made with TTD for different RTAA. (a) Swelling ratio as a function of degradation time; (b) Curcumin release profile measured using absorbance @ 420 nm.

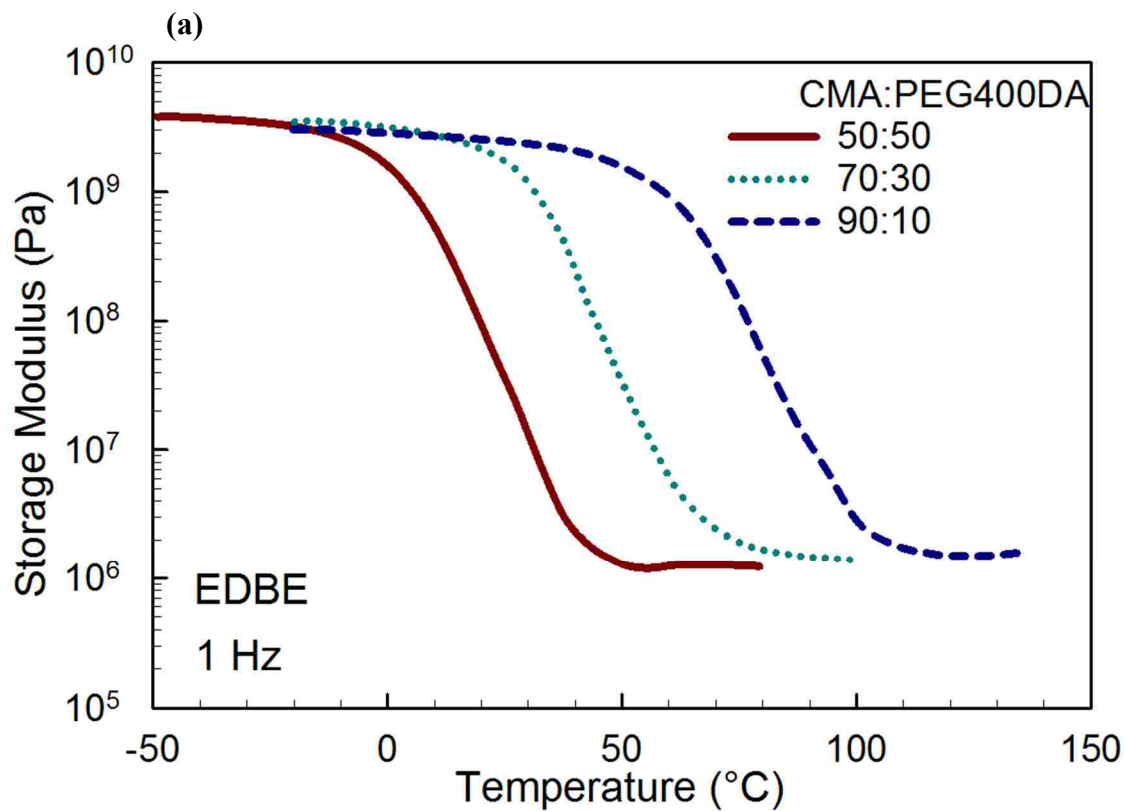


**Figure 5.11:** Dynamic mechanical properties of different CMA:PEG400DA fillms made with EDDBE crosslinker. (a) Storage modulus vs. Temperature (°C) at 1 Hz; (b) Tan  $\delta$  vs. Temperature (°C) at 1 Hz.

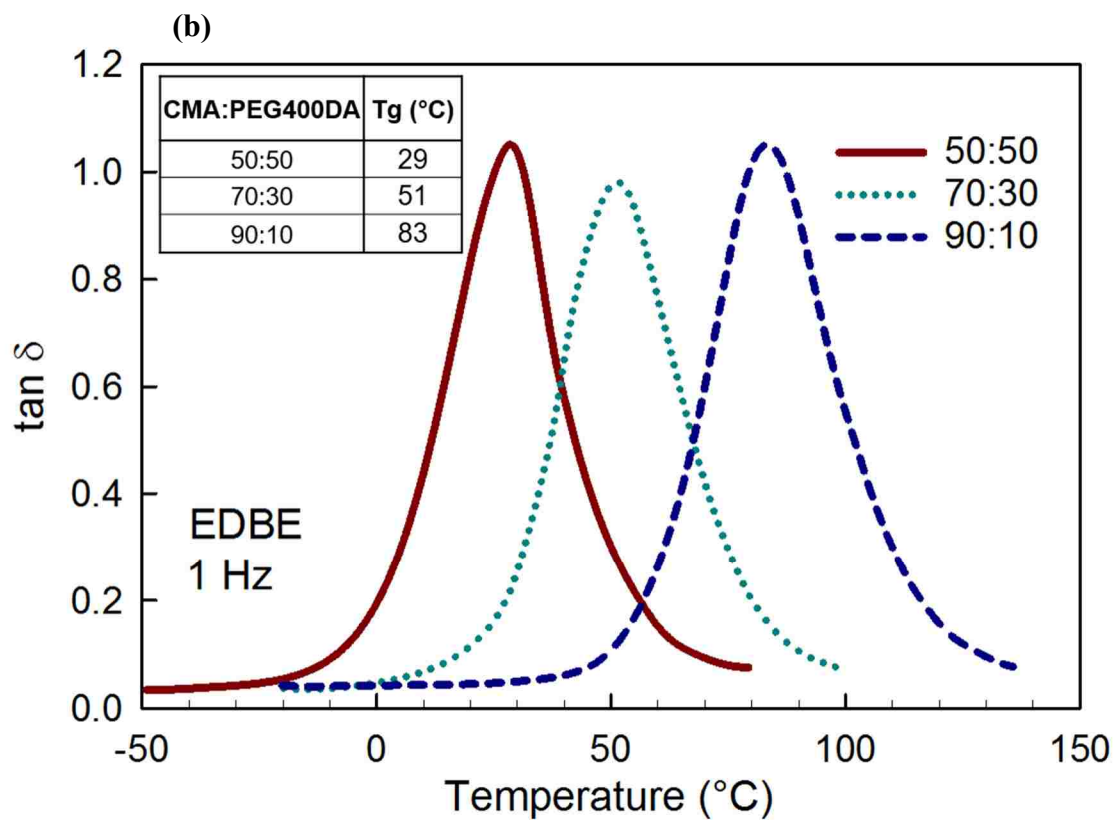


**Figure 5.11:** Dynamic mechanical properties of different CMA:PEG400DA films made with EDDB crosslinker. (a) Storage modulus vs. Temperature (°C) at 1 Hz; (b) Tan  $\delta$  vs. Temperature (°C) at 1 Hz.

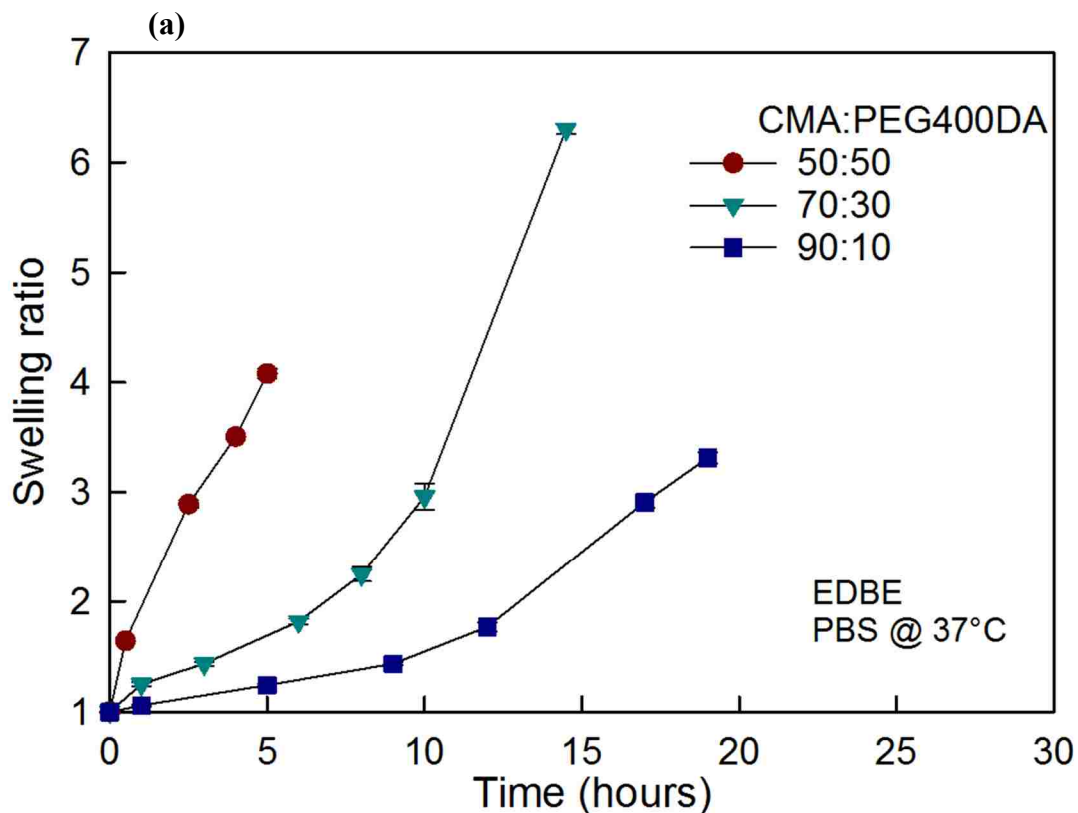


**Figure 5.12:** Degradation in PBS (0.1 % SDS) for different CMA:PEG400DA films made with EDDB crosslinker. (a) Swelling ratio as a function of degradation time; (b) Curcumin release profile measured using absorbance @ 420 nm; (c) Antioxidant capacity of supernatants measured using TEAC in-vitro antioxidant capacity measurement assay.

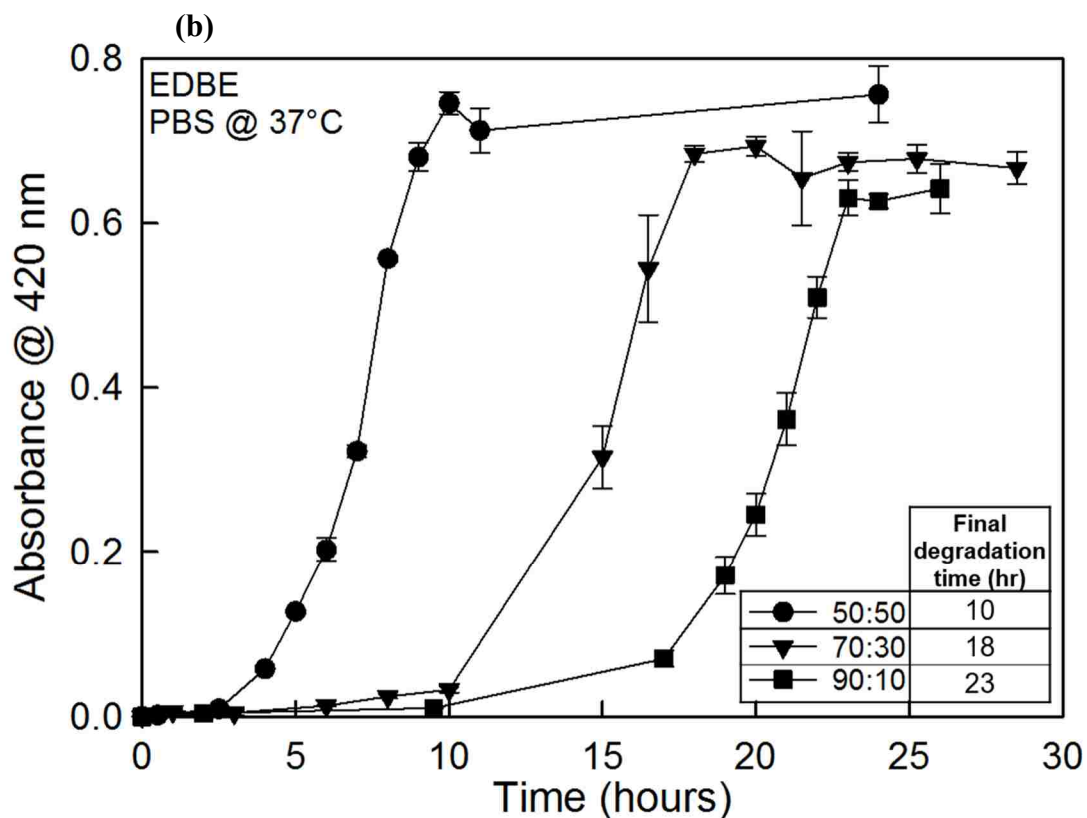


**Figure 5.12:** Degradation in PBS (0.1 % SDS) for different CMA:PEG400DA films made with EDDB crosslinker. (a) Swelling ratio as a function of degradation time; (b) Curcumin release profile measured using absorbance @ 420 nm; (c) Antioxidant capacity of supernatants measured using TEAC in-vitro antioxidant capacity measurement assay.

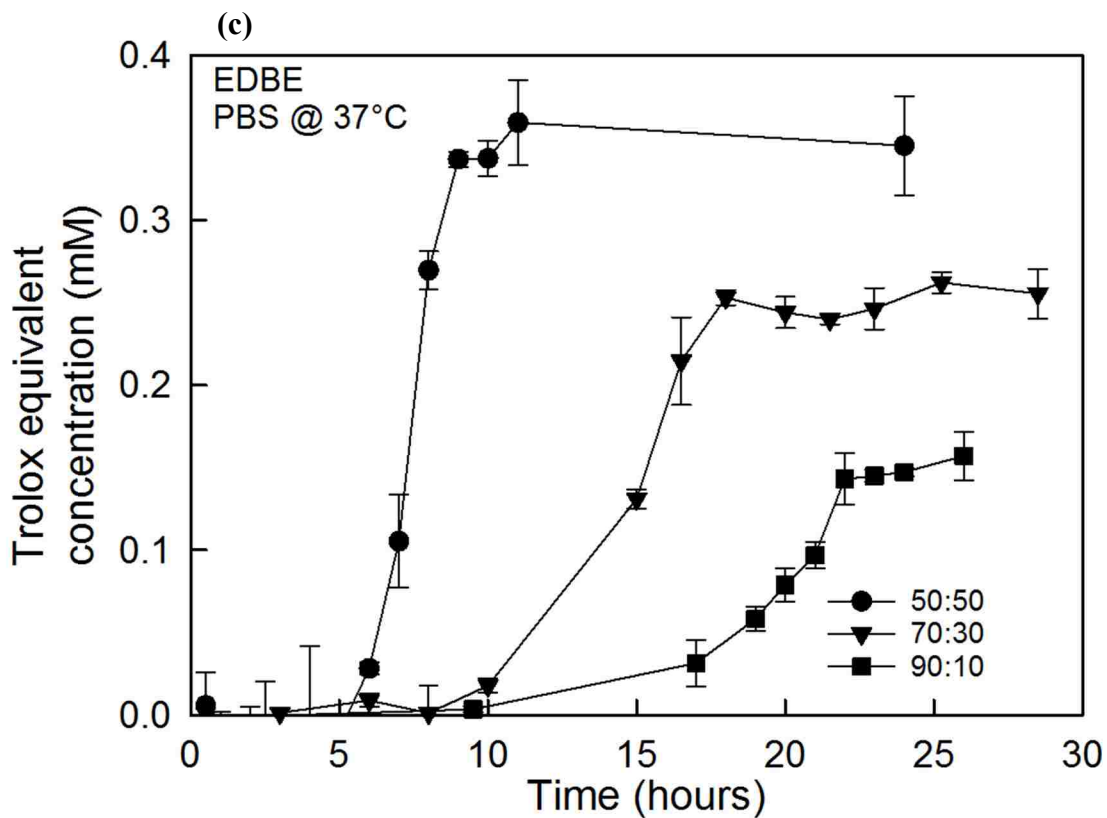


**Figure 5.12:** Degradation in PBS (0.1 % SDS) for different CMA:PEG400DA films made with EDDBE crosslinker. (a) Swelling ratio as a function of degradation time; (b) Curcumin release profile measured using absorbance @ 420 nm; (c) Antioxidant capacity of supernatants measured using TEAC in-vitro antioxidant capacity measurement assay.

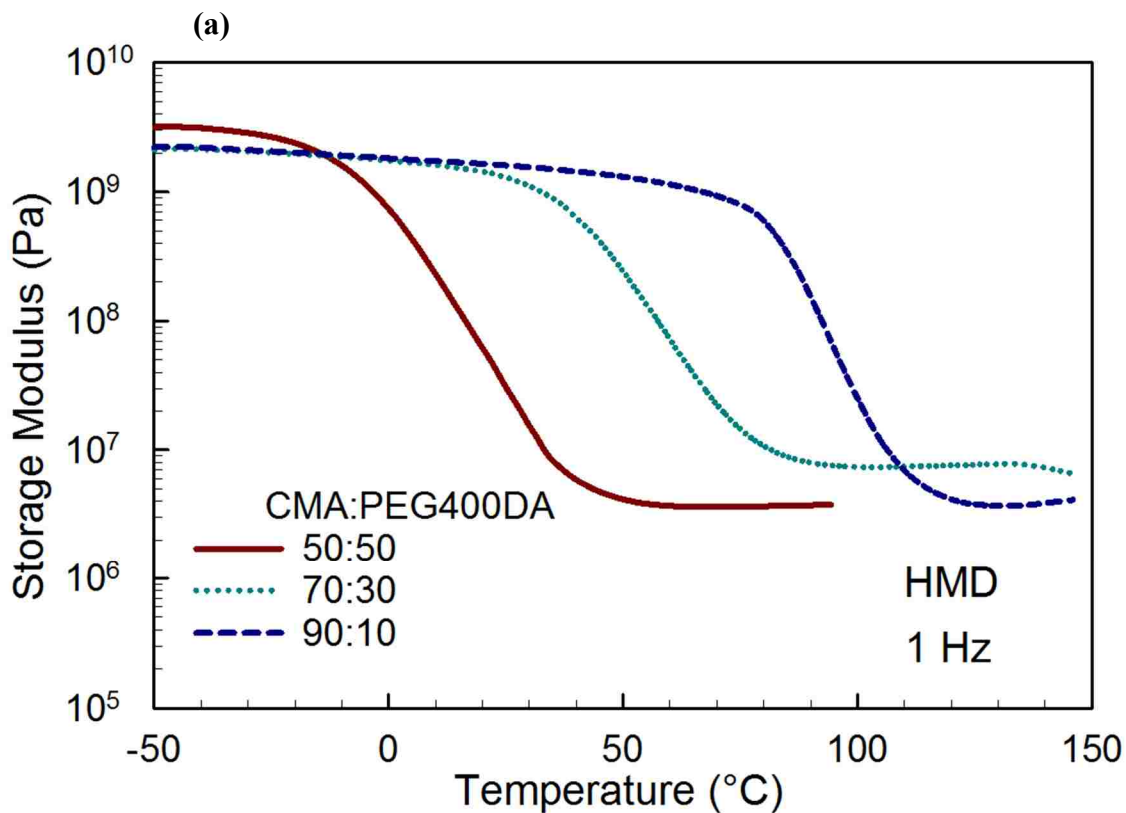


**Figure 5.13:** Dynamic mechanical properties for PCBAE films of different CMA:PEG400DA composition made with HMD crosslinker. (a) Storage modulus vs. Temperature (°C) at 1 Hz; (b) Tan  $\delta$  vs. Temperature (°C) at 1 Hz.

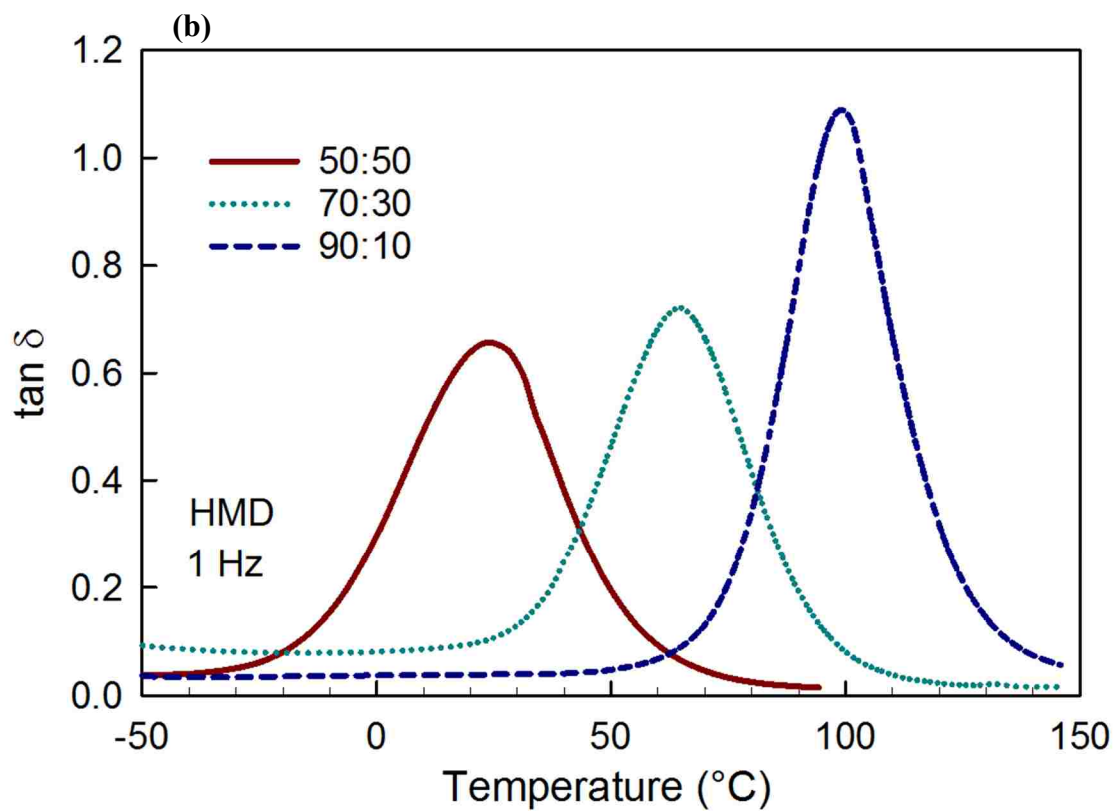


**Figure 5.13:** Dynamic mechanical properties for PCBAE films of different CMA:PEG400DA composition made with HMD crosslinker. (a) Storage modulus vs. Temperature ( $^{\circ}\text{C}$ ) at 1 Hz; (b) Tan  $\delta$  vs. Temperature ( $^{\circ}\text{C}$ ) at 1 Hz.

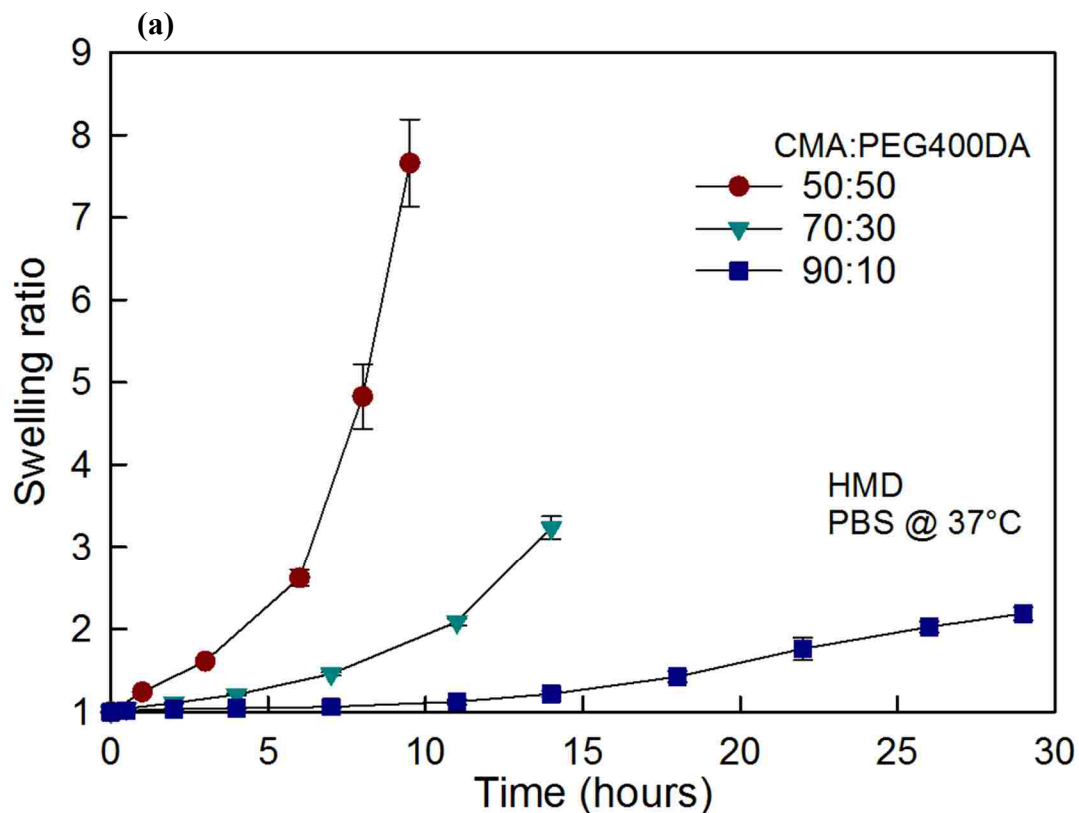


**Figure 5.14:** Degradation in PBS (0.1 % SDS) for different CMA:PEG400DA films made with HMD crosslinker. (a) Swelling ratio as a function of degradation time; (b) Curcumin release profile measured using absorbance @ 420 nm; (c) Antioxidant capacity of supernatants measured using TEAC in-vitro antioxidant capacity measurement assay.

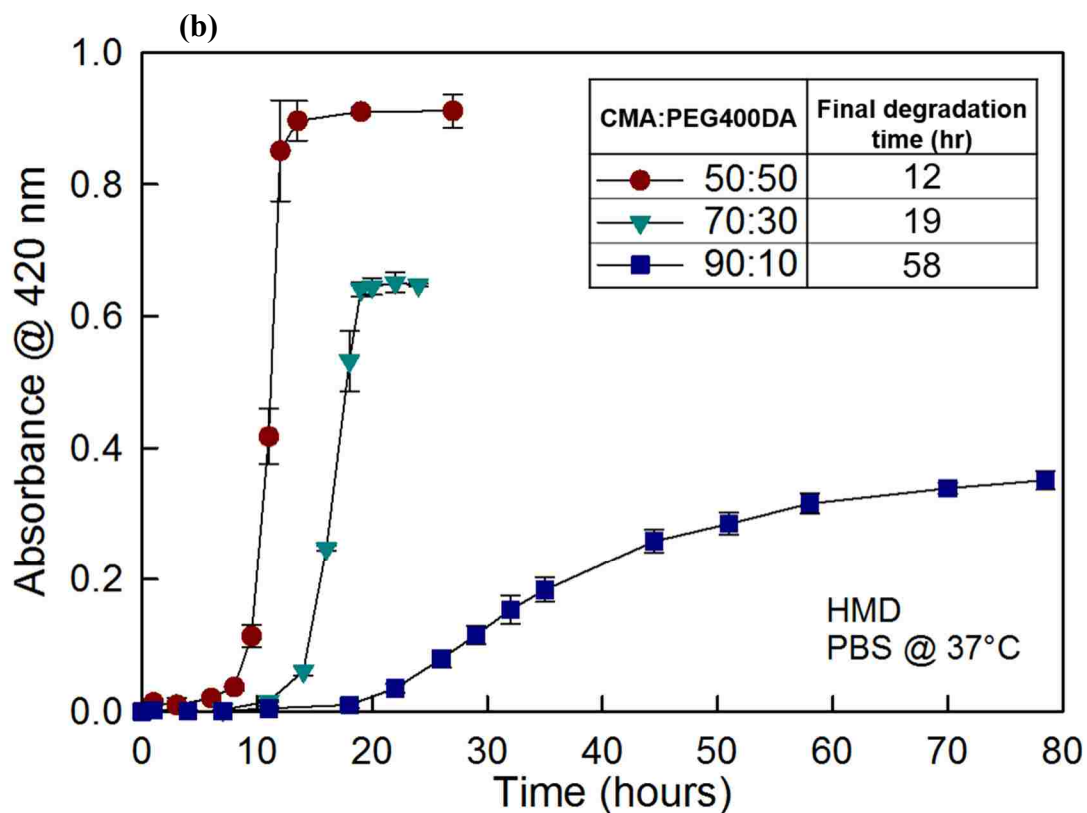


**Figure 5.14:** Degradation in PBS (0.1 % SDS) for different CMA:PEG400DA films made with HMD crosslinker. (a) Swelling ratio as a function of degradation time; (b) Curcumin release profile measured using absorbance @ 420 nm; (c) Antioxidant capacity of supernatants measured using TEAC in-vitro antioxidant capacity measurement assay.

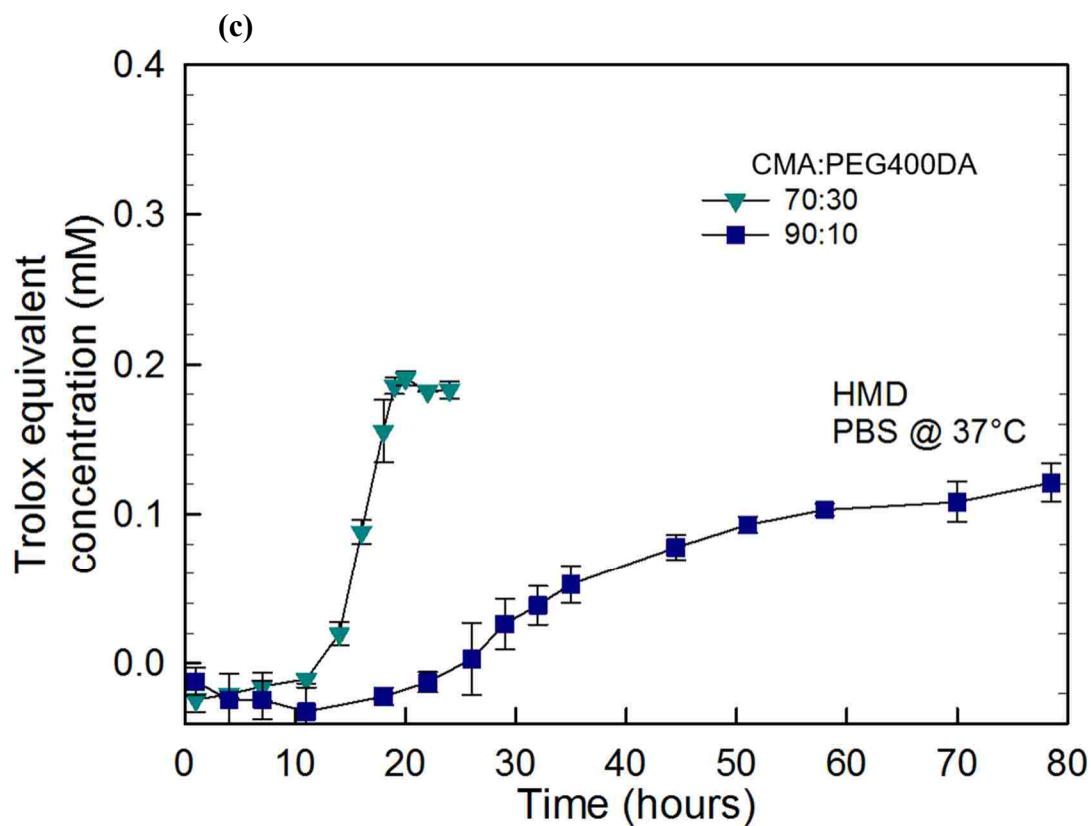


**Figure 5.14:** Degradation in PBS (0.1 % SDS) for different CMA:PEG400DA films made with HMD crosslinker. (a) Swelling ratio as a function of degradation time; (b) Curcumin release profile measured using absorbance @ 420 nm; (c) Antioxidant capacity of supernatants measured using TEAC in-vitro antioxidant capacity measurement assay.

## **Chapter 6: Poly( $\beta$ -amino ester) based tablet formulation for improved oral bioavailability of a hydrophobic drug**

### **6.1 Introduction**

Oral dosage of drugs remains the most commonly used form of drug delivery due to patient compliance and ease of administration. Oral formulations are used for treating a wide range of diseases localized to the gastrointestinal (GI) tract, such as gastritis, enterocolitis, enteritis, inflammatory bowel diseases, as well as for delivering drugs to the whole body for systemic disorders [208-210]. However, the efficacy of oral formulations is often limited by poor stability and solubility of the drug, which is usually overcome by the use of enteric coatings. These coatings rely on pH dependent swelling for drug release [211]. However, enteric coatings can be ineffective if the patient is taking proton pump inhibitors, which result in increased stomach pH, or when the coatings are broken. If the coatings are compromised, dose dumping can raise the drug concentration in the body to toxic levels [212].

Inflammatory bowel diseases such as Crohn's disease, ulcerative colitis, infectious colitis, or ischemic colitis are caused by the formation and cascade of reactive oxygen species that lead to a chronic inflammatory response [27, 210, 213]. The resulting oxidative stress can be overcome by the use of antioxidants, which can scavenge the reactive oxygen species, reducing oxidative stress signaling and thus allowing the tissue to heal and reverse inflammation [133, 214, 215]. In addition, colon-specific delivery has applications in the treatment of colon cancer and for delivering proteins and peptides due to the close-to-neutral pH in the colon [216]. Different approaches have been explored for colon-specific

delivery that include enzymatic degradation of polymers such as gaur gum, polymers with pH dependent solubility, timed release systems and osmotically controlled release systems [211, 217-219]. While all promising, each possesses limitations that hamper their applicability. For instance, in the case of gaur gum based tablets, a seven-day enzyme induction period is needed before actually using the tablets. Also, as the pH of the gastrointestinal tract is known to vary under different conditions and with the use of proton pump inhibitors, it may be difficult to deliver drugs to the desired site based solely upon pH dependent solubility of the polymer excipients [220]. Similarly, due to the considerable variation in transit time through the GI tract, timed release systems don't always work, and the manufacturing process of osmotically controlled release systems can be complex and expensive. A sustained delivery of antioxidants to the colon is needed for effective reduction of oxidative stress without systemic side effects, while also providing a better strategy to deliver poorly soluble drug molecules.

One possible way to overcome these limitations is the use of a new polymeric prodrug hydrogel i.e. poly( $\beta$ -amino ester) (PBAE). A drug molecule of interest is incorporated into the polymer hydrogel network through covalent bonding, which improves the stability of the drug by hindering motion of the labile groups on the molecule and also by limiting the access of degradative agents to these groups. Once inside the body, PBAE undergoes hydrolytic degradation to release the drug. The degradation of PBAE is relatively slow at lower pH, such that only minimal degradation is anticipated in the upper gastrointestinal tract, with more substantial degradation upon reaching higher pH environments. Induction treatments and enteric coatings are eliminated with the use of PBAEs, making the crosslinked polymer network an advantageous drug delivery system

that can provide the controlled release of antioxidants upon hydrolytic degradation of polymer which can be tailored for different release times and drug loadings.

In this study, we have developed oral hydrogel formulations for the delivery of curcumin, which is a hydrophobic drug. Curcumin is a polyphenolic compound found in the Indian food spice turmeric, which has anti-oxidant and anti-inflammatory properties. Poly(curcumin  $\beta$ -amino ester) (PCBAE) hydrogels with release times from 5 to 25 hours have been developed previously by tuning the hydrophobic composition of the network [69], and *in vitro* studies have shown PCBAE to be non-toxic [124]. In this chapter, we have investigated an oral PCBAE tablet formulation appropriate for colon-targeted drug delivery. The formulation contained PCBAE (20% by weight) and microcrystalline cellulose (MCC; 80% by weight). The tablets were evaluated for sustained curcumin release as well as overall stability, which is an important commercial consideration. The results of detailed release studies are presented for the as-prepared hydrogel films, hydrogel microparticles, and the tablet formulation exposed to a range of controlled storage conditions.

## **6.2 Experimental**

### **6.2.1 Materials**

Curcumin was purchased from Chem-impex International, Inc. Acryloyl chloride, triethyl amine, 4,7,10-trioxa-1,13-tridecanediamine (TTD) and magnesium stearate were all purchased from Sigma-Aldrich. Poly(ethylene glycol) 400 diacrylate (PEG400DA) was purchased from Polysciences. Avicel® PH-102 NF (microcrystalline cellulose) was obtained from FMC BioPolymer. Sodium dodecyl sulfate, sodium bromide and sodium chloride were all obtained from Fisher Scientific. All organic solvents were purchased from

Pharmco-AAPER. The molecular sieves were added to all solvents to remove any trace moisture present.

### **6.2.2 Synthesis of poly(curcumin $\beta$ amino ester) gel films**

PCBAE films were formed by reacting commercial diacrylate (PEG400DA) with a primary diamine (TTD) in combination with acrylate functionalized curcumin. Curcumin was functionalized with acrylate by reaction with acryloyl chloride to form curcumin multiacrylate (CMA) according to an established protocol [69]. The solvent used for synthesis of the films was dichloromethane (DCM) and the amount used was 1.5 mL of solvent per gram of total monomer weight. The CMA:PEG400DA molar ratio used for synthesis of the films was 90:10. PEG400DA was mixed with half of the total solvent amount and CMA was dissolved in the remaining half. TTD was added to the PEG400DA solution and allowed to pre-polymerize for 5 minutes at room temperature. The CMA solution was then added under continuous mixing and the entire mixture was transferred to a casting ring assembly. This set up was kept at room temperature for 1 hour and subsequently incubated in a convection oven at 50°C for 24 hours. The resulting films were washed in acetonitrile for 5 hours on an orbital shaker (with solvent change every hour), followed by drying overnight at 50°C in a vacuum oven. The as-synthesized films had a thickness of approximately 350 microns.

### **6.2.3 Particle size analysis**

90:10 CMA:PEG400DA PCBAE gel films were cryomilled using the SPEX®SamplePrep 6770 Freezer/Mill® with 1% magnesium stearate. Particle size of the cryomilled gel powder was analyzed using a Shimadzu SALD-7101 nano particle size analyzer with particles suspended in phosphate buffered solution (PBS). PBS was used as

a blank to cancel the background signal. The powder suspension was stirred continuously during the analysis.

#### **6.2.4 PCBAE prodrug tablet synthesis**

The blend used for tableting was made by mixing microcrystalline cellulose (80% by weight) and 90:10 CMA:PEG400DA PCBAE prodrug gel powder (20% by weight). Microcrystalline cellulose (MCC) was used as a binder as well as diluent. This blend was then compacted and milled using mortar and pestle. Tablets were prepared by directly compressing the blend in a tablet die (10 mm diameter) using a hydraulic press at 42.5 MPa. All tablets had an approximate weight of 400 mg.

In addition to the prodrug (i.e. PCBAE-containing) tablets, tablets based on free curcumin were prepared as a control. The free curcumin tablets were formulated from as-received curcumin powder (10.54% by wt.), cryomilled powder of 0:100 CMA:PEG400DA (9.46% by wt.) and MCC (80% by wt.) using same method.

#### **6.2.5 Tablet dissolution and curcumin release**

The dissolution studies were completed in a USP (United States Pharmacopoeia) apparatus II in PBS at 37°C with an impeller speed of 100 RPM. Phosphate buffered solution (PBS) with 0.1% (w/w) sodium dodecyl sulfate (SDS) was used as the dissolution media. SDS was added to PBS to improve the solubility of curcumin; this was based on the United States Food and Drug administration (USFDA) recommendation for dissolution testing of sparingly soluble drugs [221]. 1 mL aliquots were taken and the reservoir was replenished with 1 mL of fresh dissolution media for each sample time point. The sample aliquots were stored at -20°C until further analysis. All tablet and gel degradation studies were carried out using this method unless otherwise specified. Aliquots were analyzed by

UV-Visible spectrophotometry (Cary® 50 UV spectrophotometer) and reverse phase high-performance liquid chromatography (HPLC; Waters Phenomenex C18 Column, 5  $\mu\text{m}$ , 250 mm (length) x 4.6 mm (I.D.) on a Shimadzu Prominence LC-20 AB HPLC system). The wavelength used for detection of curcumin in both UV-vis and HPLC was 420 nm, which is the peak absorbance wavelength for curcumin. The curcumin release data are presented as  $M_t/M_\infty$ , where  $M_t$  is the absorbance at 420 nm for time  $t$  and  $M_\infty$  is the absorbance corresponding to the theoretical curcumin loading for a given sample. In the analysis of samples using HPLC, a gradient method file from 50/50 acetonitrile/water to 100/0 acetonitrile/water over 13 minutes at 1 mL/min was used for all samples with an injection volume of 50  $\mu\text{L}$ . Curcumin elution quantities were determined from the HPLC chromatograms based on a corresponding calibration curve of peak area versus curcumin concentration.

### **6.2.6 Anti-oxidant activity using TEAC assay**

Anti-oxidant activity of released curcumin was evaluated using the standard trolox equivalent anti-oxidant activity concentration (TEAC) assay. 2,2'-azinobis-(3-ethylbenzothiazoline-6-sulfonate) (ABTS) cation radical solution was prepared by reacting ABTS and potassium persulfate overnight. The absorbance intensity of the cation radical solution was decreased to 0.4 by dilution with PBS. Using a 96-well microplate, 10  $\mu\text{L}$  of sample to be analyzed was introduced to each well followed by 200  $\mu\text{L}$  of cation radical solution. The absorbance was measured after 5 minutes at 734 nm and compared against the standard trolox curve. For the TEAC assay, a decrease in absorbance is seen as the antioxidant concentration increases.

### 6.2.7 Standard and accelerated storage stability

The stability of the tablets was studied under standard and accelerated storage conditions as prescribed by USP (USP <1150>). The recommended standard conditions are 25°C and relative humidity (RH) of 57% and the recommended accelerated conditions are 40°C and 75% RH. These conditions were maintained in an air tight chamber with beakers containing saturated salt solutions of sodium bromide and sodium chloride, respectively [222]. Different sets of tablets were stored in both conditions for 1, 2, 3, and 4 weeks. Moisture absorption was assessed and the tablet dissolution profile was measured for each distinct exposure history.

## 6.3 Results

### 6.3.1 Film degradation and tablet dissolution

90:10 CMA:PEG400DA hydrogel film was used for making microparticles needed for prodrug tablet synthesis. The corresponding theoretical drug loading in the film was 52.7% (weight of curcumin/weight of hydrogel). Particle size analysis of the cryo-milled 90:10 CMA:PEG400DA gel powder was performed using the Shimadzu nano particle size analyzer by suspending the microparticles in PBS. The particle size distribution data for these particles is presented in **Figure 6.1**. Particle size was found to be below 40 microns for 70 % of the particles.

In **Figure 6.2**, curcumin release profiles from aqueous degradation of the 90:10 CMA:PEG400DA film along with results for the (microparticle-containing) prodrug tablet and free curcumin tablet are presented. For the first 12 hours of film degradation, very little release is observed. However, after 12 hours, the polymer starts to display significant

swelling due to hydrolysis of ester bonds [69] and this leads to curcumin release from the hydrogel film. A sustained curcumin release up to approximately 26 hours is observed.

The PCBAE prodrug tablet underwent rapid disintegration (within the first 30 minutes) thereby releasing MCC and PCBAE gel particles, followed by hydrolytic degradation of the PCBAE gel particles. Since curcumin is covalently bonded in the polymer network and unreacted monomers were removed during the washing step, no initial burst release is seen during the degradation of these gels. This is one of the advantages of PC $\beta$ AE based prodrug approach, since initial burst release is a common problem encountered in the traditional approach of physically entrapping drug molecules in a polymer network [223]. Curcumin release from the microparticles was assessed by measuring the absorbance at 420 nm. A sustained curcumin release is observed over about 16 hours. The inset plot in Figure 6.2 shows the curcumin release from as-prepared microparticles compared to the release measured for the prodrug tablet. It can be seen that the excipients used in tablet formulation do not affect the curcumin release profile and that the release is governed solely by microparticle (i.e. hydrogel) degradation.

Similar to the prodrug tablet, tablets compounded with “free” curcumin powder disintegrated within the first 30 minutes of immersion in PBS. An almost immediate dumping is seen with the free curcumin tablet as compared to the controlled release of curcumin that is observed for the PCBAE prodrug tablet (re: Figure 6.2). The PCBAE prodrug tablet displayed a final  $M_t/M_\infty$  value of 0.5, which is 2.5 times the value obtained for the free curcumin tablet ( $M_t/M_\infty$  value of 0.2); a higher  $M_t/M_\infty$  value is desired as it represents higher drug recovery as well as higher *in-vitro* drug solubility in PBS. The  $M_t/M_\infty$  value for the free curcumin tablet is significantly lower than the PCBAE result due

to the crystalline character of hydrophobic curcumin, which limits its dissolution and results in the presence of solid curcumin precipitate in the PBS medium. Poor solubility is a concern with many hydrophobic crystalline drugs such as indomethacin, nifedipine, and griseofulvin, and amorphous forms of these drugs are often prepared as a way to enhance their dissolution [206, 224-226]. A higher value of  $M_t/M_\infty$  is obtained for the prodrug tablet as PCBAE is an amorphous polymer network, and the released curcumin dissolves completely without crystal formation or precipitation.

The release of native curcumin was confirmed by HPLC analysis of the degradation aliquots as shown in **Figure 6.3**. A continuous release of curcumin (HPLC elution time between 5.2 and 6 minutes) is seen with an increase in degradation time. Along with curcumin, curcumin monoacrylate (elution time between 7.6 and 8.5 minutes) and a small amount of curcumin diacrylate (elution time between 10 and 10.8 minutes) are also recovered from the HPLC column. The individual species of the curcumin acrylation mixture have been identified by Liquid chromatography–Mass spectrometry (LCMS) as reported in an independent study [173].

### **6.3.2 Tablet storage stability**

In order to study the stability of the tablet formulations according to USP protocol, tablets were held under standard and accelerated storage conditions. The effect of storage conditions on tablet stability was then assessed by comparing the moisture absorption and curcumin release profiles for tablets with varying storage exposure history. Images of an as-prepared tablet and tablets after storage at standard and accelerated conditions for 1 week are presented in **Figure 6.4**. Tablets stored at accelerated conditions exhibited a more intense orange surface coloration compared to the as-prepared tablet and tablets stored at

standard conditions. The weights of the tablets were measured before and after exposure at standard and accelerated conditions to quantify the moisture absorption of the tablets. The percentage weight change due to moisture absorption is shown in **Figure 6.5**. Tablets stored at the accelerated conditions had higher moisture absorption than those stored at standard conditions for a given exposure time. Also, overall moisture absorption increased with longer storage times at the standard condition, while tablets stored at the accelerated condition reached equilibrium weight within a week.

Aqueous dissolution studies were performed on all tablets held at standard and accelerated storage conditions for different times. The curcumin release data for these studies are reported in **Figure 6.6**. The time needed for total curcumin release from prodrug tablets stored at standard storage conditions decreased as the prior storage time was increased, with tablets stored for 4 weeks showing a total release time of just 1 hour. All of the tablets stored at standard conditions disintegrated within the first two hours of the dissolution study, followed by the release of curcumin from microparticles that had undergone partial degradation during the storage.

For the accelerated storage conditions, tablets held for 1 week had the fastest curcumin release rate. The overall curcumin release time increased as exposure time was increased, with tablets stored for 4 weeks prior to testing requiring 24 hours for complete release. This delay in curcumin release for tablets stored over longer times was not anticipated, and appears to reflect a change in the physical disintegration dynamics of these tablets as compared to those samples stored under standard conditions. Specifically, for tablets stored at accelerated conditions, the observed disintegration times in PBS were 4 hours, 8 hours, 14 hours and 20 hours for prior storage times of 1 week, 2 weeks, 3 weeks

and 4 weeks, respectively. These results were in direct contrast to the behavior observed for tablets held at standard conditions, which all disintegrated within two hours regardless of prior storage history. The time needed for total curcumin release from tablets stored at accelerated conditions correlated closely with the disintegration time of each tablet, suggesting that the delayed physical disintegration of the tablets was the controlling mechanism for curcumin release for this series of tablets. However, even though the as-prepared tablets and tablets held at standard and accelerated conditions had different degradation times, all of them reached the same plateau  $M_t/M_\infty$  value with a final curcumin concentration corresponding to 21.5  $\mu\text{g/mL}$  (based on UV-Vis measurement).

HPLC elution curves for selected release time points are presented in Figure 6.3. Analysis of the elution curves for the final release time points was performed to determine the concentration of curcumin in the degradation products obtained for each tablet exposure history; these data are reported in **Figure 6.7**. The concentration of curcumin for 100% theoretical release would be 42.2  $\mu\text{g/mL}$ , indicating only a 25% to 40% recovery of pure curcumin from the dissolved tablets. These lower values reflect the presence of acrylated curcumin and PEG-curcumin adducts in the degradation products from the PCBAE network. A higher overall curcumin concentration is indicated for the tablets exposed to the accelerated storage conditions; for the standard conditions, a modest increase in curcumin concentration is observed with an increase in prior storage time.

To further understand the delay in release seen for tablets stored at the accelerated conditions (40°C and RH = 75%), another set of tablets was stored at the same conditions and the tablets were then crushed into powder before adding to the dissolution apparatus. The curcumin release curves from dissolution of these two sets of tablets are shown in

**Figure 6.8.** It was observed that essentially all of the curcumin release from the crushed tablets occurred within the first hour, whereas at least 20 hour was required for full curcumin release from the uncrushed tablets. This result confirmed that the PCBAE microparticles present in the tablets degrade extensively to curcumin during the 4 week storage at accelerated conditions, and that an increase in the time needed for total curcumin release in the uncrushed tablets primarily reflects the difference in the physical disintegration characteristics of the tablets, as noted above.

The effect of temperature on tablet stability in the absence of surrounding moisture was analyzed by storing tablets in a desiccant chamber (RH = 0%) for 2 weeks at 25°C and 40°C; the corresponding curcumin release curves for these PCBAE prodrug tablets are presented in **Figure 6.9**. The release profile for tablets stored at 25°C was not significantly affected; however, tablets stored at 40°C showed total curcumin release within 3 hours. This suggests that the small amount of moisture present in the microcrystalline cellulose (MCC) binder could be contributing to a thermally-driven degradation of the microparticles at elevated temperature, even in the absence of ambient moisture.

To further understand the influence of temperature and moisture on the storage stability of the tablet formulation, as-prepared gel films were stored at 40°C for 4 weeks in a desiccant chamber (RH = 0%). The curcumin release profile for the degradation of these gels is reported in **Figure 6.10**. For the gel films, no degradation was seen at 40°C in the absence of surrounding moisture, which was in contrast with the release profile for tablets stored at the same conditions (re: Figure 6.9). This confirms that the small amount of moisture present in the MCC binder in the prodrug tablet is sufficient to cause the

degradation of PCBAE at 40°C, with a dramatic impact on the resulting curcumin release properties.

### **6.3.3 Antioxidant activity**

Selected degradation samples were analyzed using the TEAC assay, which measures the antioxidant activity of released curcumin in comparison with the trolox standard. The TEAC release profiles for prodrug tablets exposed to both standard and accelerated storage conditions are presented in **Figure 6.11**, and show data trends similar to the curcumin release profiles as reported in Figure 6.6. The TEAC results confirm that the curcumin released during the tablet dissolution studies maintains antioxidant activity. The final equivalent trolox concentration for all curves is consistent with the final curcumin release concentration as determined from UV spectroscopy.

## **6.4 Discussion**

In this work, PCBAE based tablets were synthesized for controlled release of curcumin with improved bioavailability. The advantage of this formulation is that stability of the drug is improved through protection of labile groups via covalent conjugation of curcumin within the polymer network. Colon specific drug delivery was achieved from a hydrolytically degradable polymeric prodrug without the use of enteric coatings. It was determined from a previous study that PCBAE hydrogels with 90:10 CMA:PEG400DA composition degraded over 25 hours [69]. In addition, the 90:10 composition had the highest glass transition temperature ( $T_g = 67^\circ\text{C}$ ) among the samples studied, which reflects favorable overall stability of the network and potential long term stability for oral drug formulation. For these reasons, PCBAE films with the 90:10 CMA:PEG400DA composition were used for the tablet formulations characterized in this work.

A sustained curcumin release was measured from the PCBAE prodrug tablet formulation over approximately 16 hours, while for 90:10 CMA:PEG400DA hydrogel films, curcumin release was observed over 25 hours (Figure 6.2). Also, the PCBAE prodrug tablet had a continuous release from the start with no lag phase, while the as-prepared hydrogel film did not show measurable curcumin release until approximately 12 hours. These differences in release characteristics are primarily the result of the difference in the characteristic size scale of the microparticles (on the order of 40 microns) as compared to the hydrogel film (approx. 350 microns). Smaller gel particle size leads to a potentially faster swelling due to higher surface to volume ratio. Poly( $\beta$ -amino ester) hydrogels typically undergo bulk erosion which is not a size dependent phenomena [103, 227]. However, the effect of degradation products on the release and degradation of hydrogels has been well studied, and in the case of samples with larger dimensions, degradation products leach out much more slowly as compared to samples with smaller dimensions [103, 228]. The effect of particle size on degradation of poly(lactic-co-glycolic acid) (PLGA) microspheres has been studied where diffusion of degradation products from the particles affected the degradation [229, 230]. In our system, it is possible that the slow leaching of curcumin-containing degradation products from the hydrogel film leads to an increase in the concentration of these products in the film, slowing the film degradation, which leads to a lag in the curcumin release during gel film degradation.

A much higher  $M_t/M_\infty$  curcumin release value was obtained for the PCBAE prodrug tablet as compared to the free curcumin tablet (re: Figure 6.2). A sustained curcumin release is seen from the prodrug tablets, while short-time dumping was encountered with the free curcumin tablet. For the free curcumin tablet,  $\sim 80\%$  of the curcumin precipitates as

crystalline solid, emphasizing its poor solubility and uptake [207]. This poor solubility along with rapid first pass metabolism has resulted in rather poor outcomes in clinical trials [231]. For instance, from a study by Sharma et. al and Garcea et. al. on the patients with colorectal cancer, results showed that very small concentration of curcumin was present in plasma and urine which led to lower efficiency of curcumin in the treatment of the condition under study [232-235]. Curcumin has low aqueous solubility due to its hydrophobic and crystalline nature. The incorporation of curcumin in PCBAE hinders the crystal formation and increases bioavailability of curcumin since curcumin dumping is avoided due to the controlled release characteristics of the hydrogel. Furthermore, the aqueous solubility of curcumin is increased by the PCBAE degradation products. A controlled release of curcumin is crucial for improving the efficacy of the drug since dumping of curcumin contributes to faster excretion from the body due to low solubility.

The release of the original form of curcumin was confirmed by HPLC for unexposed tablets, as well as tablets stored under controlled conditions (see Figure 6.3). Curcumin monoacrylate and curcumin diacrylate were also detected in the HPLC eluent. These species were formed from the hydrolysis of partially reacted curcumin triacrylate and curcumin diacrylate, respectively. Curcumin released in all dissolution studies retained its antioxidant activity as confirmed by TEAC analysis (see Figure 6.11).

The storage stability of the tablets was studied to understand the role of excipients in the long term storage behavior of the tablet formulations and also because it is an important consideration for the commercialization of any formulation. The stability study of PCBAE prodrug tablets at standard conditions indicated that after one week PCBAE polymer within the tablet was partially degraded as evidenced by the reduction in the final

release time obtained; and the extent of degradation during storage continued to increase with longer storage times and higher moisture absorption (see Figure 6.5 & 6.6). For standard conditions, final release time (i.e. total tablet degradation time) did not coincide with the tablet disintegration time (2 hours), which shows that degradation followed similar hydrolytic degradation process as with the control prodrug tablet. For tablets held at accelerated storage conditions, partial PCBAE degradation observed in one week was comparable to the partial PCBAE degradation observed in 3 weeks at standard condition (see Figure 6.6). This enhanced rate of PCBAE degradation in tablets correlated with the higher moisture absorption at these conditions (see Figure 6.5), which led to enhanced hydrolytic degradation of gel. Also, higher temperature expedited the hydrolysis process [236]. For the accelerated conditions, tablet disintegration times and final release times overlapped. Since 1 week was enough to degrade the gel present in the tablet, it suggests that the delay in the release for longer storage times at accelerated condition was likely due to a delay in the tablet disintegration. This observed delay in tablet disintegration resulted in an enhanced diffusional barrier to curcumin release, meaning that the final release time depended on the tablet disintegration time. This mechanism was confirmed by studying the dissolution of curcumin from crushed tablets, which verified that all the gel particles had degraded after 1 week storage at accelerated condition (see Figure 6.8).

Tablet stability was explored in detail by studying the effect of storage conditions and temperature on the PC $\beta$ AE prodrug tablet. Tablets underwent degradation when stored at high temperature for 2 weeks even in the apparent absence of environmental moisture (see Figure 6.9). However, gel films (without tablet excipient) were stable at these same anhydrous conditions (see Figure 6.10). As, the only difference between gel film and

tablets was the MCC (binder) used for making tablets, which affected the stability, it is believed that the MCC, which has equilibrium moisture of about 3-5% under ambient conditions, is the source of water inducing hydrolysis [237, 238]. It shows that small amount of moisture present in the MCC can cause degradation at high temperature. Based on this evidence, using excipients with low equilibrium moisture content would be recommended for the development of PCBAE based oral formulations.

From Figure 6.9, it was observed that tablets were stable at 25°C for at least 2 weeks and had a release profile similar to the unexposed tablets. However, tablets exhibited PCBAE degradation when incubated at 40°C and had complete release within 4 hours. At standard conditions tablets underwent degradation in 2 weeks. This shows that higher moisture and high temperature both cause the degradation of tablet, though high temperature (40°C) affected the tablet stability to a greater extent than high moisture (RH = 57%).

## **6.5 Conclusions**

Tablet formulations were developed for colon specific delivery using PCBAE gel microparticles. PCBAE provide a novel approach for colon specific drug delivery which is not exclusively dependent on the pH of GI tract. This formulation was able to achieve a sustained curcumin release of about 16 hours which was confirmed by HPLC analysis and activity measurements. PCBAE prodrug tablets improved the bioavailability of curcumin compared to curcumin dumping obtained with free curcumin tablets. Stability studies exhibited a step wise change in the degradation of prodrug tablet with increase in storage time. Stability studies demonstrated that high temperature and high humidity can lead to PCBAE degradation in the formulation, necessitating a low moisture

environment for storage. Small amount of equilibrium moisture present in the excipients affected the stability of PCAE prodrug tablets; the stability can be further improved by using excipients such as mannitol which have less equilibrium moisture content. This approach can also be expanded to colon specific delivery of other drugs which have hydroxyl groups present in their molecular structure.

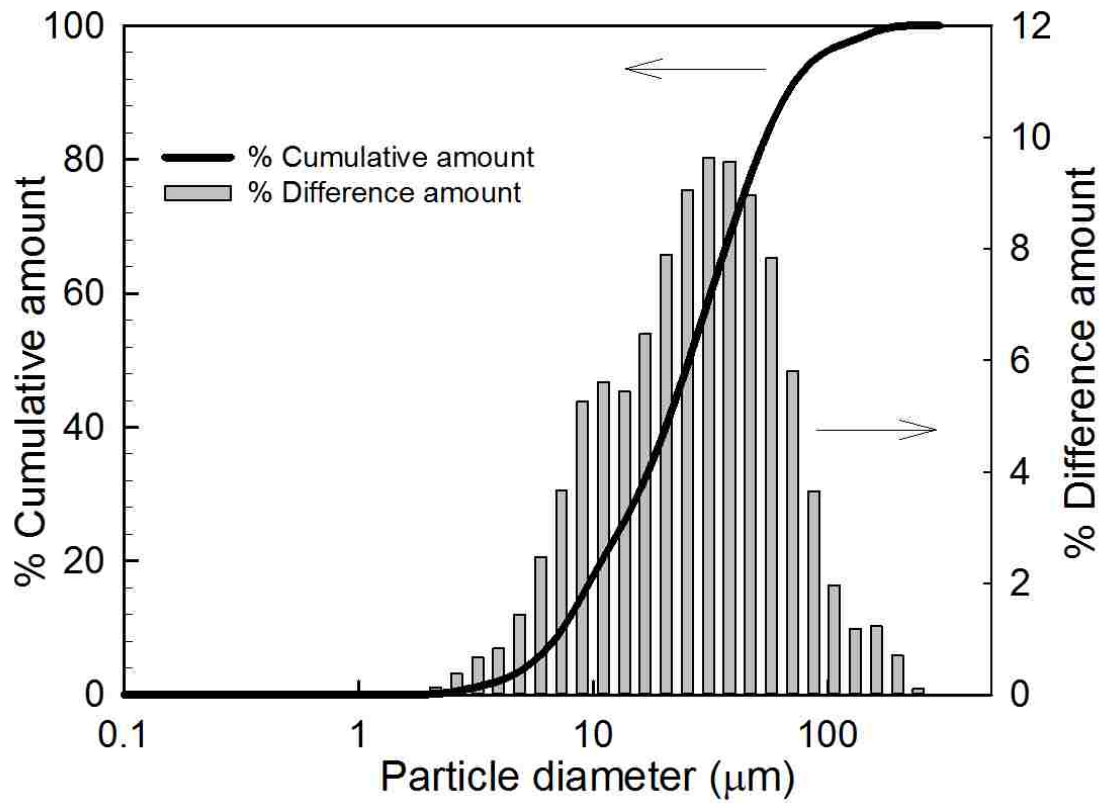


**Figure 6.1:** Particle size distribution for 90:10 CMA:PEG400DA PCBAE microparticles analyzed using Shimadzu SALD-7101 nano particle size analyzer.

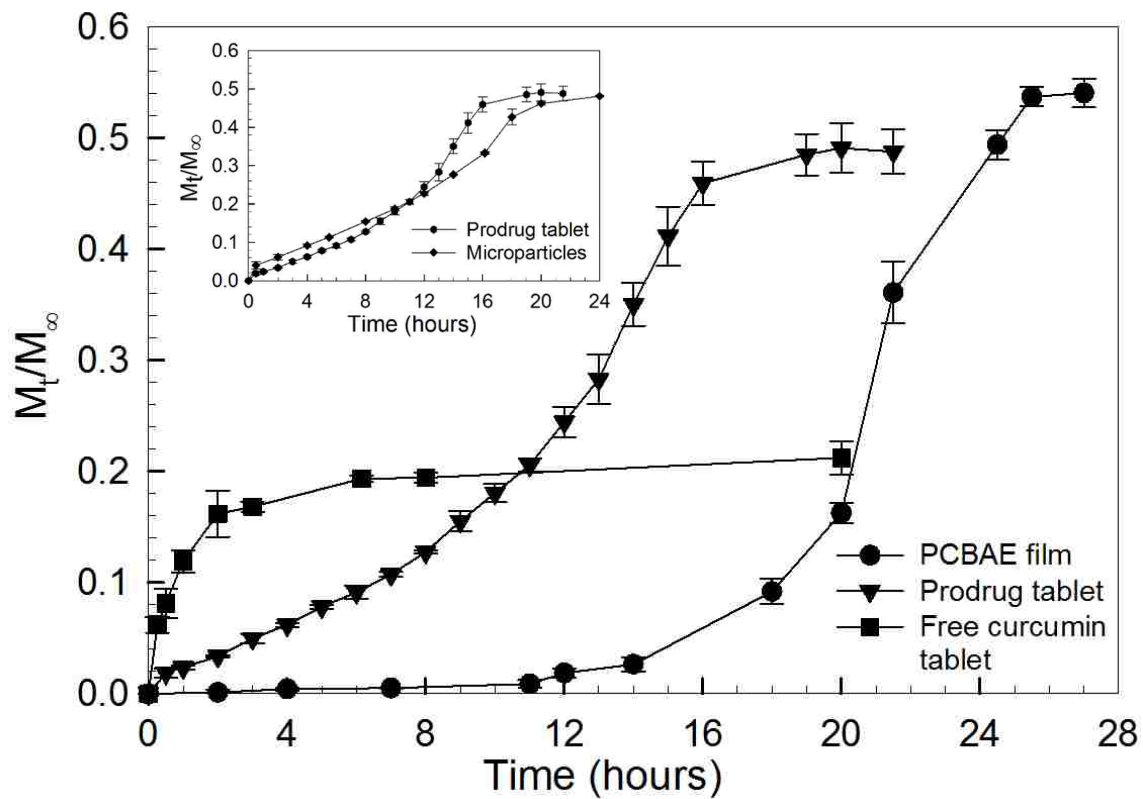


**Figure 6.2:** Curcumin release profiles for 90:10 CMA:PEG400DA PCBAE hydrogel film and tablets containing PCBAE microparticles (i.e. prodrug tablet) and free curcumin powder, respectively, in PBS (0.1 % SDS) at 37°C using USP apparatus II. Inset plot shows curcumin release for prodrug tablet vs 90:10 CMA:PEG400DA microparticles.

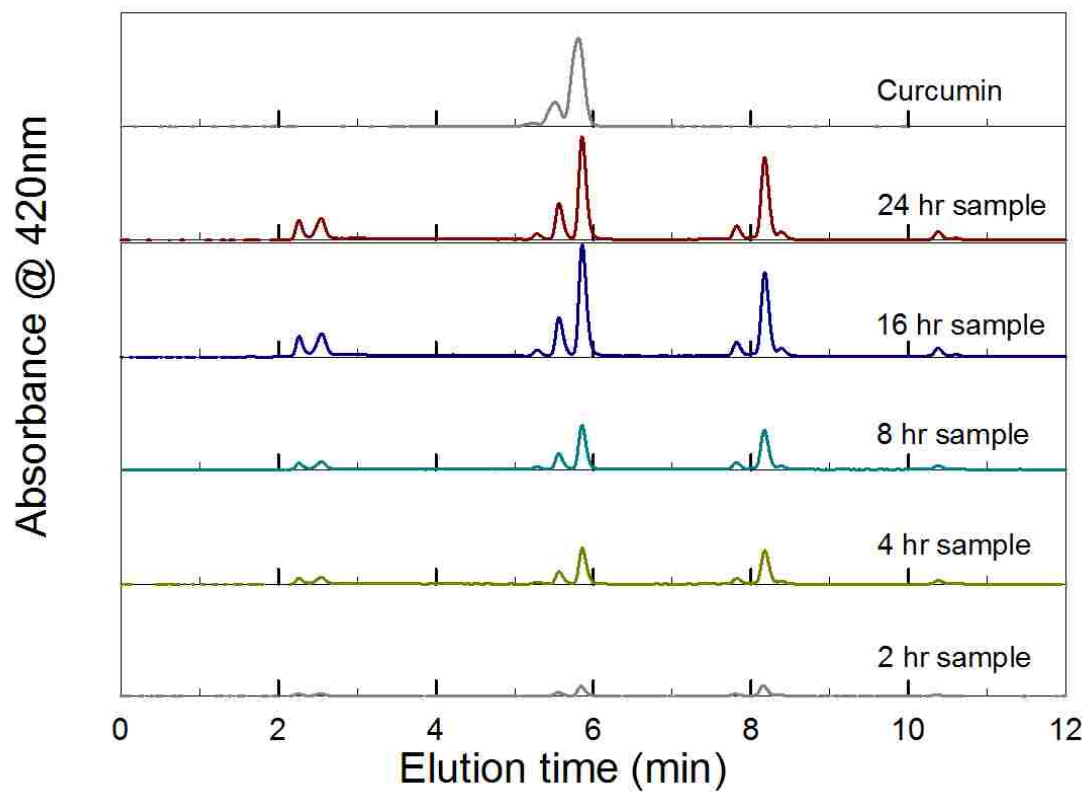


**Figure 6.3:** HPLC peak elution profile (420 nm) for supernatant samples collected during aqueous dissolution of the PCBAE prodrug tablet.

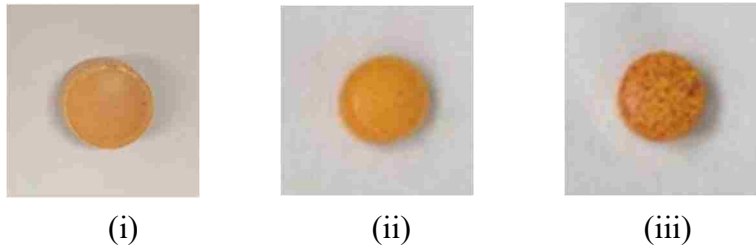


**Figure 6.4:** PCBAE tablets after 1week storage. (i) unexposed tablet; (ii) tablet from standard storage conditions i.e., 25°C and 57% RH; (iii) tablet from accelerated storage conditions i.e., 40°C and 75% RH.

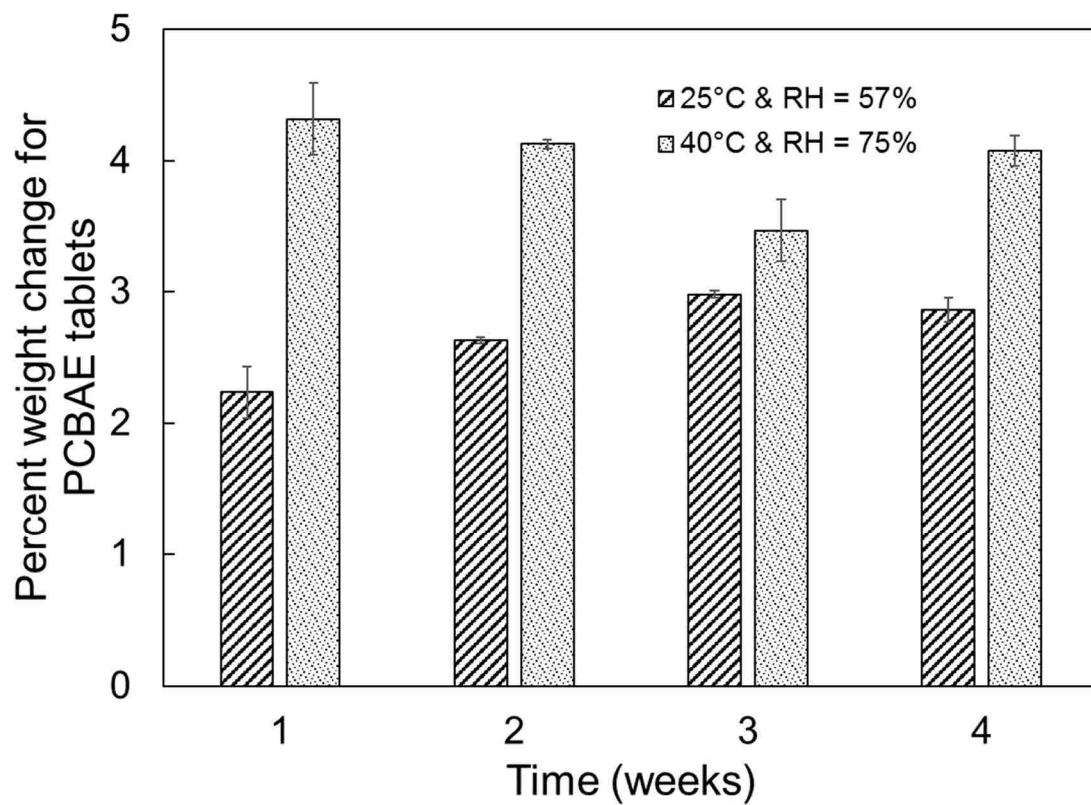


**Figure 6.5:** Prodrug (PCBAE) tablet moisture absorption as a function of storage time for standard and accelerated storage conditions.

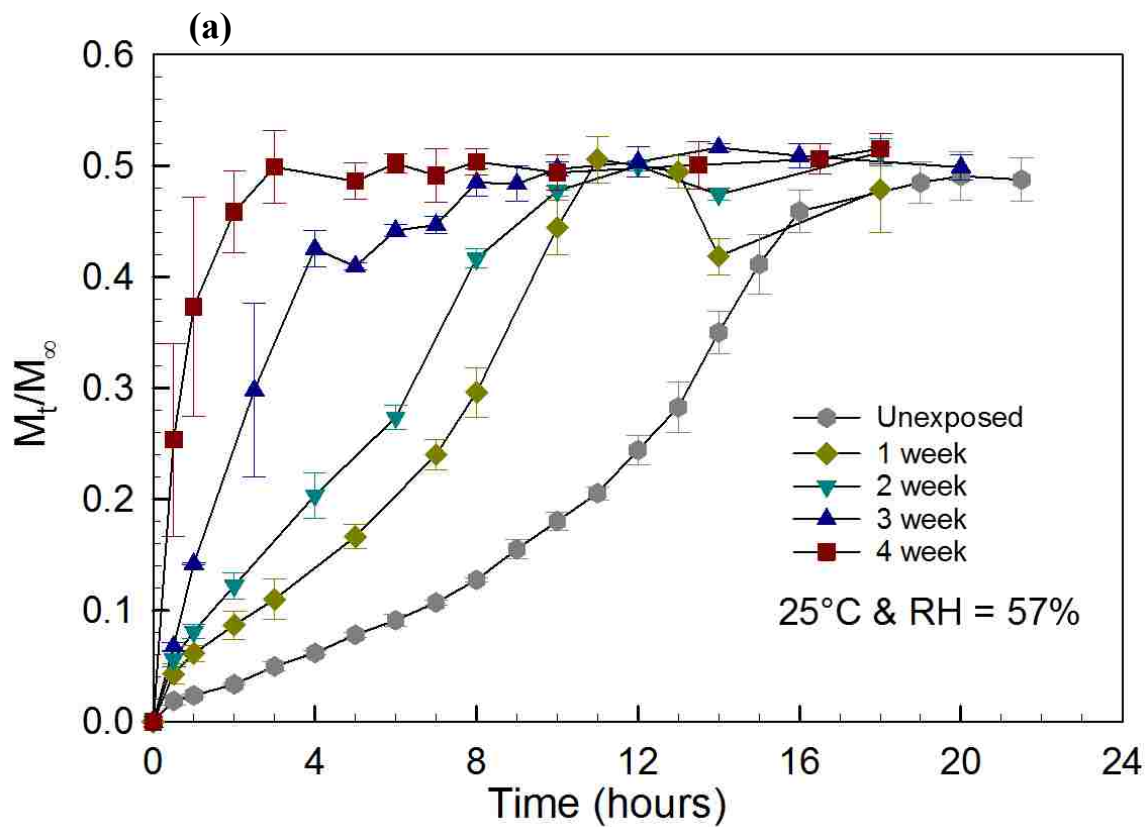


**Figure 6.6:** Curcumin release profiles from dissolution of PCBAE prodrug tablets stored at (a) standard conditions of 25°C & RH = 57%; (b) accelerated conditions of 40°C & RH = 75%.

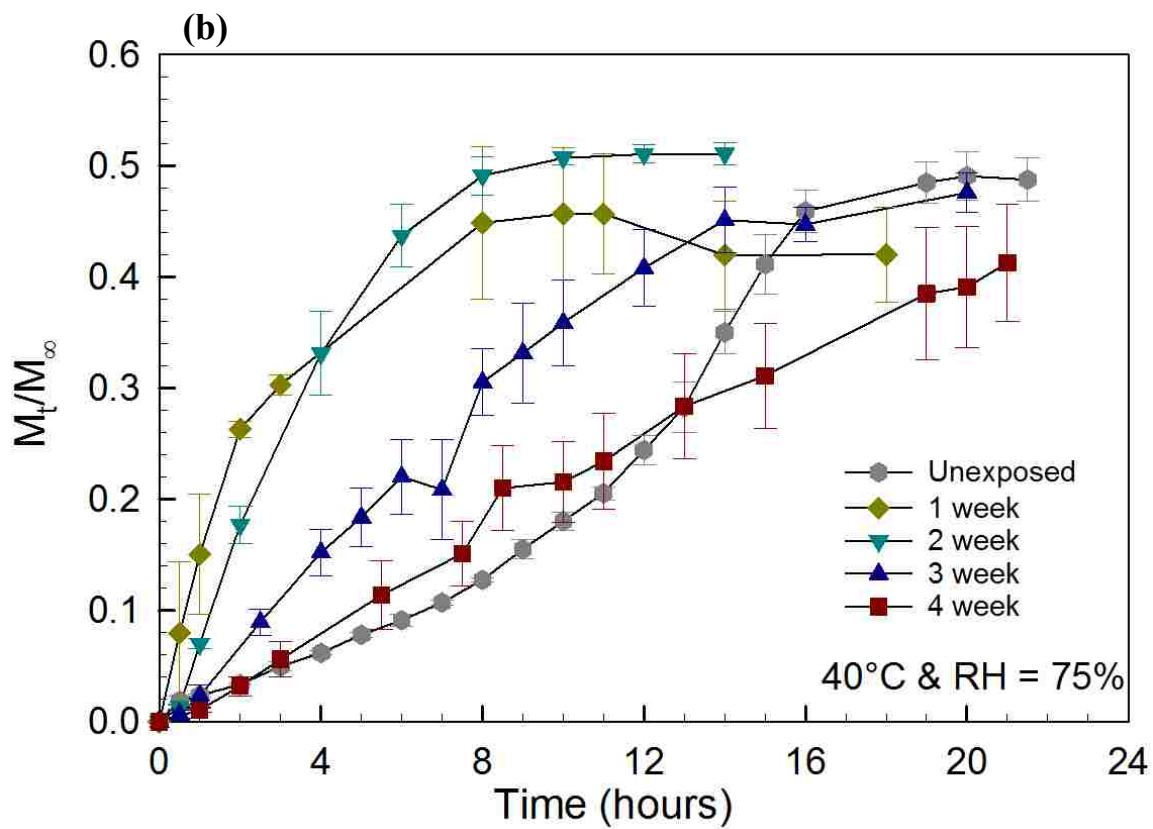


**Figure 6.6:** Curcumin release profiles from dissolution of PCBAE prodrug tablets stored at (a) standard conditions of 25°C & RH = 57%; (b) accelerated conditions of 40°C & RH = 75%.

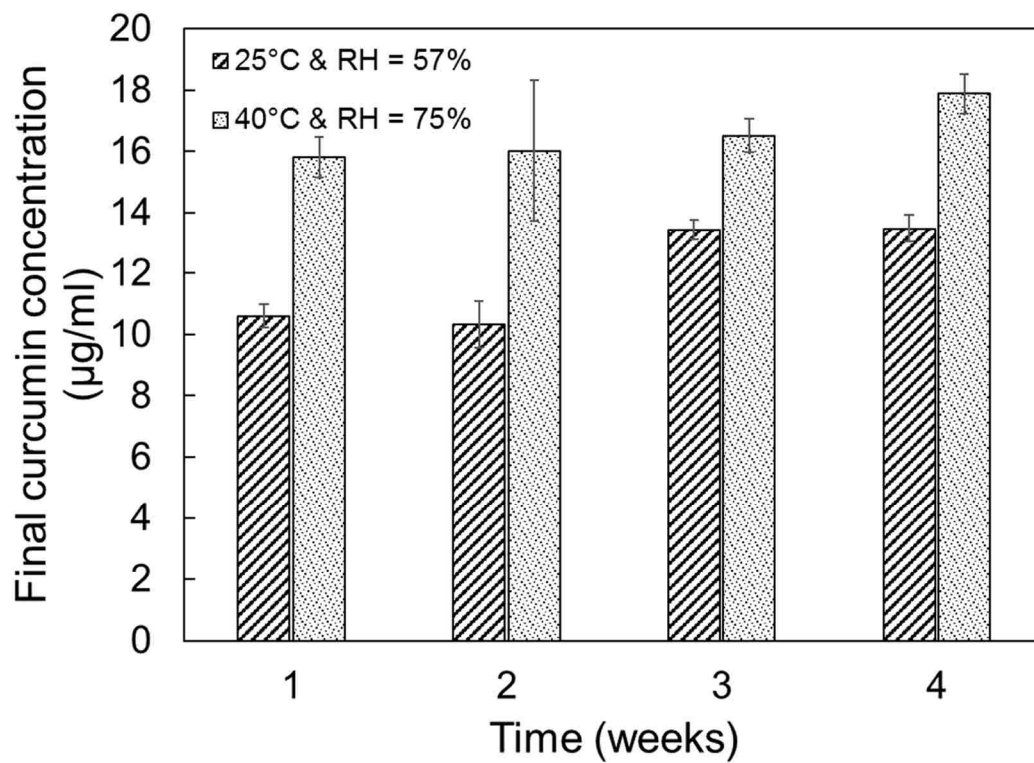


**Figure 6.7:** HPLC analysis of the final degradation supernatants collected from the dissolution of PCBAE prodrug tablets stored at standard and accelerated conditions.

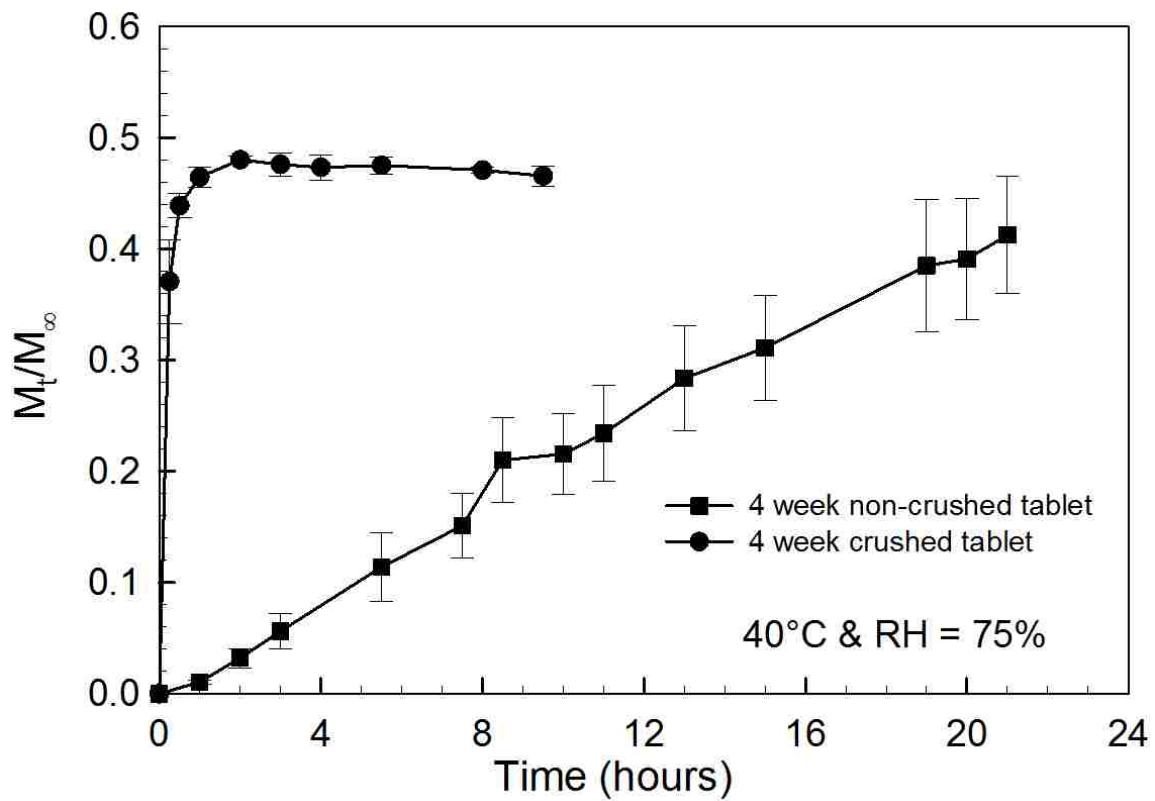


**Figure 6.8:** Curcumin release profiles for PCBAE prodrug tablets stored at accelerated conditions for 4 weeks. Crushed tablet compared with non-crushed tablet.

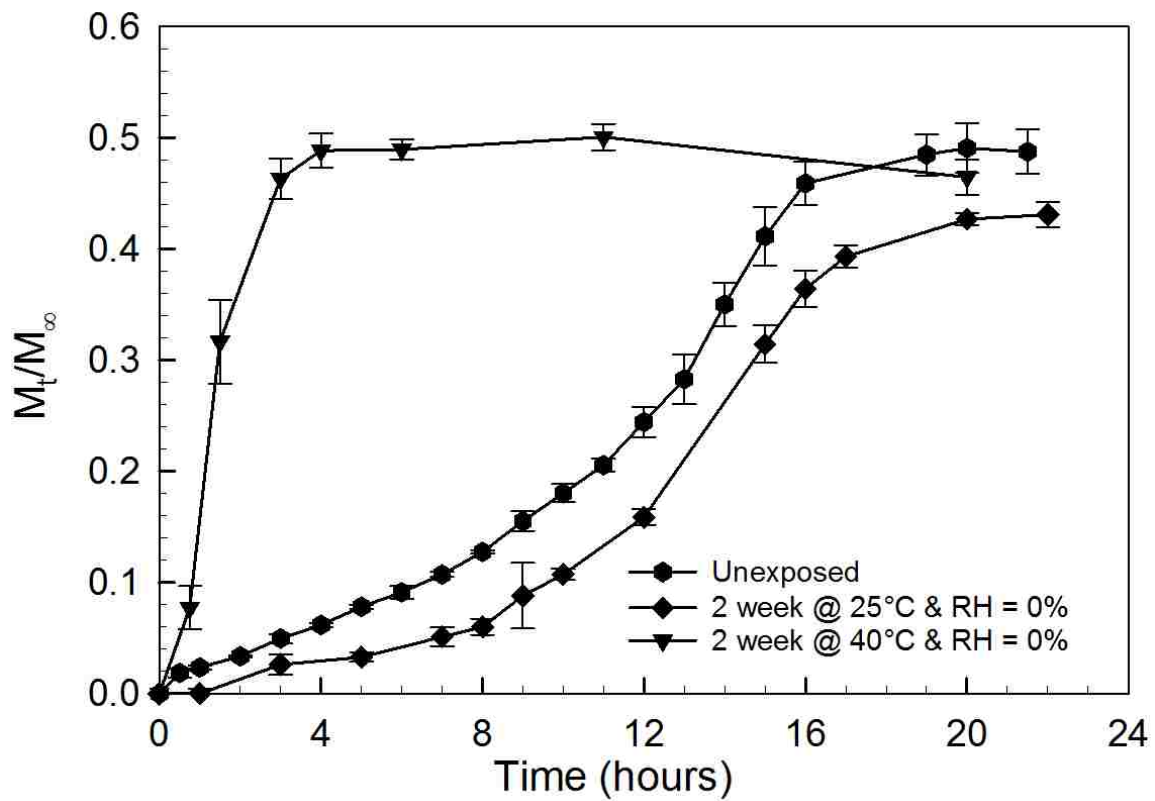


**Figure 6.9:** Curcumin release profiles for PCBAE prodrug tablets stored at 25°C and 40°C for 2 weeks in the absence of surrounding moisture.

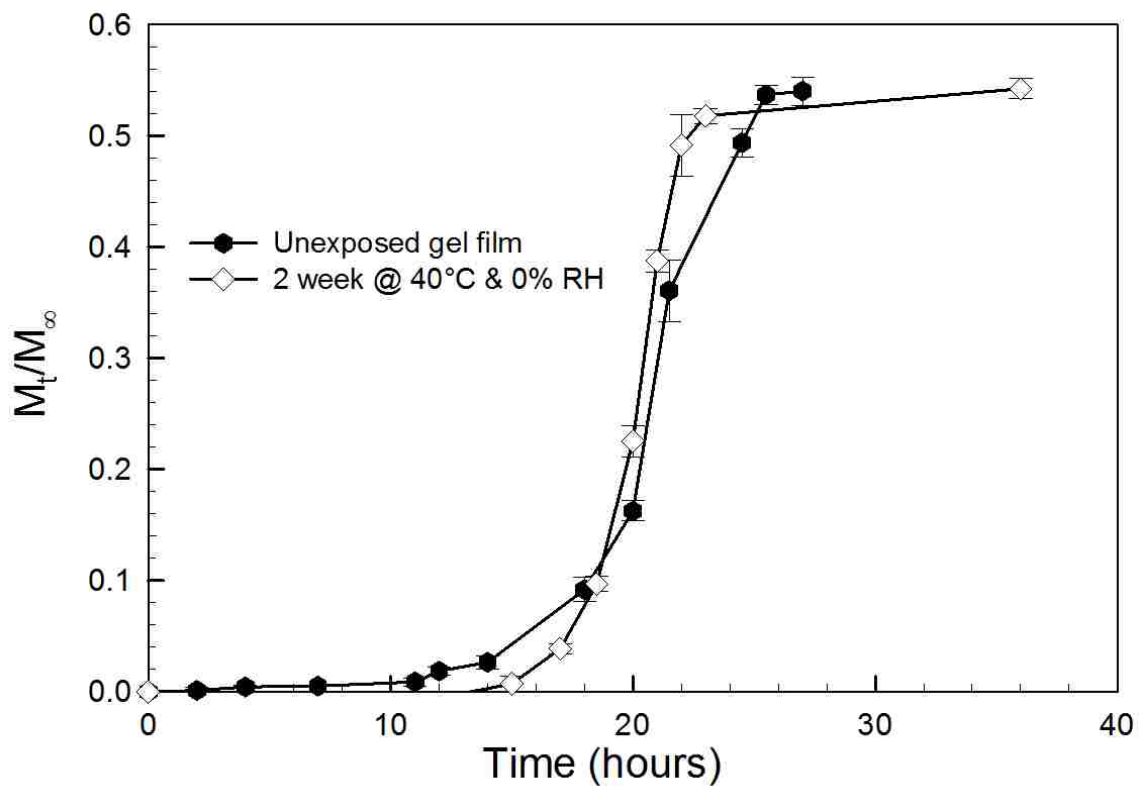


**Figure 6.10:** Curcumin release profiles in PBS for 90:10 CMA:PEG400DA PCBAE hydrogel films as-prepared at ambient conditions, and stored at 40°C for 2 weeks in the absence of moisture (i.e. RH = 0%).

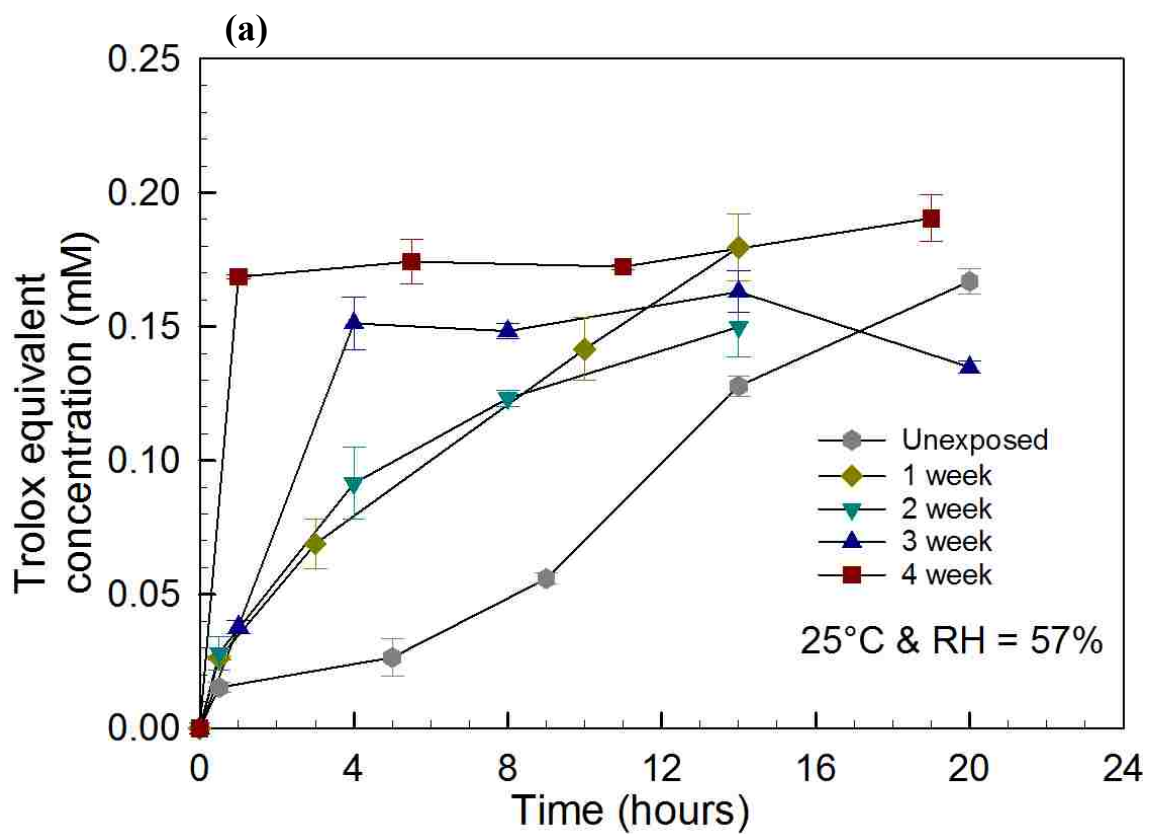


**Figure 6.11:** Antioxidant capacity of tablet dissolution supernatants measured for all storage times at standard conditions using TEAC in-vitro antioxidant measurement assay.

(a) Standard conditions of 25°C & RH = 57%; (b) Accelerated conditions of 40°C & RH = 75%.

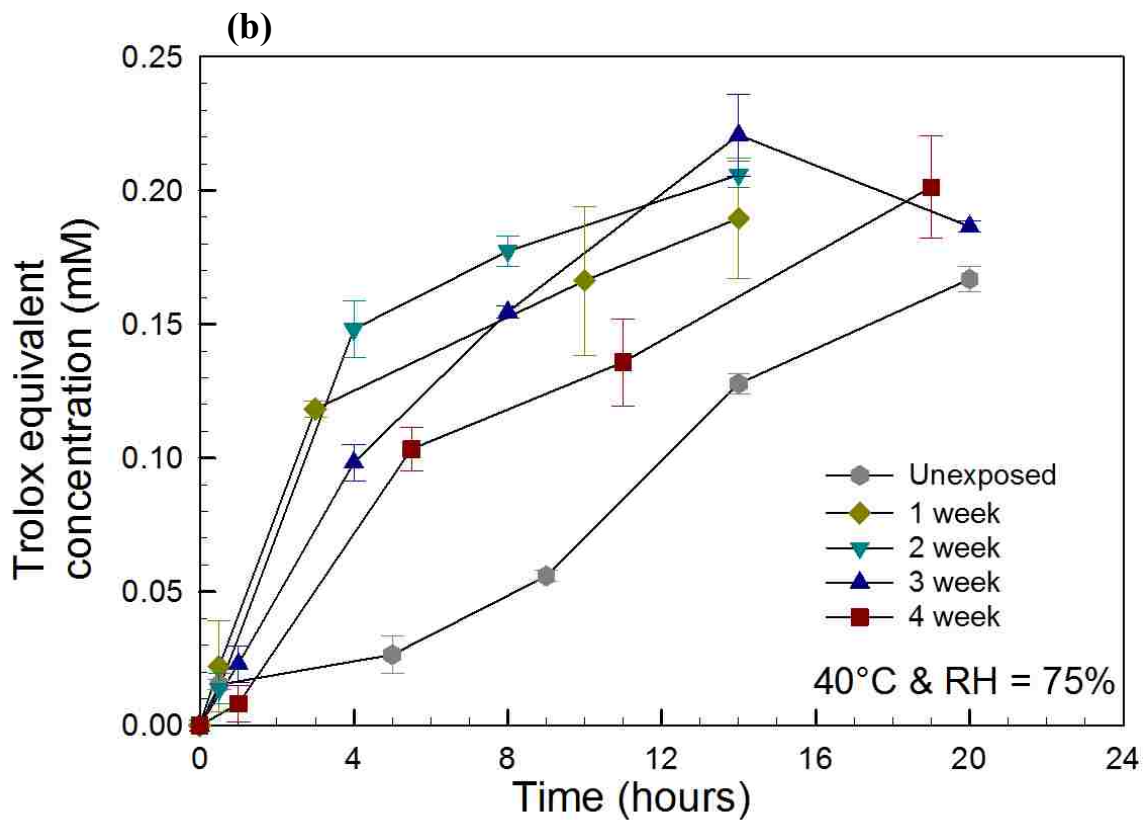


**Figure 6.11:** Antioxidant capacity of tablet dissolution supernatants measured for all storage times at standard conditions using TEAC in-vitro antioxidant measurement assay. (a) Standard conditions of 25°C & RH = 57%; (b) Accelerated conditions of 40°C & RH = 75%

## Chapter 7: Conclusions

In this dissertation, the development of a hydrolytically degradable crosslinked hydrogel network, i.e. poly(curcumin  $\beta$  amino ester) (PCBAE), has been investigated for the controlled release of curcumin. Curcumin, which has been shown to possess antioxidant and anti-inflammatory properties, was functionalized with acrylate groups that allowed a Michael-addition reaction between the curcumin and a primary diamine to form crosslinked PCBAE networks through a single-step polymerization method.

In **Chapter 3**, the extent of curcumin acrylation was tuned through variation in the reaction stoichiometry, and the individual products present in the resulting curcumin multiacrylate (CMA) mixture were characterized. The curcumin multiacrylate was subsequently used for the synthesis of PCBAE networks. In **Chapter 4**, PCBAE networks based on varying CMA:PEG400DA ratios were synthesized and degradation and network properties were characterized. The degradation of PCBAE networks was found to slow with an increase in CMA content in the network. An increase in thermomechanical stability was seen with an increase in CMA composition. Dielectric analysis of PCBAE showed the presence of three molecular relaxation processes in PCBAE networks: two sub-glass relaxations ( $\beta_1$  &  $\beta_2$ ) and one glass-rubber ( $\alpha$ ) relaxation. The sub glass relaxations had their origin in the local motion of ethylene oxide units present in PEG, independent of network composition.

In **Chapter 5**, the degradation and thermomechanical properties of PCBAEs were explored in detail through variation in reaction parameters such as amine crosslinker, diacrylate monomer and acrylate to amine ratio. The degradation properties were measured

through swelling response and curcumin release, while thermomechanical properties were measured using dynamic mechanical analysis. For the gels without curcumin, reduction in the molecular length and hydrophilicity of amine crosslinker had no effect on the thermomechanical properties, but did slow the degradation of the gels. In a similar study with diacrylate monomers, for gels without curcumin, a reduction in hydrophilicity and molecular length of the diacrylate monomer produced an increase in thermomechanical stability and slowed the degradation of the gels. For PCBAE gels made with EDDBE as well as HMD, an increase in curcumin content was found to increase the thermomechanical stability and slowed the degradation due to an increase in overall curcumin composition of the network. An increase in the thermomechanical stability due to increase in total acrylate to amine ratio (RTAA) was also reported. In addition to this, degradation of PCBAEs also slowed down at high RTAA values. Both of these results were due to the high curcumin composition at high RTAA values. However, interestingly, at low RTAA values, degradation also slowed. This was likely due an increase in amine content creating a much tighter network. In general, the PCBAE networks were shown to increase the stability and solubility of curcumin while providing a controlled release as seen from the curcumin release profiles and antioxidant activity measurements. This study of various parameters helped establish fundamental material design rules that will allow for development of tailored networks for specific applications.

To demonstrate the use of PCBAEs in the pharmaceutical field, tablet formulations based on PCBAE microparticles were developed for improving oral bioavailability of curcumin in **Chapter 6** [239]. An improved curcumin solubility was obtained in comparison with the free curcumin tablets and a sustained curcumin release was obtained

for 20 hours, which is suitable for the treatment of inflammatory diseases related to the colon.

Due to the ease of tunability of the thermomechanical and degradation properties of PCBAEs through various process parameters, these hydrogel networks could potentially provide benefit in controlling oxidative stress present in various diseases and with efficacy for a range of applications such as wound healing, tissue engineering, and orthopedic devices. As shown in this work, the solubility and stability of curcumin was also improved through the PCBAE platform. The PCBAE material platform is readily adaptable for use with other drugs containing phenolic groups (e.g. quercetin), leading to a range of possibilities for controlled release systems.

## References:

1. *Health, Unites States, 2015*. 2015 [cited 2016 08-22-2016]; 121]. Available from: <http://www.cdc.gov/nchs/data/hus/hus15.pdf#019>.
2. Heron, M. and B. Tejada-Vera, *Deaths: leading causes for 2005*. National vital statistics reports: from the Centers for Disease Control and Prevention, National Center for Health Statistics, National Vital Statistics System, 2009. **58**(8): p. 1-97.
3. Heitzer, T., et al., *Endothelial dysfunction, oxidative stress, and risk of cardiovascular events in patients with coronary artery disease*. *Circulation*, 2001. **104**(22): p. 2673-2678.
4. Dhalla, N.S., R.M. Temsah, and T. Netticadan, *Role of oxidative stress in cardiovascular diseases*. *Journal of hypertension*, 2000. **18**(6): p. 655-673.
5. Stephens, N.G., et al., *Randomised controlled trial of vitamin E in patients with coronary disease: Cambridge Heart Antioxidant Study (CHAOS)*. *The Lancet*, 1996. **347**(9004): p. 781-786.
6. Poljsak, B., *Strategies for reducing or preventing the generation of oxidative stress*. *Oxid Med Cell Longev*, 2011. **2011**: p. 194586.
7. Murrell, G.A., M.J. Francis, and L. Bromley, *Modulation of fibroblast proliferation by oxygen free radicals*. *Biochemical Journal*, 1990. **265**(3): p. 659-665.
8. Schreck, R., P. Rieber, and P.A. Baeuerle, *Reactive oxygen intermediates as apparently widely used messengers in the activation of the NF-kappa B transcription factor and HIV-1*. *The EMBO journal*, 1991. **10**(8): p. 2247.
9. Turrens, J.F., *Mitochondrial formation of reactive oxygen species*. *The Journal of physiology*, 2003. **552**(2): p. 335-344.
10. Murphy, M.P., *How mitochondria produce reactive oxygen species*. *Biochemical Journal*, 2009. **417**(1): p. 1-13.
11. Valko, M., et al., *Free radicals, metals and antioxidants in oxidative stress-induced cancer*. *Chem Biol Interact*, 2006. **160**(1): p. 1-40.
12. Pacht, E.R., et al., *Deficiency of vitamin E in the alveolar fluid of cigarette smokers. Influence on alveolar macrophage cytotoxicity*. *Journal of Clinical Investigation*, 1986. **77**(3): p. 789.
13. Glauert, H.P., et al., *Role of oxidative stress in the promoting activities of PCBs*. *Environmental toxicology and pharmacology*, 2008. **25**(2): p. 247-250.
14. Fahmy, B. and S.A. Cormier, *Copper oxide nanoparticles induce oxidative stress and cytotoxicity in airway epithelial cells*. *Toxicology in Vitro*, 2009. **23**(7): p. 1365-1371.
15. Sánchez, O., et al., *Study of biomaterial-induced macrophage activation, cell-mediated immune response and molecular oxidative damage in patients with dermal bioimplants*. *Immunobiology*, 2012. **217**(1): p. 44-53.
16. Li, J.J., et al., *Autophagy and oxidative stress associated with gold nanoparticles*. *Biomaterials*, 2010. **31**(23): p. 5996-6003.
17. Kim, S., et al., *Oxidative stress-dependent toxicity of silver nanoparticles in human hepatoma cells*. *Toxicology in vitro*, 2009. **23**(6): p. 1076-1084.
18. Penttinen, P., et al., *Ultrafine particles in urban air and respiratory health among adult asthmatics*. *European respiratory journal*, 2001. **17**(3): p. 428-435.

19. Weichenthal, S., A. Dufresne, and C. Infante-Rivard, *Indoor ultrafine particles and childhood asthma: exploring a potential public health concern*. *Indoor air*, 2007. **17**(2): p. 81-91.
20. Uttara, B., et al., *Oxidative stress and neurodegenerative diseases: a review of upstream and downstream antioxidant therapeutic options*. *Current neuropharmacology*, 2009. **7**(1): p. 65-74.
21. Davidovich, N., et al., *Cyclic Stretch-Induced Oxidative Stress Increases Pulmonary Alveolar Epithelial Permeability*. *American journal of respiratory cell and molecular biology*, 2013. **49**(1): p. 156-164.
22. Chapman, K.E., et al., *Cyclic mechanical strain increases reactive oxygen species production in pulmonary epithelial cells*. *American Journal of Physiology-Lung Cellular and Molecular Physiology*, 2005. **289**(5): p. L834-L841.
23. Ali, M.H., et al., *Mitochondrial requirement for endothelial responses to cyclic strain: implications for mechanotransduction*. *American Journal of Physiology-Lung Cellular and Molecular Physiology*, 2004. **287**(3): p. L486-L496.
24. Spencer, J.P., et al., *Evaluation of the pro-oxidant and antioxidant actions of L-DOPA and dopamine in vitro: implications for Parkinson's disease*. *Free radical research*, 1996. **24**(2): p. 95-105.
25. Murphy, M.E., et al., *Antioxidant depletion in aortic crossclamping ischemia: increase of the plasma  $\alpha$ -tocopheryl quinone/ $\alpha$ -tocopherol ratio*. *Free Radical Biology and Medicine*, 1992. **13**(2): p. 95-100.
26. Won, S.J., et al., *Assessment at the single-cell level identifies neuronal glutathione depletion as both a cause and effect of ischemia-reperfusion oxidative stress*. *The Journal of Neuroscience*, 2015. **35**(18): p. 7143-7152.
27. Rana, S., et al., *Role of oxidative stress & antioxidant defence in ulcerative colitis patients from north India*. *The Indian journal of medical research*, 2014. **139**(4): p. 568.
28. Ayala, A., M.F. Muñoz, and S. Argüelles, *Lipid peroxidation: production, metabolism, and signaling mechanisms of malondialdehyde and 4-hydroxy-2-nonenal*. *Oxidative medicine and cellular longevity*, 2014. **2014**.
29. Yin, H., L. Xu, and N.A. Porter, *Free radical lipid peroxidation: mechanisms and analysis*. *Chemical reviews*, 2011. **111**(10): p. 5944-5972.
30. Griffiths, H.R., et al., *Biomarkers*. *Molecular aspects of medicine*, 2002. **23**(1): p. 101-208.
31. Esterbauer, H., R.J. Schaur, and H. Zollner, *Chemistry and biochemistry of 4-hydroxynonenal, malonaldehyde and related aldehydes*. *Free radical Biology and medicine*, 1991. **11**(1): p. 81-128.
32. Jomova, K. and M. Valko, *Advances in metal-induced oxidative stress and human disease*. *Toxicology*, 2011. **283**(2): p. 65-87.
33. Roberts Li, L.J. and J.D. Morrow, *Measurement of F2-isoprostanes as an index of oxidative stress in vivo*. *Free Radical Biology and Medicine*, 2000. **28**(4): p. 505-513.
34. Sultana, R., M. Perluigi, and D.A. Butterfield, *Lipid peroxidation triggers neurodegeneration: a redox proteomics view into the Alzheimer disease brain*. *Free Radical Biology and Medicine*, 2013. **62**: p. 157-169.

35. Reed, T.T., *Lipid peroxidation and neurodegenerative disease*. Free Radical Biology and Medicine, 2011. **51**(7): p. 1302-1319.
36. Dalle-Donne, I., et al., *Protein carbonyl groups as biomarkers of oxidative stress*. Clinica chimica acta, 2003. **329**(1): p. 23-38.
37. Oliver, C.N., et al., *Age-related changes in oxidized proteins*. Journal of Biological Chemistry, 1987. **262**(12): p. 5488-5491.
38. Stadtman, E., et al., *Implication of protein oxidation in protein turnover, aging, and oxygen toxicity*, in *Oxygen Radicals in Biology and Medicine*. 1988, Springer. p. 331-339.
39. Stadtman, E.R., *Metal ion-catalyzed oxidation of proteins: biochemical mechanism and biological consequences*. Free Radical Biology and Medicine, 1990. **9**(4): p. 315-325.
40. Dean, R., et al., *Biochemistry and pathology of radical-mediated protein oxidation*. Biochem. J, 1997. **324**: p. 1-18.
41. Malik, Q. and K.E. Herbert, *Oxidative and non-oxidative DNA damage and cardiovascular disease*. Free radical research, 2012. **46**(4): p. 554-564.
42. Ames, B.N., M.K. Shigenaga, and T.M. Hagen, *Mitochondrial decay in aging*. Biochimica et Biophysica Acta (BBA)-Molecular Basis of Disease, 1995. **1271**(1): p. 165-170.
43. Stadtman, E.R., *Protein oxidation in aging and age-related diseases*. Annals of the New York Academy of Sciences, 2001. **928**(1): p. 22-38.
44. Croteau, D.L. and V.A. Bohr, *Repair of oxidative damage to nuclear and mitochondrial DNA in mammalian cells*. Journal of Biological Chemistry, 1997. **272**(41): p. 25409-25412.
45. Cooke, M.S., et al., *Oxidative DNA damage: mechanisms, mutation, and disease*. The FASEB Journal, 2003. **17**(10): p. 1195-1214.
46. Mecocci, P., U. MacGarvey, and M.F. Beal, *Oxidative damage to mitochondrial DNA is increased in Alzheimer's disease*. Annals of neurology, 1994. **36**(5): p. 747-751.
47. Klaunig, J.E. and L.M. Kamendulis, *The role of oxidative stress in carcinogenesis*. Annu. Rev. Pharmacol. Toxicol., 2004. **44**: p. 239-267.
48. Loft, S. and H.E. Poulsen, *Cancer risk and oxidative DNA damage in man*. Journal of molecular medicine, 1996. **74**(6): p. 297-312.
49. Vanessa Fiorentino, T., et al., *Hyperglycemia-induced oxidative stress and its role in diabetes mellitus related cardiovascular diseases*. Current pharmaceutical design, 2013. **19**(32): p. 5695-5703.
50. Nicholas, S.H., *Clinical applications of body ventilators*. Chest, 1986. **90**(6): p. 897-905.
51. Gifford, R., et al., *Protein interactions with subcutaneously implanted biosensors*. Biomaterials, 2006. **27**(12): p. 2587-2598.
52. Zhou, T., et al., *Development of a multiple-drug delivery implant for intraocular management of proliferative vitreoretinopathy*. Journal of Controlled Release, 1998. **55**(2): p. 281-295.
53. Anderson, J.M., *Mechanisms of inflammation and infection with implanted devices*. Cardiovascular Pathology, 1993. **2**(3): p. 33-41.

54. Udipi, K., et al., *Modification of inflammatory response to implanted biomedical materials in vivo by surface bound superoxide dismutase mimics*. Journal of Biomedical Materials Research Part A, 2000. **51**: p. 12.
55. Anderson, J.M., *Inflammation and the foreign body response*. Problems in General Surgery, 1994. **11**(2): p. 147-160.
56. Anderson, J.M. and M.S. Shive, *Biodegradation and biocompatibility of PLA and PLGA microspheres*. Advanced drug delivery reviews, 2012. **64**: p. 72-82.
57. Nilsson, B., et al., *The role of complement in biomaterial-induced inflammation*. Molecular immunology, 2007. **44**(1): p. 82-94.
58. Broughton 2nd, G., J.E. Janis, and C.E. Attinger, *The basic science of wound healing*. Plastic and reconstructive surgery, 2006. **117**(7 Suppl): p. 12S-34S.
59. Szpaderska, A.M. and L.A. DiPietro, *Inflammation in surgical wound healing: friend or foe?* Surgery, 2005. **137**(5): p. 571-3.
60. Stramer, B.M., R. Mori, and P. Martin, *The inflammation–fibrosis link? A Jekyll and Hyde role for blood cells during wound repair*. Journal of Investigative Dermatology, 2007. **127**(5): p. 1009-1017.
61. Tsaryk, R., et al., *Response of human endothelial cells to oxidative stress on Ti6Al4V alloy*. Biomaterials, 2007. **28**(5): p. 806-813.
62. Evens, A., J. Mehta, and L. Gordon, *Rust and corrosion in hematopoietic stem cell transplantation: the problem of iron and oxidative stress*. Bone marrow transplantation, 2004. **34**(7): p. 561-571.
63. Kalbacova, M., et al., *The effect of electrochemically simulated titanium cathodic corrosion products on ROS production and metabolic activity of osteoblasts and monocytes/macrophages*. Biomaterials, 2007. **28**(22): p. 3263-3272.
64. Dziubla, T.D., et al., *Nanoscale antioxidant therapeutics*, in *Oxidative stress, Disease and Cancer*, K.K. Singh, Editor. 2006: Imperial College Press, London.
65. Zolnik, B.S., et al., *Minireview: nanoparticles and the immune system*. Endocrinology, 2010. **151**(2): p. 458-465.
66. Moyano, D.F., et al., *Nanoparticle hydrophobicity dictates immune response*. Journal of the American Chemical Society, 2012. **134**(9): p. 3965-3967.
67. Thomas, C., V. Gupta, and F. Ahsan, *Influence of surface charge of PLGA particles of recombinant hepatitis B surface antigen in enhancing systemic and mucosal immune responses*. International journal of pharmaceutics, 2009. **379**(1): p. 41-50.
68. Fink, J., et al., *Stimulation of monocytes and macrophages: possible influence of surface roughness*. Clinical hemorheology and microcirculation, 2008. **39**(1–4): p. 205-212.
69. Patil, V.S., T.D. Dziubla, and D.S. Kalika, *Static and dynamic properties of biodegradable poly(antioxidant  $\beta$ -amino ester) networks based on incorporation of curcumin multiacrylate*. Polymer, 2015. **75**: p. 88-96.
70. Huang, D., B. Ou, and R.L. Prior, *The chemistry behind antioxidant capacity assays*. Journal of agricultural and food chemistry, 2005. **53**(6): p. 1841-1856.
71. Huang, D., et al., *Development and validation of oxygen radical absorbance capacity assay for lipophilic antioxidants using randomly methylated  $\beta$ -cyclodextrin as the solubility enhancer*. Journal of Agricultural and Food Chemistry, 2002. **50**(7): p. 1815-1821.

72. Antolovich, M., et al., *Methods for testing antioxidant activity*. Analyst, 2002. **127**(1): p. 183-198.
73. Prior, R.L., X. Wu, and K. Schaich, *Standardized methods for the determination of antioxidant capacity and phenolics in foods and dietary supplements*. Journal of agricultural and food chemistry, 2005. **53**(10): p. 4290-4302.
74. Chen, X., et al., *Release kinetics of tocopherol and quercetin from binary antioxidant controlled-release packaging films*. J Agric Food Chem, 2012. **60**(13): p. 3492-7.
75. Göpferich, A., *Mechanisms of polymer degradation and erosion*. Biomaterials, 1996. **17**(2): p. 103-114.
76. Amass, W., A. Amass, and B. Tighe, *A review of biodegradable polymers: uses, current developments in the synthesis and characterization of biodegradable polyesters, blends of biodegradable polymers and recent advances in biodegradation studies*. Polymer International, 1998. **47**(2): p. 89-144.
77. Shastri, V.P., *Non-degradable biocompatible polymers in medicine: past, present and future*. Current pharmaceutical biotechnology, 2003. **4**(5): p. 331-337.
78. Mathiesen, E.B., et al., *Wear of the acetabular socket: Comparison of polyacetat and polyethylene*. Acta Orthopaedica Scandinavica, 1986. **57**(3): p. 193-196.
79. San Pio, J.R., et al., *Repair of giant incisional hernias with polypropylene mesh: a retrospective study*. Scandinavian journal of plastic and reconstructive surgery and hand surgery, 2003. **37**(2): p. 102-106.
80. Cox, A.J. and T.D. Wang, *Skeletal implants in aesthetic facial surgery*. Facial plastic surgery, 1999. **15**(01): p. 3-12.
81. Berard, X., et al., *[Retrospective study of the one-year patency of a cuffed polytetrafluoroethylene Venaflo-type graft placed for venous hemodialysis access]*. Journal des maladies vasculaires, 2003. **28**(2): p. 73-78.
82. Morris-Stiff, G.J. and L.E. Hughes, *The outcomes of nonabsorbable mesh placed within the abdominal cavity: literature review and clinical experience*. Journal of the American College of Surgeons, 1998. **186**(3): p. 352-367.
83. Mii, S., et al., *Fifteen-year experience in axillofemoral bypass with externally supported knitted Dacron prosthesis in a Japanese hospital*. Journal of the American College of Surgeons, 1998. **186**(5): p. 581-588.
84. DiMaio, F.R., *The science of bone cement: a historical review*. Orthopedics, 2002. **25**(12): p. 1399-1407.
85. Breusch, S. and K.-D. Kühn, *Knochenzemente auf basis von polymethylmethacrylat*. Der Orthopäde, 2003. **32**(1): p. 41-50.
86. Moreira-Gonzalez, A., et al., *Clinical outcome in cranioplasty: critical review in long-term follow-up*. Journal of Craniofacial Surgery, 2003. **14**(2): p. 144-153.
87. Gu, S., et al., *Effectiveness of Norplant® implants through seven years: a large-scale study in China*. Contraception, 1995. **52**(2): p. 99-103.
88. Pollack, I.P., H.A. Quigley, and T. Harbin, *The Ocusert pilocarpine system: advantages and disadvantages*. Southern medical journal, 1976. **69**(10): p. 1296-1298.
89. Asafo-Adjei, T.A., T.D. Dziubla, and D.A. Puleo, *Synthesis and characterization of a poly (ethylene glycol)–poly (simvastatin) diblock copolymer*. RSC advances, 2014. **4**(102): p. 58287-58298.

90. Fu, Y. and W.J. Kao, *Drug release kinetics and transport mechanisms of non-degradable and degradable polymeric delivery systems*. Expert opinion on drug delivery, 2010. **7**(4): p. 429-444.
91. Nair, L.S. and C.T. Laurencin, *Biodegradable polymers as biomaterials*. Progress in polymer science, 2007. **32**(8): p. 762-798.
92. Collins, M.N. and C. Birkinshaw, *Hyaluronic acid based scaffolds for tissue engineering—A review*. Carbohydrate polymers, 2013. **92**(2): p. 1262-1279.
93. Liechty, W.B., et al., *Polymers for drug delivery systems*. Annual review of chemical and biomolecular engineering, 2010. **1**: p. 149.
94. Park, H., K. Park, and W.S. Shalaby, *Biodegradable hydrogels for drug delivery*. 2011: CRC Press.
95. Kotla, N.G., et al., *Facts, fallacies and future of dissolution testing of polysaccharide based colon-specific drug delivery*. J Control Release, 2014. **178**: p. 55-62.
96. Champion, J.A., Y.K. Katare, and S. Mitragotri, *Particle shape: a new design parameter for micro-and nanoscale drug delivery carriers*. Journal of Controlled Release, 2007. **121**(1): p. 3-9.
97. Pillai, O. and R. Panchagnula, *Polymers in drug delivery*. Current opinion in chemical biology, 2001. **5**(4): p. 447-451.
98. Middleton, J.C. and A.J. Tipton, *Synthetic biodegradable polymers as orthopedic devices*. Biomaterials, 2000. **21**(23): p. 2335-2346.
99. Uhrich, K.E., et al., *Polymeric systems for controlled drug release*. Chemical reviews, 1999. **99**(11): p. 3181-3198.
100. Jain, J.P., et al., *Role of polyanhydrides as localized drug carriers*. Journal of Controlled Release, 2005. **103**(3): p. 541-563.
101. Sundararaj, S.C., et al., *Design of a multiple drug delivery system directed at periodontitis*. Biomaterials, 2013. **34**(34): p. 8835-42.
102. Sundararaj, S.C., et al., *Bioerodible system for sequential release of multiple drugs*. Acta Biomater, 2014. **10**(1): p. 115-25.
103. Lao, L.L., et al., *Modeling of drug release from bulk-degrading polymers*. Int J Pharm, 2011. **418**(1): p. 28-41.
104. Peppas, N.A., et al., *Hydrogels in biology and medicine: from molecular principles to bionanotechnology*. Advanced Materials, 2006. **18**(11): p. 1345-1360.
105. Slaughter, B.V., et al., *Hydrogels in regenerative medicine*. Advanced materials, 2009. **21**(32-33): p. 3307-3329.
106. Hoffman, A.S., *Hydrogels for biomedical applications*. Advanced drug delivery reviews, 2012. **64**: p. 18-23.
107. Hoare, T.R. and D.S. Kohane, *Hydrogels in drug delivery: progress and challenges*. Polymer, 2008. **49**(8): p. 1993-2007.
108. Jordan, C., et al., *The role of carrier geometry in overcoming biological barriers to drug delivery*. Current pharmaceutical design, 2016. **22**(9): p. 1259-1273.
109. Champion, J.A. and S. Mitragotri, *Role of target geometry in phagocytosis*. Proceedings of the National Academy of Sciences of the United States of America, 2006. **103**(13): p. 4930-4934.

110. Rolland, J.P., et al., *Direct fabrication and harvesting of monodisperse, shape-specific nanobiomaterials*. Journal of the American Chemical Society, 2005. **127**(28): p. 10096-10100.
111. Velev, O.D., A.M. Lenhoff, and E.W. Kaler, *A class of microstructured particles through colloidal crystallization*. Science, 2000. **287**(5461): p. 2240-2243.
112. Dendukuri, D., et al., *Controlled synthesis of nonspherical microparticles using microfluidics*. Langmuir, 2005. **21**(6): p. 2113-2116.
113. Sozzani, P., et al., *Complete shape retention in the transformation of silica to polymer micro-objects*. Nature materials, 2006. **5**(7): p. 545-551.
114. Hsieh, D.S., W.D. Rhine, and R. Langer, *Zero-order controlled-release polymer matrices for micro-and macromolecules*. Journal of pharmaceutical sciences, 1983. **72**(1): p. 17-22.
115. Kuo, C.K. and P.X. Ma, *Ionicly crosslinked alginate hydrogels as scaffolds for tissue engineering: Part I. Structure, gelation rate and mechanical properties*. Biomaterials, 2001. **22**(6): p. 511-521.
116. Xing, B., et al., *Hydrophobic interaction and hydrogen bonding cooperatively confer a vancomycin hydrogel: a potential candidate for biomaterials*. Journal of the American Chemical Society, 2002. **124**(50): p. 14846-14847.
117. Kim, D. and K. Park, *Swelling and mechanical properties of superporous hydrogels of poly (acrylamide-co-acrylic acid)/polyethylenimine interpenetrating polymer networks*. Polymer, 2004. **45**(1): p. 189-196.
118. Authimoolam, S.P., et al., *Layer-by-Layers of Polymeric Micelles as a Biomimetic Drug-Releasing Network*. Macromol Biosci, 2015.
119. Scott, R.A. and N.A. Peppas, *Highly crosslinked, PEG-containing copolymers for sustained solute delivery*. Biomaterials, 1999. **20**(15): p. 1371-1380.
120. Kharkar, P.M., et al., *Thiol-ene click hydrogels for therapeutic delivery*. ACS Biomaterials Science & Engineering, 2016. **2**(2): p. 165-179.
121. Anderson, D.G., et al., *Structure/property studies of polymeric gene delivery using a library of poly(beta-amino esters)*. Mol Ther, 2005. **11**(3): p. 426-34.
122. Anderson, D.G., et al., *A Combinatorial Library of Photocrosslinkable and Degradable Materials*. Advanced Materials, 2006. **18**(19): p. 2614-2618.
123. Zawko, S.A., Q. Truong, and C.E. Schmidt, *Drug-binding hydrogels of hyaluronic acid functionalized with beta-cyclodextrin*. Journal of Biomedical Materials Research Part A, 2008. **87**(4): p. 1044-1052.
124. Wattamwar, P.P., et al., *Synthesis and characterization of poly(antioxidant beta-amino esters) for controlled release of polyphenolic antioxidants*. Acta Biomater, 2012. **8**(7): p. 2529-37.
125. Wattamwar, P.P., et al., *Tuning of the pro-oxidant and antioxidant activity of trolox through the controlled release from biodegradable poly (trolox ester) polymers*. Journal of Biomedical Materials Research Part A, 2011. **99**(2): p. 184-191.
126. Tønnesen, H.H., M. Måsson, and T. Loftsson, *Studies of curcumin and curcuminoids. XXVII. Cyclodextrin complexation: solubility, chemical and photochemical stability*. International Journal of Pharmaceutics, 2002. **244**(1): p. 127-135.
127. Hood, E., et al., *Nanocarriers for vascular delivery of antioxidants*. Nanomedicine, 2011. **6**(7): p. 1257-1272.

128. Simone, E.A., et al., *Filamentous polymer nanocarriers of tunable stiffness that encapsulate the therapeutic enzyme catalase*. *Biomacromolecules*, 2009. **10**(6): p. 1324-1330.
129. Giovagnoli, S., et al., *Biodegradable microspheres as carriers for native superoxide dismutase and catalase delivery*. *AAPS PharmSciTech*, 2004. **5**(4): p. 1-9.
130. Yallapu, M.M., et al., *Fabrication of curcumin encapsulated PLGA nanoparticles for improved therapeutic effects in metastatic cancer cells*. *Journal of colloid and interface science*, 2010. **351**(1): p. 19-29.
131. Pool, H., et al., *Antioxidant effects of quercetin and catechin encapsulated into PLGA nanoparticles*. *Journal of Nanomaterials*, 2012. **2012**: p. 86.
132. Altunbas, A., et al., *Encapsulation of curcumin in self-assembling peptide hydrogels as injectable drug delivery vehicles*. *Biomaterials*, 2011. **32**(25): p. 5906-5914.
133. Wattamwar, P.P., et al., *Antioxidant Activity of Degradable Polymer Poly(trolox ester) to Suppress Oxidative Stress Injury in the Cells*. *Advanced Functional Materials*, 2010. **20**(1): p. 147-154.
134. Cochran, D.B., et al., *Suppressing iron oxide nanoparticle toxicity by vascular targeted antioxidant polymer nanoparticles*. *Biomaterials*, 2013. **34**(37): p. 9615-9622.
135. Kwon, J., et al., *Inflammation-responsive antioxidant nanoparticles based on a polymeric prodrug of vanillin*. *Biomacromolecules*, 2013. **14**(5): p. 1618-1626.
136. Tirouvanziam, R., et al., *High-dose oral N-acetylcysteine, a glutathione prodrug, modulates inflammation in cystic fibrosis*. *Proceedings of the National Academy of Sciences of the United States of America*, 2006. **103**(12): p. 4628-4633.
137. Inoue, M., et al., *Mitochondrial generation of reactive oxygen species and its role in aerobic life*. *Current medicinal chemistry*, 2003. **10**(23): p. 2495-2505.
138. Wattamwar, P.P. and T.D. Dziubla, *Modulation of the Wound Healing Response Through Oxidation Active Materials*, in *Engineering Biomaterials for Regenerative Medicine*. 2012, Springer. p. 161-192.
139. Sharma, O.P., *Antioxidant activity of curcumin and related compounds*. *Biochemical Pharmacology*, 1976. **25**.
140. Motterlini, R., et al., *Curcumin, an antioxidant and anti-inflammatory agent, induces heme oxygenase-1 and protects endothelial cells against oxidative stress*. *Free Radical Biology and Medicine*, 2000. **28**(8): p. 1303-1312.
141. Gururaj, A.E., et al., *Molecular mechanisms of anti-angiogenic effect of curcumin*. *Biochemical and biophysical research communications*, 2002. **297**(4): p. 934-942.
142. Tonnesen, H.H., J. Karlsen, and G.B. van Henegouwen, *Studies on curcumin and curcuminoids VIII. Photochemical stability of curcumin*. *Zeitschrift für Lebensmittel-Untersuchung und -Forschung*, 1986. **183**.
143. Paradkar, A., et al., *Characterization of curcumin-PVP solid dispersion obtained by spray drying*. *International journal of pharmaceutics*, 2004. **271**(1): p. 281-286.
144. Bisht, S., et al., *Polymeric nanoparticle-encapsulated curcumin ("nanocurcumin"): a novel strategy for human cancer therapy*. *Journal of nanobiotechnology*, 2007. **5**(1): p. 18.

145. Tang, H., et al., *Curcumin polymers as anticancer conjugates*. *Biomaterials*, 2010. **31**(27): p. 7139-49.
146. Manju, S. and K. Sreenivasan, *Conjugation of curcumin onto hyaluronic acid enhances its aqueous solubility and stability*. *Journal of colloid and interface science*, 2011. **359**(1): p. 318-325.
147. Cassano, R., et al., *Preparation, characterization and in vitro activities evaluation of curcumin based microspheres for azathioprine oral delivery*. *Reactive and Functional Polymers*, 2012. **72**(7): p. 446-450.
148. Gogoi, B., et al., *Polycurcumin acrylate and polycurcumin methacrylate: Novel bio-based polymers for explosive chemical sensor*. *Sensors and Actuators B: Chemical*, 2013. **181**: p. 144-152.
149. Killi, N., V.L. Paul, and R.V.N. Gundloori, *Antibacterial non-woven nanofibers of curcumin acrylate oligomers*. *New Journal of Chemistry*, 2015. **39**: p. 7.
150. Ishii, Y., et al., *[Possible candidates for the compound which is expected to attenuate dioxin toxicity]*. *Fukuoka igaku zasshi= Hukuoka acta medica*, 2005. **96**(5): p. 204-213.
151. Kitture, R., et al., *Fe<sub>3</sub>O<sub>4</sub>-citrate-curcumin: promising conjugates for superoxide scavenging, tumor suppression and cancer hyperthermia*. *Journal of Applied Physics*, 2012. **111**(6): p. 064702.
152. Cochran, D.B., et al., *Degradable poly (apigenin) polymer inhibits tumor cell adhesion to vascular endothelial cells*. *Journal of Biomedical Materials Research Part B: Applied Biomaterials*, 2015. **104**(7).
153. Gupta, P., et al., *Quercetin conjugated poly ( $\beta$ -amino esters) nanogels for the treatment of cellular oxidative stress*. *Acta biomaterialia*, 2015. **27**: p. 194-204.
154. Nagao, T., et al., *Ingestion of a tea rich in catechins leads to a reduction in body fat and malondialdehyde-modified LDL in men*. *The American journal of clinical nutrition*, 2005. **81**(1): p. 122-129.
155. Li, Y. and Y. Ding, *Minireview: Therapeutic potential of myricetin in diabetes mellitus*. *Food Science and Human Wellness*, 2012. **1**(1): p. 19-25.
156. Zhang, A., et al., *Dendronized polymers: recent progress in synthesis*. *Macromolecular Chemistry and Physics*, 2003. **204**(2): p. 328-339.
157. Payton, F., P. Sandusky, and W.L. Alworth, *NMR Study of the Solution Structure of Curcumin*. *Journal of Natural Products*, 2007. **70**(2): p. 143-146.
158. Zawadiak, J. and M. Mrzyczek, *UV absorption and keto-enol tautomerism equilibrium of methoxy and dimethoxy 1,3-diphenylpropane-1,3-diones*. *Spectrochimica Acta Part A: Molecular and Biomolecular Spectroscopy*, 2010. **75**(2): p. 925-929.
159. Kawano, S.-i., et al., *Analysis of keto-enol tautomers of curcumin by liquid chromatography/mass spectrometry*. *Chinese Chemical Letters*, 2013. **24**(8): p. 685-687.
160. Pan, J., et al., *Separation and determination of the structural isomers of madecassoside by HPLC using  $\beta$ -cyclodextrin as mobile phase additive*. *Chromatographia*, 2007. **66**(1-2): p. 121-123.
161. Riddell, N., et al., *Branched perfluorooctane sulfonate isomer quantification and characterization in blood serum samples by HPLC/ESI-MS (/MS)*. *Environmental science & technology*, 2009. **43**(20): p. 7902-7908.

162. Gutsche, C.D., et al., *Calixarenes 9: conformational isomers of the ethers and esters of calix [4] arenes*. Tetrahedron, 1983. **39**(3): p. 409-426.
163. Pumera, M. and C.H.A. Wong, *Graphane and hydrogenated graphene*. Chemical Society Reviews, 2013. **42**(14): p. 5987-5995.
164. Fu, K., et al., *Visual evidence of acidic environment within degrading poly (lactico-glycolic acid)(PLGA) microspheres*. Pharmaceutical research, 2000. **17**(1): p. 100-106.
165. Fleming, C., et al., *A carbohydrate-antioxidant hybrid polymer reduces oxidative damage in spermatozoa and enhances fertility*. Nature Chemical Biology, 2005. **1**(5): p. 270-274.
166. Bat, E., et al., *In vivo behavior of trimethylene carbonate and  $\epsilon$ -caprolactone-based (co) polymer networks: Degradation and tissue response*. Journal of Biomedical Materials Research Part A, 2010. **95**(3): p. 940-949.
167. Williams, S.R., et al., *Synthesis and Characterization of Poly (ethylene glycol)–Glutathione Conjugate Self-Assembled Nanoparticles for Antioxidant Delivery*. Biomacromolecules, 2008. **10**(1): p. 155-161.
168. Pulla Reddy, A.C. and B. Lokesh, *Effect of dietary turmeric (< i> curcuma longa</i>) on iron-induced lipid peroxidation in the rat liver*. Food and chemical toxicology, 1994. **32**(3): p. 279-283.
169. Wright, J.S., *Predicting the antioxidant activity of curcumin and curcuminoids*. Journal of Molecular Structure: THEOCHEM, 2002. **591**(1): p. 207-217.
170. Brey, D.M., et al., *Controlling poly(beta-amino ester) network properties through macromer branching*. Acta Biomater, 2008. **4**(2): p. 207-17.
171. Biswal, D., et al., *A single-step polymerization method for poly( $\beta$ -amino ester) biodegradable hydrogels*. Polymer, 2011. **52**(26): p. 5985-5992.
172. Hawkins, A.M., et al., *Synthesis and analysis of degradation, mechanical and toxicity properties of poly(beta-amino ester) degradable hydrogels*. Acta Biomater, 2011. **7**(5): p. 1956-64.
173. Patil, V.S., et al., *Curcumin acrylation for biological and environmental applications*. 2017.
174. Fumio, U., et al., *Swelling and mechanical properties of poly (vinyl alcohol) hydrogels*. International journal of pharmaceutics, 1990. **58**(2): p. 135-142.
175. Anseth, K.S., C.N. Bowman, and L. Brannon-Peppas, *Mechanical properties of hydrogels and their experimental determination*. Biomaterials, 1996. **17**(17): p. 1647-1657.
176. Safranski, D.L., et al., *Thermo-Mechanical Properties of Semi-Degradable Poly(beta-amino ester)-co-Methyl Methacrylate Networks under Simulated Physiological Conditions*. Polymer, 2011. **52**(21): p. 4920-4927.
177. Kannurpatti, A.R., J.W. Anseth, and C.N. Bowman, *A study of the evolution of mechanical properties and structural heterogeneity of polymer networks formed by photopolymerizations of multifunctional (meth) acrylates*. Polymer, 1998. **39**(12): p. 2507-2513.
178. Williams, G., et al., *Further considerations of non symmetrical dielectric relaxation behaviour arising from a simple empirical decay function*. Transactions of the faraday Society, 1971. **67**: p. 1323-1335.

179. Kalakkunnath, S., et al., *Segmental Relaxation Characteristics of Cross-Linked Poly(ethylene oxide) Copolymer Networks*. *Macromolecules*, 2005. **38**: p. 8381-8393.
180. Kremer, F. and A. Schönhals, *Broadband dielectric spectroscopy*. 2003: Springer.
181. Kalakkunnath, S., et al., *Molecular relaxation in cross-linked poly(ethylene glycol) and poly(propylene glycol) diacrylate networks by dielectric spectroscopy*. *Polymer*, 2007. **48**(2): p. 579-589.
182. Havriliak, S. and S. Negami, *A complex plane representation of dielectric and mechanical relaxation processes in some polymers*. *Polymer*, 1967. **8**: p. 161-210.
183. Havriliak, S. and S.J. Havriliak, in *Dielectric and mechanical relaxation in materials*. 1997: Cincinnati:Hanser.
184. Ferry, J.D., *Viscoelastic properties of polymers*. 1980: John Wiley & Sons.
185. Jin, X., S. Zhang, and J. Runt, *Observation of a fast dielectric relaxation in semicrystalline poly(ethylene oxide)*. *Polymer*, 2002. **43**(23): p. 6247-6254.
186. Borns, M.A., et al., *Dynamic relaxation characteristics of crosslinked poly(ethylene oxide) copolymer networks: Influence of short chain pendant groups*. *Polymer*, 2007. **48**(25): p. 7316-7328.
187. Peppas, N.A., *Hydrogels and drug delivery*. *Current opinion in colloid & interface science*, 1997. **2**(5): p. 531-537.
188. Nicolson, P.C. and J. Vogt, *Soft contact lens polymers: an evolution*. *Biomaterials*, 2001. **22**(24): p. 3273-3283.
189. Kopecek, J., *Hydrogels: From soft contact lenses and implants to self-assembled nanomaterials*. *Journal of Polymer Science Part A: Polymer Chemistry*, 2009. **47**(22): p. 5929-5946.
190. Lynn, D.M. and R. Langer, *Degradable poly( $\beta$ -amino esters): synthesis, characterization, and self-assembly with plasmid DNA*. *Journal of the American Chemical Society*, 2000. **122**(44): p. 10761-10768.
191. Eltoukhy, A.A., et al., *Effect of molecular weight of amine end-modified poly( $\beta$ -amino ester)s on gene delivery efficiency and toxicity*. *Biomaterials*, 2012. **33**(13): p. 3594-3603.
192. Keeney, M., et al., *Development of poly( $\beta$ -amino ester)-based biodegradable nanoparticles for nonviral delivery of minicircle DNA*. *ACS nano*, 2013. **7**(8): p. 7241-7250.
193. Little, S.R., et al., *Poly- $\beta$  amino ester-containing microparticles enhance the activity of nonviral genetic vaccines*. *Proceedings of the National Academy of Sciences of the United States of America*, 2004. **101**(26): p. 9534-9539.
194. Devalapally, H., et al., *Poly(ethylene oxide)-modified poly(beta-amino ester) nanoparticles as a pH-sensitive system for tumor-targeted delivery of hydrophobic drugs: part 3. Therapeutic efficacy and safety studies in ovarian cancer xenograft model*. *Cancer chemotherapy and pharmacology*, 2007. **59**(4): p. 477-484.
195. Brey, D.M., I. Erickson, and J.A. Burdick, *Influence of macromer molecular weight and chemistry on poly( $\beta$ -amino ester) network properties and initial cell interactions*. *Journal of Biomedical Materials Research Part A*, 2008. **85**(3): p. 731-741.
196. Jere, D., et al., *Poly( $\beta$ -amino ester) as a carrier for si/shRNA delivery in lung cancer cells*. *Biomaterials*, 2008. **29**(16): p. 2535-2547.

197. McBath, R.A. and D.A. Shipp, *Swelling and degradation of hydrogels synthesized with degradable poly ( $\beta$ -amino ester) crosslinkers*. Polymer Chemistry, 2010. **1**(6): p. 860-865.
198. Azagarsamy, M.A., et al., *Photocontrolled nanoparticles for on-demand release of proteins*. Biomacromolecules, 2012. **13**(8): p. 2219-2224.
199. An, T., et al., *Hyaluronic acid-coated poly ( $\beta$ -amino) ester nanoparticles as carrier of doxorubicin for overcoming drug resistance in breast cancer cells*. RSC Advances, 2016. **6**(45): p. 38624-38636.
200. Cai, X., et al., *pH-responsive copolymers based on pluronic P123-poly ( $\beta$ -amino ester): Synthesis, characterization and application of copolymer micelles*. Colloids and Surfaces B: Biointerfaces, 2016. **142**: p. 114-122.
201. Safranski, D.L., et al., *Effect of poly(ethylene glycol) diacrylate concentration on network properties and in vivo response of poly(beta-amino ester) networks*. J Biomed Mater Res A, 2011. **96**(2): p. 320-9.
202. Kozielski, K.L., S.Y. Tzeng, and J.J. Green, *A bio-reducible linear poly ( $\beta$ -amino ester) for siRNA delivery*. Chemical Communications, 2013. **49**(46): p. 5319-5321.
203. Balashanmugam, M.V., et al., *Preparation and characterization of novel PBAE/PLGA polymer blend microparticles for DNA vaccine delivery*. The Scientific World Journal, 2014. **2014**.
204. Gupta, P., et al., *Controlled curcumin release via conjugation into PBAE nanogels enhances mitochondrial protection against oxidative stress*. International Journal of Pharmaceutics, 2016. **511**(2): p. 1012-1021.
205. Perni, S. and P. Prokopovich, *Poly-beta-amino-esters as pro-drug delivery system in cartilages*. Osteoarthritis and Cartilage, 2016. **24**: p. S525.
206. Mayersohn, M. and M. Gibaldi, *New method of solid-state dispersion for increasing dissolution rates*. Journal of pharmaceutical sciences, 1966. **55**(11): p. 1323-1324.
207. Anand, P., et al., *Bioavailability of curcumin: problems and promises*. Molecular pharmaceutics, 2007. **4**(6): p. 807-818.
208. Brown, K.M., M. Kass, and R. Wilson Sr, *Isolated Granulomatous Gastritis: Treatment with Corticosteroids*. Journal of clinical gastroenterology, 1987. **9**(4): p. 442-446.
209. Enzmann, F. and B. Lachmann, *Transdermal, oral and intravenous formulations of 2, 3-dimethoxy-5-methyl-6-decaprenyl-1, 4-benzoquinone*. 2004, Google Patents.
210. Fraser, A., T. Orchard, and D. Jewell, *The efficacy of azathioprine for the treatment of inflammatory bowel disease: a 30 year review*. Gut, 2002. **50**(4): p. 485-489.
211. Fukui, E., et al., *Preparation of enteric coated timed-release press-coated tablets and evaluation of their function by in vitro and in vivo tests for colon targeting*. International journal of pharmaceutics, 2000. **204**(1): p. 7-15.
212. Wen, H. and K. Park, *Oral controlled release formulation design and drug delivery*. 2011: John Wiley & Sons.
213. Solem, C.A., et al., *Correlation of C-reactive protein with clinical, endoscopic, histologic, and radiographic activity in inflammatory bowel disease*. Inflammatory bowel diseases, 2005. **11**(8): p. 707-712.

214. Millar, A., et al., *Evaluating the antioxidant potential of new treatments for inflammatory bowel disease using a rat model of colitis*. Gut, 1996. **39**(3): p. 407-415.
215. Mitov, M.I., et al., *Chapter Six - In Vitro Cellular Assays for Oxidative Stress and Biomaterial Response*, in *Oxidative Stress and Biomaterials*. 2016, Academic Press. p. 145-186.
216. Yan, F., et al., *Colon-specific delivery of a probiotic-derived soluble protein ameliorates intestinal inflammation in mice through an EGFR-dependent mechanism*. The Journal of clinical investigation, 2011. **121**(6): p. 2242-2253.
217. Khan, M.Z.I., Ž. Prebeg, and N. Kurjaković, *A pH-dependent colon targeted oral drug delivery system using methacrylic acid copolymers: I. Manipulation of drug release using Eudragit® L100-55 and Eudragit® S100 combinations*. Journal of Controlled Release, 1999. **58**(2): p. 215-222.
218. Makhija, S.N. and P.R. Vavia, *Controlled porosity osmotic pump-based controlled release systems of pseudoephedrine: I. Cellulose acetate as a semipermeable membrane*. Journal of controlled release, 2003. **89**(1): p. 5-18.
219. Prasad, Y.R., Y. Krishnaiah, and S. Satyanarayana, *In vitro evaluation of guar gum as a carrier for colon-specific drug delivery*. Journal of controlled release, 1998. **51**(2): p. 281-287.
220. Youngberg, C.A., et al., *Comparison of gastrointestinal pH in cystic fibrosis and healthy subjects*. Digestive diseases and sciences, 1987. **32**(5): p. 472-480.
221. Shah, V.P., et al., *In vitro dissolution profile of water-insoluble drug dosage forms in the presence of surfactants*. Pharmaceutical research, 1989. **6**(7): p. 612-618.
222. Rockland, L.B., *Saturated salt solutions for static control of relative humidity between 5° and 40° C*. Analytical Chemistry, 1960. **32**(10): p. 1375-1376.
223. Serra, L., J. Doménech, and N.A. Peppas, *Drug transport mechanisms and release kinetics from molecularly designed poly (acrylic acid-g-ethylene glycol) hydrogels*. Biomaterials, 2006. **27**(31): p. 5440-5451.
224. Babu, N.J. and A. Nangia, *Solubility advantage of amorphous drugs and pharmaceutical cocrystals*. Crystal Growth & Design, 2011. **11**(7): p. 2662-2679.
225. Xiang, T.X. and B.D. Anderson, *Molecular dynamics simulation of amorphous indomethacin-poly (vinylpyrrolidone) glasses: Solubility and hydrogen bonding interactions*. Journal of pharmaceutical sciences, 2013. **102**(3): p. 876-891.
226. Yuan, X., D. Sperger, and E.J. Munson, *Investigating miscibility and molecular mobility of nifedipine-PVP amorphous solid dispersions using solid-state NMR spectroscopy*. Molecular pharmaceutics, 2013. **11**(1): p. 329-337.
227. Basarkar, A. and J. Singh, *Nanoparticulate systems for polynucleotide delivery*. International journal of nanomedicine, 2007. **2**(3): p. 353.
228. Li, S., H. Garreau, and M. Vert, *Structure-property relationships in the case of the degradation of massive poly ( $\alpha$ -hydroxy acids) in aqueous media*. Journal of Materials Science: Materials in Medicine, 1990. **1**(4): p. 198-206.
229. Dunne, M., O. Corrigan, and Z. Ramtoola, *Influence of particle size and dissolution conditions on the degradation properties of polylactide-co-glycolide particles*. Biomaterials, 2000. **21**(16): p. 1659-1668.

230. Panyam, J., et al., *Polymer degradation and in vitro release of a model protein from poly (D, L-lactide-co-glycolide) nano-and microparticles*. Journal of Controlled Release, 2003. **92**(1): p. 173-187.
231. Hsu, C.-H. and A.-L. Cheng, *Clinical studies with curcumin*, in *The Molecular Targets and Therapeutic Uses of Curcumin in Health and Disease*. 2007, Springer. p. 471-480.
232. Garcea, G., et al., *Detection of curcumin and its metabolites in hepatic tissue and portal blood of patients following oral administration*. British journal of cancer, 2004. **90**(5): p. 1011-1015.
233. Garcea, G., et al., *Consumption of the putative chemopreventive agent curcumin by cancer patients: assessment of curcumin levels in the colorectum and their pharmacodynamic consequences*. Cancer Epidemiology Biomarkers & Prevention, 2005. **14**(1): p. 120-125.
234. Sharma, R.A., et al., *Pharmacodynamic and pharmacokinetic study of oral Curcuma extract in patients with colorectal cancer*. Clinical Cancer Research, 2001. **7**(7): p. 1894-1900.
235. Sharma, R.A., et al., *Phase I clinical trial of oral curcumin biomarkers of systemic activity and compliance*. Clinical Cancer Research, 2004. **10**(20): p. 6847-6854.
236. Simanenko, Y.S., et al., *The Effect of Temperature on the Rate of Alkaline Hydrolysis of Esters in Concentrated Aqueous Solutions of Et<sub>4</sub>NCl*. Theoretical and Experimental Chemistry, 2004. **40**(1): p. 17-24.
237. Chaudhari, S.P. and R.H. Dave, *To prepare and characterize microcrystalline cellulose granules using water and isopropyl alcohol as granulating agents and determine its end-point by thermal and rheological tools*. Drug development and industrial pharmacy, 2015. **41**(5): p. 744-752.
238. Shi, L., Y. Feng, and C.C. Sun, *Initial moisture content in raw material can profoundly influence high shear wet granulation process*. International journal of pharmaceutics, 2011. **416**(1): p. 43-48.
239. Patil, V.S., et al., *Poly( $\beta$ -amino ester) based tablet formulation for improved oral bioavailability of a hydrophobic drug*, 2017.

## VITA

Vinod Shivaji Patil was born on 28<sup>th</sup> June, 1990 in Sangli, Maharashtra, India. He completed Bachelors in Chemical Engineering from Institute of Chemical Technology (formerly known as UDCT) in May 2011. He joined University of Kentucky in August 2011 to pursue PhD in Chemical Engineering,

### HONORS AND AWARDS

- “Best Poster” (1st place) award at MACE Spring Symposium, University of Kentucky, May 2016
- Graduate School Travel Award, Nov 2013 & Nov 2015
- Graduate School Academic Year Fellowship, Jan 2012
- Narotam-Sekhsaria Scholarship for UG studies, May 2009

### PUBLICATIONS

- **V.S. Patil**, T.D. Dziubla and D.S. Kalika, “Static and dynamic properties of biodegradable poly(antioxidant  $\beta$ -amino ester) networks based on incorporation of curcumin multiacrylate”. **Polymer**, 75, 88-96 (2015)
- M.I. Mitov, **V.S.Patil**, M.C. Alstott, T.D. Dziubla and D.A. Butterfield, Chapter Six - *In vitro* cellular assays for oxidative stress and biomaterial response. In *Oxidative stress and Biomaterials*, Academic Press, 145-186 (2016)
- **V.S. Patil**, Benjamin Burdette, T.D. Dziubla and D.S. Kalika, “Poly( $\beta$ -amino ester) based tablet formulation for hydrophobic drug”, (Under review)

- **V.S. Patil**, A.M. Gutierrez, M Sunkara, A.J. Morris, D.S. Kalika, and T.D. Dziubla “Curcumin acrylation for biological and environmental applications” (Journal of Natural Products), (Under Review)
- P. Gupta, C. Lacerda, **V.S. Patil**, P. P. Wattamwar, D. Biswal, J. Z. Hilt, T.D. Dziubla, “Degradation of Poly( $\beta$ -amino esters) in alcohols through transesterification: A method to conjugate drugs into the hydrogel matrix”, (Polymer Chemistry (Royal Society of Chemistry)), (Under review)

### **SELECTED CONFERENCE PRESENTATIONS**

- **V.S. Patil**, D.S. Kalika, T.D. Dziubla, “Static and dynamic properties of biodegradable PA $\beta$ AE networks based on incorporation of curcumin diacrylate”, *AIChE Annual Meeting*, San Francisco, Nov 2013
- **V.S. Patil**, D.S. Kalika, T.D. Dziubla, P.M. Bummer, “Polymeric prodrug formulations for the stabilizations of labile compounds”, *CPD semi-annual meeting*, Georgia Institute of Technology, Atlanta, Nov 2013
- **V.S. Patil**, B.C. Burdette, D.S. Kalika, T.D. Dziubla, “P $\beta$ AE based tablet formulation for a hydrophobic drug”, *Biomaterials day*, Lexington, Sept 2014
- **V.S. Patil**, D.S. Kalika, T.D. Dziubla, “P $\beta$ AE based tablet formulation for a hydrophobic drug”, *AIChE Annual Meeting*, Atlanta, Nov 2014
- **V.S. Patil**, D.S. Kalika, T.D. Dziubla, “Influence of composition and reaction conditions on the static and dynamic properties of biodegradable PC $\beta$ AE networks”, *AIChE Annual Meeting*, Salt Lake City, Nov 2015